Applications of *in vitro* and *in vivo* hepatic models to investigate drug and chemical toxicity

Alistair Callum Leitch

BSc, MRes.

Thesis submitted for the degree of Doctor of Philosophy

Newcastle University

Faculty of Medical Sciences

Institute of Cellular Medicine

September 2018

Declaration

I hereby declare that this thesis has been composed by myself and has not been accepted in application of a degree. All work was performed by myself unless otherwise stated. All sources of information have been acknowledged appropriately by means of a reference.

Alistair Leitch

Abstract

Hepatocytes are the primary cell of the liver, performing the majority of its unique functions, including the metabolism and clearance of xenobiotics and as a result, the liver plays an important role in drug and chemical toxicity. There are numerous *in vitro* and *in vivo* models currently used to investigate drug and chemical toxicity. The application of these models was used to investigate drug- and chemical-induced lipid dysregulation in hepatocytes and to determine the hepatic toxicity of an ionic liquid found in the environment, 3-methyl-1-octyl-1H-imidazol-3-ium (M8OI).

Hepatocyte-like B-13/H cells have previously been shown to express functional metabolising enzymes and have been suggested as an alternative to primary hepatocytes for *in vitro* toxicity screening. B-13/H cells accumulated lipids in response to being exposed to fatty acids and the liver X receptor activator T0901317. Phospholipidosis, a lipid storage disorder characterised by the accumulation of phospholipids was also observed in B-13/H cells exposed to cationic amphiphilic drugs. This effect was reduced by the over-expression of lysosomal phospholipase A2.

M8OI induced apoptotic cell death in several *in vitro* hepatic models including primary human hepatocytes and the inhibition of mitochondrial oxidative phosphorylation was determined as the cause of this toxic effect. Hepatic injury and glycogen depletion was observed in *in vivo* mouse models exposed to M8OI. Finally, M8OI was shown to be metabolised in primary human hepatocytes and in mice to less toxic hydroxyl and carboxyl metabolites.

These data indicate that B-13/H cells are an effective *in vitro* model in which to study the hepatic lipid dysregulation in response to drugs and chemicals and M8OI induces hepatotoxic effects *in vitro* and *in vivo* models.

Acknowledgements

Firstly, I would like to thank my supervisors Matthew Wright and George Kass. Especially to Matt for his support, guidance and enthusiasm for the past four years. He has made the experience enjoyable and motivated me throughout.

I would also like to thank all of Team Wright, past and present, especially to Philip Probert, Emma Fairhall, Stephanie Meyer, Anne Lakey and Rodrigo Figueiredo for their advice and assistance over the years and for the terrible jokes and even more terrible singing, I will always remember to shake it off.

Thanks also to Michael, Scott and Sarah who were always around for a drink when something did not go as planned, or when it did. And to Amanda and Euan who kept me sane from a distance.

Special thanks to Loranne Agius for a constant supply of mouse hepatocytes, Satomi Miwa for her assistance with all the seahorse and mitochondrial work and to Mick Dunn for all of his help and analysis of the Mass Spectroscopy work.

Finally, I would like to thank my family, to my Mum, Dad and sister, Shannon, who have always been around to support me.

Publications and Abstracts

Publications

Leitch, A.C., Lakey, A.F., Hotham, W.E., Agius, L., Kass, G.E.N., Blain, P.G., Wright, M.C. 2018. 'The ionic liquid 1-octyl-3-methylimidazolium (M8OI) is an activator of the human estrogen receptor alpha', Biochem Biophys Res Commun, 503, 2167-2172.

Fairhall, E.A., **Leitch, A.C**., Lakey, A.F., Abdelghany, T.M., Ibrahim, I., Tosh, D., Kass, G.E.N., Wilson, C. and Wright, M.C. 2018 'HNF4alpha expression amplifies the glucocorticoid-induced conversion of a human pancreatic cell line to an hepatocyte-like cell', *Biochem Biophys Res Commun*, 503, 1633-1640.

Probert, P.M., **Leitch, A.C**., Dunn, M.P., Meyer, S.K., Palmer, J.M., Abdelghany, T.M., Lakey, A.F., Cooke, M.P., Talbot, H., Wills, C., McFarlane, W., Blake, L.I., Rosenmai, A.K., Oskarsson, A., Figueiredo, R., Wilson, C., Kass, G.E., Jones, D.E., Blain, P.G., Wright, M.C. 2018. Identification of a xenobiotic as a potential environmental trigger in primary biliary cholangitis. *J Hepatol*, 69(5), 1123-1135.

Fairhall, E. A., **Leitch, A. C**., Lakey, A. F., Probert, P. M. E., Richardson, G., De Santis, C. & Wright, M. C. 2018. Glucocorticoid-induced pancreatic-hepatic trans-differentiation in a human cell line in vitro. *Differentiation*, 102, 10-18.

Meyer, S.K., Probert, P.M., Lakey, **Leitch A.C.**, A.K., Blake, L.I., Jowsey, P.A., Cooke, M.P., Blain, P.G., Wright M,C, 2017. Environmental Xenoestrogens Super-Activate a Variant Murine ER Beta in Cholangiocytes. *Toxicol Sciences*, 156, 54-71.

Meyer, S.K., Probert, P.M., Lakey, A.K., Axon, A.A., **Leitch, A.C.**, Williams, F.M., Jowsey, P.A., Blain, P.G., Kass, G.E.N., Wright, M.C. 2017b. Hepatic effects of tartrazine (E 102) after systemic exposure are independent of oestrogen receptor interactions in the mouse. *Toxicology Letters*, 273, 55-68.

Leitch, A. C., Probert, P. M. E., Shayman, J. A., Meyer, S. K., Kass, G. E. N. & Wright, M. C. 2017. B-13 progenitor-derived hepatocytes (B-13/H cells) model lipid dysregulation in response to drugs and chemicals. *Toxicology*, 386, 120-132.

Presented abstracts

Leitch, A.L., Figueiredo, R., Dunn, M.P., Blain, P.G., Wilson, C., Wright, M.C. Evidence that CYP3A4 metabolises the ionic liquid M8OI British Toxicological Society Congress 2018

Leitch, A.L., Axon, A., Williams, F.M., Blain, P.G., Kass, G.E.N., Wright, M.C. An ionic liquid activates the human ERs in vitro. British Toxicological Society Congress 2017

Leitch, A.L., Probert, P.M.E., P.G., Kass, G.E.N., Wright, M.C. Methapyrilene induced phospholipidosis does not significantly contribute to hepatotoxicity in rat hepatocytes (B-13/H cells). British Toxicological Society Congress 2016

Leitch, A.L., Probert, P.M.E., P.G., Kass, G.E.N., Wright, M.C. B-13 Progenitor-Derived Hepatocytes (B-13/H cells) as a Model for Lipid Dysregulation. EFSA's second scientific conference 2015

Leitch, A.L., Probert, P.M.E., P.G., Kass, G.E.N., Wright, M.C. B-13 Progenitor-Derived Hepatocytes (B-13/H cells) Model Lipid Dysregulation in Response to Drugs and Chemicals. British Toxicological Society Congress 2015

Table of Contents

List of Figures

List of Tables

List of Abbreviations

18S rRNA	18S ribosomal RNA
2-OADCs	2-oxoacid dehydrogenase complexes
ADFP	Adipocyte differentiation-related protein
ADH	Alcohol dehydrogenase
ADP	Adenosine diphosphate
ADRs	Adverse drug reactions
AhR	Aromatic hydrocarbon receptor
ALD	Alcoholic liver disease
ALDH	Aldehyde dehydrogenase
ALP	Alkaline phosphatase
ALT	Alanine transaminase
AMA	Antimitochondrial antibody
AMPK	AMP- activated protein kinase
ANAs	Antinuclear antigens
ANIT	α-naphthylisothiocyanate
ARNT	AhR nuclear translocator
ATP	Adenosine Triphosphate
β-NF	β-naphthoflavone
B13	AR42J-B-13
B13/H	B13 derived hepatocyte-like cell
BD	Bile duct
BECs	Biliary epithelial cells
BSA	Bovine serum albumin

BSEP	Bile salt exporter pump
CADs	Cationic amphiphilic drugs
CAR	Constitutive androstane receptor
cDNA	Complementary DNA
CEBP-β	CCAAT/enhancer-binding protein-β
ChREBP	Carbohydrate-responsive element-binding protein
CK-19	Cytokeratin 19
CMC	Carboxymethyl cellulose
COOH7IM	Carboxylic acid - 1-(7-carboxyheptyl)-3-methyl-1H-imidazol-3-ium
CV	Central vein
CYP450s	Cytochrome P450s
DAPI	4’6’-diamino-2-phenylindole
DBD	DNA binding domain
DEX	Dexamethasone
DILI	Drug induced liver injury
DIPL	Drug induced phospholipidosis
DMEM	Dulbecco’s modified eagle medium
DMEs	Drug metabolising enzymes
DMSO	Dimethyl sulfoxide
DNA	Deoxyribonucleic acid
DNL	*De novo* lipogenesis
DTT	Dithiothreitol
E2	17β oestradiol
ECAR	Extracellular acidification rate
ECM	Extracellular Matrix

EDTA	Ethylenediaminetetraacetic acid
EE	Ethinyloestradiol
EpCAM	Epithelial cell adhesion molecule
ERE	Estrogen response elements
ERs	Estrogen receptors
ETC	Electron transport chain
FAD	Flavin adenine dinucleotide
FAS	Fatty acid synthase
FCCP	Carbonyl cyanide-4 (trifluoromethoxy) phenylhydrazone
FCS	Fetal calf serum
FFAs	Free fatty acids
FXR	Farnesoid X receptor
GAPDH	Glyceraldehyde 3-phosphate dehydrogenase
GR	Glucocorticoid receptor
GSK3	Glycogen synthase kinase 3
H&E	Haematoxylin and eosin
HA	Hepatic artery
HBSS	Hank's Balanced Salt Solution
HCC	Hepatocellular carcinoma
HCV	Hepatitis C virus
hERα	Human estrogen receptor α
hERβ	Human estrogen receptor β
hESCs	Human embryonic stem cells
HNFα	Hepatocyte nuclear factor 1α
HO8IM	3-(8-hydroxyoctyl)-1-methyl-1H-imidazol-3-ium

HPLC	High performance liquid chromatography
hPSCs	Human pluripotent stem cells
HSCs	Hepatic stellate cells
i.p.	Intra-peritoneally
IDILI	Idiosyncratic drug induced liver injury
ILs	Ionic Liquids
IVIS	*In vivo* imaging system
LB	Luria-Bertani medium
LBD	Ligand binding domain
LDL	Low density lipoproteins
LPLA2	Lysosomal phospholipase A2
LPS	Lipopolysaccharide
LXR	Liver X receptor
M8OI	3-methyl-1-octyl-1H-imidazol-3-ium
MAS	Mitochondrial assay media
MDR-3	Multidrug resistance-associated protein 3
mER	Mouse estrogen receptor
mERα	Mouse estrogen receptor α
mERβv1	Mouse estrogen receptor β transcript variant 1
mERβv2	Mouse estrogen receptor β transcript variant 2
MHC	Major histocompatibility complex
M-MLV	Moloney murine leukemia virus
MPTP	Mitochondrial permeability transition pore
mRNA	Messenger RNA
MTT	3-(4,5-Dimethylthiazol-2-Yl)-2,5-Diphenyltetrazolium Bromide

NADH	Nicotinamide adenine dinucleotide
NADPH	Nicotinamide adenine dinucleotide phosphate
NAFLD	Non-alcoholic fatty liver disease
NASH	Non-alcoholic steatohepatitis
NEFA	Nonesterified fatty acid pool
NF-κB	Nuclear factor κB
OCA, INT-747	Obeticholic acid
OCR	Oxygen consumption rate
P80	Polysorbate 80
PB	Phenobarbital
PBC	Primary biliary cholangitis
PBREM	PB responsive enhancer modules
PBS	Phosphate buffer saline
PCR	Polymerase Chain Reaction
PDC	Pyruvate dehydrogenase complex
PDC-E2	Pyruvate dehydrogenase complex - dihydrolipoamide acetyltransferase
PDK1	3-phosphoinositide dependent protein kinase 1
PHHs	Primary human hepatocytes
PhIP	Progenotoxin 2-amino-1-methyl-6-phenylimidazo(4,5-b)pyridine
PI3K	Phosphatidylinositol-4,5-bisphosphate 3-kinase
PLD	Phospholipidosis
PMP	Plasma membrane permeabilizer
PNPLA3	Patatin-like phospholipase domain-containing protein 3
PPAR-α	Peroxisome proliferator activated receptor-alpha
PV	Portal vein

PXR	Pregnane X receptor
ROS	Reactive oxygen species
RT-PCR	Reverse transcription polymerase chain reaction
RXR	Retinoic X receptor
SD	Standard deviation
SDS	Sodium dodecyl sulphate
SECs	Sinusoidal endothelial cells
SREBP-1c	Sterol regulatory element binding protein 1c
TAG	Triacylglycerol
TCA	Citric acid cycle/tricarboxylic acid
TCDD	2,3,7,8-tetrachlorodibenzodioxin
Tcf/Lef	T-cell factor/lymphoid enhancer factor
TEM	Transmission electron microscope
TEMED	Tetramethylethylenediamine
TFF1	Trefoil factor 1
TG	Triglyceride
TLC	Thin layer liquid chromatography
TLR4	Toll-like receptor 4
TNFα	Tumour necrosis factor alpha
UDCA	Ursodeoxycholic acid
VLDL	Very low-density lipoprotein
XRE	Xenobiotic response element
XREM	Xenobiotic responsive enhancer module

Chapter 1. Introduction

1.1 The Liver

1.1.1 Liver anatomy

The liver is the largest internal organ in the human body, weighing approximately 1.5kg and contributing to ~2% of the total body weight of a healthy adult. It is located under the diaphragm in the upper right region of the abdominal cavity, surrounded by a layer of collagenous tissue called the Glisson's capsule. The human liver is most commonly described as consisting of four lobes; the left lobe and the larger right lobe, separated by the falciform filament, and the caudate and quadrate lobes (located at the posterior and inferior sides of the right lobe respectively). The Couinaud classification is a more accurate way to describe the anatomy of the liver (Figure 1.1). This classification divides the liver into eight segments based on vascular inflow and outflow. (Dancygier, 2009).

The liver receives its blood supply from two sources, the portal vein and the hepatic artery. The portal vein delivers around 70-75% of the blood. This blood is deoxygenated and rich in nutrients and toxins from the gut, pancreas and spleen. Around 25-30% of blood is delivered by the hepatic artery, this blood is oxygenated and low in nutrients. The two supplies are mixed in the liver sinusoids, at the edge of the portal tract and drained by the hepatic vein (Kuntz and Kuntz, 2009).

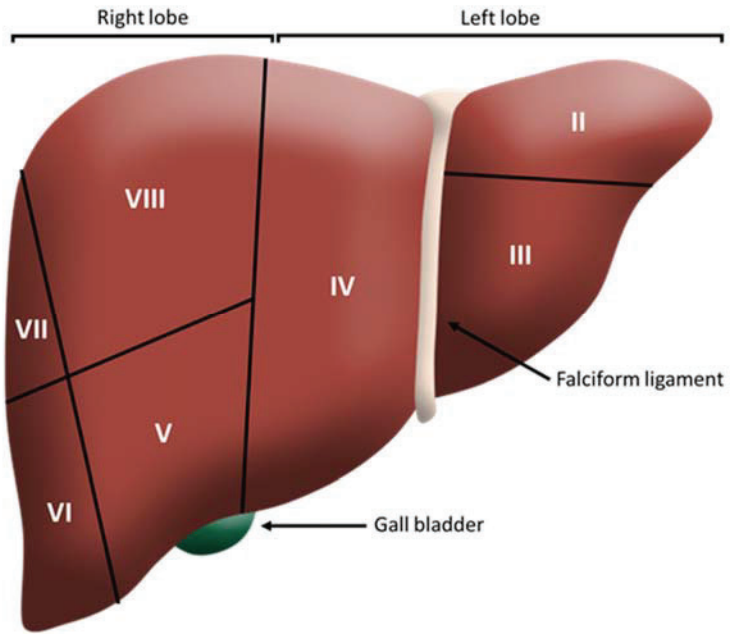

Figure 1.1: Anatomy of the human liver. Segmentation shown according to Couinaud. Segment I not shown, found at the posterior. Adapted from (Monga and Cagle, 2010)

1.1.2 Functional units of the liver

The functional unit of the liver tissue is based around the entry and exit of blood. Several models have been proposed to describe the functional units of the liver. The two most widely used models are the liver lobule and liver acinus. The liver lobule model describes the functional unit of the liver on a structural basis. The lobule is a polygonal unit with the central vein at its centre. Blood enters through the portal vein and hepatic artery at the periphery and flows towards the central vein (Figure 1.2A). The liver acinus model describes the unit on a functional level. Similarly, in this model blood flows from the portal tract to the central vein. However, the liver acinus model considers the levels of oxygen and substrates available to the hepatocytes based on their distance from the portal tract (Figure 1.2B). They are designated into three zones with zone 1, being closest to the portal tract, receiving the most oxygen and substrates, and zone 3 receiving the least. Hepatocyte function, such as enzymatic and metabolic capacity, is not identical within all hepatocytes and differs based on zonation, for example cytochrome P450 expression increases from zone 1 towards zone 3 (Dancygier, 2009; Kuntz and Kuntz, 2009).

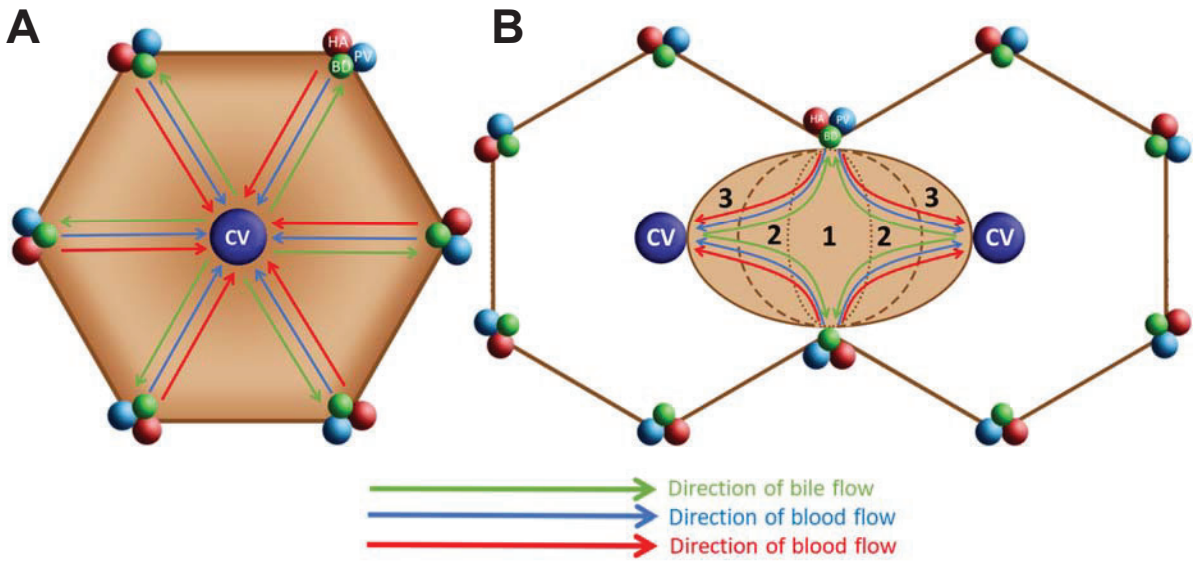

Figure 1.2: Functional units of the liver. A, Liver lobule. Blood flows from the portal tract towards the central vein. Blood flows into adjacent lobules. Oxygen and the concentration of nutrients decrease as blood flows away from the portal tract. Bile flows from the central vein towards the bile duct in the portal tract. **B, Liver acinus.** Blood flows from portal tract to central vein. Blood flows in a single acinus through zones 1 to 3. Oxygen and nutrient concentration decreases as blood flows through from zones 1 to 3. Abbreviations: BD, bile duct; CV, central vein; HA, hepatic artery; PV, portal vein. Adapted from (Wallace *et al.*, 2008).

Within the lobule acinus, hepatocytes are organised into plates that extend from the portal tract towards the central vein. These plates consist of 15-25 hepatocytes from portal tract to central vein and each plate is one cell thick (Figure 1.3). The space between these plates is called the sinusoid and is where the exchange of materials between blood (supplied from the portal vein and hepatic artery) and hepatocytes takes place. Fenestrated endothelial cells (sinusoidal endothelial cells, SECs) line the sinusoid and the space between these endothelial cells and hepatocytes is known as the space of Dissé. Extracellular components are found within the space of Dissé, as well as hepatic stellate cells in a quiescent state in the absence of inflammation. Hepatocytes are polarised so that microvilli are present on the sinusoidal surface that aid in the exchange of materials with the blood. On their lateral surface they form bile canaliculi where they secrete bile that flows towards the bile duct in the portal tracts (Dancygier, 2009).

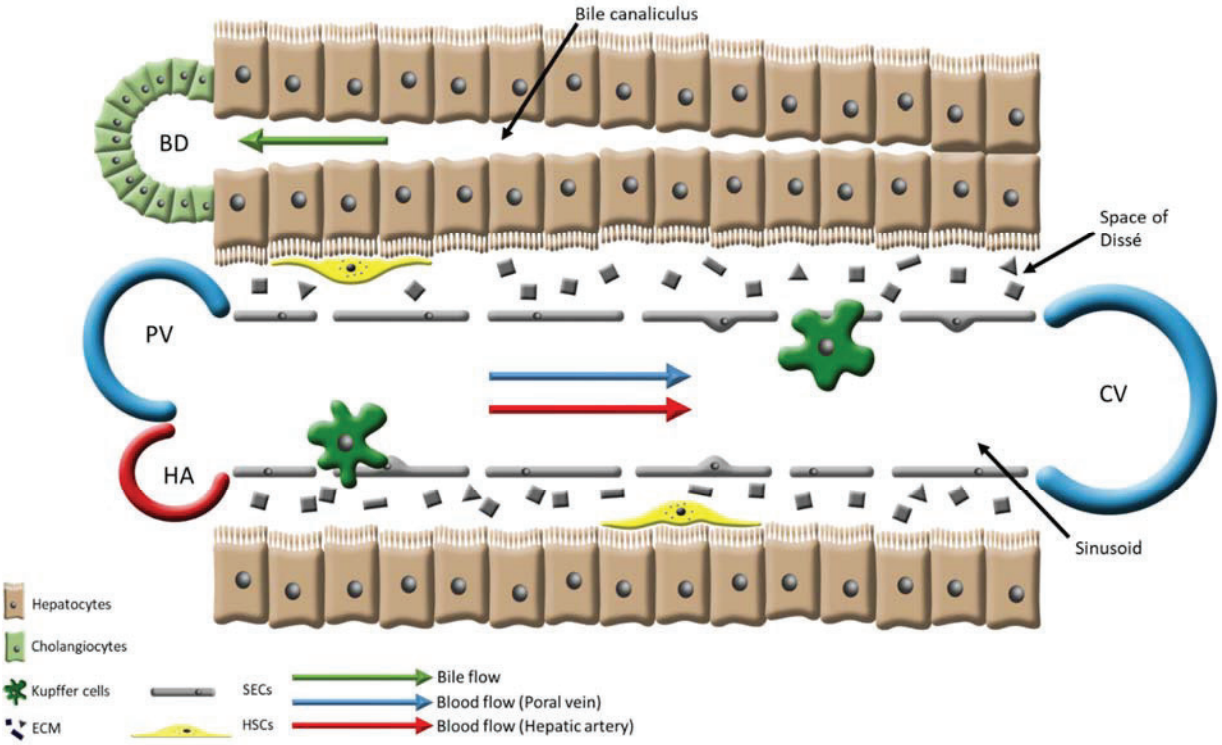

Figure 1.3: The microarchitecture of the liver. Blood flows from the portal vein and hepatic artery towards the central vein. The two blood supplies are mixed in the liver sinusoid. Materials are exchanged between the sinusoid and the hepatocytes. Hepatocytes secrete bile into the bile canaliculus where it flows towards the bile duct in the opposite direction to blood. Hepatic stellate cells are found are found in the space of Dissé and Kupffer cells in the sinusoid. Abbreviations: BD, bile duct; CV, central vein; ECM, extracellular matrix; HA, hepatic artery; HSCs, hepatic stellate cells; PV, portal vein; SECs, sinusoidal endothelial cells. Adapted from (Wallace *et al.*, 2008).

1.1.3 The biliary system

The biliary system is a network of ducts that transport bile acids that are synthesised from cholesterol by hepatocytes, from the liver to the gall bladder or duodenum. These ducts are lined with cholangiocytes – the bile duct epithelium cell. Bile is secreted by hepatocytes into the smallest ducts, the canaliculi, and they increase in size as they move towards the portal tract where they converge on intra-hepatic ducts. Bile then leaves the liver via the common hepatic duct, followed by either the cystic duct towards the gall bladder or the common bile duct to the duodenum. Bile that travels to the gall bladder is stored as it is not required. The bile that travels to the duodenum is used to emulsify lipids and lipophilic vitamins in the intestine to aid digestion and most is recirculated back to the liver via the portal vein. Bile also plays a role in the excretion of xenobiotic metabolites produced by hepatocytes. These products are too hydrophobic to by excreted by the kidneys without the presence of bile (Kuntz and Kuntz, 2009).

1.1.4 Cells of the liver

1.1.4.a Hepatocytes

Hepatocytes are the main functional cell in the liver, accounting for 60-70% of total cell number. The hepatocyte has many essential functions in the liver, including xenobiotic detoxification, protein synthesis and the metabolism of amino acids, lipids and carbohydrates. To aid in these functions hepatocytes contain high levels of smooth and rough endoplasmic reticulum, mitochondria and electron dense glycogen particles. The hepatocyte is unique compared to other epithelia, as they are structurally and functionally polarised. This gives rise to three distinct membrane domains; sinusoidal (basolateral), lateral, and canalicular (apical). The sinusoidal membrane faces the sinusoids and microvilli extend into the space of Dissé to facilitate exchange of substrates and proteins. The lateral membrane forms a blood-bile barrier by fusing alongside the bile canaliculi to form tight junctions. The canalicular membrane faces the bile canaliculus and transports bile constituents (bile acids, phospholipids etc.) to the bile duct (Monga and Cagle, 2010).

1.1.4.b Sinusoidal endothelial cells

Sinusoidal endothelial cells act as a barrier between the blood and hepatocytes and regulate the exchange of materials between them. SECs do not have a basal membrane but instead have fenestrations. It is these fenestrations that allow the transport of fluids and filtration of solutes and particles. For example, the

pores allow the access of smaller lipoproteins to the hepatocytes, however larger sized lipoproteins do not cross until they have been sufficiently broken down by lipases (Malarkey *et al.*, 2005; Dancygier, 2009).

1.1.4.c Biliary epithelial cells

Biliary epithelial cells (BECs), also known as cholangiocytes, are the epithelial cell of the bile ducts that make up the biliary tree and are essential to the transport of bile to the gall bladder and duodenum. BECs display functional and morphological heterogeneity that is dependent on their location within the biliary tree. For example, the BECs of the small bile ducts possess proliferative capabilities. Whereas those lining the large bile ducts secrete hormones and electrolytes to alkalinize the bile (Glaser *et al.*, 2009; Monga and Cagle, 2010).

1.1.4.d Hepatic stellate cells

Hepatic stellate cells (HSC) are located in the space of Dissé, between the SECs and hepatocytes. In normal conditions these cells are quiescent, functioning to store and metabolise vitamin A and secrete extracellular matrix components (ECM). When the liver is in an injured state, pro-inflammatory signalling, such as reactive oxidative species (ROS), cytokines and chemokines, activate the HSCs. This leads to a loss of vitamin A and they differentiate into a more proliferative, pro-fibrogenic myofibroblast. In their activated state they also increase their expression of α-smooth muscle actin (α-SMA), increase in contractility and secrete more extracellular components as well as cytokines (Monga and Cagle, 2010).

1.1.4.e Kupffer cells

Kupffer cells are the hepatic macrophages that are located in the lumen of sinusoids, adhered to the SECs. Kupffer cells number, size and activity is greatest at the periportal region (zone 1) and least active that the pericentral region (zone 3). The role of the Kupffer cell is to phagocytose foreign materials along with the processing and presentation of antigenic material. Kupffer cells are also involved in the liver's response to stresses such as infection, toxins and ischemia. Once activated they release pro-inflammatory cytokines such as tumour necrosis factor alpha (TNFα) and ROS that regulate the liver's inflammatory response (Roberts *et al.*, 2007; Monga and Cagle, 2010).

1.1.4.f Hepatic progenitor cells

Hepatic progenitor cells can differentiate into two types of liver epithelial cells, the hepatocytes and the cholangiocytes. These progenitor cells are believed to be involved in tissue repair and the proliferation of hepatocytes and cholangiocytes in response to liver injury, when the normal proliferative capabilities of these endothelial cells are impaired. These cells are likely to be in the canals of Hering as these ductal structures expand in response to liver injury (Tanimizu and Mitaka, 2014). Recent studies have suggested that these liver progenitor cells originate from biliary epithelium (Rodrigo-Torres *et al.*, 2014; Lu *et al.*, 2015)

1.1.5 Functions of the liver

The liver is responsible for numerous metabolic and homeostatic processes that are essential to the functioning of a healthy organism. These include the metabolism of endogenously produced substances such as bilirubin, a toxic product formed from the breakdown of haemoglobin. Glucocorticoids, androgens, estrogens and gestagens are cholesterol derived, steroid hormones that are inactivated in the liver, and eliminated in the bile or urine. This is important in the regulation for hormonal homeostasis (Kuntz and Kuntz, 2009).

The liver is also involved in the metabolism of proteins, lipids and carbohydrates. Some protein synthesis occurs in the liver as well as the degradation of essential amino acids. This degradation results in the production of ammonia a toxic product that is rapidly converted to urea by the urea cycle. Lipid metabolism within the liver includes the synthesis and degradation of free fatty acids as well as the synthesis and secretion of lipoproteins. Lipoproteins transport lipids through the blood and are essential for the maintenance of plasma lipid levels. The liver is essential in the regulation of carbohydrate metabolism, and the maintenance of blood glucose levels. The hepatocytes take up glucose in response to insulin released by the pancreas and can transform it into glycogen for storage. In response to low blood glucose concentrations, the pancreas releases glucagon that promotes the hepatocyte to catabolise glycogen to release glucose and increase blood glucose levels (Kuntz and Kuntz, 2009).

Bile acid metabolism is an important specialised function of the liver, more specifically of the hepatocytes. Primary bile acids are formed from cholesterol through a series of enzymatic reactions. These are used to aid the digestion and absorption of lipids in the duodenum or are stored in the gall bladder (Kuntz and Kuntz, 2009).

1.2 Xenobiotic metabolism

The body is exposed to various exogenous compounds (xenobiotics) every day. These xenobiotics are generally lipophilic and are therefore poorly soluble in water and almost completely reabsorbed by the renal tubules. In order for the body to be able to excrete these exogenous compounds, they need to be converted into more water-soluble products. The primary organ for the biotransformation of xenobiotics is the liver as hepatocytes contain drug metabolising enzymes, mainly in the smooth endoplasmic reticulum, and partially in the mitochondria. Traditionally biotransformation of exogenous compounds takes place in two phases, phase I – xenobiotic modification and phase II – conjugation (Monga and Cagle, 2010).

1.2.1 Phases of metabolism

Phase I metabolism acts to modify xenobiotics by introducing a functional polar group, such as hydroxyl (-OH), amino ($-NH_2$), sulfhydryl (-SH), or carboxyl (-COOH) groups. Enzymes achieve this using the functional reactions of oxidation, reduction, hydrolysis and hydration. The main enzymes responsible for phase I metabolism are the cytochrome P450s (CYP450) and the flavin-containing monooxygenases (FMO) (Monga and Cagle, 2010).

Phase II reactions are synthetic, involving the conjugation of the xenobiotic with endogenous substances. This is carried out by transferases such as UDP glucoronosyl transferases, N-acetyl transferases and sulphotransferases. The endogenous ligands for these transferases are described in Table 1.1. Once conjugated the xenobiotic is usually detoxified (but not always) and hydrophilic enough to be excreted in the bile or urine (Monga and Cagle, 2010).

Reaction Type	Conjugating enzyme	Endogenous conjugation agent
Glucuronidation	UDP glucoronosyl transferases	UDP-glucuronic acid
Acetylation	N-acetyl transferases	Acetyl CoA
Glutathione conjugation	Glutathione transferases	Glutathione
Sulphation	Sulphotransferases	Phosphoadenosyl phosphosulate
Methylation	Methyl transferases	s-adenosyl-methionine
Amino acid conjugation	ATP dependent acid:CoA ligases and Acyl:CoA amino acid N-acyltransferases	Amino acids

Table 1.1: Major phase II pathways of xenobiotic metabolism. Adapted from (Monga and Cagle, 2010)

1.2.2 Cytochrome P450s

The largest group of drug metabolising enzymes are the CYP450s. There are 57 separate human genes encoding CYP450s that are categorised into families (eg CYP1), subfamilies (CYP1A), and individual genes (CYP1A1). The main families in the liver are CYP1, CYP2 and CYP3 that account for the biotransformation of 70-80% of currently used clinical drugs (Zanger and Schwab, 2013).

CYP450 reactions are mono-oxygenation reactions that oxidise xenobiotics. The cytochrome P450 catalytic cycle is shown in Figure 1.4. CYP450 combines with the reduced xenobiotic. An electron is then donated from dihydronicotinamide-adenine dinucleotide phosphate (NADPH) by cytochrome P450 oxidoreductase. Molecular oxygen then binds and a second electron is donated by CYP reductase or cytochrome b_5. The complex then dissociates and releases water and the oxidised xenobiotic, with one electron used to oxidised one oxygen atom to water and the other oxidising the xenobiotic (Monga and Cagle, 2010).

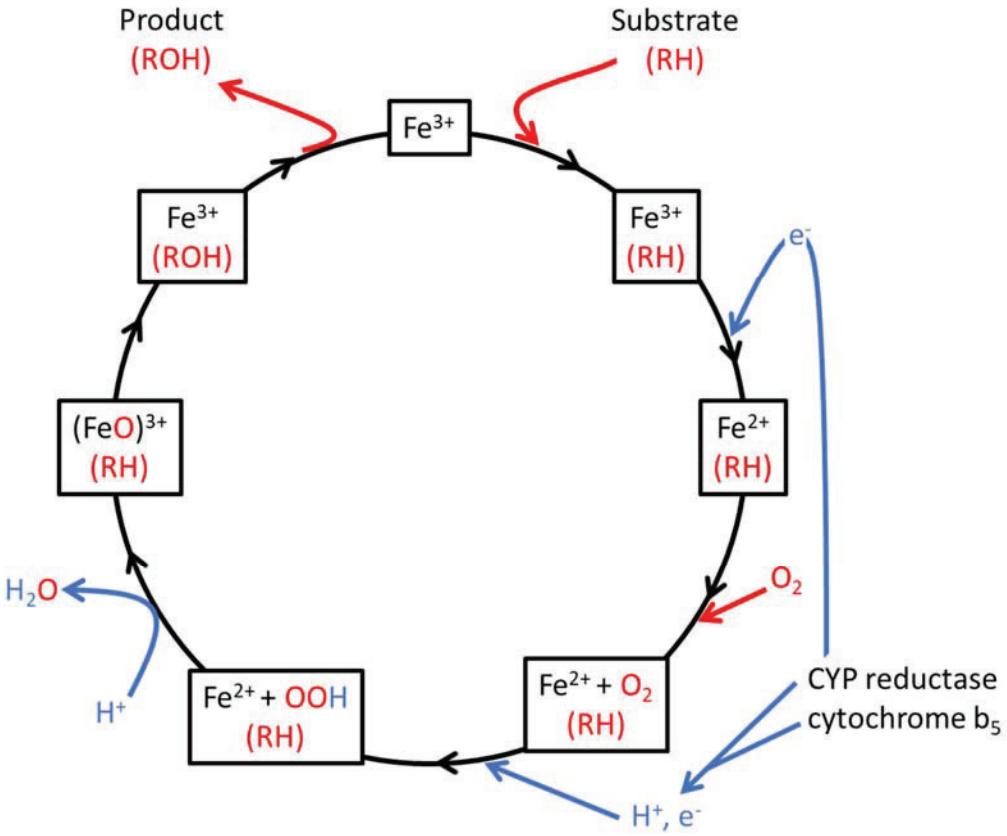

Figure 1.4: The cytochrome P450 catalytic cycle. Adapted from (Monga and Cagle, 2010)

1.2.3 Influences on CYP450 expression and function

Numerous factors influence the expression of CYP450 enzymes, including polymorphisms, epigenetics, sex, age and disease. Knowledge of these factors is important in clinical pharmacology when predicting pharmacokinetics and drug response. Polymorphisms in CYP450 genes can lead to a loss of function or gain of function. This results in a spectrum of pharmacokinetic phenotypes that range from poor metabolisers to intermediate metabolisers to ultra-rapid metabolisers based on their allelic expression. Clinically this means an individual defined as a poor metaboliser with respect to a particular CYP450 would show a reduced clearance and increased plasma concentration of administered drugs metabolised by that CYP450. It is therefore important to know how efficiently a patient will metabolise a drug to avoid toxic effects or a lack of therapeutic response, especially with drugs that have a narrow therapeutic window, such as warfarin (Sconce *et al.*, 2005).

Epigenetics via DNA methylation and histone protein modification is another factor that influences CYP450 expression. One example of this is the methylation of the CYP1A1 promoter in human lung tissue. This methylation is lowest in tobacco smokers compared to non-smokers, resulting in CYP1A1 expression in the lungs being higher in smokers (Anttila *et al.*, 2003). Sex also influences CYP450 expression with most clinical studies showing women metabolise drugs quicker than men. One genome wide gene expression study showed that ~40 drug metabolising enzymes and metabolising enzyme related genes displayed bias towards one sex compared to the other (Zhang *et al.*, 2011). Finally, age has an influence on drug metabolising enzyme expression, particularly in new-borns and the elderly. New born children show low levels of metabolising capacity due to the low expression of several enzymes. In the elderly there is also a decrease in metabolising capability. Contributing factors to this are diseases such as fatty liver disease (Naik *et al.*, 2013), reduced liver blood flow and the administration of multiple drugs that could also lead to inhibition of metabolising enzymes (Zanger and Schwab, 2013).

1.2.4 CYP450 induction and regulation

The regulation of CYP450 expression is important for ensuring the drug metabolising function meets the demand of metabolism. Thus, the liver has developed a mechanism to modulate CYP450 expression. The primary method in which this is achieved is via ligand activated receptors. The ligands of these receptors are usually substrates for the CYP450 that the receptor regulates. The four major receptors are the aryl hydrocarbon receptor (AhR), constitutive androstane receptor (CAR), pregnane X receptor (PXR) and the peroxisome proliferator activated receptor-alpha (PPAR-α) (Monga and Cagle, 2010).

The AhR up-regulates CYP1A1, CYP1A2 and CYP1B1 expression, the enzymes that activate polyaromatic hydrocarbons and arylamines (Honkakoski and Negishi, 2000). Inducers of CYP1A1 via the AhR include β-naphthoflavone (β-NF), 3-methylcholanthrene and 2,3,7,8-tetrachlorodibenzodioxin (TCDD) (Hankinson, 1995; Ma and Lu, 2007). The ligand bound AhR translocates into the nucleus where is associates with AhR nuclear translocator (ARNT). The AhR-ARNT complex then binds to xenobiotic response element (XRE) sites, recruits transcriptional activators and machinery and up-regulates gene expression (Beischlag *et al.*, 2008).

The CAR and PXR are orphan nuclear receptors that are primarily expressed in the liver. CAR activators include phenobarbital (PB), bilirubin and 6-(4-chlorophenyl)imidazo[2,1-b][1,3]thiazole-5-carbaldehyde-O-(3,4-dichlorobenzyl)oxime (CITCO). CAR activation can be induced directly by the binding of ligands, such as CITCO. In direct activation, the ligand binds and induces the association of CAR with the co-activator

SRC-1 and protein phosphates A2 (PP2A). PP2A catalyses the dephosphorylation of CAR and leads to its translocation to the nucleus where it associates with the retinoic X receptor (RXR). Gene expression is then regulated by the binding to the xenobiotic responsive enhancer module (XREM) or PB responsive enhancer modules (PBREM) (Timsit and Negishi, 2007). Activation can also be induced indirectly where the ligand (such as PB) does not bind to CAR but rather promotes the interaction of CAR with the factors required for its dephosphorylation. After dephosphorylation this mechanism acts much like the direct mechanism (Mutoh *et al.*, 2013).

PXR ligands include rifampicin and hyperforin and their regulation of CYP450 is similar to the CAR. However, in absence of ligand binding, the PXR is believed to act as a gene silencer with active co-repressors (Wang *et al.*, 2012). When activated through ligand binding, the co-repressors dissociate allowing the binding of co-activators. This induces the binding to XREM and PBREM in the same way as CAR (i.e. RXR) (di Masi *et al.*, 2009). Due to both the CAR and PXR binding XREM and PBREM there is overlap in their CYP450 induction, however they have different affinities for direct, indirect and everted repeats of the responsive elements. This results in CAR favouring CYP2B regulation whereas the PXR favours CYP3A regulation (Xie *et al.*, 2000; Wang *et al.*, 2012).

The final main regulatory receptor is the nuclear receptor, PPAR-α. PPAR-α promotes fatty acid oxidation, ketogenesis, lipid transport and gluconeogenesis in the liver (Chakravarthy *et al.*, 2009). The ligands for PPAR-α include endogenous fatty acids and metabolites from fatty acid anabolism and catabolism. They are also activated by fibrate drugs such as clofibrate and bezafibrate (Pyper *et al.*, 2010). The PPAR-α forms heterodimers with the RXR in the absence of ligand binding. This leads to the inhibition of the transcription by binding and recruiting of co-repressors to the peroxisome proliferator response element (PPRE). When ligands bind, the co-repressor complex is released and co-activator complex proteins are recruited, initiating transcription (Pyper *et al.*, 2010). Activation of PPAR-α induces CYP4A genes (Johnson *et al.*, 2002) and in the human liver the major CYP4A is CYP4A11 which has been shown to be upregulated in hepatocytes in response to PPAR-α ligands (Raucy *et al.*, 2004; Savas *et al.*, 2009).

1.2.5 Xenobiotic hepatic bioactivation & toxicity

The aim of xenobiotic metabolism is the detoxification and clearance of xenobiotics. However, in some cases the opposite can occur where the metabolite is more toxic than the parent compound. This is termed bioactivation. Bioactivation can induce cell damage by generating reactive metabolites that can generate

electrophiles and free radicals that covalently bind to macromolecules (Amacher, 2012; Gomez-Lechon *et al.*, 2016) or generate ROS, inducing oxidative stress.

Idiosyncratic drug induced liver injury (IDILI) is a rare disease that occurs due to the administration of drugs. The pathogenesis of IDILI is poorly understood due to lack of reliable models to test IDILI as well as difficultly in the diagnosis of patients (Fontana, 2014). IDILI is usually unexpected with very few drugs having a predictable toxic mechanism, such as paracetamol (Bjornsson, 2015) which induces its toxicity via an increase in the production of the reactive metabolite N-acetyl-p-benzoquinoneimine (NAPQI) by CYP2E1 (James *et al.*, 2003).

The liver has developed several detoxification mechanisms to defend itself from potentially toxic metabolites. Including the conjugation of reduced glutathione by glutathione S-transferases (GSH) and ROS scavenging enzymes (James *et al.*, 2003). However, if these defence mechanisms become saturated (e.g. glutathione conjugation in paracetamol overdose) then hepatotoxicity will occur.

1.3 *In vitro* models of hepatotoxicity

Adverse drug reactions (ADRs) are a problem in drug development, with drug toxicity accounting for ~21% of pharmaceutical failures during development and safety testing (Williams *et al.*, 2013). This has financial consequences for pharmaceutical companies, with the further a drug gets in development, the greater the financial loss if the drug fails. For this reason, these drug companies aim to identify potentially toxic drugs as early as possible to minimise loss (Bass *et al.*, 2009).

Hepatocytes are responsible for the metabolism of clinical drugs and are therefore the target of the majority of potential drug toxicity. *In vitro* approaches in drug development are important in the identification of a drugs properties and potential toxicity and are generally cheaper and have a higher throughput than *in vivo* models (Bass *et al.*, 2009). These include the use of primary human hepatocytes (PHHs), pluripotent stem cell-derived hepatocyte-like cells and hepatocyte derived cell lines (e.g. HepG2 cells).

While *in vitro* models have their advantages of cost and throughput, they also have their limitations. These limitations include the lack of ability to replicate the complexity of the interacting cell types within the liver, inability to perform longer term studies, limited availability of some models such as PHHs, and reduced metabolic ability (Kyffin *et al.*, 2018).

1.3.1 Species differences in hepatic models

Major challenges in toxicology are understanding the differences between species and translating from *in intro* to *in vivo* models. Some structures and processes are highly conserved between species such as the transcription and translation of DNA and oxidative phosphorylation via the electron transport chain. One significant difference between species is the variation of expression, substrate specificity and catalytic efficiency for drug metabolising enzymes such as CYP450s (Bogaards *et al.*, 2000). As a result, there are differences between species in their drug metabolising capabilities and differing toxicities. One example of this 5-n-Butyl-7-(3,4,5-trimethoxybenzoylamino)-pyrazolo[1,5-a]pyrimidine that is metabolised by CYP1A2 in humans to a hepatotoxin. In rat it is metabolised via a different route that does not generate the same metabolite (Kuribayashi *et al.*, 2009). The expression of PPARα is an example of species difference as expression is greater in rodents than humans and activation of the receptor in rodents leads to an increase in hepatocyte proliferation, inhibition of apoptosis and hepatocarcinogenesis (Oliver and Roberts, 2002). This effect is not observed in humans.

1.3.2 Primary hepatocytes

Primary human hepatocytes are the gold standard for toxicity screening and are considered the closest model to hepatocytes found *in vivo*. PHHs express functional drug metabolising enzymes that are important for investigating the hepatic uptake, kinetics, clearance and interactions of drugs and chemicals. However, there are several limitations with using PHHs. Their availability is a major issue as they are primarily sourced from livers that are not suitable for transplantation or from sections of liver resected during surgery (Guguen-Guillouzo and Guillouzo, 2010). To try and increase the supply of PHHs, cryopreservation of hepatocytes (Hengstler *et al.*, 2000) and sourcing of hepatocytes from explanted diseased livers (Kleine *et al.*, 2014) has been suggested. Rat and mouse hepatocytes also provide another more readily available source of primary hepatocytes. However, the relevance of these for human drug interactions could be questioned due to species differences.

Human liver sources also raise the issue of variability as these donor livers could be considered diseased and not representative of a healthy liver. These donors could also be on a range of drugs that could affect the expression of metabolising enzymes. This along with interindividual variability within the population means that reproducibility of results can be difficult (Zeilinger *et al.*, 2016).

Finally, the isolation protocol of PHHs induces ischemic injury and the loss of ECM that results in cultured cells to rapidly dedifferentiate. This is caused by the induction of inflammatory (via nuclear factor κB, NF-κB) and proliferative (via mitogen-activated protein kinase, MAPK) responses. Induction of this signalling represses transcription factors, such as hepatocyte nuclear factor 1α (HNFα), that is thought to lead to the dedifferentiation of hepatocytes and therefore the loss of expression of drug metabolising enzymes (DMEs) (Fraczek *et al.*, 2013). This means that all experiments on PHHs must be carried out as soon after isolation as possible to observe optimal expression of DMEs. Various culture models have been developed to try and increase the longevity of functionally metabolising hepatocytes in culture including sandwich culture (Liu *et al.*, 1999), spheroid culture (Bell *et al.*, 2016), and 3D-bioprinted human liver tissue (Nguyen *et al.*, 2016; Tetsuka *et al.*, 2017).

1.3.3 Stem cell derived hepatocyte-like cells

Stem cell derived hepatocytes are a potential solution to the lack of availability of PHHs. Stem cells are proliferative and pluripotent, meaning theoretically there is an infinite supply and they can be used to generate multiple cell types, including hepatocytes. Two sources of stem cells have been used in the generation of hepatocytes, human embryonic stem cells (hESCs) and pluripotent stem cells (hPSCs). Stem cell differentiation to hepatocytes involves the mimicking of liver embryogenesis towards hepatocyte maturation using combinations of growth factors, cytokines and small molecules (Kia *et al.*, 2013; Asumda *et al.*, 2018). Ethically, hPSCs are superior to the hESCs due to them being produced by reprogrammed somatic cells and therefore avoiding the use of embryonic tissue (Kia *et al.*, 2013).

Development of stem cell derived human hepatocytes is therefore of interest to pharmaceutical companies for use in toxicity screening as an alternative to PHHs. However, there are some limitations with the use of stem cell derived hepatocytes. Like PHHs, stem cell derived hepatocyte phenotype is not stable when cultured (Goldring *et al.*, 2017). No standard protocol has been established and current methods are not perfect, resulting in cell populations of mixed phenotype (Gomez-Lechon and Tolosa, 2016). Additionally, hepatocytes derived from stem cells have limited functionality and are not functionally similar to adult human hepatocytes (Takayama *et al.*, 2012). Currently used methods for generation of stem cell derived hepatocytes are also expensive with many growth factors being required.

1.3.4 Liver Cell Lines

Immortalised cell lines are widely used *in vitro* models in toxicology studies as an alternative to PHHs. They have several advantages over PHHs and iPSCs in that they are proliferating, easier and cheaper to culture, with stable gene expression profiles providing higher reproducibility with experiments. The HepG2 cell line was derived in the 1970s from a male human hepatoblastoma and have since been used in early phase toxicological assessments. HepG2 cells have been shown to express similar levels of phase II enzymes such as glutathione S-transferases (GSTs) and N-acetyl-transferase-1 (NAT1) compared to PHHs (Westerink and Schoonen, 2007b). However, their expression of phase I CYP450 enzymes are in general, relatively low. CYP1A1, 1A2, 2A6, 2B6, 2C8, 2C9, 2C19, 2D6, 2E1, and 3A4 are all present but at low levels compared to PHHs (Westerink and Schoonen, 2007a), resulting in low activity of these enzymes. It has been suggested that HepG2 cells resemble more of a fetal state of liver as they express detectable levels of CYP3A7 and express higher levels of 1A1 compared to 1A2 (Wilkening *et al.*, 2003). Additionally, the AhR, CAR and PXR are all expressed in HepG2 cells, although levels of CAR and PXR are low. Yet the inducibility of DMEs though these receptors are relatively poor, with the exception of CYP1A1 (regulated though the AhR) (Gerets *et al.*, 2012).

Due to the low activity of phase I metabolism the use of HepG2 cells in the toxicological assessment is considered to be limited as there is no bioactivation of drugs tested. Attempts have been made to modify and increase the activity of metabolising enzymes in HepG2 cells. Culturing HepG2 cells in a 3D model in spheroids showed an upregulation of genes involved in xenobiotic and lipid metabolism (Chang and Hughes-Fulford, 2009; Kyffin *et al.*, 2018). HepG2 cells can use adenoviral or lentiviral transfection to express DMEs. This has been done by simultaneously expressing multiple enzymes (Tolosa *et al.*, 2013) or by developing multiple cell lines each expressing a different enzyme (Xuan *et al.*, 2016). Transfected HepG2 models are limited as enzyme induction is lost as well as potential drug interactions. Multiple cell lines expressing different enzymes would also mean the testing of the same compound in each model instead of in one 'complete' model.

HepaRG cells are a more recent model used for drug metabolism and toxicity studies. These cells were derived from a female human hepatocellular carcinoma and are proliferative in their non-differentiated state. When the cells are confluent they are treated with 2% dimethyl sulfoxide (DMSO) for approximately 2 weeks to differentiate them into both biliary and hepatocyte like cells (Gripon *et al.*, 2002). Unlike the HepG2 cells, the differentiated HepaRG cells express phase I CYPs at levels similar to those observed in PHHs. These include CYP2C9, 3A4 and 2D6 that account for the metabolism of approximately 90% of

currently used drugs (Aninat *et al.*, 2006; Antherieu *et al.*, 2012) with CYP3A4 appearing to be expressed at levels greater than PHHs. Phase II enzymes and nuclear receptors are also expressed in differentiated HepaRG cells. CYP enzymes have also been shown to be inducible by nuclear receptor agonists β-NF, phenobarbital, and rifampicin (agonists of AhR, CAR and PXR respectively), suggesting that the nuclear receptors are functional (Gerets *et al.*, 2012). Further developments of the HepaRG model aim to more closely resemble *in vivo* drug bioactivation. These include the use of 3D culture (Leite *et al.*, 2012) and using glutathione-depleted cells (Xu *et al.*, 2018). The time it takes for differentiation is a major limitation of the HepaRG cells, requiring 1-2 weeks to become confluent, and a further 2 weeks of 2% DMSO treatment to culture fully differentiated cells. The use of 2% DMSO has also been suggested to potentially protective against apoptosis, an undesirable response when trying to investigate the toxicity of drugs and chemicals (Gerets *et al.*, 2012).

Much research has gone into the comparison of PHHs, HepG2 and HepaRG cells in terms of expression, DME activity and the prediction of drug hepatotoxicity (Guo *et al.*, 2011; Gerets *et al.*, 2012; Saito *et al.*, 2016; Yokoyama *et al.*, 2018). With the limited availability of PHHs, it has been suggested that the use of both HepG2 and HepaRG cells are required for toxicity screening as HepaRGs are more predictive for metabolism and toxicity whereas HepG2 cells appear to be more predictive for toxicogenomic studies (Jennen *et al.*, 2010; Guo *et al.*, 2011).

1.3.5 AR42J-B-13 cells

The AR42J cell line is a pancreatic acinar cell line that was derived from a pancreatic adenocarcinoma from studies where Wistar/Lewis rats were treated with azaserine (Longnecker *et al.*, 1979; Christophe, 1994). The Kojima lab sub-cloned the AR42J-B13 (B-13) cell line from the AR42J cell line in 1996 and showed that treating the AR42J cells with hepatocyte growth factor (HGF) and activin A resulted in some cells producing insulin. These cells were then isolated to produce the B-13 cell line (Mashima *et al.*, 1996a; Mashima *et al.*, 1996b). It was then discovered that treatment of the B-13 cell line with the synthetic glucocorticoid, dexamethasone (DEX), caused a phenotypic change and blocked proliferation (Shen *et al.*, 2000). It was shown that 14 days of DEX treatment resulted in an upregulation of liver specific markers such as albumin and glucose-6-phosphatase, resulting in a more hepatocyte-like cells that are known as B-13/H cells (Shen *et al.*, 2000).

The effects of glucocorticoid induced exocrine pancreatic differentiation have also been investigated *in vivo*. Rats treated for 25 days with DEX showed an increase in glutamine synthase, carbamoyl phosphate

synthase and CYP2E1 expression within the pancreas compared to control rats (Wallace *et al.*, 2009). An increase in hepatic expression was also observed in pancreata of mice that were genetically modified to secrete elevated levels of endogenous glucocorticoids (Wallace *et al.*, 2010b). This response has also been demonstrated in humans. Immortalized adult human acinar cells express hepatic markers when exposed to DEX (though at higher concentrations than B-13 cells) (Fairhall *et al.*, 2013a). Finally, hepatic markers in the pancreas were observed in a patient who had been treated with glucocorticoids for over 20 years (Fairhall *et al.*, 2013b). This evidence suggests that this response is conserved between species and is not unique to the B-13 cell line.

The exact mechanism responsible for the transdifferentiation of B-13 to B-13/H cells is not fully understood. Current understanding of the mechanism is summarised in Figure 1.5 and suggests the involvement of the glucocorticoid receptor (GR) and the induction of the transcription factor CCAAT/enhancer-binding protein-β (CEBP-β) (Shen *et al.*, 2000; Tosh *et al.*, 2002). The GR becomes activated in response to DEX treatment. This induces the serine/threonine kinase SGK1 (serum- and glucocorticoid-regulated kinase 1) which in turn phosphorylates β-catenin (Wallace *et al.*, 2011; Probert *et al.*, 2015). Phosphorylation of β-catenin results in a loss of β-catenin nuclear localisation and a reduction in T-cell factor/lymphoid enhancer factor (Tcf/Lef) transcriptional activity. Downregulation of Tcf/Lef increases CEBP-β expression and therefore the induction of transdifferentiation. A reduction in Tcf/Lef also leads to a down regulation of Wnt signalling. The reduction in Wnt proteins reduces their interaction with the frizzled receptor that phosphorylate glycogen synthase kinase 3 (GSK3) when active (Wallace *et al.*, 2009). The reduction of GSK3 phosphorylation leads to an increase in β-catenin phosphorylation and ultimately the upregulation of CEBP-β and transdifferentiation (Wallace *et al.*, 2011; Probert *et al.*, 2015). Phosphatidylinositol-4,5-bisphosphate 3-kinase (PI3K) signalling also plays a role in the transdifferentiation of B-13 cells. The glucocorticoid receptor activates PI3K which in turn activates 3-phosphoinositide dependent protein kinase 1 (PDK1). PDK1 then activates SGK1, increasing the phosphorylation of β-catenin and up regulation of C/ERPβ (Wallace *et al.*, 2011).

A short pulse exposure of DEX of 6 hours has been shown to be sufficient to activate the GR and irreversibly initiate the transdifferentiation of B-13 to B-13/H cells. Evidence suggests that this caused by epigenetic changes, with B-13 cell DNA becoming rapidly methylated and de-methylated (and possible other epigenetic changes) in response to continuous and pulse DEX exposure (Fairhall *et al.*, 2016). The transdifferentiation of B-13 to B-13/H cells has been shown to be inhibited with the treatment of the

methylation inhibitor 5-azacytidine, supporting the involvement of epigenetic changes (Fairhall *et al.*, 2016).

Hepatic DME and transporter expression, as well as the possible use of B-13/H cells for toxicity studies has been investigated. It has been shown that the B-13/H cells express hepatic genes, including phase I and phase II metabolising enzymes and transporter proteins (Shen *et al.*, 2000; Marek *et al.*, 2003; Kurash *et al.*, 2004; Burke *et al.*, 2006; Wallace *et al.*, 2009; Probert *et al.*, 2014; Probert *et al.*, 2015; Probert *et al.*, 2016). B-13 cells did not show detectable levels of CYP2C11, CYP2A, CYP2E and CYP3A1 whereas after differentiation to B-13/H cells, there was significant expression of these enzymes (Marek *et al.*, 2003). Functional CYP activity was also confirmed in this study by the hydroxylation of testosterone (Marek *et al.*, 2003). Further studies found that B-13/H cells did not express functional CYP1A2, however the human CYP1A2 could be stably transfected into B-13 cells to express metabolically functioning CYP1A2 when differentiated into B-13/H cells (Probert *et al.*, 2014). Functional AhR, CAR and PXR were also shown to be capable of inducing DMEs in response to agonists (Probert *et al.*, 2014). Phase II genes were shown to be expressed in B-13 cells and become upregulated following transdifferentiation. Finally, the transporter proteins, bile salt exporter pump (BSEP), p-glycoprotein, breast cancer resistance protein (BCRP) and multidrug resistance-associated protein (MRP) were shown to be expressed and functional in B-13/H cells (Probert *et al.*, 2014).

Utility of B-13/H cells in toxicological studies have also been shown. Paracetamol was toxic to B-13/H cells but not B-13 cells, suggesting the bioactivation of paracetamol to its reactive, toxic metabolite (Marek *et al.*, 2003). A similar response was observed with the bioactivation of methapyrilene to a toxic metabolite by B-13/H cells (Probert *et al.*, 2014). The genotoxicity of a metabolic product of progenotoxin 2-amino-1-methyl-6-phenylimidazo(4,5-b)pyridine (PhIP) has been shown in CYP1A2 stable transfection B-13/H cells, as has the bioactivation of 1'-hydroxyestragole to 1'-sulphoxyestragole by SULT2B1 (Probert *et al.*, 2016). Both show the requirement of functional DMEs for the bioactivation of drugs (phase I for PhIP and phase II for 1'-hydroxyestragole), and therefore the B-13/H cells could serve as a potential model for toxicity studies.

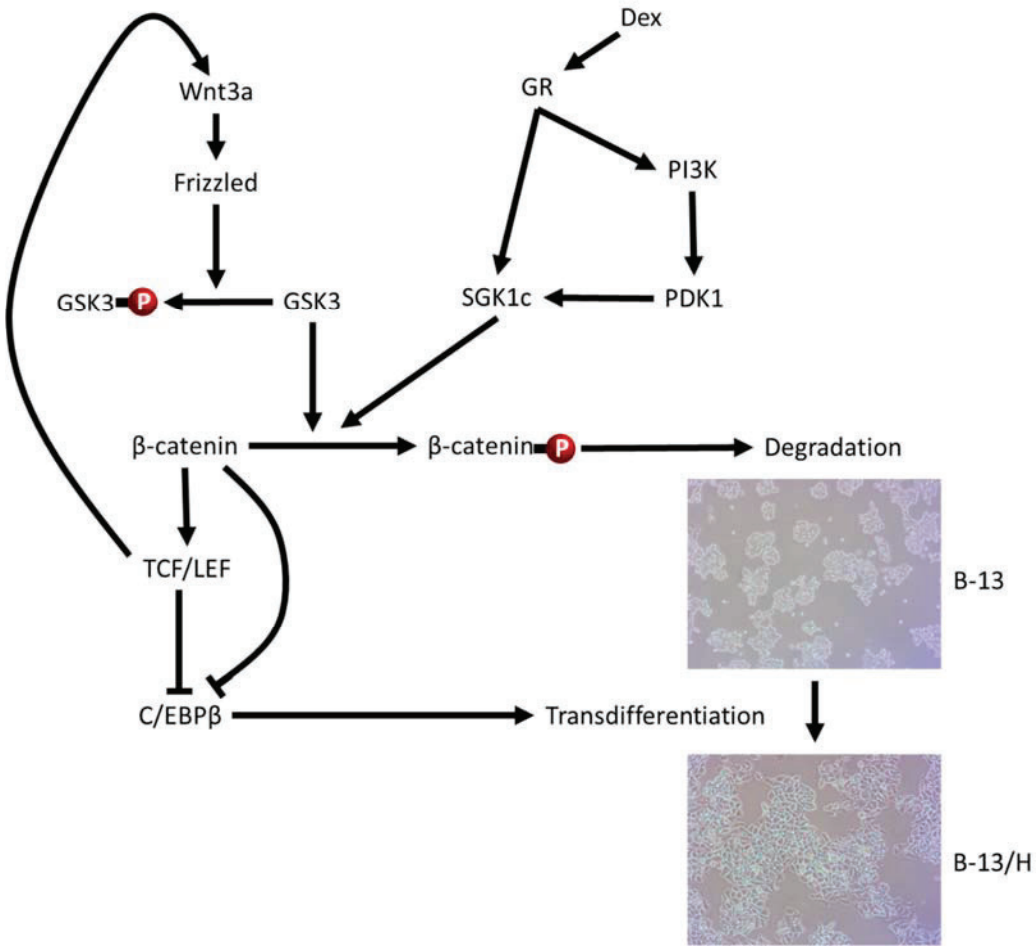

Figure 1.5: B-13 to B-13/H transdifferentiation pathway. See text for details. Abbreviations: Dex, dexamethasone; GR, glucocorticoid receptor; P, phosphorylated.

1.4 Liver disease and fibrosis

Liver disease is a growing health problem in the UK with the number of people at risk of liver disease and mortality caused by liver disease increasing whereas mortality from other diseases is falling (Figure 1.6) (Williams *et al.*, 2014). According to a report published by Public Health England (PHE), liver disease is the third commonest cause of premature death in the UK, with 600,000 people in England and Wales having some form of liver disease, and 60,000 of these having liver cirrhosis (Public Health England, 2017). Table 1.2 breaks down the number of people at risk or affected by liver disease in the England and Wales. The number of people at risk of liver damage in England is believed to be 15,120,000, with 2,240,000 of these being at risk of alcohol related liver damage. This is due to life-style/diet, with approximately 27% of the population being obese and 4% being higher risk drinkers (Public Health England, 2017). The three main

causes of liver disease – alcohol related liver disease, fatty liver disease and viral hepatitis (B&C), accounting for approximately 90% of liver disease (Public Health England, 2017). Other less common causes include autoimmune hepatitis, primary biliary cholangitis (PBC), primary sclerosing cholangitis (PSC) and drug induced liver injury (DILI). The increase incidence of liver disease is therefore having a financial burden on health services such as the NHS in England, and with such a large percentage being due to life-style choices, this burden could be significantly reduced with an increase in more healthy life-style such choices as a balanced diet, exercise and a reduction in alcohol consumption.

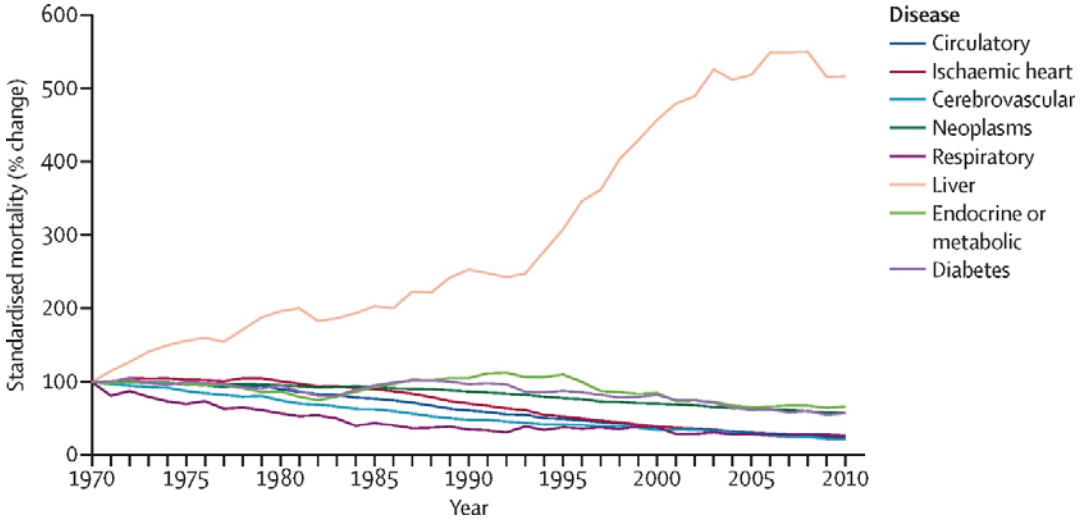

Figure 1.6: Standardised UK mortality rate. Taken from (Williams *et al.*, 2014)

Liver Disease / Risk	Number at risk/affected in the UK
At risk of liver disease	15,120,000
At risk of alcohol related liver damage	2,245,000
With (at least) significant liver disease	600,000
With (at least) chronic viral hepatitis B and C	400,000
With Cirrhosis	30,000-60,000
Underlying cause of death is liver disease	13,937 (2015)
Have primary liver cancer	4585 (new cases in 2014)
Liver organ transplants	925 (2015/16)

Table 1.2: Number of people in the UK at risk/affected by liver disease in the England and Wales. Adapted from (Public Health England, 2017)

1.4.1 Liver disease progression

Liver disease progression is triggered by epithelial stress that activates Kupffer and stellate cells which signal an inflammatory and wound healing response that in exposure to chronic injury leads to fibrogenesis, cirrhosis and cancer/terminal liver failure. The only treatment currently available for liver failure is a liver transplant, with 925 patients undergoing a liver transplant in England in 2015/16 (Public Health England, 2017). However, there are a limited number of donor livers for transplantation, which is becoming more problematic with the rising number of cases of liver disease.

Chronic liver disease begins with persistent epithelial cell stress and damage induced by xenobiotic toxicity or metabolic dysregulation. These cells undergo apoptosis or necrosis with the aim to remove the damaged cell and reduce potential further damage. The liver has a regenerative capacity, with rats and mice being able to restore full liver mass after 5-7 days post partial hepatectomy (Michalopoulos, 2010). Undamaged hepatocytes are capable of replicating, and hepatic progenitor cells can differentiate into hepatocytes (or cholangiocytes) to replace dead liver cells (Friedman, 2008). Persistent fibrotic injury restricts hepatocyte replication and results in the loss of hepatic function.

The epithelial cells that undergo cell death in response to injury release their cellular components, resulting in the activation of Kupffer cells and stellate cells, triggering the release of pro-inflammatory mediators such as cytokines, resulting in an inflammatory response. This inflammatory response promotes the recruitment of leukocytes as well as the activation of HSCs to myofibroblasts (Dooley and ten Dijke, 2012). These activated myofibroblasts secrete ECM in the space of Dissé and a change in hepatic ECM composition from a matrix composed mainly of collagens IV and VI to fibrillar collagens I and III and fibronectin, stimulating fibrogenesis (Hernandez-Gea and Friedman, 2011). The change in ECM results in the loss of fenestrations and hepatocyte microvilli, impairing the metabolic exchange between hepatocytes and the blood. These changes are summarised in Figure 1.7.

The pattern of fibrosis differs depending on the aetiology, for example viral hepatitis as well as PBC primarily affects periportal hepatocytes (periportal fibrosis) whereas alcoholic liver disease (ALD), non-alcoholic fatty liver disease (NAFLD) and DILI affect centrilobular regions (centrilobular fibrosis) (Hernandez-Gea and Friedman, 2011). Regardless of aetiology, continuous liver damage and fibrogenesis have the potential to lead to cirrhosis, an advanced and final stage of fibrosis. Cirrhosis is characterised by liver architecture disruption, nodule formation and portal hypertension due to an increase in hepatic

resistance to blood flow (Hernandez-Gea and Friedman, 2011). Ultimately this can lead to the progression of hepatocellular carcinoma and/or liver failure.

Studies suggest that the removal of the cause of liver damage results in the reversal of liver fibrosis in fibrosis models (such as carbon tetrachloride in rats) as well as in patients (Iredale *et al.*, 1998; Sun and Kisseleva, 2015). This reversal is induced by the degradation of fibrillar ECM (Ramachandran and Iredale, 2009) and the senescence (Krizhanovsky *et al.*, 2008) and apoptosis (Issa *et al.*, 2001) of activated stellate cells, as shown with gliotoxin (Wright *et al.*, 2001) and an antibody targeting myofibroblasts inducing apoptosis (Douglass *et al.*, 2008).

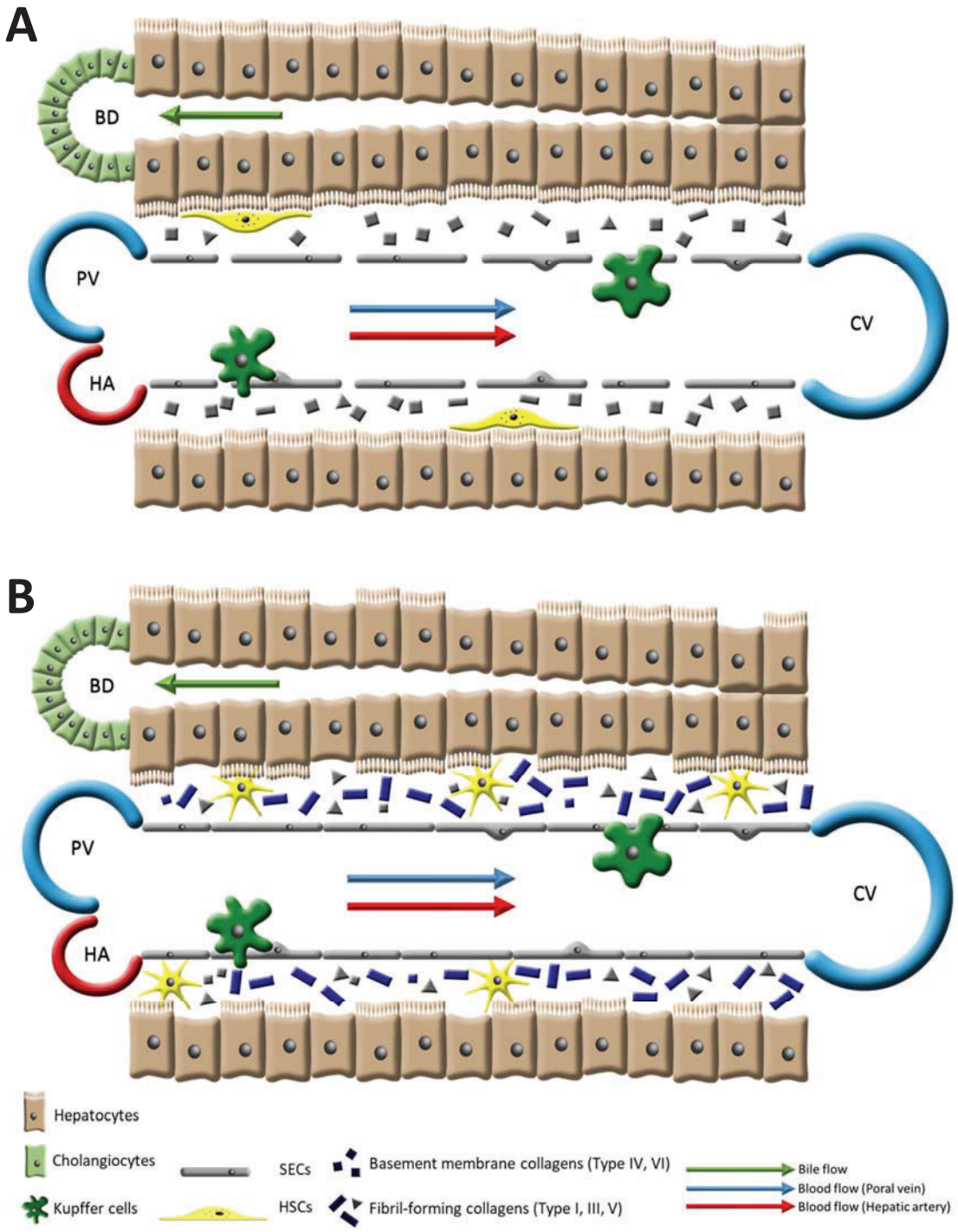

Figure 1.7: Alterations in hepatic fibrosis. A, normal liver parenchyma. Hepatocytes have microvilli and SECs have fenestrations. Space of Dissé contains low-density basement membrane-like matrix and quiescent, vitamin A containing HSCs. **B, Fibrotic liver.** HSCs become active, lose their vitamin A and secrete more fibril-forming collagens leading to hepatocytes loss of microvilli and SECs loss of fenestrations. Abbreviations: BD, bile duct; CV, central vein; HA, hepatic artery; HSCs, hepatic stellate cells; PV, portal vein; SECs, sinusoidal endothelial cells. Adapted from (Hernandez-Gea and Friedman, 2011)

1.4.2 Hepatitis C

The hepatitis C virus (HCV) is estimated to have currently infected 160,000 people in England (Williams *et al.*, 2014). In developed countries the primary route of transmission is though intravenous drug abuse. The viral RNA of HCV is contained in a lipoviral particle (a lipid membrane formed by low density lipoproteins, LDL, and very low-density lipoprotein, VLDL) (Morozov and Lagaye, 2018). The lipoprotein binds to receptors on the surface of hepatocytes where it is endocytosed into the cell. Here the viral RNA is released, translated and replicated. Newly synthesised viral RNA is then recruited into particles made of VLDLs and directed to the plasma membrane using the VLDL secretory pathway to be released from the cell (Morozov and Lagaye, 2018).

HCV causes damage to liver cells, however the exact mechanism is not known but damage is likely to be induced by the hosts immune system (Morozov and Lagaye, 2018). It is also possible that there are HCV induced cellular responses such as endoplasmic reticulum stress, autophagy and apoptosis that could induce cellular stress/damage (Ke and Chen, 2012). This damage could go on to release cytokines and chemokines, activating HSCs and induce fibrosis and, if left untreated, to cirrhosis and liver failure/hepatocellular carcinoma (HCC). Current recommended treatment for HCV is the administration of pegylated interferon (PEG-IFN) and ribavirin. More recently, direct acting antiviral drugs, such as telaprevir, sofosbuvir, daclatasvir and boceprevir have been used (Ghany *et al.*, 2009; Liang and Ghany, 2013). These drugs inhibit an HCV viral protein involved in the virus's replication, transcription and translation.

1.4.3 Alcoholic liver disease

In England, 2,240,000 people are believed to be at risk or already have alcohol related liver damage and it is believed that this number will continue to increase (Public Health England, 2017). Alcoholic liver disease is a spectrum of disorders, starting with the development of steatosis and steatohepatitis progressing to fibrosis and HCC. Only 30-35% of heavy drinkers develop advanced fibrosis and cirrhosis, suggesting factors such as sex, obesity and diet may be significantly influence progression (Gao and Bataller, 2011).

Development of steatosis is the earliest response of prolonged alcohol abuse and is believed to occur due to the inhibition of PPARα and upregulation of the transcription factor sterol regulatory element binding protein 1c (SREBP-1c) that promote fatty acid synthesis (Ceni *et al.*, 2014). Ethanol is metabolised to acetaldehyde by alcohol dehydrogenase (ALD) which is then further metabolised to acetate by aldehyde

dehydrogenases (ALDH). Both of these steps increase the production of NADH (Figure 1.8), creating a shift in the NADH/NAD^+ ratio towards NADH. NADH inhibits the activity of many enzymes of fatty acid oxidation (Ceni *et al.*, 2014). Additionally, the final product of ethanol metabolism, acetate, is used in the TCA cycle. The citrate made via the citric acid cycle (tricarboxylic acid, TCA) is then converted into acetyl-CoA that is then made into lipids via *de novo* lipogenesis. Many factors contribute to the development of fibrosis following alcohol abuse. The NADH generated from ethanol metabolism is converted back to NAD^+ by the mitochondrial electron transport chain during which ROS is generated. ROS can then go onto induce lipid peroxidation, DNA mutations and the destruction of cell membranes (Gao and Bataller, 2011; Ceni *et al.*, 2014). Acetaldehyde is the metabolite produced by ethanol metabolism, and while is rapidly metabolised further to acetate, it is highly reactive and therefore potentially toxic to hepatocytes (Farfan Labonne *et al.*, 2009).

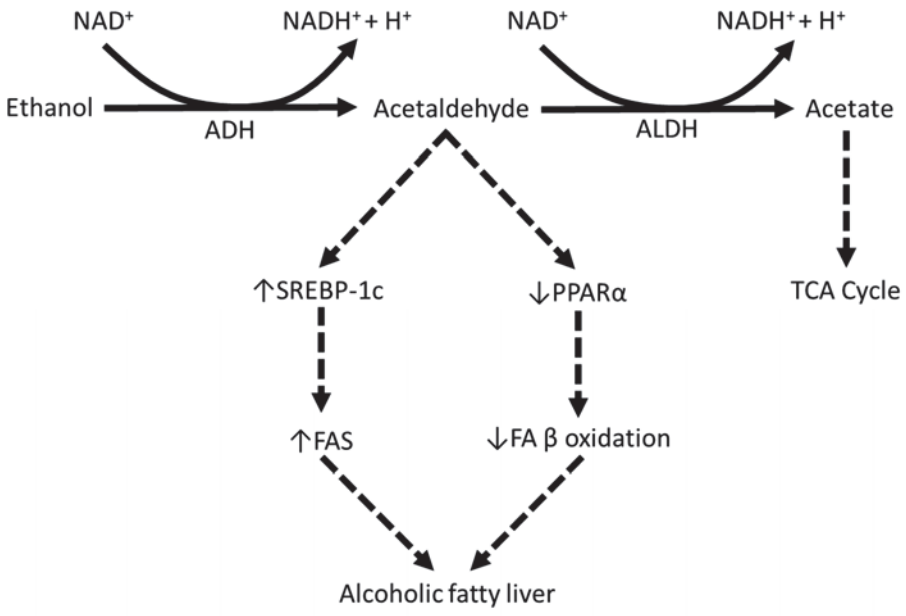

Figure 1.8: Mechanisms of alcoholic fatty liver. Abbreviations: ADH, alcohol dehydrogenase; ALDH, aldehyde dehydrogenase; FA, fatty acid; FAS, fatty acid synthesis; PPARα, peroxisome proliferator-activated receptor alpha; SREBP-1c, sterol regulatory element binding protein 1c; TCA, citric acid cycle. Adapted from (Gao and Bataller, 2011).

Alcohol consumption has also been shown to increase gut permeability (Enomoto *et al.*, 2001; Szabo, 2015). The increase in gut permeability allows the translocation of bacteria derived lipopolysaccharide (LPS) from the gut to reach the liver. Once in the liver, LPS binds to the toll-like receptor 4 (TLR4) receptors of Kupffer cells, inducing the release of ROS and proinflammatory cytokines such as TNFα that go onto activate HSCs (Gao and Bataller, 2011). Additionally, LPS itself can activate HSCs directly via TLR4 (Seki *et*

al., 2007). Acetaldehyde can also act on HSCs by directly increasing the expression of collagen I (Mello *et al.*, 2008). ALD has several unique factors towards the development of HCC that other liver disease aetiologies do not. Such as the production of acetaldehyde that is a carcinogen and ethanol mediated induction of CYP2E1, which metabolises the procarcinogenic compounds in some alcoholic drinks (Gao and Bataller, 2011).

Treatment of ALD primarily involves the reduction and elimination of alcohol consumption. One therapeutic treatment is the use of disulfiram, an inhibitor of acetaldehyde dehydrogenase. However, this cannot be given to patients with more advanced forms of ALD due to potential hepatoxicity (Gao and Bataller, 2011). New targets for the treatment of ALD are emerging including the use of anti-TNFα agents and targeting the gut microbiota and LPS pathway (Gao and Bataller, 2011).

1.4.4 Non-alcoholic fatty liver disease and non-alcoholic steatohepatitis

The prevalence of obesity is increasing in western counties due to changes in diet and a more sedentary lifestyle (Hardy *et al.*, 2016). Multiple health risks are associated with obesity, including type 2 diabetes, cardiovascular disease, cancer and non-alcoholic fatty liver disease (NAFLD) (Williams *et al.*, 2014). It has been estimated that 20-30% of the general population in the UK have NAFLD (Public Health England, 2017), and this number is likely to increase as the prevalence of obesity increases as studies have shown NAFLD in 80-90% of obese patients (Bellentani *et al.*, 2010). Like ALD, NAFLD is considered to be a spectrum of liver disease that begins with steatosis and progresses to non-alcoholic steatohepatitis (NASH) and to fibrosis, cirrhosis and HCC.

There is a heritable susceptibility to the development of NAFLD, and a major susceptibility has been associated with a polymorphism in patatin-like phospholipase domain-containing protein 3 (PNPLA3). In addition, associations have been made to polymorphisms in a protein that is related to adipose triglyceride lipase, glucokinase regulator (GCKR) which regulates glucokinase activity and glucose metabolism, and transmembrane 6 superfamily 2 (TM6SF2), the function of which is currently unknown (Hardy *et al.*, 2016). Diet can also increase susceptibility to NAFLD. Increased consumption of fructose has been shown to be a predictor of fatty liver in humans (Abid *et al.*, 2009) and has been shown to increase lipid accumulation in mice (Bergheim *et al.*, 2008), more so than any other sugar.

It is generally considered that under normal conditions the liver maintains lipid homeostasis, balancing the uptake and turnover of free fatty acids (FFAs). FFAs in the liver are sourced primarily from fats stored in

adipose tissue and transported via the plasma nonesterified fatty acid pool (NEFA) bound to albumin, as well as *de novo* lipogenesis (DNL), and diet (Donnelly *et al.*, 2005) (summarised in Figure 1.9). Hepatocytes then process these fatty acids by converting them either into triacylglycerol (TAG) for storage as lipid droplets, oxidised by the mitochondria, secreted in VLDL or synthesised into phospholipids (Hardy *et al.*, 2016). The NEFA pool is regulated by lipolysis in the adipose tissue. An increase in lipolysis increases FFAs levels which are then transported to the liver. Hormone sensitive lipases control lipolysis in adipocytes, with insulin being one hormone that acts to inhibit lipolysis (Browning and Horton, 2004). DNL is the process of synthesising fatty acids from carbohydrates in a state of energy excess. DNL and the lipogenic enzymes involved are transcriptionally regulated by insulin and glucose via SREBP-1c and carbohydrate-responsive element-binding protein (ChREBP) respectively. These two proteins are also regulated by the liver X receptor (LXR) (Cha and Repa, 2007). The LXR also induces the fatty acid synthesis enzymes acetyl-CoA carboxylase (ACC) and fatty acid synthase (FAS) (Hardy *et al.*, 2016).

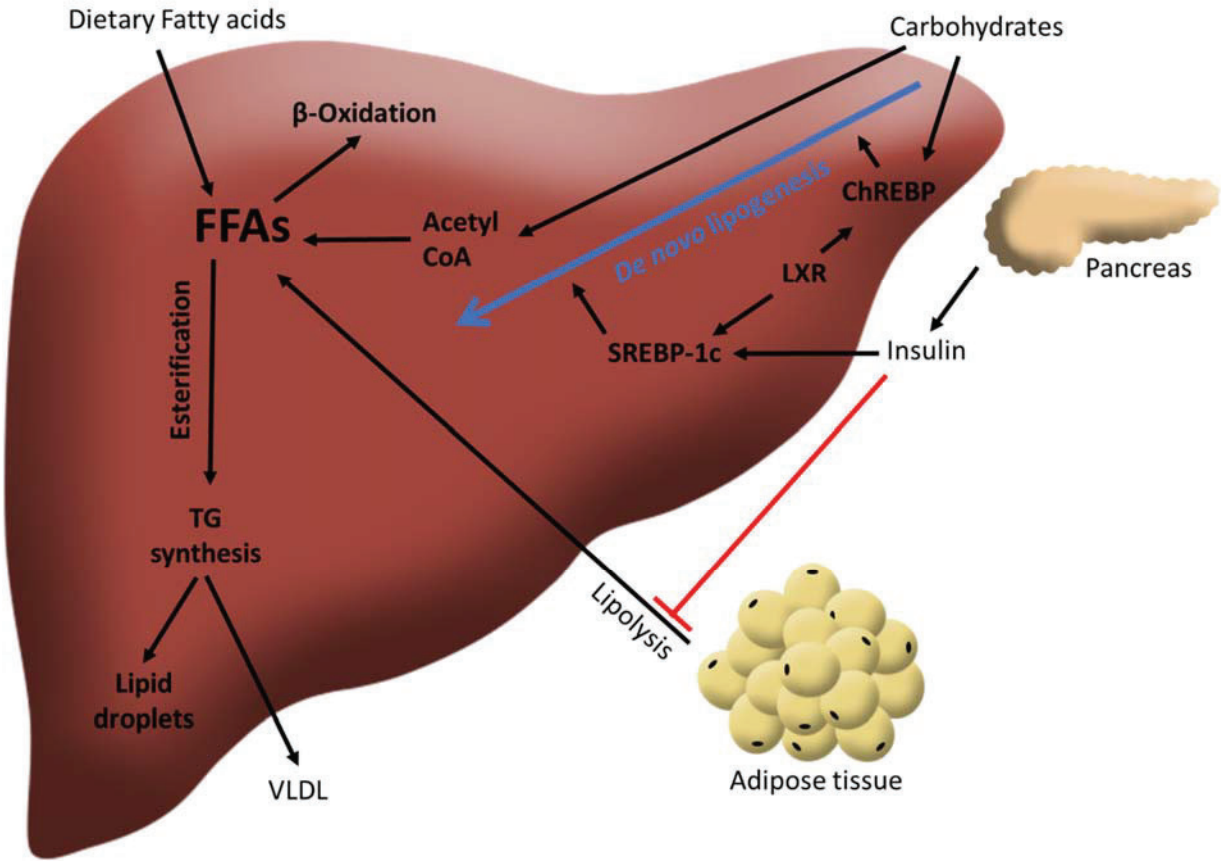

Figure 1.9: Sources of free fatty acids and lipid handling by the liver. The free fatty acid pool is made up of fatty acids from the lipolysis of adipose tissue, *de novo* lipogenesis and from dietary fatty acids. *De novo* lipogenesis converts carbohydrates into acetyl CoA by β-oxidation. This is transcriptionally regulated by ChREBP and SREBP-1c which are activated by glucose and insulin respectively. Additionally, they are both regulated by the LXR. Lipogenesis from the adipose tissue is regulated by insulin. Fatty acids are either oxidised to generate energy or synthesised into triglycerides where they are either stored as lipid droplets or secreted as VLDL. Abbreviations: Acetyl CoA, acetyl coenzyme A; ChREBP, carbohydrate-responsive element-binding protein; FFA, free fatty acids; LXR, liver X receptor; SREBP-1c, sterol regulatory element-binding protein 1c; TG, triglyceride; VLDL, very low-density lipoprotein. Adapted from (Hardy *et al.*, 2016)

Steatosis occurs when there is dysfunction in the regulation of lipid metabolism and storage, characterised by the formation of lipid droplets within the cell and can be further classified based on the size of the lipid droplets being formed, with macrovesicular steatosis being lipid droplets large enough to displace the nucleus to the periphery of the cells and microvesicular steatosis being smaller lipid droplets (Fishbein *et al.*, 1997). The primary cause of steatosis is insulin resistance. The adipose tissue plays a crucial role in insulin resistance as it is more likely to undergo inflammation and secrete cytokines such as tumour necrosis factor α (TNFα) and Il-6 that go on to inhibit insulin sensitivity and activate pro-inflammatory pathways (Hardy *et al.*, 2016). In patients with insulin resistance, the levels of insulin and glucose increase,

leading to the overstimulation of SREBP-1c and ChREBP respectively and thus an increase in DNL (Browning and Horton, 2004). Additionally, insulin resistance results in increased hormone sensitive lipase activity and an increase lipolysis therefore a greater FFA flux to the liver and a larger NEFA pool. Steatosis can also be induced through exposure to xenobiotics (Amacher, 2011), such as tamoxifen (Larosche *et al.*, 2007). The mechanism of drug induced steatosis has been linked to a decrease in β-oxidation and decrease lipoprotein secretion (Amacher, 2011).

Steatosis could be considered to be an adaptive response to an increase in lipotoxic FFAs in order to store them as less toxic TAGs in the form of lipid droplets (Hardy *et al.*, 2016). In persistent exposure to FAs, the liver will eventually not be able to sufficiently store FFAs, leading to lipotoxicity, cell damage, apoptosis and/or necrosis. It is this injury and not steatosis that could be seen as the initiating events of NASH. Lipotoxic effects include an increase in oxidative stress that leads to DNA damage, phospholipid membrane disruption and release of cytokines (Sanyal *et al.*, 2001). ER stress has also been shown to develop in excess FFAs, leading to the misfolding or unfolding of proteins, which could lead to autophagy (Hardy *et al.*, 2016). Finally, it has been shown that that mice on high fat diets have an altered microbiota leading to an increase in the levels of LPS (Cani *et al.*, 2009). Intestinal permeability is increased in patients with NAFLD and so there is an increase in the levels of LPS that are delivered to the liver, which then binds to TLR4 on Kupffer cells, inducing proinflammatory response, as in ALD. This response is summarised in Figure 1.10.

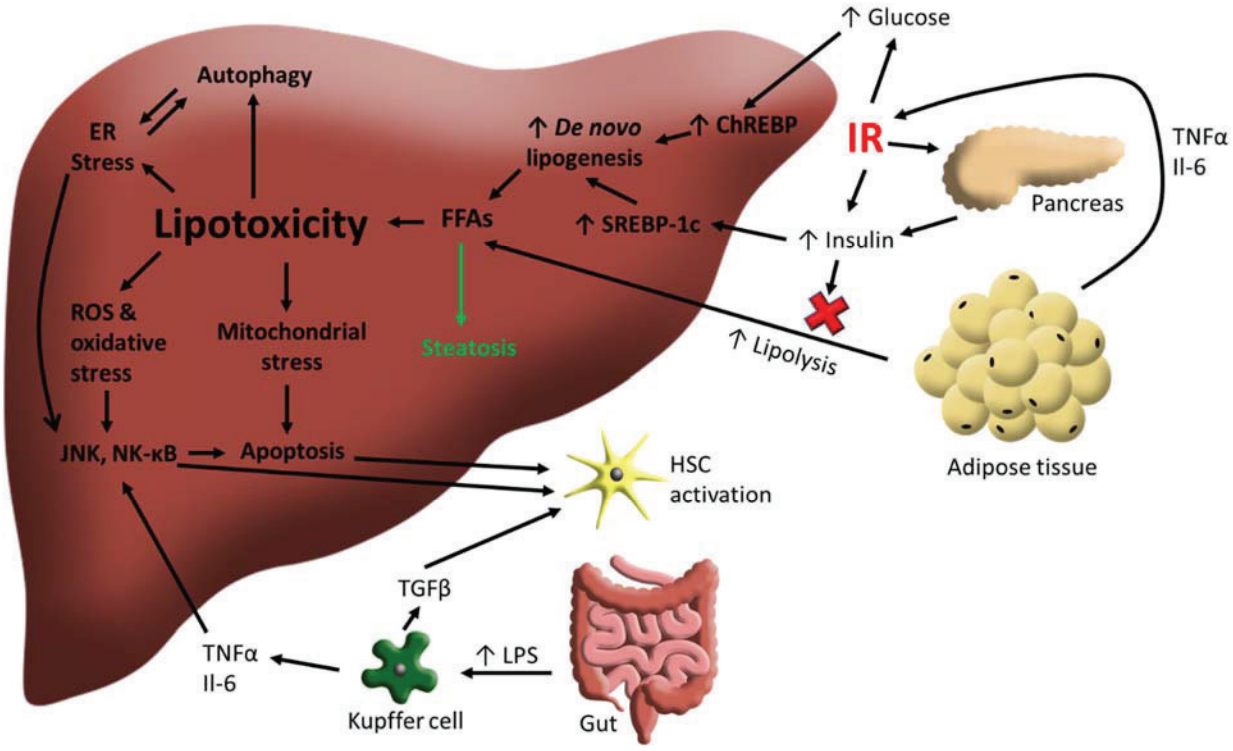

Figure 1.10: Insulin resistance, lipid dysregulation and liver injury. Insulin resistance increases insulin and glucose levels which increase SREBP-1c and ChREBP which in turn increase *de novo* lipogenesis and free fatty acid levels. Additionally, insulin receptors involved in the lipogenesis of adipose tissue become resistant and lipogenesis is increased. An increase in free fatty acids induce ER stress, autophagy, the production of ROS, oxidative stress and mitochondrial stress leading to the induction of apoptosis and the activation of HSCs. Obesity increases gut permeability and therefore and increase in LPS levels in the liver, activating Kupffer cells. Kupffer cells can induces HSC activation directly by TGFβ or via the NF-κB pathway by TGFα. Abbreviations: ChREBP, carbohydrate-responsive element-binding protein; ER, endoplasmic reticulum; FFA, free fatty acids; HSC, hepatic stellate cells; IR, insulin resistance; LPS, lipopolysaccharide; JNK, c-Jun N-terminal kinase; NK-κB, nuclear factor kappa-light-chain-enhancer of activated B cells; ROS, reactive oxygen species; SREBP-1c, sterol regulatory element-binding protein 1c; TGF, transforming growth factor. Adapted from (Hardy *et al.*, 2016)

The above stress and injury will ultimately lead to the activation of HSCs, NASH and hepatic fibrogenesis. NASH progression shares some profibrogenic mechanisms as other previously described liver diseases such as induction of CYP2E1, oxidative stress, apoptosis, and inflammation (Hardy *et al.*, 2016). There are some mechanisms that appear to be unique to NAFLD and NASH such as adipokines. Leptin is an adipokine that is secreted from the adipose tissue and is recognised by leptin receptors found on HSCs, leading to HSCs activation, however no evidence has been found for leptin and fibrosis progression in human studies (Ding *et al.*, 2005). Insulin resistance can affect HSCs as they express insulin receptors and altered glucose

metabolism upregulates TGFβ and connective tissue growth factor (Paradis *et al.*, 2001). Other mechanisms include the renin-angiotensin system, PPARγ and free cholesterol (Hardy *et al.*, 2016).

1.5 Primary Biliary Cholangitis

Primary biliary cholangitis (PBC), formally known as primary biliary cirrhosis (Beuers *et al.*, 2015), is an autoimmune liver disease that is characterised by the gradual destruction of the intrahepatic bile ducts, resulting in the impairment of the flow of bile from the liver to the duodenum (cholestasis). The progression of cholestasis leads to inflammation within the periportal region that develops to fibrosis and eventually to cirrhosis and liver failure. PBC is a much rarer liver disease than HCC, ALD and NASH, with data suggesting that the prevalence of the disease in the UK is 35/100,000 (Hirschfield *et al.*, 2018). This rate is similar to the rate in other northern European and North American countries. While it has been widely shown that the rate of PBC varies around the world, there is usually a significant female predominance with the female to male ratio being 10:1 (Lleo *et al.*, 2017). The disease is diagnosed primarily in the over 50s and is associated with other autoimmune diseases, smoking, urinary tract infections, pruritus during pregnancy, hormone replacement therapy and exposure to nail polish or hair dye (Hirschfield and Gershwin, 2013).

1.5.1 Symptoms and diagnosis

Around 20-60% of patients are diagnosed with PBC without any presentation of symptoms (Lleo *et al.*, 2017). Two of the most common symptoms of PBC are fatigue and pruritus. Fatigue is described as feeling of tiredness and weakness and is the most common symptom of PBC, occurring in 70% of patients (Lleo *et al.*, 2017). Pruritus (itch) affects majority of patients during the progression of the disease and occurs in other cholestatic diseases (Beuers *et al.*, 2014). Other symptoms include osteopenia (about 30% of patients), osteoporosis (10% of patients), hyperlipidemia and other autoimmune diseases (Lleo *et al.*, 2017). Lastly, as with other advance liver diseases, portal hypertension and jaundice may develop.

The diagnosis of PBC requires two out of three criteria to be present. These are an antimitochondrial antibody (AMA) serum titer higher than 1:40, unexplained alkaline phosphatase (ALP) levels over 1.5 times the upper limit of normal for more than 6 months, and liver histology (Bowlus and Gershwin, 2014). The AMAs in the serum are normally reactive to the lipoylated domains of 2-oxoacid dehydrogenase complexes (2-OADCs), including pyruvate dehydrogenase (PDC-E2), 2-oxo glutarate dehydrogenase (OADC-E2) and branched-chain 2-oxo acid dehydrogenase (BCOADC-E2) complexes (Bowlus and Gershwin, 2014). The

most prevalent of these autoantigens is PDC-E2 with 95% of patients displaying the AMAs against it (Jones, 2007). Antinuclear antigens (ANAs) are also detected in around 50% of PBC patients and is diagnostically significant in patients who are AMA negative (Hirschfield and Gershwin, 2013). These include ANAs against proteins in the nuclear pore complex, mainly glycoprotein 210 (gp210, a type I integral membrane protein) and nucleoporin 62 (Duarte-Rey *et al.*, 2012), as well as multiple nuclear dots nuclear body speckled 100kDa (sp100) (Hirschfield and Gershwin, 2013). ALPs are a group of enzymes that dephosphorylates compounds and are traditionally used as an indirect marker of cholestasis (Poupon, 2015). This is caused by an increase in hepatic synthesis and release of ALP in the sinusoidal blood flow (Poupon, 2015). Finally, liver histology identifies the stage of PBC, looking for portal inflammation, bile duct lesions, fibrosis and cirrhosis (Bowlus and Gershwin, 2014).

1.5.2 PBC treatment

The first-generation therapy for PBC was ursodeoxycholic acid (UDCA). UDCA is a hydrophilic bile acid that accounts for about 4% of bile acid composition in the human bile. It's proposed mechanism of action is that it modifies the bile acid pool and reduces proinflammatory cytokines and apoptosis, and stimulates the impaired secretion of hydrophobic bile acids, stabilising the HCO_3^- umbrella, maintaining bile pH and protecting the cholangiocytes from the toxic effects of bile acids (Beuers *et al.*, 2010; Khanna and Jones, 2017). However approximately 40% of patients show no or insufficient response to UDCA treatment (Lleo *et al.*, 2017), meaning new, novel therapies are required.

Obeticholic acid (OCA, INT-747) is a derivative of the human bile acid chenodeoxycholic acid and has recently been approved for use in the USA and Europe (Khanna and Jones, 2017; Hirschfield *et al.*, 2018). OCA is a FXR ligand, therefore inhibits bile acid synthesis from cholesterol in hepatocytes and increases the clearance of bile acids from hepatocytes, thus reducing the bile acid pool (Khanna and Jones, 2017). Activation of the FXR also has anti-fibrotic and anti-inflammatory mediated effects (Khanna and Jones, 2017). Several studies have found a reduction in ALP levels following OCA treatment, however, there was no improvement in the symptoms of PBC, with OCA treatment exacerbating pruritus in a dose-related manner (Hirschfield *et al.*, 2015).

Other therapeutics include the use of fibrates such as fenofibrate and benzafibrate that act as PPAR activators, upregulating multidrug resistance-associated protein 3 (MDR-3) and the FXR and therefore inhibiting bile salt synthesis (Mousa *et al.*, 2015). The targeting of the immune system has also been suggested (Mousa *et al.*, 2015). Towards the end stages of PBC the only available treatment is liver

transplant. Liver transplant outcome is good, with 1 and 5 year survival rates being 92-93% and 82-90% respectively, and recurrence of PBC post-transplant occurring in 25% of patients after 5 years (Lleo *et al.*, 2017).

1.5.3 PBC and autoimmunity

Under normal, healthy conditions, an organism's immune system develops tolerance against self-components to avoid their destruction. In autoimmune diseases there is a loss of tolerance against a particular component(s). In PBC there is primarily a loss of tolerance to, and production of AMAs against members of 2-OADC, targeting primarily cholangiocytes and bile duct destruction. 2-OADCs are found in the inner membrane of the mitochondria and are involved in the oxidative phosphorylation pathway. The main target of the AMA response is the pyruvate dehydrogenase complex (PDC), particularly to the dihydrolipoamide acetyltransferase (E2) subunit of this complex (Jones, 2007). The E2 subunit contains a lipoyl domain that covalently binds to the co-factor, lipoic acid, at the lysine residue at position 173 (Figure 1.11) (Hirschfield and Gershwin, 2013). This lysine binding domain is highly conserved between organisms. The binding of lipoic acid is also shared with other members of the 2-OADC that are targeted by AMAs. As well as AMAs, ANAs are also detected in 50% of PBC patients but the mechanisms involved are not understood (Duarte-Rey *et al.*, 2012). Common AMAs and ANAs are listed in Table 1.3.

Antigen group		Antigen	Patient frequency (%)
Mitochondrial (>95%)	E2 subunits of 2-OADC	PDC-E2	95*
		OGDC-E2	40-90
		BCOADC-E2	10
	PDC	PDC-E3BP	95*
		PDC-E1α	40-60
		PDC-E1β	10
Nuclear (~50%)	Nuclear pore complex	gp210	10-40
		Nucleoporin 62	20-30
	Multiple nuclear dots	sp100	10-30
	Centromeres	-	10

Table 1.3: Autoantibodies and PBC. * PDC-E2 and PDC-E3BP are fully crossreactive. Abbreviations: BCOADC, branched-chain 2-oxo-acid dehydrogenase complex; E3BP, E3-binding protein; gp210, glycoprotein 210; OGDC, oxoglutarate dehydrogenase complex; sp100, nuclear body speckled 100 kDa; PDC, pyruvate dehydrogenase complex; PML, promyelocytic leukemia; 2-OADC, 2-oxo-acid dehydrogenase complex. Adapted from (Jones, 2007; Hirschfield and Gershwin, 2013).

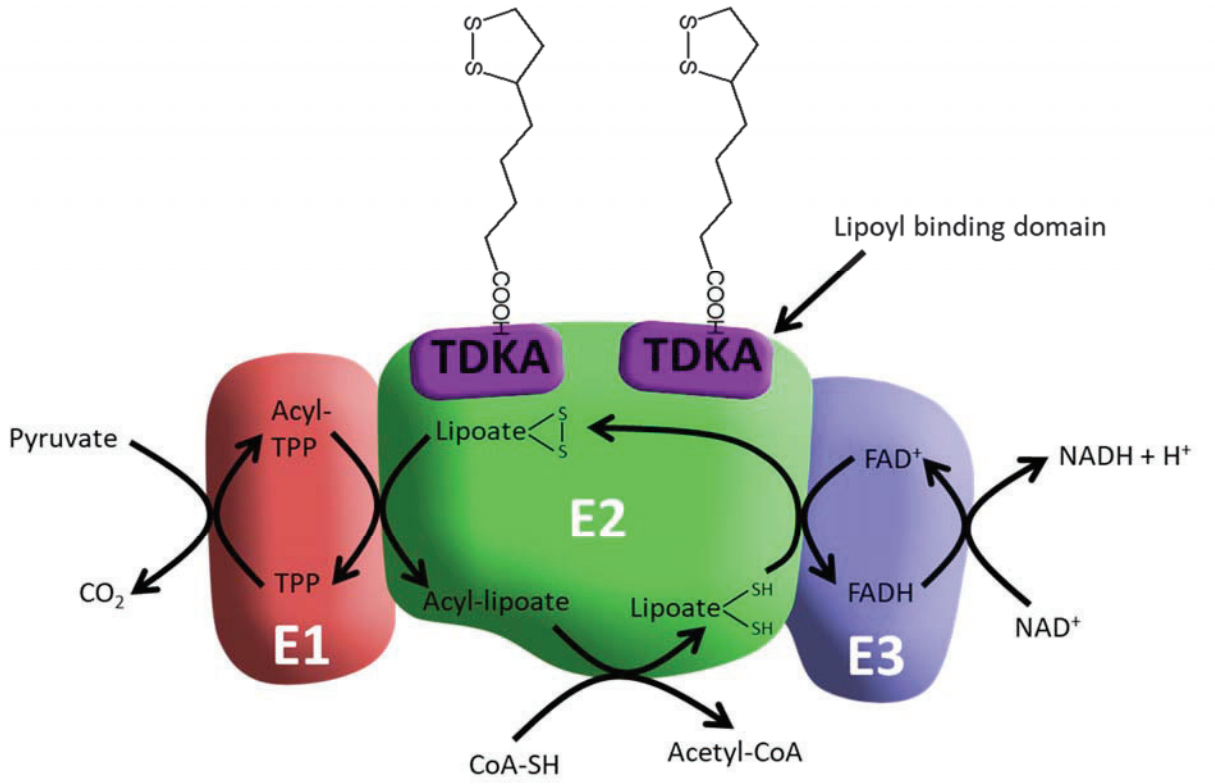

Figure 1.11: The PDC-E2 lipoyl binding domains and pyruvate dehydrogenase reaction. Lipoic acid binds to the lysine (K) residue of the lipoyl binding domain. Pyruvate dehydrogenase (E1) decarboxylates pyruvate. The acetyl group is transferred to thiamine pyrophosphate (TPP) which is then transferred to lipoic acid bound to dihydrolipoyl transferase (E2). The acetyl group is then transferred to CoA resulting in 2 SH-groups forming on lipoic acid which is then is re-oxidised back to the disulphide form by FAD and dihydrolipoyl dehydrogenase (E3). This produces $FADH_2$ which is then oxidised back to FAD^+ by NAD^+ producing NADH that is then used in mitochondrial oxidation.

The pathogenesis of PBC (summarised in Figure 1.12) has been suggested to involve the T-lymphocytes due to the high concentration of CD4 and CD8 T cells in the portal triads of PBC patients (Kita *et al.*, 2002) as well as a role for natural killer cells (Chuang *et al.*, 2008). These cells are recruited by chemokines CXCL10, CXCL9 and CX_3CL1. The PDC-E2 autoepitope is presented by antigen presenting cells via the major histocompatibility complex (MHC) class II receptor to CD4+ T cells. The CD4+ T cells can then go onto activate CD8 cytotoxic T cells that play a role in the degradation and death of cholangiocytes (Liaskou *et al.*, 2014). There is also a reduction in regulator T cells (Lan *et al.*, 2006). Lastly, PDC-E2 specific B cells are activated and differentiate into plasma cells to produce PDC-E2 AMAs (Liaskou *et al.*, 2014).

The cholangiocytes are also believed to play a role in the pathogenesis of PBC. Cholangiocytes express cell surface adhesion molecules that are recognised by lymphocytes. It has been demonstrated that they can

increase the expression of these adhesion molecules as well as TNF-α, MHC class I and II, INF-γ and IL-1 when stimulated by pro-inflammatory cytokines (Invernizzi *et al.*, 2010). It has also been shown that MHC class II receptors are expressed on the surface of cholangiocytes (Ayres *et al.*, 1993). The cholangiocytes in the small bile ducts are susceptible to apoptosis. In most cells undergoing apoptosis, including epithelial cells, PDC-E2 undergoes covalent modification by glutathione. In PBC, the cholangiocytes fail to bind glutathione to the lysine-lipoyl residue (Figure 1.13) (Odin *et al.*, 2001). This means PDC-E2 remains immunologically intact in apoptotic blebs forming an 'apotope' which can be recognised by AMAs. This could explain the tissue specificity of injury in PBC.

The apotopes, AMAs and immune induced cytotoxicity results in the production of pro-inflammatory cytokines such as TNF-α, IL-6 and IL-10 leading to the further recruitment of immune cells, apoptosis, biliary destruction and ultimately to fibrosis and cirrhosis.

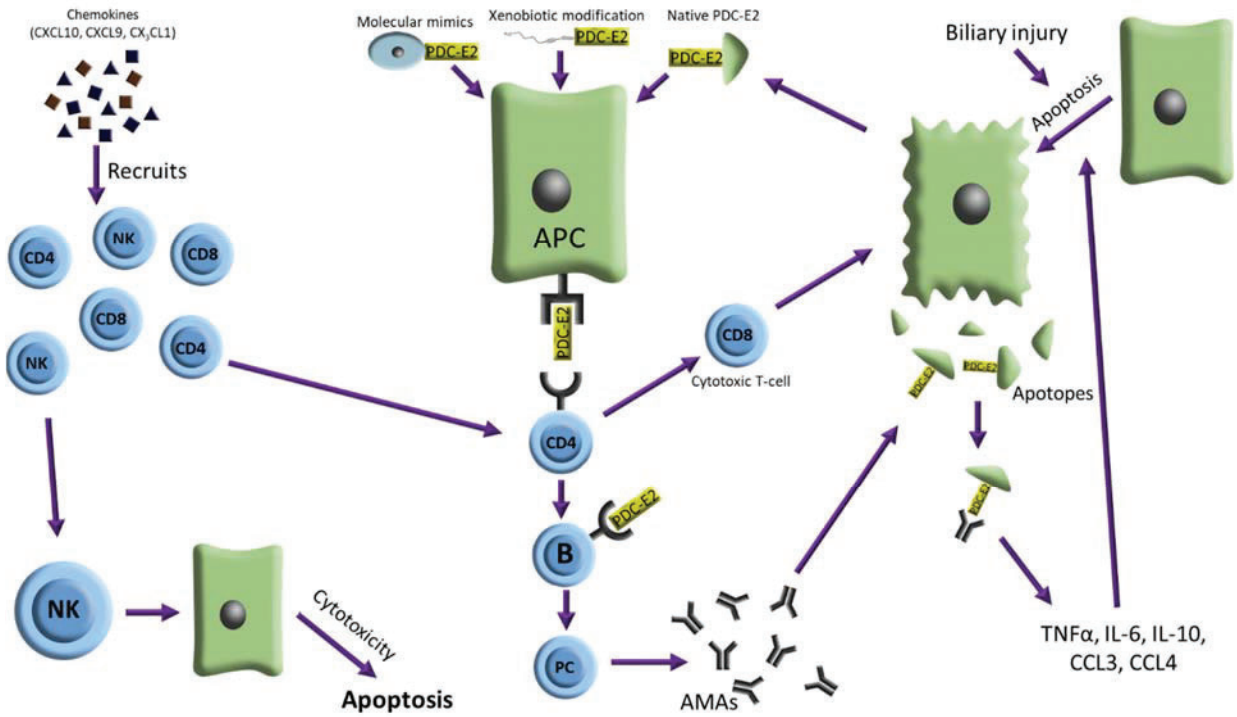

Figure 1.12: Pathogenesis of PBC. Chemokines in the portal tracts recruit CD4, CD8 and NK cells. CD4+ T cells recognise autoantigenic stimuli on the MHC class II on an antigen presenting cell (including cholangiocytes). Stimuli provided by native PDC-E2, molecular mimics of PDC-E2 or PDC-E2 modified by a xenobiotic. CD4+ T cells can then either activate CD8 cytotoxic T cells which damage cholangiocytes or activate PDC-E2 cells specific B cells that mature into plasma cells and produce AMA. These AMAs recognise PDC-E2 presented on apotopes of cholangiocytes undergoing apoptosis (induced from biliary damage). AMAs recruit cytokines to induce further apoptosis. Abbreviations: AMAs, antimitochondrial antibodies; PC, plasma cell; PDC-E2, pyruvate dehydrogenase complex E2 subunit; TNFα, tumour necrosis factor α. Adapted from (Liaskou *et al.*, 2014).

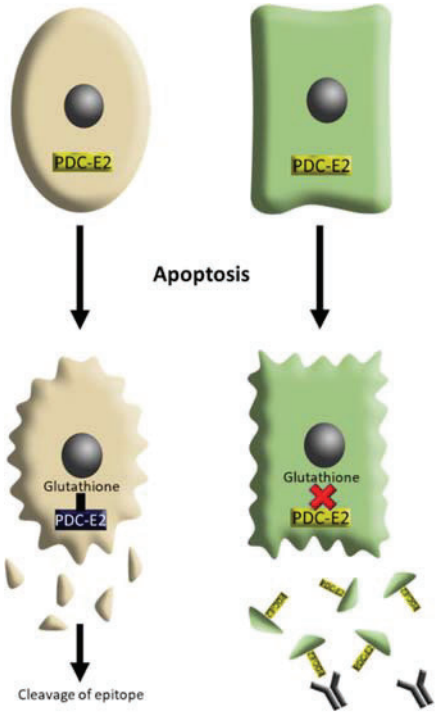

Figure 1.13: PDC-E2 remains intact in cholangiocytes undergoing apoptosis. When most cells undergoing apoptosis, PDC-E2 is covalently bound to glutathione (brown cell). Cholangiocytes (green cell) do not undergo glutathione modification during apoptosis. Resulting in PDC-E2 remaining intact on the apotope that is recognised by AMAs inducing an immune response. This immune response occurs specifically in the bile duct. Abbreviations: PDC-E2, pyruvate dehydrogenase complex – E2 subunit.

1.5.4 PBC aetiology – genetic and environmental components

The exact aetiology of PBC is unknown, however a combination of genetic factors and exposure to environmental factors is regarded as a possible trigger that leads to the loss of immune tolerance to PDC-E2. Studies have shown a strong genetic predisposition in PBC, with first degree relatives of PBC patients having a 6% increased risk of PBC (Gershwin *et al.*, 2005) and monozygotic twins have been shown to have a 63% concordance for PBC (Selmi *et al.*, 2004). Genome-wide association studies (GWAS) have shown associations with single nucleotide polymorphisms (SNPs) within the HLA region (human leukocyte antigen) (Donaldson *et al.*, 2006; Invernizzi *et al.*, 2012). GWAS have also identified 27 non-HLA genes associated with PBC, such as IL12RB2, NKKB1, STAT4 and STAT1 (Lleo *et al.*, 2017). The non-HLA genes all appear to be involved in the regulation of the immune system, including antigen presentation and T cell differentiation.

Genes alone do not seem to be sufficient to trigger PBC and exposure to an environmental factor may be required. Two environmental factors have been primarily studied in PBC, exposure to infectious agents and exposure to xenobiotics. Geographical studies support the existence of environmental factors as it has been reported that the incidence rate of PBC varies between regions. The first demonstrated case was in 1980 in Sheffield and was suggested to be linked to a water reservoir (Triger, 1980). Other studies have shown higher incidence in former areas of heavy mining in Newcastle-upon-Tyne (Prince *et al.*, 2001) and in residential proximity to a superfund toxic waste site in New York City (Ala *et al.*, 2006). This clustering of incidence rate of PBC suggests that there may be some environmental exposure in these locations that could trigger PBC in susceptible individuals.

Human PDC-E2 has a similar structure to that of some bacterial PDC-E2 (Tanaka *et al.*, 2018). Therefore, it is possible that bacterial infection and bacterial PDC-E2 could trigger a loss of immunological tolerance to host PDC-E2 through molecular mimicry. Associations between PBC and urinary tract infection by *Escherichia Coli* have been shown (Corpechot *et al.*, 2010). The lipoyl domain sequences of Human and *E. coli* PDC-E2 are similar and have been shown to be cross-reactive (Bogdanos *et al.*, 2004). Another bacterium shown to have a structurally similar PDC-E2 and has been suggested to be more reactive than *E. coli* is *Novosphingobium aromaticivorans*, a xenobiotic metabolising bacterium (Selmi *et al.*, 2003; Hirschfield and Gershwin, 2013).

Epidemiological studies and animal models suggest that xenobiotics play a role in the development of PBC. The hypothesised mechanism of how xenobiotics trigger auto-immune responses is through the modification of the molecular structure of the protein leading to the modified protein not being recognised by the immune system. In the case of PBC, the potential xenobiotic is likely to couple to the lysine residue in the inner lipoyl domain that conjugates to lipoic acid (Tanaka *et al.*, 2018). 2-octynoic acid has been suggested as one xenobiotic with reactivity against PBC patient sera with the potential capability to modify PDC-E2 (Amano *et al.*, 2005). This chemical is of particular interest as 2-octynoic acid methyl esters are widely used in several products including perfumes, lipsticks and as a food flavouring. Recently AMAs have been shown to have specificity toward 2-octynoic acid modified PDC-E2 than lipoylated PDC-E2 (Shuai *et al.*, 2017). Other structurally similar cosmetic components have also been identified as potential xenobiotic triggers for PBC such as 2-nonynoic acid (Rieger *et al.*, 2006). *In vivo* models investigating xenobiotics and PBC have shown that mice immunised with 2-octynoic acid with bovine serum albumin (BSA) displayed autoimmune cholangitis, AMAs and other immunological markers after 24 weeks (Wakabayashi *et al.*, 2008). 6-bromohexanate immunisation has also shown an induction of AMAs (Leung

et al., 2003) in addition to being shown to incorporate into PDC-E2 *in vitro* (Walden *et al.*, 2008). It has therefore been shown in several models *in vitro* and *in vivo*, the possibility of environmental triggers in the aetiology of PBC.

1.5.5 PBC and estrogens

PBC has a strong female bias and primarily affects post-menopausal women and there is also a history of cholestasis during pregnancy, suggesting there is potentially some influence between hormones and PBC (Sun *et al.*, 2015). Numerous immune related genes including genes involved in the maintenance of immune tolerance are found on the X chromosome and diseases caused by X monosomy are associated with autoimmune features (Bianchi *et al.*, 2012). Women with PBC also have a higher frequency of X monosomy in peripheral blood cells (Invernizzi *et al.*, 2004). These suggests the X chromosome may play a role in autoimmune related genes, including PBC.

Another possible explanation for the female bias in PBC are effects of estrogens, as elevated estrogen levels have been shown to induce cholestasis (Stieger *et al.*, 2000; Ozkan *et al.*, 2015). Estrogens are a class of steroid hormone, defined as the primary female sex hormone and bind to and activate estrogen receptors (ERs). Two estrogen receptors are found in humans, ERα and ERβ and differ in their distribution within the body (Bondesson *et al.*, 2015). ERα is expressed in high levels in uterine, ovarian and pituitary gland and adipose tissue, whereas ERβ is expressed in high levels in the ovary, lung, epiderymis, prostate, colon and specific brain regions **(www.nursa.org)**.

Some have shown ERα to be expressed in hepatocytes (Ahlbory-Dieker *et al.*, 2009) and regulate levels of circulating estrogen through metabolism (Bondesson *et al.*, 2015). Other have also shown ERα and ERβ are both expressed in cholangiocytes in rats (Alvaro *et al.*, 2000) however in normal human livers ERs were not shown to be, but are expressed in response to injury (Alvaro *et al.*, 2006). ERβ levels were also increased in PBC stage IV whereas ERα expression disappeared (Alvaro *et al.*, 2004). The current hypothesis is that ERα and ERβ are believed to regulate the expression of growth factors and cytokines and modulate the proliferative response of cholangiocytes to damage.

Xenoestrogens are exogenous chemicals that mimic the activity of estrogens and therefore disrupt normal estrogen signalling. It has therefore been hypothesised that since estrogens are cholestatic, exposure to xenoestrogens could play a role in the development of PBC. Sunset yellow, a coal-derived food and tartrazine, a cosmetic colouring have been shown to be xenoestrogens (Axon *et al.*, 2012; Meyer *et al.*,

2017b). Recently, evidence of a xenoestrogen has been shown to be in high levels in the proximity of a landfill site that is in a region of high incidence rate of PBC (Meyer *et al.*, 2017a). This landfill xenoestrogen could link geographical PBC incidence variation, environmental xenobiotic exposure and estrogenic effects.

1.6 Project hypothesis and aims

The main hypothesis of this thesis was that B-13/H cells could be used as a model for lipid dysregulation (steatosis and phospholipidosis). To test this hypothesis, the main aims were to:

- Examine the effects of fatty acids on lipid accumulation in B-13 and B-13/H cells.
- Examine the effects of alcohol on lipid accumulation in B-13 and B-13/H cells.
- Investigate the effects of xenobiotics in their ability to induce phospholipid and lipid accumulation.

Chapter 2. Materials and Methods

2.1 Materials

Unless otherwise stated, all materials were purchased from Sigma-Aldrich (Merck) at the highest purity available (Poole, UK). The expression construct encoding the human lysosomal phospholipase A2 (LPLA2) was kindly donated by Professor James Shayman (University of Michigan, USA). The LXR responsive gene construct, TK-LXRE-LUC, was donated by Professor David Mangelsdorf (University of Texas Southwestern Medical Center, USA). Wnt3a condition medium and 10% RSPO1 conditioned medium was donated by Dr Andrew Bennett (University of Nottingham, UK).

2.2 Animals

2.2.1 Ethics and husbandry

All animal work was carried out in accordance to Home Office regulations and experiments were performed under a UK Home Office license (PPL - P1FF204BF). Protocols were designed for each study and approved by a Senior Animal Technician/Named Animal Care and Welfare Officer before the start of the study.

Animals were housed in the Comparative Biology Centre (CBC) at Newcastle University and were kept in an air-conditioned environment on a 12-hour light/dark cycle with a humidity of 50% ± 10% and a temperature of 23^{o}C ± 1^{o}C. Mice were kept in saw-dust filled and filter topped, individually ventilated cages and kept no more than 6 to a cage. Food and water were provided ad-libitum and bedding was changed twice weekly.

2.2.2 C57BL/6 mice

C57BL/6 mice (wild type) were purchased from Charles River (Kent, UK) and housed as outlined in 2.2.1. Mice were at least 6 weeks old and between 15-22g body weight at the beginning of all experiments.

2.2.3 3x-κB-luc C57BL/6 mice (NF-κB-luc mice)

Transgenic NF-κB-luc mice (bearing a transgene composed of three NF-κB sites from the Ig κlight chain promoter coupled to the gene encoding Firefly luciferase) (Carlsen *et al.*, 2002) were re-derived from zygotes from Charles River and the colony expanded in house. Mice were housed as described in 2.2.1 and

genotyped as described in 2.2.4 (transgenic NF-κB-luc mice show a basal level of NF-κB-driven luciferase activity). Animals were at least 6 weeks old at the beginning of experiments.

2.2.4 In vivo luminescent imaging

Transgenic NF-κB-luc mice were imaged with the *In Vivo* Imaging System (IVIS), Xenogen Spectrum imaging system. Luminescence was quantified and analysed using the Living Image 4.0 software (Caliper Life Sciences, Hoplinton, USA).

Mice were anaesthetized with isoflurane and their abdominal fur shaved off prior to imaging. Mice were then injected intra-peritoneally (i.p.) with 5ml/kg body weight D-luciferin (Perkin Elmer, Waltham, USA) at 15mg/ml in PBS. Optimum time post injection for imaging was determined and used throughout the experiment using 300 seconds exposure time. Following imaging, mice were returned to their cage or culled by cervical dislocation for tissue collection. Using captured images, regions of interest were manually selected and total flux values (photons/seconds) were calculated using the Living Image 4.0 software.

2.3 Cell culture

2.3.1 Culture of adherent cell lines

Adherent cell line sourcing and appropriate medium for their culture are described in Table 2.1. Cells were maintained at 37^{o}C and 5% CO_2. Medium was changed every 2-3 days.

Cell line	Source	Species/Morphology	Culture medium
AR42J-B13	Gift from Dr Philip Probert	rat pancreatic acinar	Dulbecco's Modified Eagle Medium (1g glucose/L, DMEM), 10% fetal calf serum (FCS), 2mM glutamine, 100U/ml penicillin, 100µg/ml streptomycin
HepG2	ATCC (catalogue HB-8065, Manassas, Virginia)	human hepatoma	
HEK293	ECACC (catalogue 85120602, Porton Down, UK)	human embryonic kidney	
MCF7	Gift from Dr Katherine Rennie, (Newcastle University, UK)	human breast cancer	
603B	Gift from Dr Yedidya Saiman (Mount Sinai School of Medicine, New York, US)	murine biliary epithelial	
LTPA	ATCC (catalog CRL-2389, Manassas, Virginia)	murine pancreatic epithelial	Minimum Essential Medium Eagle (MEME), 10% FCS, 2mM glutamine, 100U/ml penicillin, 100µg/ml streptomycin, 1% (v/v) non-essential amino acids (NEAA), 1mM sodium pyruvate
H69	Gift from Prof John Kirby (Newcastle University, UK)	human biliary epithelial	DMEM:Ham's F12 (2:1), 10% (v/v) FCS, 2mM glutamine, 100U/ml penicillin, 100µg/ml streptomycin, 180µM adenine, 2nM triiodothyronine, 5.5µM epinephrine, 1x ITS solution, 1µM hydrocortisone

Table 2.1: Adherent cell lines, source, species and culture medium.

2.3.2 Isolation of primary mouse hepatocytes

Primary mouse hepatocytes were generously donated by Professor Loranne Agius (Newcastle University, UK) and were isolated following collagenase perfusion. The protocol was essentially as follows: the mouse was anaesthetized by isoflurane (IsoFlo 100%, Zoetis UK Ltd) for 2 minutes. The mouse was injected intraperitoneally with 300 µl heparin (3mg/ml in sterile 150mM NaCl) and then returned to the isoflurane chamber. After 4 minutes from first exposure to isoflurane the mouse was removed and dissected to expose the heart and liver. A suture was placed below the heart under the vena cava and a 20Gauge x 32 mm i.v. catheter (Versatus, SR+DU2032PX) was inserted into the inferior vena cava. The needle insert was then removed and when the cannula filled with blood, the suture was tied securely, and the portal vein was cut approximately 1 cm distal to the liver. The cannula was then connected to a peristaltic pump linked to calcium-free perfusate (containing per litre: 8000mg NaCl, 400mg KCl, 130mg KH_2PO_4, 76mg EGTA, 20mg phenol red, 10mmol HEPES, pH 7.4). The liver was perfused at 5 ml/min for 6 minutes. The cannula was then connected to a calcium plus collagenase Hanks medium buffered with 5mM $NaHCO_3$, 20mM HEPES and containing 10mg/100ml collagenase and it was perfused for between 15 and 20 min. On termination of the perfusion the liver was transferred to a petri dish and gently dissociated in ~40ml Minimum Essential Medium. The cell suspension was filtered through a 200-micron mesh, sedimented at

50g and the pellet was washed in medium at 50g. The pellet was suspended in Minimum Essential Medium supplemented with Non-Essential Amino acids; 2mM glutamine; 100U/ml penicillin and 100µg/ml streptomycin, 5% (vol/vol) FCS, 10nM DEX and 10nM insulin. Cell viability was determined by trypan blue stain as described in 2.3.11 and were seeded at a density of 100,000 cells/ml on collagen-coated plates (Greiner bio-one, Stonehouse, UK).

2.3.3 Primary mouse hepatocyte culture

Primary mouse hepatocytes were initially cultured in Minimum Essential Medium as described in 2.3.2 for 4 hours to allow hepatocytes to adhere to the culture plates. Once adhered, culture medium was replaced with Minimum Essential Medium supplemented with Non-Essential Amino acids; 2mM glutamine; 100U/ml penicillin and 100µg/ml streptomycin, 10nM DEX and 10nM insulin. Cells were maintained at 37^{o}C and 5% CO_2.

2.3.4 Isolation of primary human hepatocytes

Primary human hepatocytes were isolated at the Freeman Hospital with the assistance of Mr Rodrigo Figueiredo. Livers unsuitable for transplantation and offered for research were used for hepatocyte isolation. Prior to isolation, the liver was re-conditioned with blood for 6 hours at 37^{o}C with a target pO_2 of 20 kPa using a BioMedicus pump perfusion system (Figure 2.1). Circulating blood was drained and the liver was washed with EBSS (without Ca^{2+} and Mg^{2+}). A section of liver weighing approximately 300-500g was anatomically split from the rest of the liver and any transected ducts or vessels ligated. Cannulation of the suprahepatic inferior vena cava, portal vein, and hepatic artery was maintained to allow the circulation of perfusates using the BioMedicus pump. The following perfusates were then perfused at 37^{o}C; Perfusate 1 (1x EBSS (without Ca^{2+} and Mg^{2+}) + 0.5mM EGTA) was perfused and run to waste. Perfusate 2 (1L 1x EBSS (without Ca^{2+} and Mg^{2+}) was perfused and run to waste. Perfusate 3 (EBSS (without Ca^{2+} and Mg^{2+}) + 1mM CaCl2 + 300mg/L collagenase A) was then circulated at 37^{o}C until the liver was digested (approximately 25-30 minutes). The liver was then passed through a sieve and gauze into sterile beaker, with 1x EBSS (without Ca^{2+} and Mg^{2+}).

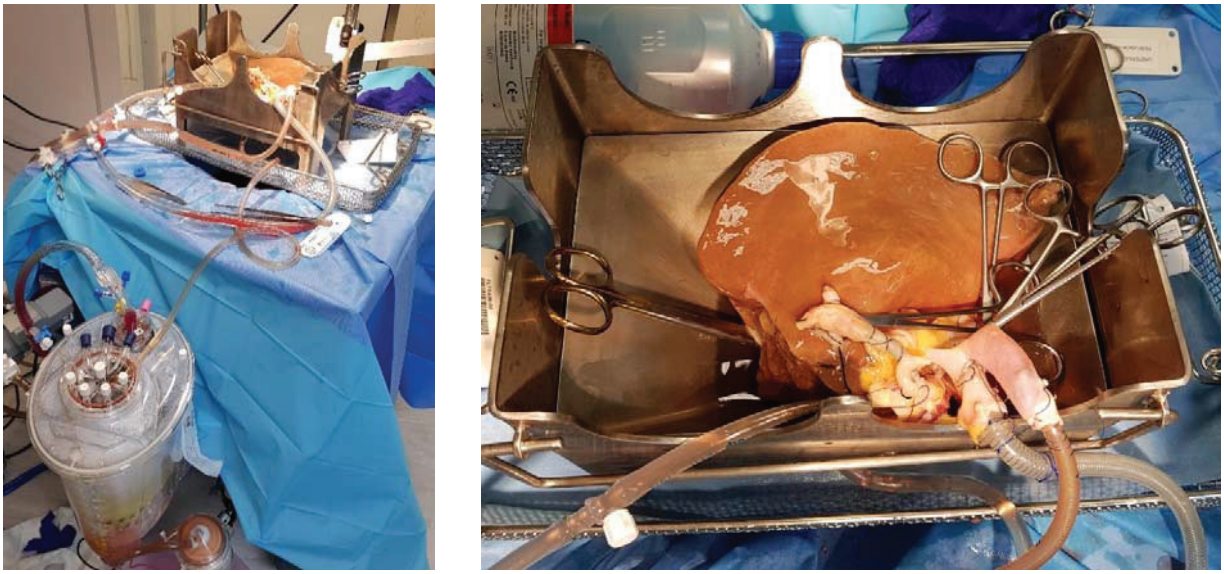

Figure 2.1: Hepatocyte isolation set up. BioMedicus pump set-up (left panel). Cannulation of a section of liver (right panel).

2.3.5 Primary human hepatocyte culture

The EBSS suspension was then span at 50g for 3 minutes and the hepatocytes were resuspended in Williams E medium, 10% FCS, 2mM glutamine, 100U/ml penicillin, 100µg/ml streptomycin, 50mg/ml gentamycin and 10mg/ml insulin. Cell viability was determined by trypan blue stain as described in 2.3.11. Cells were then seeded at a density of 250,000 cells/ml on collagen-coated plates for 4 hours to allow the hepatocytes to adhere.

Once primary human hepatocytes were adhered, the medium was replaced with Williams E medium, 2mM glutamine, 100U/ml penicillin, 100µg/ml streptomycin, 50µg gentamycin and 1µg insulin. Cells were maintained at 37^{o}C and 5% CO_2.

2.3.6 Cell passage

Once adherent cell lines reached 75-95% confluence, they were passaged. The cell media was removed, and the cells were washed twice with sterile 1x phosphate buffer saline (PBS, 137mM NaCl, 2.6mM KCl, 10mM KH_2PO_4, pH 7.4). The cells were then incubated with 1x trypsin-EDTA diluted in PBS at 37^{o}C and 5% CO_2 for 5-10 minutes to detached cells. The trypsin was then inactivated by adding an equal volume of cell culture media, and the cell suspension was transferred to a centrifuge tube (Fisher, Loughborough, UK).

The cell suspension was centrifuged at 2000rpm for 5 minutes. Supernatant was discarded, and the cell pellet was re-suspended in fresh media before the cell were reseeded.

2.3.7 Long-term cell storage

Cell lines were routinely frozen down and stored long term at -80°C. Cells were detached and pelleted by centrifugation as described in 2.3.8. Cells were re-suspended in freezing media (10% (v/v) DMSO in FCS). The cell suspension was then aliquoted into sterile cryovials (2ml/cryovial). Aliquots were cooled in an isopropanol filled Mr. Frosty freezing container (Thermo scientific, Loughborough, UK) and chilled at -80°C. The cells were cooled at a rate of 1°C per hour and left at -80°C or transferred to liquid nitrogen for long term storage.

2.3.8 Cell stock revival

Cell stocks were removed from liquid nitrogen or -80°C storage and thawed at 37°C in a water bath. The cells were then transferred into a 50ml centrifuge tube containing pre-warmed medium (10x volume of cryovial). Cells were centrifuged at 600rpm, the supernatant discarded, and the pellet resuspended in fresh culture medium. Cells were then transferred into a tissue culture flask and incubated overnight to adhere. Once adhered, medium was removed and replaced with fresh medium.

2.3.9 Determining cell number and viability by trypan blue exclusion

Cell number and viability was assessed using trypan blue staining. Trypan blue is excluded by cells with an intact plasma membrane (live cells), whereas dead cells or cells that have a compromised plasma membrane, allows the passing of trypan blue into the cell, staining them blue.

After cell trypsinisation, pelleting and resuspension as described in 2.3.8, an aliquot of cells was diluted 1:1 (v/v) with 0.4% (w/v) trypan blue in PBS. The cell suspension was then placed onto a haemocytometer counting grid and the number of viable cells was determined by counting the total number of colourless cells. The total number of non-viable (blue stained) cells was also determined and cell number and viability calculated:

$$\%\ \text{viability} = 100\ \times \left(\frac{\text{mean number of viable cells}}{\text{total cell number}}\right)$$

2.3.10 B-13 transdifferentiation

B-13 cells were transdifferentiated into hepatocyte like cells (B-13/H) by culturing the cells with B-13 medium (described in 2.3.1) containing 10nM dexamethasone (DEX). DEX was added to the culture medium from a 1000x stock solution in ethanol (10µM). Cells were treated for 14 days to achieve full transdifferentiation, with medium changes every 2-3 days. After 14 days, cells were used for experiments unless otherwise stated.

2.3.11 Revival of EPCAM+ve progenitor cells

Human hepatic EPCAM+ve progenitor cells were kindly donated by Dr Andrew Bennett (University of Nottingham, UK). Organoids/isolated cells were thawed at 37^{o}C using a water bath and transferred to a centrifuge tube containing 10ml of isolation medium (Expansion medium + 10µM Y-27632, 25ng/ml noggin, 30% (vol/vol) wnt3a-conditioned medium) before centrifugation at 300g for 5 minutes. Dissociated cells/organoids were then re-suspended in Matrigel (SLS, Nottingham, UK) and seeded onto 48-well low attachment plates (25µl per well). The Matrigel was solidified by incubation at 37^{o}C for 5 minutes. Once the Matrigel had solidified, isolation medium was added to each well. After 6 days of culture in isolation medium (with medium change every 2-3 day), the medium was removed and replaced with expansion medium (1% penicillin/streptomycin, 1% L-glutamine, 10mM HEPES, 1% N2 supplement, 1% B27 supplement, 1.25mM N-acetylcysteine, 10nM gastrin, 10mM nicotinamide, 50ng/ml EGF, 100ng/ml FGF10, 25ng/ml HGF, 5µM A83.01, 5µM forskolin, 10% RSPO1 conditioned medium) (summarised in Figure 2.2).

2.3.12 EPCAM+ve progenitor cell passage and maintenance

Expansion medium was changed every 2-3 days. After 7-10 days the organoids were used for desired experiments or sub-cultured. To sub-culture the organoids they were first pipetted from the well and added to cold medium, the matrix washed from the organoids and the organoids dissociated through pipetting. The organoids were then centrifuged at 400g for 5 minutes and resuspended in Matrigel and seeded as described in 2.3.6 with the exception that expansion medium was added to each well (not isolation medium).

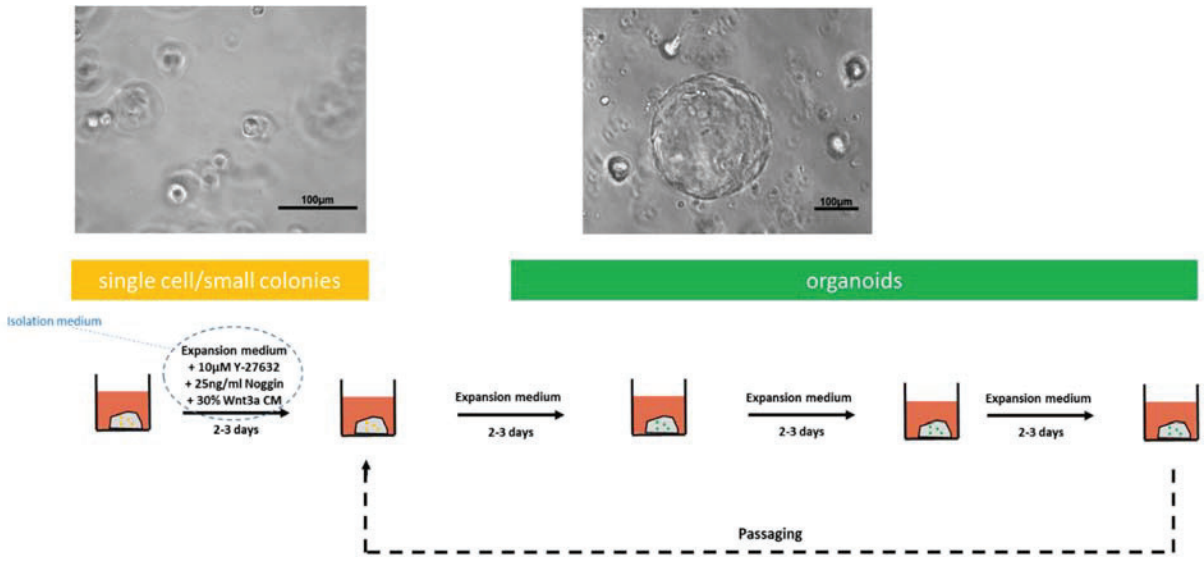

Figure 2.2: EPCAM+ve organoid culture protocol.

2.4 Cell transfection

2.4.1 Effectene transfection

603B and LTPA cells were transfected using effectene transfection reagent (Qiagen, Manchester, UK). Cells were transfected once they reached 70-80% confluency. For a 24 well plate, 6µg of plasmid DNA was added to 480µl of EC buffer and 36µl of enhancer buffer. The mixture was vortexed and incubated at room temperature for 5 minutes. 38.4µl effectene was mixed and incubated for a further 10 minutes. The mixture was added to 3.6ml of media and added dropwise to cells containing fresh media and incubated for 1-2 days before the continuation of experiments. The volumes of reagents and plasmid DNA were scaled accordingly for transfection in different multi-well plates.

2.4.2 Lipofectamine 2000 transfection

B-13/H, HepG2 and H69 cells were transfected using Lipofectamine 2000 (Invitrogen, Paisley, UK). Cells were transfected once they reached 70-80% confluency. For a 24 wells plates, 15µg of plasmid DNA was added to 600µl of serum free media, 60µl of lipofectamine was added to a separate vial 600µl of serum free media. The two mixtures were mixed together and incubated at room temperature for 5 minutes. 50µl of the final mixture was added dropwise to the cells with fresh medium and incubated for 1-2 days

before the continuation of experiments. The volumes of reagents and plasmid DNA were scaled accordingly for transfection in different multi-well plates.

2.4.3 Polyethyleneimine (PEI) transfection

HEK293 and MCF7 cells were transfected using polyethyleneimine (PEI). PEI working stocks were made to 1mg/ml in distilled water (dH_2O), pH7 (using NaOH). Stocks were filter sterilised (0.22µm), aliquoted and stored a -20^oC. Cells were transfected once they reached 70-80% confluency. For a 24 well plate, 12µg of plasmid DNA was added to 600µl of serum free medium. 72µl of 1mg/ml PEI was added and the mixture was vortexed and incubated at room temperature for 15 minutes. The mixture was then added to 3.6ml of serum free medium and 170µl was added dropwise to cells with no medium and incubated for 2 hours. After incubation fresh culture medium was added to each well and the cells were further incubated for 1-2 days before the continuation of experiments. The volumes of reagents and plasmid DNA were scaled accordingly for transfection in different multi-well plates.

2.5 Dual-Glo Luciferase Assay System

The Dual-Glo Luciferase Assay System (Promega, Southampton, UK) allows the quantification of a stable luminescent signal from two separate reporter genes in a single sample. Cells were co-transfected with two different plasmids resulting in the expression of Firefly (*Photinus phyralis*) and Renilla (*Renilla reniformis*, sea pansy) luciferase. Firefly luciferase is usually regulated by response elements in conjunction with a minimal promoter whereas Renilla luciferase control is from a constitutively active promoter. The assay system used provides the substrates for both luciferases, initiating their activity and producing a luminescent signal that can be quantified.

Cells were transfected with reporter constructs (Table 2.2) and a control construct, RL-TK at a ratio of no less than 6:1. Cells were transfected for 24-48 hours and then incubated with treatments for a further 24 hours. After treatment, the culture medium was removed, and the cells were washed with PBS. The cells were then lysed using Passive Lysis Buffer (Promega, Southampton, UK) and left at room temperature on an orbital shaker for 10-15 minutes. 50µl of the lysate was transferred to a well of a white 96-well microplate. 50µl of luciferase buffer was then added to each well and Firefly luminescence was measured using a luminometer (MicroLumaPlus, Berthold technologies). 50µl of Stop and Glo reagent was added to each well (inhibiting firefly luminescence), and Renilla luminescence was measured. Background luminescence (non-transfected cells) was subtracted from the samples and Firefly luciferase activity

(reporter construct) was normalised to Renilla activity. All sample measurements were then further normalised to the control group.

Plasmid	Expresses/promotor	Cell Used
pcDNA3-LLPL-HA tagged	human lysosomal phospholipase A2	B-13
TK-LXRE3-LUC	LXR responsive reporter gene	B-13/H and HepG2
(ERE)3-pGL3promotor	estrogen-responsive reporter gene luciferase construct	MCF7, 603B, HEK293, H69
3XERE TATA Luc	estrogen-responsive reporter gene luciferase construct	LTPA
pcDNA3.1-mERα	mouse estrogen receptor alpha	LTPA
pcDNA3.1-mERβv1	mouse estrogen receptor beta, variant 1	603B
pcDNA3.1-mERβv2	mouse estrogen receptor beta, variant 2	603B
pcDNA-Flag-Erβ	human estrogen receptor beta	HEK293 and H69
RL-TK	renilla luciferase - thymidine kinase	All cells

Table 2.2: Plasmids and cell lines use for transfections.

2.6 Plasmid DNA constructs and sequencing

2.6.1 Competent cell transformation

TOP10 chemically competent *E. coli* (Invitrogen) were used to replicate plasmid DNA. Cells stocks were stored at -80^{o}C and thawed on ice before use. 50-100ng of plasmid DNA was added to a vial (50µl of cells) and incubated on ice for 30 minutes. The cells were then heat shocked at 42^{o}C for 30 seconds using a water bath. The cells were then moved back onto ice. 250µl of prewarmed S.O.C medium was added to each vial and shaken at 37^{o}C for 1 hour at 225 rpm. The transformed cells were spread onto LB (LB (luria broth-10g NaCl, 10g Tryptone, 5g yeast in 1litre dH_2O) agar plates containing required antibiotics (kanamycin 25µg/ml or ampicillin 100µg/ml). The plates were then incubated upside down overnight at 37^{o}C.

Colonies were selected and placed in LB medium and incubated overnight at 37^{o}C shaking at 220rpm. The grown cells were then either frozen and stored as glycerol stocks of or used in miniprep culture.

2.6.2 Miniprep isolation of plasmid DNA

Miniprep (Qiagen) was carried out essentially as described in the manufacturer's protocol. 1-5ml of culture was centrifuged at 10000rpm for 1 minute. The pellet was then resuspended in 250µl of buffer P1 (containing RNase to remove contaminating RNA), followed by buffer P2 (highly concentrated salt buffer containing sodium dodecyl sulphate, SDS). The buffers were mixed by inversion and buffer N3 was added

and mixed. Samples were centrifuged for 10 minutes at 13000rpm and the supernatant removed and added to a Qiaprep spin column and centrifuged for a further minute. The flow through was discarded and 750µl of buffer PE was added to the column and centrifuged again to remove excess salt. Finally, 50µl of buffer EB was added to the column to elute the DNA into a sterile microcentrifuge tube. DNA was then quantified as described in 2.7.2 and stored at -20°C.

2.6.3 Maxiprep isolation of plasmid DNA

Maxiprep isolation was used to purify larger quantities of plasmid DNA and carried out following the manufacturer's protocol. The process is largely similar to that of a miniprep isolation but on a larger scale. 200-300ml of overnight culture was separated into 50ml centrifuge tubes and centrifuged at 6000g for 10 minutes at 4°C. The bacterial pellet was lysed by adding buffers P1, P2 and after mixing and incubating for 5 minutes at room temperature, buffer P3. The lysate was transferred to a QIAfilter cartridge (that had been equilibrated with prechilled buffer P3) and incubated at room temperature for 10 minutes. The lysate was then filtered through the cartridge into a HiSpeed Tip (that had been equilibrated with buffer QBT). The lysate was filtered through to waste, and the HiSpeed Tip washed with 60ml of buffer QC to waste. The DNA was then eluted using 15ml of buffer QF and precipitated by adding 10.5ml of isopropanol and incubating for 5 minutes. The eluate-isopropanol was filtered through a QIApreciptator and the precipitator was washed by filtering through 2ml of 70% ethanol. The membrane was then dried by pressing air through the precipitator. 1ml of buffer TE was used to elute the DNA into a sterile microcentrifuge tube. DNA was then quantified as described in 2.7.2 and stored at -20°C.

2.6.4 Storage of transformed bacterial cultures

For long term storage, 500µl of overnight culture was diluted 1:1 (v/v) with LB containing 30% glycerol (v/v), transferred to cryovial and frozen at -80°C. When required, glycerol stocks of bacteria were removed from storage, thawed and a small volume (20-30µl) spread onto a LB agar plate containing required antibiotics. The plate was then incubated, and colonies picked as described in 2.6.1.

2.6.5 Restriction digest

Plasmid DNA was analysed to confirm the purification of the correct plasmid by digestion with restriction using endonucleases. Restriction digests were carried out as described in the manufacture's protocol (New

England Biolabs). The reaction mixture was made from 2µl 10X reaction buffer, 0.2µl of acetylated bovine serum albumin (BSA, 10µg/µl), 1µg of plasmid DNA, and 0.5µl of restriction enzyme(s). Nuclease free water was added to make the total volume 20µl. The mixture was incubated for 1-3 hours at 37°C. After incubation, DNA loading buffer was added to the sample and the DNA fragments separated by agarose gel electrophoresis as described in 2.7.5.

2.6.6 DNA extraction from agarose gel

DNA fragments in an agarose gel were imaged using a UV box and bands of interest identified. These bands were cut out using a sterile scalpel blade and place in a nuclease free microcentrifuge tube. DNA was then extracted from the gel using QIAquick gel extraction kit (Qiagen). Extraction was carried out as described in the manufacturer's protocol. Buffer QG was added to the gel at a ratio of 3:1 and placed in a heat block at 50°C for 10 minutes. 1 volume of isopropanol was added and mixed. The sample was applied to the QIAquick column and centrifuged for 1 minutes at 16,000g, discarding the flow through. 750µl of buffer PE was added to the column and centrifuged as before to wash the DNA. The column was centrifuged once more to dry it. DNA was eluted by applying 50µl of nuclease free water to the column and centrifuged as before into a fresh, sterile, nuclease free microcentrifuge tube. The DNA was quantified as described in 2.7.2

2.6.7 Sequencing and analysis

Plasmid DNA was sequenced by DNAseq (Dundee, UK) using either M13 or sequence specific primers. Sequencing chromatograms were analysed using Chromas software (Technelysium, Brisbane, Australia).

2.7 Isolation of RNA and quantification

2.7.1 RNA isolation

RNA was isolated from cells and tissue using TRIzol (Invitrogen). For cells, medium was removed, and the cells were washed with sterile 1x PBS. 1ml of TRIzol was added directly to the cells and incubated at room temperature on the orbital shaker for 5 minutes. Alternatively, after the cells were washed they were scraped in PBS and centrifuged at 16,000g for 1 minute, the supernatant discarded and 1ml of TRIzol added and pipetted up and down to mix. The TRIzol with cells were then transferred into an RNAse free microcentrifuge tube. 200µl of chloroform was added, the mixture vortexed, and centrifuged at 16000g

for 15 minutes at 4°C. The upper aqueous layer containing the RNA was then transferred into a fresh RNase microcentrifuge tube and 500µl of ice-cooled isopropanol was added and mixed by inversion before being incubated on ice for 10 minutes. The mixture was centrifuged at 16000g for 10 minutes at 4°C and the supernatant discarded. The pellet was then gently dislodged and washed with ice-cooled 70% ethanol before being centrifuged again at 16000g for 10 minutes at 4°C. The supernatant was removed and the pellet air dried for 5-10 minutes before being resuspended in 20-30µl of RNase free water (Qiagen). RNA samples were quantified as described in 2.7.2 and stored at -80°C.

RNA isolation from tissue samples followed the same protocol with the exception that tissue was snap frozen in TRIzol and when needed were thawed, homogenized using a hand homogeniser and sonicated before continuing with the RNA isolation.

2.7.2 DNAse I treatment of RNA

Contaminating DNA was removed from TRIzol purified RNA samples by treatment with RQ1 RNAse-free DNAse (Promega). To 10µl of RNA, 1µl of RQ1 RNAse-free DNAse and 1µl of 10x DNAse buffer were added and incubated for 30 minutes at 37°C. 1µl of DNAse stop solution added and incubated at 65°C for 10 minutes to inhibit DNAse activity.

2.7.3 RNA and DNA quantification

The concentration and purity of RNA and DNA was determined using a NanoDrop 2000 spectrophotometer (Thermo Scientific) to measure the absorbance at 260nm and 280nm, using RNase free water as the blank. Pure nucleic acids should have a 260nm/280nm ratio between 1.8 and 2.0, deviation from these values suggests contamination, likely to be by phenol or protein.

2.7.4 cDNA synthesis by reverse transcription of RNA

RNA was diluted to 200ng/µl and 5µl was transferred to a 200µl reaction tube. 1µl of 50ng/µl random primers (Promega) was added to each tube and incubated for 3 minutes at 90°C to melt the RNA secondary structure. The temperature was rapidly reduced to 4°C to anneal the random primers to the RNA. 14µl of reverse transcription master mix was added to each sample. The master mix contained 1µl of Moloney Murine Leukemia Virus reverse transcriptase (M-MLV, an RNA-dependent DNA polymerase), 2µl of 10x reverse transcription buffer, 2µl of 10mM dNTPs and 9µL of nuclease free water. The samples were

incubated for 1 hour at 42°C. Samples were diluted to desired concentration with nuclease free water and stored at -20°C.

2.7.5 *Primer Design*

DNA primer sequences were designed using the NCBI database (www.ncbi.nlm.nih.gov). Primers were designed to be 20-25 bases in length with a 40-60% guanine and cytosine content and with melting temperatures (Tm) close to 60°C. The optimum annealing temperature for a set of primers was determined, starting at 5oC below the Tm.

2.7.6 Polymerase chain reaction (PCR)

Polymerase Chain Reaction (PCR) is a technique that use DNA polymerases and thermal cycling to amplify target DNA sequences. As shown in Figure 2.3, double-stranded DNA is denatured at high temperatures (95°C), then short 5'-3' oligonucleotides (primers) anneal to complementary DNA (cDNA) at the target sequence (amplicon) enabling selective amplification. DNA polymerase binds and elongates the DNA strand 5' to 3'. The amplicon is the exponentially amplified as DNA generated from previous cycles can act as a target itself.

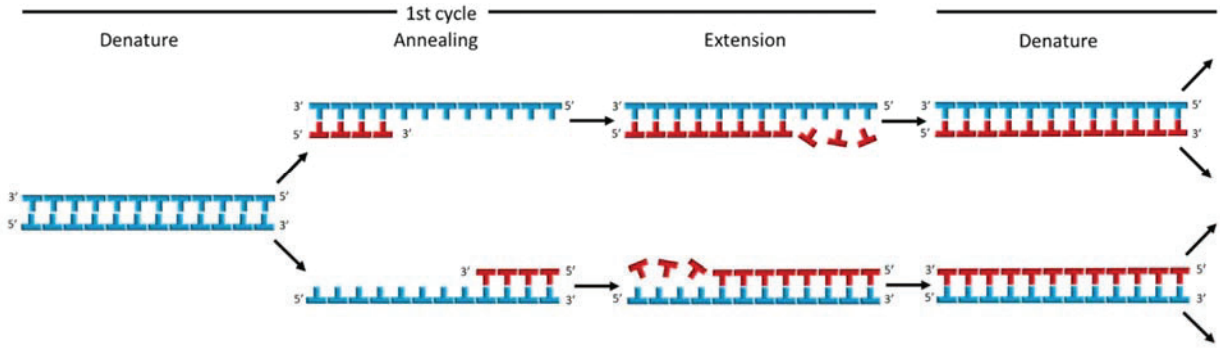

Figure 2.3: The PCR cycle. Double stranded DNA is denatured at 95°C. Primers are annealed to the resulting single stranded molecules at approximately 60°C. Polymerase extends the single stranded DNA at 72°C, generating new double stranded DNA. The new double stranded DNA is then denatured, and the cycle starts again for 25-35 cycles to amplify enough product for detection.

Semi-quantitative PCR was carried out using GoTaq green master mix. For each reaction, 1µl of cDNA (40ng) was added to a reaction tube with 19µl of PCR master mix. The master mix contained 10µl 2x GoTaq green master mix, 2µl of 10µM upstream and downstream primers (10nM final concentration), and 6µl of

nuclease free water. Thermal cycling was then carried out using a Px2 (Thermo Scientific) thermocycler. The PCR program was optimised to the primers (Table 2.3) used. The standard program was as follow:

Initial denaturing	-	95°C	1 minute	
Denature	-	95°C	1 minute	30-35 cycles
Anneal	-	X°C (based on primers)	1 minute	
Elongate	-	72°C	1 minute	
Final elongation	-	72°C	5 minutes	
Hold	-	4°C	∞	

PCR products were then separated on an agarose gel (1-2%, dependent on amplicon size), as described in 2.7.6, and visualised using a UV box.

Oligo ID	5'-3' sequence	Comments
rAdh1 US **rAdh1 DS**	CAGCCTAAGGGAGCTTTGCT CGATTTTGGCCACCGCTATG	Will amplify 130bp fragment from rat alcohol dehydrogenase (NM_019286.4).
rAdh4 US **rAdh4 DS**	CTGTGCAGGAACAGCTCAGA TTCCCTTTACAGAACGGCCC	Will amplify 143bp fragment from rat alcohol dehydrogenase (NM_017270.2).
rAdh5 US **rAdh5 DS**	CCCGAAGCTGGTGTCTGAAT GGTCGAAGGACAGATTGCCA	Will amplify 77bp fragment from rat alcohol dehydrogenase (NM_001126120.1).
rAdh6a US **rAdh6a DS**	GTCACCGACTGTCTCAACCC TGTGGTTGCAGGAGTTCCAA	Will amplify 145bp fragment from rat alcohol dehydrogenase (NM_001106475).
rAdh6 US **rAdh6 DS**	CCAAAGCGAGCTTCCCAAGG GGCCACTTCGATCTCCTCAA	Will amplify 113bp fragment from rat alcohol dehydrogenase (NM_001012084) Also X4 (XM_008761508.1), X6 (XM_006233375.2) and X7 (XM_006233374.1) transcript variants.
rAldh1a1 US **rAldh1a1 DS**	TGCTTTCTGTCGTAGCTCCC CGAGAAGCAGTTCAAGGGGT	Will amplify 100bp fragment from rat aldehyde dehydrogenase (NM_022407.3).
rAldh1a2 US **rAldh1a2 DS**	AGGCTCTCATGGTGTCCTCT TCCCGTAAGCCAAACTCACC	Will amplify 139bp fragment from rat aldehyde dehydrogenase (NM_053896.2).
rAldh2 US **rAldh2 DS**	ACGGAAGTGAAGACGGTCAC CCAAGACGCTTTGGTGAAGG	Will amplify 163bp fragment from rat aldehyde dehydrogenase (NM_032416.1) Also amplifies transcript variant X1 to give 192bp (XM_006249385.2).
rAldh3a1 US **rAldh3a1 DS**	GAAGCTTGGAGGAGGCCATT GCTGGATGTCTCTGCGATCA	Will amplify 113bp fragment from rat aldehyde dehydrogenase (NM_031972.1).
rAldh3a2 US **rAldh3a2 DS**	ACTCAGGTACCCTCCCAACA TCACAGCTGATCCTTGACGA	Will amplify 145bp fragment from rat (NM_031731.2).
rCD36 US **rCD36 DS**	TCCTCGGATGGCTAGCTGATT GCACTTGCTTCTTGCCAACT	Will amplify 187bp fragment from rat CD36 molecule/thrombospondin receptor (NM_031561.2).
rSlc27a1 US **rSlc27a1DS**	CTGCGAGAACCCGTGAGGAA ACCCACGTACACACCGAAC	Will amplify 166bp fragment from rat solute carrier family 27 (fatty acid transporter) Slc27a1 (NM_053580.2).
rSlc27a2 US **rSlc27a2 DS**	GAATGTTTACGGTGTGCCCG GGCAGGTACTCCGAGATGTG	Will amplify 123bp fragment from rat solute carrier family 27 (fatty acid transporter) Slc27a2 (NM_031736.1).
rSlc27a4 US **rSlc27a4 DS**	GCAACTGTAGCTTGGGCAAC AGCGGATGGGGTACACAAAG	Will amplify 87bp fragment from rat solute carrier family 27 (fatty acid transporter) Slc27a4 (NM_001100706.1).
rSlc27a5 US **rSlc27a5 DS**	CATTCGATGGGGCTTGTCCT ACTGTCACACTGTACTGCCG	Will amplify 122bp fragment from rat solute carrier family 27 (fatty acid transporter) Slc27a5 (NM_024143.2).
rAcsl US **rAcsl DS**	GCAGGGGTGCTTCACTTACT CCGATGATTTCCACCCCACA	Will amplify 249bp fragment from predicted rat) acyl-CoA synthetase long-chain family member 1 transcript variant X6 Acs1 (XM_006253125.2) and 7 other transcript variants.
rAcs4 US **rAcs4 DS**	CTACTGGAAGAGTTGGCGCT GACACGTACTCTCCGGCTTG	Will amplify 301bp fragment from predicted rat) acyl-CoA synthetase long-chain family member 4 Acs4 transcript variant X4 (XM_006257316.2) and 4 other transcript variants.
rAcs5 US	TGACCCCAAAGGAGCTATGC	Will amplify 134bp fragment from rat Acs5 (NM_053607.1).

rAcs5 DS	ACATATGGGCCAAGGGAAGG	
rAcaca US **rAcaca DS**	GGGAACATCCCCACGCTAAA CATGCGTTGACAAGGTGGTG	Will amplify 126bp fragment from rat acetyl-CoA carboxylase alpha Acaca (NM_022193.1).
rAcacb US **rAcacb DS**	GGTCCTGATTGCCTCTCACC ACGCCATACAGACGACCTTG	Will amplify 197bp fragment from rat acetyl-CoA carboxylase beta Acacb (NM_053922.1) and 6 other transcript variants.
rAcly US **rAcly DS**	ATCCGGGGAGTTGGGGTAAG CTTTGCCGGTCTGCTCTGAA	Will amplify 125bp fragment from rat ATP citrate lyase Acly transcript variant 2 (NM_001111095.1) and also transcript variant 1.
rMpc1 US **rMpc1 DS**	ATGAGTACGCACTTCTGGGG AATGAGCTGAGCGACTTCGT	Will amplify 213bp fragment from rat mitochondrial pyruvate carrier Mpc1 (NM_133561.1).
rMpc2 US **rMpc2 DS**	GTGCTGATGGCTACAGGGTT ACTGGATTCCTTTAGATTTGAGTTC	Will amplify 163bp fragment from rat mitochondrial pyruvate carrier Mpc2 (NM_001077643.1).
rSlc25a1 US **rSlc25a1 DS**	CCAAGGAGACAACCCCAACA AATACGATGGCCACGTCCAG	Will amplify 255bp fragment from rat mitochondrial citrate carrier Slc25a1 (NM_017307.3).
rFasn US **rFasn DS**	CCCTCACATCAAGTGGGACC TGGTACACTTTCCCGCTCAC	Will amplify 387bp fragment from rat fatty acid synthase (NM_017332.1).
rPlin1 US **rPlin1 DS**	GTGGCTCTCAGCTGCATGT ATTCTCCTGTTCAGGGAGGTCT	Will amplify 87bp fragment from rat perilipin 1 Plin1 (NM_001308145.1). May also amplify variant X1 (XM_008759499.1) yielding a 143bp fragment.
rPlin2 US **rPlin2 DS**	CAGTACTTGCCGCTCACTCA GTGCACATTCTTCCTGGCGAA	Will amplify 240bp fragment from rat perilipin 2 (Adrp) Plin2 (NM_001007144.1) intrinsic lipid storage droplet protein. Also amplifies X1 and X3 transcript variants.
rPlin3 US **rPlin3 DS**	AGCAGTGGATGTGACCTGTG TGTGGCAATCAGGGCTAGTT	Will amplify 202bp fragment from predicted rat Plin3 (XM_001061015.2) cDNA.
rPlin4 US **rPlin4 DS**	ATGGGACTAGAGGTTCCCCC GGAGATGGAGGGACAGGAGT	Will amplify 166bp fragment from 47 predicted rat Plin4 transcript variants (e.g. XM_006244382.2).
rPlin5 US **rPlin5 DS**	GCTCTACACAGCAGGATGTCCG CAGCTCCTCTGATTTGCCCAG	Will amplify 534bp fragment from rat Plin5 (NM_001134637.1). Will also amplify transcript variant X1 (XM_008766770.1) yielding a 498bp fragment.
rFXR US **rFXR DS**	TGGAGTGCTAACAGAGCACG TTCGGAAGAAACCTTTGCAGC	Will amplify 383bp fragment from rat nuclear receptor subfamily 1, group H, member 4 Nr1h4, FXR, (NM_021745.1). Also amplifies X1, X2 and X3 transcript variants.
rLXRα US **rLXRα DS**	CTGCGATCGAGGTGATGCTT CTCTGAATGGACGCTGCTCA	Will amplify 392bp fragment from rat nuclear receptor subfamily 1, group H, member 3 Nr1h3, LXRα, (NM_031627.2). Also amplifies 4 other transcript variants.
rLXRβ US **rLXRβ DS**	GGCATCCACCATCGAGATCAT AAGGAAGCGTCCATCTGCAA	Will amplify 529bp fragment from rat nuclear receptor subfamily 1, group H, member 2 Nr1h2, LXRβ, (NM_031626.1).
rPNPLA3 US **rPNPLA3 DS**	CTCACCAGAGTGTCCGATGG CACAGGGACGTTGTCACTCA	Will amplify 174bp fragment of rat PNPLA3 (NM_001282324.1). Also, transcript variant X1.
rLYPLA2 US **rLYPLA2 DS**	GGTGCCTGGTGATTTGGGTA CCACGTTCCTTTTGCTTGGG	Will amplify 278bp fragment of rat LYPLA2 (NM_001004277.2).
rCYP2E1 US **rCYP2E1 DS**	TCGACTACAATGACAAGAAGTGT CAAGATTGATGAATCTCTGGATCTC	Will amplify 525bp fragment of rat CYP2E1 (NM_031543).
hHNF4α US **hHNF4α DS**	GGACATGGCCGACTACAGTG CTCGAGGCACCGTAGTGTTT	Will amplify 192bp fragment of human HNF4α (NM_004133.4). Also 6 other transcript variants.
hSOX9 US **hSOX9 DS**	AGGAAGTCGGTGAAGAACGG TCCCTCCCGGGAAGCATAAA	Will amplify 261bp fragment of human SOX9 (NM_000346.3).
hSOX17 US **hSOX17 DS**	CACGACTTGCCCAGCATCTTG CAAGGGCGAGTCCCGTATC	Will amplify 132bp fragment of human SOX17 (NM_022454.3).
hTFF1 US **hTFF1 DS**	GTGCAAATAAGGGCTGCTGT CCGAGCTCTGGGACTAATCA	Will amplify 177bp fragment of human trefoil factor 1 TFF1 (NM_003225.2).
hCD24 US **hCD24 DS**	GAACAAAGCAAGGGCTTCGGG TAGTTGGATTTGGGGCCAACC	Will amplify 402bp fragment of human CD24 (NM_001291737.1) and variant X1 (XM_024446293.1).
hCD133 US **hCD133 DS**	TGCCTTGAGTGAATGACCCC GCCCATTTTCCTTCTGTCGC	Will amplify 660bp fragment of human CD133 (NM_006017.2). Also 24 other transcript variants.
hrmGAPDH US **hrmGAPDH DS**	TGACATCAAGAAGGTGGTGAAG TCTTACTCCTTGGAGGCCATGT	Will amplify 243bp of rat (NM_017008), mouse (NM_008084) or human (NM_002046) of glyceraldehyde 3 phosphate dehydrogenase.
hrm18S US **hrm18S DS**	CCCGAAGCGTTTACTTTGAA CCCTCTTAATCATGGCCTAC	Will amplify 136bp fragment of rat, mouse and human 18S rRNA.

Table 2.3: DNA oligonucleotide sequences used in RT-PCR and SYBR green Realtime PCR.

2.7.7 Agarose gel electrophoresis

Agarose gel electrophoresis was used to separate DNA fragments. The sugar phosphate backbone of DNA is negatively charged and therefore migrate towards the positive electrode when an electric field is applied across the agarose gel. Larger fragments migrate slower as they experience more resistance in a polymerized agarose matrix.

Agarose gels were made with 1-2% (w/v) agarose in TAE buffer (40mM Tris, 20mM acetic acid, 1mM EDTA). In general, 1.5% gels were used, however for amplicons smaller than 400bp, 2% was used. The gel mixture was boiled in the microwave until dissolved and left to cool to approximately 50°C. Once cool enough, 1µl/100ml of ethidium bromide was added. Ethidium bromide is an intercalating agent that fluoresces when expose to UV light, allowing for visualisation. The gel was poured into a gel cast with a sample comb and left to set at room temperature.

Once set, the gel was placed into a gel tank filled with 1 x TAE buffer and the samples were loaded into the wells created by removing the sample comb. 100bp and 1kb DNA ladders were also loaded so that fragment size to be determined. Gels were then run for approximately 45-60 minutes at 90 volts and visualised using a UV box.

2.7.8 *Quantitative real-time PCR*

2.7.8.a Real-time PCR using SYBR green

SYBR green is a dye that fluoresces when bound to double stranded DNA, by measuring this fluorescence it is possible to determine the amount of target DNA in a sample (Figure 2.4A). A master mix was made containing; 5µl of PowerUp SYBR Green Master Mix (Applied Biosystems), 500nM of forward and reverse primers, and nuclease free water (total volume made up to 9µl before cDNA addition). 9µl of the master mix was added to each well of an optical 48 or 96 well reaction plate. 1µl of 10ng/µl cDNA was added to each well. The plate was sealed using optical film (Applied Biosystems) centrifuged at 300g for 1 minute to collect the samples to the bottom of the well. Plates were then run using a StepOne real-time PCR machine (Applied Biosystems) and accompanying software. The general method was as follows:

Initial denaturing	-	50°C	2 minutes	
		95°C	10 minutes	
Denature	-	95°C	15 seconds	40 Cycles
Anneal	-	X°C (based on primers)	1 minute	

Fluorescence was measured during the elongation phase and a melt curve analysis was run post cycling to check primer specificity. Relative amounts of target DNA were calculated using the comparative ΔΔCt

method and 18S ribosomal RNA (18S rRNA) was used as the housekeeping control. Relative expression was calculated as follows:

$$\Delta C_T = C_T target - C_T\ 18S\ rRNA$$

$$\Delta\Delta C_T = \Delta C_T\ sample - \Delta C_T\ control$$

$$Fold\ change = 2^{-\Delta\Delta C_T}$$

Standard deviation was calculated as follows:

$$STDev = \sqrt{STdev\ \Delta C_T target^2 + STdev\ \Delta C_T 18S\ rRNA^2}$$

2.7.8.b Real-time PCR using Taqman

Taqman based real-time PCR is considered to have higher specificity than SYBR Green based detection and uses fluorogenic probes that are specific to target genes. Taqman based detection works by the probe (containing a fluorescent reporter and a quencher at 5' and 3' ends respectively) annealing downstream from a primer site of a target (Figure 2.4B). The probe is then cleaved by Taq DNA polymerase, separating the reporter and quencher dye, increasing the fluorescence of the reporter. The probe is completely removed from the target, allowing the extension of the primer and therefore the continuation of the PCR process.

The protocol for Taqman based real time PCR is similar to SYBR Green. A master mix was made containing; 10µl LightCycler TaqMan Master Mix (Roche), 0.5µl TE buffer, 0.5µl probe, 7µl PCR grade water (total volume made up to 18µl before cDNA addition). 18µl of the master mix was added to each well of an optical 48 or 96 well reaction plate. 2µl of 10-100ng/µl cDNA was added to each well. The rest of the plate set up, program (with no melt curve) and comparative ΔΔCt calculation was the same as described in 2.7.7a.

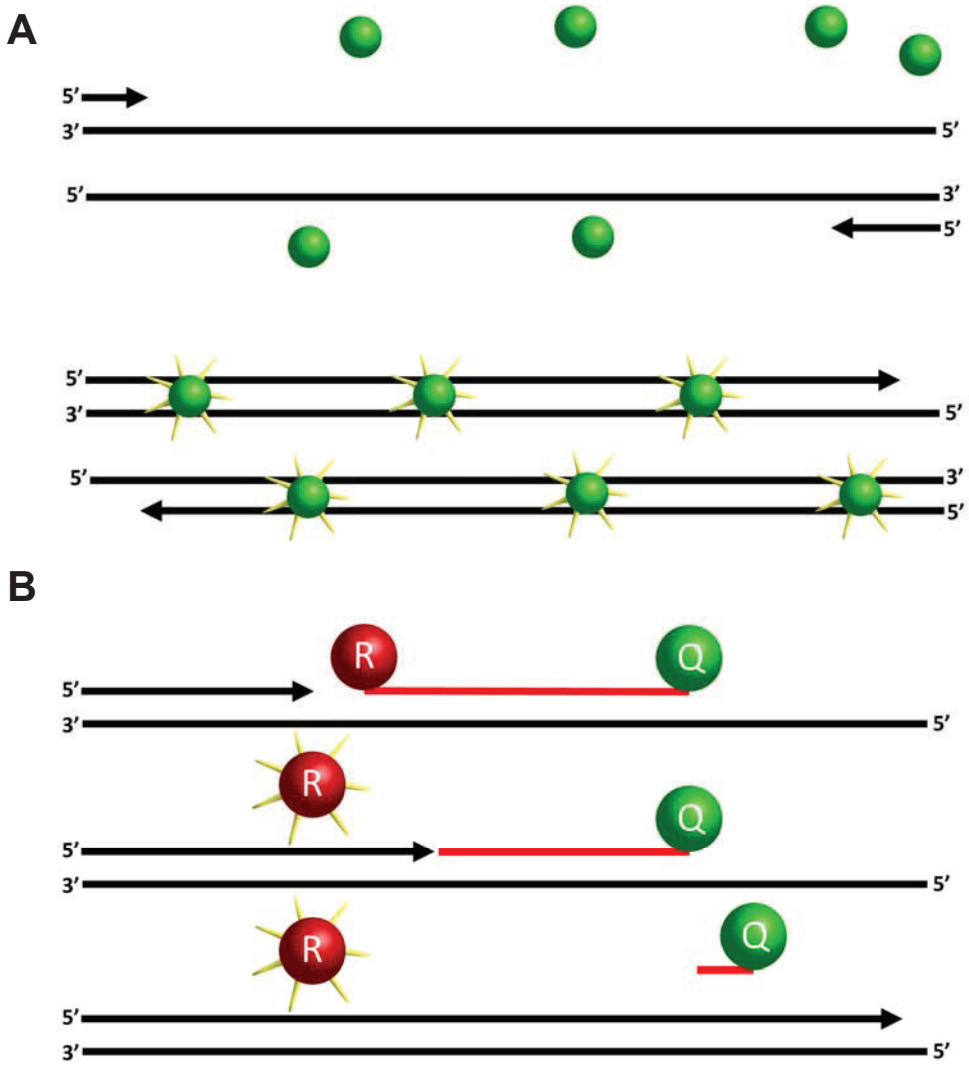

Figure 2.4: Real-time PCR chemistry. (A) SYBR green and **(B)** Taqman. See text for detail.

2.8 Protein isolation and analysis

2.8.1 Cell lysate preparation

Cells were washed with PBS and then scraped in ice cold PBS and transferred into a fresh microcentrifuge tube. Samples were centrifuged at 16,000g for 5 minutes, and the supernatant removed, and the pellet resuspended in an appropriate volume of 20mM Tris (pH 7.5). Samples were then either stored at -80^{o}C or protein content was determined by Lowry assay (2.8.3) or by Bradford assay (2.8.4).

2.8.2 Tissue lysate preparation

Tissue was flash frozen in liquid nitrogen and stored at -80^{o}C until required. Samples were thawed on ice and washed in PBS to remove any blood. The sample was homogenised using a hand homogeniser and sonicated in an appropriate volume of 20mM Tris (pH 7.5). Samples were then either stored at -80^{o}C or protein content was determined by Lowry assay (2.8.3) or by Bradford assay (2.8.4).

2.8.3 Lowry assay

The Lowry assay was used to determine protein concentration, using BSA as a standard. The BSA standards were prepared ranging from 0-20mg/ml in 20mM Tris (pH 7.5). 50µl of dH_2O was added to 5µl of sample and standard. ABC buffer was prepared, Lowry A (2% (w/v) Na_2CO_3 and 4% (w/v) NaOH), Lowry B (2% (w/v) sodium tartrate), Lowry C (1% (w/v) $CuSO_4$) were combined at a ratio of 100:1:1 (v:v:v). 1ml of ABC buffer was added to each sample and standard, vortexed and incubated at room temperature for 10 minutes. Folin-ciocalteu reagent was diluted 1:1 (v:v) with dH_2O and 100µl was added to each sample and standard, mixed and incubated at room temperature for 15-20 minutes. The absorbance at 750nm was measured using a spectrophotometer (Themo labsystems multiskan spectrum), using the 0mg/ml standard as the blank. Protein concentration was then determined from the BSA standard curve.

Some experiments in 24- and 6-well plates were normalised to protein concentration. 1ml of ABC buffer was added directly to each well and the procedure was continued as described above.

2.8.4 Bradford assay

Bradford assays were also used to determine protein concertation. BSA was used as a standard, ranging from 0-1.4mg/ml in distilled water. Protein samples were diluted 1:20 in dH_2O. 5µl of standards and samples were transferred into a flat bottom 96-well plate. 250µl of Bradford reagent was added to each well and incubated for 10 minutes. Absorbance was measured at 750nm using a spectrophotometer, using the 0mg/ml standard as a control. Protein concentration was then determined from the BSA standard curve.

Some experiments carried out in 96 well plates were normalised to protein concentration. Cells were lysed by incubating the cells with lysis buffer (250mM Tris (7.4) + 0.05% Triton) at room temperature on an

orbital shaker for 10 minutes. 250µl of Bradford reagent was added to each well and protein concentration determined as described above.

2.8.5 Sodium-dodecyl sulphate polyacrylamide gel electrophoresis (SDS-PAGE)

SDS-PAGE was used to separate proteins based on their molecular weight. Two different polyacrylamide gels different were used; a stacking gel (4%) and a resolving gel (9%). The use of a stacking gel improves resolution as they proteins accumulate at the stacking/resolving interface. A resolving gel was made using; 9% acrylamide/bis (w/v) (using acrylamide/bis-acrylamide, 37.5:1 ratio), 375mM Tris-HCL (pH 8.8), 0.1% (w/v) SDS, 0.05% (w/v) ammonium persulphate (APS) and 0.05% (v/v) tetramethylethylenediamine (TEMED). APS and TEMED were added last to catalyse polymerisation. The resolving gel solution was transferred into a 0.75mm glass plate cast, and a layer of isopropanol was pipetted on top of the gel to straighten the interface between the two gels. Once the gel was set, the isopropanol was removed and the 4% gel (4% (w/v) acrylamide, 125mM Tris buffer pH 6.8, 0.1% (w/v) SDS, 0.05% (w/v) APS and 0.1% (v/v) TEMED) was transferred on top of the 9% gel. Bubbles were removed, and a sample comb was inserted into the cast. Once the gel set, the comb was removed, and the cast was inserted into an electrophoresis tank containing electrophoresis running buffer (ERB, 25mM Tris, 0.1% (w/v) SDS and 192mM glycine (pH 8.3)).

Protein samples were diluted at 1:1 (v/v) in reducing loading buffer (120mM Tris (pH 6.8), 20% glycerol (v/v), 3.9% (w/v) SDS, 0.74% (w/v) bromophenol blue and 20mM DTT), the loading buffer contains SDS that binds to polypeptides allowing their migration though the polyacrylamide gel towards the anode. Samples were incubated at 95^{o}C for 5 minutes to denature the protein, and thereby losing their secondary, tertiary and quaternary structures. 10-20µg of protein was loaded per well, as well as a protein ladder of known molecular weights (colour pre-stained protein standard, molecular weight 11-245kDa, New England Biolabs). Electrophoresis was initially run at 100V until the migrating front had reached the interface. The voltage was then increased to 160V until the samples had reached the bottom of the gel.

2.8.6 Western blotting

Proteins separated by SDS-PAGE were detected by immunodetection using Western blotting. Filter paper and nitrocellulose membrane (Fisher) were prechilled in transfer buffer (25mM Tris, 192mM glycine and 20% (v/v) methanol, pH 8.3). The SDS-PAGE polyacrylamide gel was transferred onto the nitrocellulose membrane and sandwiched between filter paper and scouring pads in a transfer cassette and the cassette

placed into a tank filled with prechilled transfer buffer and an ice pack. Transfer was run at 100V for 2 hours.

Once transfer was complete, the nitrocellulose membrane was washed in TBS-T (200mM NaCl, 20mM Tris (pH 7.4) and 0.05% (v/v) Tween 20, pH 7.4). The membrane was blocked with 3% (w/v) skimmed milk powder in TBS-T for 1 hour at room temperature. After blocking, the blocking solution was removed, and the membrane was washed 3 times in TBS-T and incubated overnight a 4^{o}C with primary antibody in 0.3% (w/v) skimmed milk powder in TBS-T. For the primary antibodies used and dilutions, see Table 2.4. The primary antibody was removed, and the membrane washed 3 times in TBS-T and incubated in the appropriate secondary antibody (Table 2.4) for 1 hour at room temperature. The secondary antibody was removed, and the membrane washed 3 times.

Proteins were visualised using the binding of secondary antibody to the chemillumenscent Pierce ECL Western blotting substrate (Thermo Scientific). Equal volumes of reagents 1 and 2 were mixed and added to the membrane and incubated for 1 minute at room temperature. Excess reagents were removed from the membrane and the membrane was saran wrapped in a film cassette. CL-Xposure film (Thermo Scientific) was exposed to the membrane in a dark room and developed using an automated developer (RP X-OMAT, Kodak, Hertfordshire, UK).

Antigen	**Approximate molecular weight (kDa)**	**Antibody raised in**	**Dilution**	**Source (cat#)**
Primary antibodies				
β actin	44	Mouse	1 in 3000	Sigma (A2228)
CYP2E1	50	Rabbit	1 in 3000	Abcam (ab28146)
CYP3A4	52	Rabbit	1 in 2000	Abcam (ab155029)
HA Tag	variable	Rabbit	1 in 4000	Abcam (ab9110)
LXR	50	Mouse	1 in 1000	Abcam (ab41902)
P450 reductase	78	Rabbit	1 in 1000	Abcam (ab13513)
Secondary antibodies				
Anti-mouse HRP	-	Goat	1 in 3000	Dako (P0447)
Anti-rabbit HRP	-	Goat	1 in 3000	Sigma (A0545)

Table 2.4: Specifications and source of primary and secondary antibodies.

2.9 Histochemistry and staining

2.9.1 Paraffin embedded section preparation

Tissue samples were fixed in 10% formalin in PBS for 24 hours, then transferred into 70% ethanol until processed. Samples were processed and embedded by cellular pathology at the Royal Victoria Infirmary and cut by microtome onto Superfrost Plus slides (Fisher) at 5µm in thickness.

2.9.2 Haematoxylin and eosin staining (H&E)

H&E staining was used to examine the histology of tissue samples. Sections were dewaxed in xylene for 10 minutes, then rehydrated in a series of ethanol washes (100% → 90% → 70%) and dH_2O. Sections were then stained with haematoxylin, a nuclear stain, for 1 minute before being developed in Scott's tap water (2% (w/v) $NaHCO_3$ and 0.35% (w/v) $MgSO_4$ in dH_2O) for 10 seconds. The sections were then washed in dH_2O and counterstained with eosin, a cytoplasmic stain, for 1 minute and washed in dH_2O. Dehydration of sections was achieved through a series of ethanol washes (50%→70%→95%→100%) and xylene. Sections were then mounted using DPX and left to dry before imaging.

2.9.3 Periodic acid–Schiff stain (PAS)

Periodic acid–Schiff stain (PAS) is a stain used for the detection of polysaccharides such as glycogen. For each sample two sections were deparaffinised and hydrated as described in 2.9.2. One section was incubated in warm diastase (5mg/ml) for 15 minutes at 37^{o}C and washed in dH_2O. Both sections were then immersed in 0.5% periodic acid for 5 minutes and washed in dH_2O. Sections were immersed in Schiff's reagent for 15-30 minutes, until a deep magenta colour is observed. Schiff's was then washed from the sections in dH_2O for 5 minutes before being counterstained in haematoxylin for 1 minute, developed in Scott's tap water for 30 seconds and washed once more in dH_2O before being dehydrated and mounted as described in 2.9.2.

2.9.4 Transmission electron microscopy

Cells were trypsinised and transferred to a microcentrifuge tube before being centrifuged at 16000g for 5 minutes. The pellet was then fixed in 2% glutaraldehyde in cacodylate buffer. EPCAM+ve progenitor cells were left in Matrigel and fixed in fixed in 2% glutaraldehyde in cacodylate buffer. The cells were then

processed and embedded in resin by the Newcastle University Electron Microscopy Research Service. Samples were viewed using a Philips CM100 transmission electron microscope (TEM).

2.9.5 Image analysis

Stained sections were imaged using the a Lecia bright field microscope (Milton Keynes, UK) using the accompanying software. Slides were scanned using the Lecia (MODEL) at x20 magnification.

2.10 Enzyme assays

2.10.1 Alcohol dehydrogenase assay

Alcohol dehydrogenase activity was calculated by measuring the conversion of NAD to NADH by measuring the increase in absorbance at 340nm (**Clemens 1995**). Cells were washed in PBS and lysed in 1% Triton X-100 (v/v) in PBS and sonicated briefly. 250µl of lysate was added to 1ml of alcohol dehydrogenase reaction mix (0.5M Tris HCl (pH7.4) and 3mM NAD) prewarmed to 37^{o}C Background activity was measured before 2.9µl of ethanol (final concentration of 10mM) was added and mixed briefly. Absorbance was then measured at 340nm. 10mM of pyrazole was used to inhibit the reaction. Results were expressed as nmol NADH generated/minute/mg total protein.

2.10.2 CYP450 assays

Cytochrome P450 activity was measured using the luminescent CYP assay system (Promega). The assay works by providing proluciferins that act as a substrate for CYP450s. The proluciferin is converted into D-luciferin which can be detected as light when a luciferin detection reagent is used. Cells were resuspended in 100mM KPO_4, with an aliquot taken for protein determination. 12.5µl of cell suspension was added to 12.5µl of proluciferin substrate (the substrate is specific for the CYP system being used, see Table 2.5). 25µl of 3mM NADPH in 50mM Tris-HCl (pH 7.4) were added to the mixture (final concentration of 1.5mM) and incubated at room temperature for 30 minutes. 50µl of luciferin detection reagent was added to the mix and allowed to equilibrate for 20 minutes before luminescence was measured on a luminometer.

P450 Enzyme	Substrate	Volume (µl) added to 100mM KPO_4 (total volume = 12.5µl)
CYP2D6	Luciferin-ME EGE	0.15
CYP3A4	Luciferin-IPA	0.05

Table 2.5: CYP P450 enzyme substrates for luminescent assays.

2.10.3 Serum activity assays

Blood was collected from animals by tail vein bleed or after culling. The blood was left to clot at room temperature for approximately 1 hour before being centrifuged at 16000g for 5 minutes and the serum was transferred into a fresh tube. Alanine transaminase (ALT, a biomarker of hepatocyte injury) and alkaline phosphatase (ALP, a biomarker of cholangiocyte injury) activities were analysed by the Royal Victoria Infirmary Clinical Biochemistry Department, Newcastle Upon Tyne.

2.11 Total P450 dual-beam spectroscopy

Reduced CYP450 has an absorbance peak at 450nm, making it possible to calculate the total CYP450 concentration in a sample by measuring the change between reduced and oxidised samples. To measure haem-bound CYP450, cell pellets were resuspended in 2ml of TST buffer (20mM Tris, 250mM sucrose, and 0.01% (v/v) triton X-100, pH 7.4). A sample was removed for protein determination by Lowry assay as described in 2.8.3. 1-5mg of sodium dithionite was added to the sample and mixed by inversion. The solution was then split into 2 quartz cuvettes. One cuvette was bubbled with carbon monoxide for 30 seconds at a rate of around 1 bubble per second. The absorbance difference between the two cuvettes was measured between 400-500nm. Total CYP concentration was then determined using the following equation:

$$Total\ CYP450\ concentration\ (M) = \frac{OD_{450} - OD_{490}}{91000 M^{-1} cm^{-1}}$$

2.12 Cell viability assays

2.12.1 3-(4,5-Dimethylthiazol-2-Yl)-2,5-Diphenyltetrazolium Bromide (MTT) assay

MTT is a simple coulometric assay that can be used as an indicator of cell viability. In viable cells MTT is converted to the purple coloured product, formazan, by mitochondrial reductases. The colour production can be quantified by the measurement of absorbance.

Culture medium was removed from cells and the cells were washed in PBS. 5mg/ml MTT in PBS was added 1:10 (v/v) to fresh cell medium. The MTT medium was added to the cells and incubated for 1-3 hours (dependent of cell type). The MTT cell medium was discarded and isopropanol was added to each well. The plate was incubated at room temperature on an orbital shaker for 15 minutes before absorbance at 570nm and 690nm was measured. The absorbance at 690nm was subtracted from that at 570nm and cell viability calculated as a percentage of the control cells.

2.12.2 Cell titre-glo 2.0

Cell titre-glo 2.0 (Promega) is an assay that is used to determine cell viability by the quantifying that amount of adenosine triphosphate (ATP) present. The assay works by mono-oxygenating luciferin by a luciferase enzyme in the presence of ATP that is provided by the lysed cell. This generates a luminescent output that can be measured.

ATP standards of 0-10µM were prepared in cell culture medium. After desired treatment, cell titre glo 2.0 reagent was added directly to cells in cell culture medium at an equal volume to that of culture medium present (and to standards). The standards and samples were then mixed on an orbital shaker for 2 minutes and incubated for a further 10 minutes to stabilise the luminescent signal. The luminescence was then measured on a luminometer.

2.12.3 RealTime-Glo™ annexin V apoptosis and necrosis assay

RealTime-Glo™ Annexin V Apoptosis and Necrosis Assay (Promega) measures exposure of phosphatidylserine on the outer leaflet of cell membranes as an indicator of apoptosis. Phosphatidylserine brings together Annexin V-LgBiT and Annexin V-SmBiT (NanoBiT) fusion proteins that form a functional luciferase that is measurable using a luminometer. In addition to this, necrosis can also be detected when

membrane integrity is compromised, and a DNA binding fluorescent dye enters the cell producing a fluorescent signal.

Cells were dosed with equal volumes of medium containing compounds of interest at a 2X desired concentration and with 2X detection reagent (annexin V nanobit substrate, $CaCl_2$, necrosis detection reagent, annexin V-SmBiT and annexin V-LgBiT), giving a final concentration of both of 1X. Luminescence and fluorescence ($485nm_{Ex}/530nm_{Em}$) was measured every 1-6 hours over 48 hours and returned to the CO_2 incubator.

2.12.4 ApoTox-Glo™ triplex assay

The ApoTox-Glo™ triplex assay (Promega) measures three different endpoints; cell viability, caspase activation, and cytotoxicity. Cell viability is measured by a substrate that can enter viable cells and is cleaved by proteases to give a fluorescent signal. Cytotoxicity is measured by a second substrate that is cell impermeable and is cleaved by proteases that have been released by cells that have lost their membrane integrity. Caspase activity is measured by using a luminogenic substrate for caspase 3/7 where caspase cleavage of the substrate generates and luminescent signal.

After cells had been treated for desired time with compounds of interest, 20µl of viability/cytotoxicity reagent (made by adding 10µl of GF-AFC Substrate and bis-AAF-R110 Substrate to 2ml of assay buffer) and mixed on the orbital shaker for 30 seconds before being incubated for 30 minutes at 37°C. Fluorescence was then measured to determine viability ($400_{Ex}/505_{Em}$) and cytotoxicity ($485_{Ex}/520_{Em}$). 100µl of caspase-glo 3/7 reagent was added to each well and mixed on the orbital shaker for 30 seconds before being incubated at room temperature for 30 minutes. Luminescence was then measured using a luminometer.

2.12.5 Apoptotic DNA isolation

The isolation of apoptotic DNA can be used to visualise the fragmentation of DNA that occurs during apoptosis on an agarose gel. Cells were washed in PBS, scraped in ice cooled PBS, centrifuged at 16000g and the supernatant was discarded. The pellet was resuspended in 50µl of apoptosis lysis solution (1% (v/v) NP40, 20mM EDTA, 50mM Tris-HCl, pH 7.5), incubated at room temperature for 5 minutes before being centrifuged at 16000g for 5 minutes. The supernatant was transferred into a fresh microcentrifuge tube and the process was repeated with the pellet but with 10µl of apoptosis lysis buffer. The supernatant was combined and 11µl of 10% SDS and 5µl of 10mg/ml RNAse A was added. The sample was incubated

for 2 hours at 56°C. The samples were then digested with 12.5µl of 20mg/ml proteinase K for 2 hours at 37°C. 62µL of 10M ammonium acetate and 310µl of ice cooled 100% ethanol was added to the sample and incubated overnight at -80°C. The next morning the samples were centrifuged at 16000g for 15 minutes at 4°C and the supernatant removed. The pellet was washed using ice cooled 70% ethanol before being centrifuged at 16000g for 15 minutes at 4°C. All ethanol was removed, and the sample was air dried for 10 minutes. The apoptotic DNA was resuspended in 30-50µl of DNA loading solution and 10µl was run on a 1.5% agarose gel (as described in 2.7.6) for 45-60 minutes at 80V.

2.13 Lipid staining and determination

2.13.1 Oil red o staining

Oil red o is a staining method used to visualise and quantify neutral lipids. Oil red o solution was prepared by dissolving 84mg of oil red o powder in 24ml of isopropanol and left to incubate overnight at room temperature. The solution was filtered, diluted with 18ml of distilled water and incubated overnight at 4°C before being filtered twice.

Cells were washed in PBS and fixed in 3.7% formaldehyde for 30 minutes. The formaldehyde was removed, and the cells washed 3 times in PBS. At this point, blank wells were incubated twice for 10 minutes with isopropanol and washed with PBS. Oil red o solution was added to cells and incubated for 2-5 minutes. The stain was removed and washed twice with PBS. Images of cells were taken using a bright field microscope camera (Kern ODC-82 microscope camera). Isopropanol was added to each well to extract the dye and the absorbance was measured using a spectrophotometer at 515nm. The cells were washed with PBS then protein concentration was determined by Lowry assay as described in 2.8.3.

Linoleic acid and oleic acid were used as positive controls for oil red o staining. 200mM linoleic and oleic acid solution was made in ethanol at a ratio of 7:7:86 (v:v:v). 0.5g of essentially fatty acid free BSA was dissolved in 10ml of serum free medium and heated to 60°C. 50µl of 200mM fatty acid solution was added to heated BSA containing medium to give a final concentration of 1mM (ethanol used as control). The solution was then filter sterilised (0.45µm) before use.

2.13.2 LipidTOX staining

HCS LipidTOX Red Phospholipidosis Detection Reagent (Thermo Scientific) was used to stain phospholipid accumulation with a fluorescent dye. LipidTOX staining was carried out to manufacturer's instructions. 24-48 hours before end of treatment, LipidTOX reagent was added to give a final concentration of 1X. Cells were then washed in PBS, fixed in 3.7% formaldehyde in PBS for 30 min, washed again in PBS and then incubated with 20µM 4'6'-diamino-2-phenylindole (DAPI) for 10 min to stain DNA. Cells were then washed once more in PBS and stored at 4^{o}C in PBS protected from light. Cells were imaged using a Nikon Spinning Disk confocal microscope and fluorescence was measured using a fluorescent plate read to quantify LipidTOX staining ($595_{Ex}/615_{Em}$) and normalised to DAPI staining ($360_{Ex}/460_{Em}$) to control for cell number/well.

2.13.3 Chloroform methanol extraction

Lipids were extracted from cells using a chloroform/methanol extraction. Cells were washed in PBS and scraped in ice-cooled PBS, centrifuged at 16,000g for 5 minutes and the supernatant discarded. The pellet was resuspended in ice-cooled 20mM Tris (pH 7.4) with 100mM KCl and sonicated. For tissue, frozen samples were thawed on ice before being homogenised using a hand homogeniser in 20mM Tris (pH 7.4) with 100mM KCl and sonicated. An aliquot was then removed for protein determination by Lowry assay (as described in 2.8.3). 1 volume of sample was added to 10 volumes of chloroform/methanol (CM) extraction buffer (chloroform:methanol, 2:1 ratio (v/v)). Samples were vortexed and centrifuged for 1 minute a 13,000g. The lower organic phase that contains the lipid was transferred into a fresh tube and another 10 volumes of CM extraction buffer was added to the remaining upper aqueous layer and centrifuged as before. The two lower phases were then combined. An additional step was added for triglyceride determination, silica gel was then added to the lipid extract (~10mg/ml) to bind phospholipids and vortexed before being centrifuged for 1 minute at 13,000g. the supernatant was transferred into a fresh microcentrifuge and the extract evaporated at 37^{o}C. Lipids were then resuspended in CM extraction buffer.

2.13.4 Thin layer chromatography

Thin layer liquid chromatography (TLC) was used to quantitatively identify lipids in cells and tissues. A solution of chloroform, methanol and aqueous ammonia (at a ratio of 56:24:4 (v/v/v)) was poured into a

tank containing filter paper. The tank was closed and left for 20 minutes. A known volume of sample in CM extraction buffer was loaded on a silica gel TLC plate around 1cm up from the bottom of the plate. Adipose tissue was used as a positive control for triglycerides. Phospholipids and cholesterol in CM extraction buffer were also used as positive controls. The plate was place in the tank and left until the solvent had reached approximately 1 cm from the top of the plate. The plate was then dried using a hot plate and the bands visualised using iodine vapour.

2.13.5 Triglyceride determination assay

Triglyceride content was determined using a quantitative enzymatic assay. Triglycerides are hydrolysed to glycerol and fatty acids by lipoprotein lipase. The glycerol is then phosphorylated to glycerol-1-phosphoate by ATP (catalysed by glycerol kinase), which in turn is oxidised to dihydrooxyacetone phosphate and hydrogen peroxide by glycerol phosphate oxidase. Finally, hydrogen peroxide is coupled with 4-aminoantipyrine and sodium N-ethyl-N-(3-sulfopropyl) m-anisidine to produce a dye that has a maximum absorbance at 540nm that can be measured. These enzymatic reactions summarised in Figure 2.5.

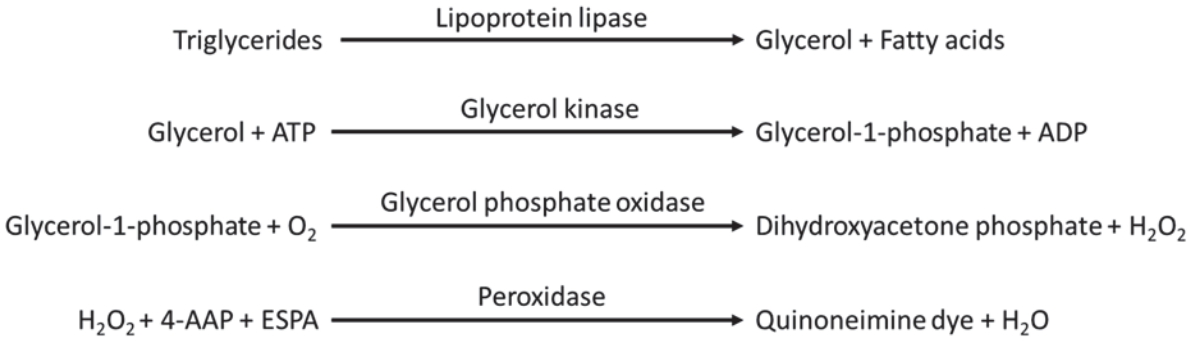

Figure 2.5: Triglyceride assay enzymatic reaction. Abbreviation: 4-AAP, 4-aminoantipyrine; ESPA, N-ethyl-N-(3-sulfopropyl) m-anisidine.

Triglyceride working reagent was made by mixing free glycerol reagent (0.75mM ATP, 3.75mM Magnesium salt, 0.188mM 4-Aminoantipyrine, 2.11mM N-Ethyl-N-(3-sulfopropyl) m-anisidine, sodium salt, 1,250 units/L Glycerol Kinase (microbial), 2,500 units/L Glycerol Phosphate Oxidase (microbial), 2,500 units/L Peroxidase (horseradish), Buffer, pH 7.0 ± 0.1, 0.05% Sodium azide) and triglyceride reagent (250,000 units/L Lipase (microbial), 0.05% Sodium azide) together at a ratio of 4:1 (v/v) and prewarmed at 37^{o}C. 5µl of sample, blank (CM extraction buffer) or standard (glycerol, 0.26mg/ml) was added to 200µl of

triglyceride working reagent and incubated for 10-20 minutes at 37°C. Absorbance was then measured at 540nm. Triglyceride content was then determined using the following equation:

$$\frac{ABS_{sample} - ABS_{blank}}{ABS_{standard} - ABS_{blank}} \; x \; concentration \; of \; standard$$

Triglyceride content was then normalised by protein concentration.

2.14 Glycogen determination

Glycogen content was determined by the anthrone method. Once the glycogen is precipitated, sulfuric acid is used to form furfural from carbohydrates. Furfural then reacts with anthrone and produces a blue colour that can be measured. 1 volume of homogenised liver (~25µl) or glycogen standard was added to 1 volume of ice cooled 4% sulphosalicylic acid and centrifuged at 1000g for 20 minutes at 4°C. 20µl of the supernantent was removed and added to 500µl of anthrone reagent (72% sulfuric acid, 1% (w/v) thiourea, 0.05% (w/v) anthrone), mixed, and incubated at 100°C for 15 minutes. The mixture was allowed to cool before the absorbance was measured at 620nm. Glycogen content was then normalised to protein from Lowry determination.

2.15 Seahorse flux analyser

The seahorse flux analyser allows the measurement of the oxygen consumption rate (OCR) and extracellular acidification rate (ECAR) in live cells as indicators of mitochondrial respiration and glycolysis. All seahorse flux analyser experiments were performed using a seahorse XFe96 analyser (Agilent, Santa Clara, US) and analysed using the Seahorse Wave software.

2.15.1 Seahorse XF cell mito stress test kit

The Seahorse XF cell mito stress test is an assay for measuring the mitochondrial function in live cells by directly measuring the OCR of cells. The assay uses modulators that target the electron transport chain (ETC) to enable the measurement of key parameters of mitochondrial function. Figure 2.6 shows the key modulators used in the mito stress test. Oligomycin is an ATP synthase (complex V) inhibitor, that causes a decrease in OCR due to protons being unable to enter the mitochondrial matrix and is used to determine ATP production. Carbonyl cyanide-4 (trifluoromethoxy) phenylhydrazone (FCCP) is an uncoupling agent that allows the free movement of protons across the mitochondrial membrane, uninhibiting the ETC and

allowing oxygen to be consumed at its maximal capacity. Rotenone and antimycin A are complex I and complex III inhibitors respectively, inducing the complete shutdown of the mitochondrial respiration and used to measure rates of non-mitochondrial respiration.

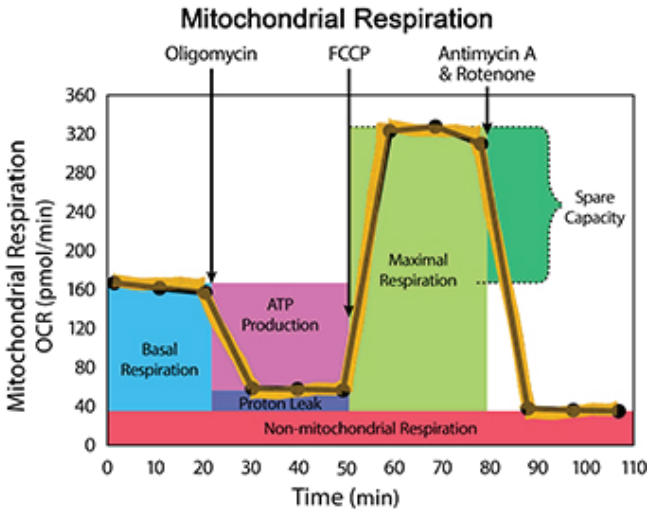

Figure 2.6: Parameters of mitochondrial function measured in the cell mito stress test. (taken from https://www.agilent.com/en/products/cell-analysis/mitochondrial-respiration-xf-cell-mito-stress-test)

The day before the experiment, the sensor cartridge was hydrated using the Seahorse XF Calibrant at 37°C in a non-CO_2 incubator and cells were plated on seahorse XF cell culture microplates (the 4 corner wells were left blank of cells). On the day of experiment the assay medium was prepared (5.5mM glucose, 1mM pyruvate, 2mM glutamine in Seahorse XF Base Medium, pH 7.4). Cell culture medium was removed from the cells and they were wash once in seahorse assay medium. 180µl of seahorse assay medium was added to each well and the plate was incubated at 37°C in non-CO_2 for 1 hour prior to the start of the experiment. Chemicals of interests and ETC modulators were prepared in seahorse assay buffer and loaded into the injection ports as follows:

Chemical	Port	Concentration in port (µM)	Volume in port (µl)	Final concentration (µM)
Chemical of interest	A	Various	20	Various
Oligomycin	B	10	22	1
FCCP	C	10	25	1
Rotenone/antimycin A	D	5/5	27	0.5/0.5

Table 2.6: Seahorse XF cell mito stress test injection preparation.

The calibrant plate with loaded ports was then inserted into the seahorse XFe96 analyser for calibration. Once done, the calibration plate was removed and replaced with the cell culture microplate and the assay was run. The general assay used was as follows:

Equilibration

Baseline - 3 cycles – mix (3 minutes), wait (0 minutes), measure (3 minutes) – *Total duration (18 minutes)*

Injection 1 – 3 cycles – mix (3 minutes), wait (14 minutes), measure (3 minutes) – *Total duration (60 minutes)*

Injection 2 – 3 cycles – mix (3 minutes), wait (0 minutes), measure (3 minutes) – *Total duration (18 minutes)*

Injection 3 – 3 cycles – mix (3 minutes), wait (0 minutes), measure (3 minutes) – *Total duration (18 minutes)*

Injection 4 – 3 cycles – mix (3 minutes), wait (0 minutes), measure (3 minutes) – *Total duration (18 minutes)*

2.15.2 Seahorse XF plasma membrane permeabilizer (PMP) assays

Seahorse XF plasma membrane permeabilizer (PMP) contains recombinant perfringolysin O, a cholestrol-dependent cytolysin that forms pores in the plasma membrane keeps the mitochondrial membrane intact (Salabei *et al.*, 2014), allowing the study of direct effects on mitochondrial function without the need of isolating mitochondrial.

The day before the assay, the sensor cartridge was hydrated using the Seahorse XF Calibrant at 37^{o}C in a non-CO2 incubator and cells were plated on seahorse XF cell culture microplates (the 4 corner wells were left blank of cells). Mitochondrial assay media (MAS) was prepared with and without essentially fatty acid free-BSA, MAS (pH 7.2) contained; 660mM mannitol, 210mM sucrose, 30mM KH_2PO_4. 15mM $MgCl_2$, 6mM HEPES and 3mM EGTA. MAS with BSA was at 0.6% (w/v).

MAS without BSA was used to prepare injection stocks as follows:

Chemical	Port	Concentration in port (µM)	Volume in port (µl)	Final concentration (µM)
ADP (pH 7.4)	A	40000	20	4000
Oligomycin	B	20	22	2
FCCP	C	40	25	4
Antimycin A	D	25	27	2.5

Table 2.7: Seahorse XF plasma membrane permeabilizer assay injection preparation.

The calibration plate with loaded ports was then inserted into the seahorse XFe96 analyser for calibration. MAS preparation for cell treatments differed depending on the complex being investigated. Preparations were as follow:

- Complex I – MAS (with BSA) plus 10mM pyruvate, 1mM malate (pH 7.4) and 10nM PMP
- Complex II – MAS (with BSA) plus 5mM succinate (pH 7.4), 5µM rotenone, 10nM PMP

Cells were then washed once with MAS (with BSA) and 180µl of complex appropriate MAS was added to each well. The calibration plate was removed and replaced with the cell culture microplate and the assay was run. The general assay used was as follows:

No equilibration

Wait – 5 minutes

Baseline – 4 cycles – mix (30 seconds), wait (30 seconds), measure (150 seconds) – *Total duration (14 minutes)*

Injection 1 – 3 cycles - mix (30 seconds), wait (30 seconds), measure (150 seconds) – *Total duration (10.5 minutes)*

Injection 2 – 3 cycles - mix (30 seconds), wait (30 seconds), measure (150 seconds) – *Total duration (10.5 minutes)*

Injection 3 – 3 cycles - mix (30 seconds), wait (30 seconds), measure (150 seconds) – *Total duration (10.5 minutes)*

Injection 4 – 3 cycles - mix (30 seconds), wait (30 seconds), measure (150 seconds) – *Total duration (10.5 minutes)*

2.16 MitoSOX assay

MitoSOX (Thermo Scientific) is a fluorescent probe used as a mitochondrial superoxide indicator. MitoSOX was prepared at 5mM in DMSO and diluted to a working solution of 5µM in HBSS (plus Ca^{2+} and Mg^{2+}).

Cells were treated with MitoSOX for 15 minutes and washed twice with pre-warmed PBS. Cells were then treated with chemicals of interest and fluorescence ($510_{Ex}/590_{Em}$) was measured over a 2-hour period using an incubated fluorescent plate reader set to 37°C.

2.17 High performance liquid chromatography (HPLC)

2.17.1 Sample preparation

Cells whose medium was to be analysed by high performance liquid chromatography (HPLC) were treated with chemicals of interest in STIM buffer. STIM buffer was composed of HBSS buffer with 20mM glucose, 1mM $CaCl_2$ 20mM $NaHCO_3$, 2mM glutamine. 1x MEM amino acids and pH 7.4. STIM buffer was sampled from cells at various time points and 1 volume of 1% HPLC grade phosphoric acid was added to 10 volumes of sample. The sample was then vortexed and centrifuged for 1 minute at 16000g. The sample was transferred into a fresh micro centrifuge tube before being analysed or stored at -20°C.

2.17.2 Mobile phase preparation and sample analysis

Samples were transferred into HPLC vials (Thermo Scientific) and run on a LC-20AD HPLC system with a Nucleosil C18 column (25cm x 3.2mm) and a mobile phase made of a gradient of (A) 0.1% phosphoric acid (Fisher) and (B) acetonitrile (Fisher) with a flow rate of 0.7ml/min. The gradient run conditions (shown in Figure 2.7) were:

0min - A = 90% / B = 10%

15min - A = 10% / B = 90%

30min - A = 10% / B = 90%

35min - A = 90% / B= 10%

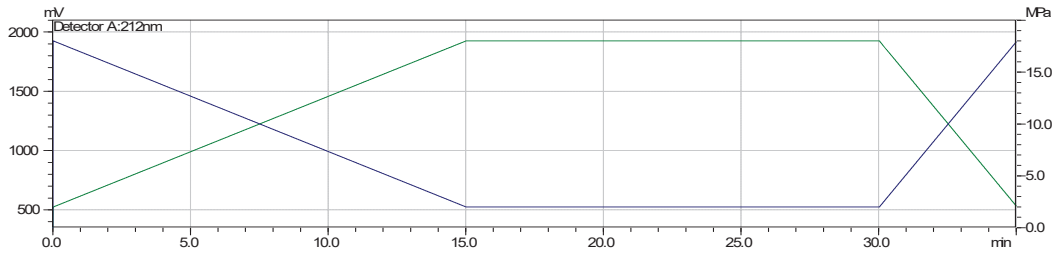

Figure 2.7: HPLC gradient conditions. (A, blue line) 0.1% phosphoric acid and (B, black line) acetonitrile.

Samples were analysed using the LC Solutions software. Area under the curve for peaks of interest were manually selected and calculated. Concentration was then calculated from a standard curve.

2.18 Mass spectroscopy

STIM buffer samples and the serum, bile and urine from animal studies were sent to the Medical Toxicology Centre at Newcastle University for mass spectroscopy analysis carried out by Dr Michael Dunn. Mass Spectroscopy was carried out using SWATH - Sequential Window Acquisition of all Theoretical fragment-ion spectra - non-targeted data independent LC-HR-MS/MS techniques, using a TripleTOF 5600+ high-resolution quadrupole time-of-flight (TOF) mass spectrometer (Sciex), equipped with a DuoSpray ion source operated in positive electrospray mode, coupled to an Eksigent Nano LC 420 system. AnalystTF version 1.7.1 was used for instrument control and data acquisition.

2.19 Statistics

Statistical analysis was performed using Graph Pad Prism and statistical significance was considered when $p<0.05$. Statistically significant differences between groups were determined by the Student's 2-tailed t-test. For comparison of multiple groups, ANOVA was carried out and where significant, differences between groups were determined using Bonferroni–Holm post-hoc tests.

Chapter 3. B-13/H cells model lipid dysregulation in response to drugs and chemicals

3.1 Introduction

Hepatocytes are the primary defining cell of the liver and are responsible for most of its functions**,** including lipid homeostasis (Wallace *et al.*, 2010a). Hepatocytes are involved in fatty acid oxidation and the synthesis of phospholipids, triglycerides and lipoprotein components used to transport lipids throughout the body. They are also capable of active cholesterol and bile acid synthesis (Nguyen *et al.*, 2008)**.** The dysregulation of these processes is a common outcome and an early hepatic response to exposure to drugs and chemicals (Klaunig *et al.*, 2003).

One form of lipid dysregulation is the storage disorder steatosis. Steatosis is defined as the accumulation of triglycerides. This occurs as a response to an imbalance of the storage and metabolism of triglycerides within the cell, leading to the formation of lipid droplets. The main cause of this imbalance is obesity and insulin resistance. These are associated with the excess of dietary carbohydrates that are converted into saturated fats and lead to an increase the free fatty acid pool and an increase fatty acid synthesis (Anderson and Borlak, 2008). Steatosis can be further defined as either micro or macrosteatosis. This is determined by the size of the lipid droplets formed, with macrosteatosis containing lipid droplets large enough to displace the nucleus to the cells periphery (Fishbein *et al.*, 1997)**.** Steatosis is a critical early event in alcoholic liver disease and in non-alcohol dependent liver diseases such as non-alcoholic steatohepatitis (NASH) (Day, 2012). It is also a problem for liver transplantation, as a donor liver with macrosteatosis has a greater chance of recipient rejection (Spitzer *et al.*, 2010; de Graaf *et al.*, 2012).

Another lipid storage disorder is phospholipidosis (PLD), a lysosomal storage disorder characterised by the accumulation of phospholipids, forming cytosolic electron dense inclusions called lamellar bodies (Shayman and Abe, 2013)**.** This may be as a result from alterations in the metabolism of phospholipids caused by drugs, hormones or cofactors (Halliwell, 1997). Drug induced phospholipidosis (DIPL) is a common response to a group of drugs known as cationic amphiphilic drugs (CADs). These drugs share a structural similarity, being made up of a hydrophobic ring structure as well as a hydrophilic side chain. This is important in the development of DIPL as these structural features allow the drugs to readily enter the cell through the cell membrane and interact with the lysosomal membrane. Once inside and exposed to the acidic environment of the lysosome, the CADs become charged and trapped though electrostatic and hydrophobic interactions with the lipids (Park *et al.*, 2012). The exact mechanism(s) of how CADs induce phospholipid accumulation is not yet fully understood, however, it is likely that CADs decrease phospholipase activity, either by interacting with enzymes or by binding to phospholipids directly and therefore inhibiting their interaction. One enzyme believed to be involved in DIPL is phospholipase A2

(LPLA2). The hypothesis for this is that CADs incorporate into the lysosomal membrane where they reduce its surface charge. This means the interactions between LPLA2 and the lysosomal membrane are weakened, as it associates with the membrane through electrostatic interactions (Shayman and Abe, 2013). This would result in the inhibition of phospholipid breakdown and therefore an accumulation of phospholipids in the lysosome.

One problem pharmaceutical companies have is that there is a lack of knowledge as to whether DIPL induces toxicity. Therefore, certain risk management strategies have become mandatory for these companies to increase safety when selecting new drugs (Chatman *et al.*, 2009). The gold standard for this was electron microscopy to look for the formation of lamellar bodies, however this is expensive and slow and so new *in vitro* models could provide a cheap high throughput alternative for drug screening for DIPL during development.

Transdifferentiated B-13 cells (B-13/H cells) have previously been used as a cost-effective model system for the study of hepatocyte function (Wallace *et al.*, 2010a). To date xenobiotic metabolism and hepatoxicity have been studied in B-13/H cells (Probert *et al.*, 2015), however lipid dysregulation has not been investigated. Therefore, it was hypothesised that the B-13/H cell could model hepatic lipid dysregulation. This was investigated using *in vitro* assays that have been established to measure lipid and phospholipid accumulation.

3.2 CADs induce an accumulation of phospholipid in B-13 and B-13/H cells.

Several *in vitro* assays have been developed to screen drugs for their capability to induce PLD, including the use of a fluorescent-labeled phospholipid analogue, NBD-PE (N-(-7-nitrobenz-2-oxa-1,3-diazol-4-yl)-1, 2-dihexadecanoyl-sn-glycero-3-phosphoethanolamine) (Fujimura *et al.*, 2007) and LipidTOX (Muehlbacher *et al.*, 2012). Numerous cell lines have utilised these assays including HepG2 cells (Almela *et al.*, 2009), yet these cell lines do not account for the metabolism and therefore could overstate the PLD inducing potential of a drug. Therefore, phospholipid accumulation was measured using LipidTOX staining in B-13 and B-13 cells transdifferentiated for 14 days using 10nM dexamethasone (B-13/H cells). These cells have been shown to express functional drug metabolising enzymes (Probert *et al.*, 2015). Many CADs have been reported to induce PLD. Known PLD inducers and negative controls (Muehlbacher *et al.*, 2012) were incubated with cells for 48 hours. CADs induced phospholipid accumulation in both B-13 and B-13/H cells (Figure 3.1A). Accumulation was greater in the B-13 cells compared to the B-13/H cells for tamoxifen, quinidine, chlorpromazine and promazine. Two of the most potent inducers were promazine and

chlorpromazine which showed a 5.2-fold and 7.4-fold increase compared to control cells. Yet they did not show any phospholipid accumulation in B-13/H cells at the same concentration. This may be due to B-13/H cells expressing functional metabolising enzymes (Probert *et al.*, 2015), and therefore could lead to these drugs being metabolised, losing their cationic amphiphilic structure required for PLD. However, 6.25µM amiodarone, a widely reported PLD inducer (Kasahara *et al.*, 2006; Park *et al.*, 2012), caused a greater accumulation in B-13/H cells (Figure 3.1A). This was observed using fluorescence microscopy which showed each cell accumulated more phospholipids in the B-13/H cells treated with amiodarone compared to B-13 cells (Figure 3.1C). To confirm that the difference in phospholipid accumulation was not due to toxicity, MTT assays were performed as an indicator of cell viability. These data showed that overall there was little to no toxicity with the majority of the drugs at the concentrations employed in both B-13 and B-13/H cells (Figure 3.1B). Cyclosporine A, quinidine and promazine in B-13 cells and menadione in B-13/H cells reduced MTT activity significantly. Ketoconazole showed significant toxicity in both cell types. In B-13 cells, 50µM reduced cell viability to 2.3% of control cells and is most likely why no PLD was detected in these cells despite being a known CAD.

Exposing B-13/H cells to 5µM amiodarone for 48 hours showed a time-dependent response that reached a threshold when incubated for longer (Figure 3.2). Phospholipid accumulation did not increase after 48 hours in cells that were not washed and accumulation was not reversed when amiodarone was extensively washed out and incubated for a further 48 hours. It has been shown that the combination of two different CADs have an additive effect on phospholipid accumulation (Glock *et al.*, 2016). This was tested in B-13/H cells with the combination of amiodarone and quinidine. Individually they induced PLD 1.5-fold and 1.7-fold, but together induced an additive effect as they increased phospholipid accumulation 2.3-fold (Figure 3.3A). This combination did not have a toxic effect on B-13/H cells (Figure 3.3B). These data suggest that B-13 and B-13/H cells can be used as a model for PLD (Amacher, 2011).

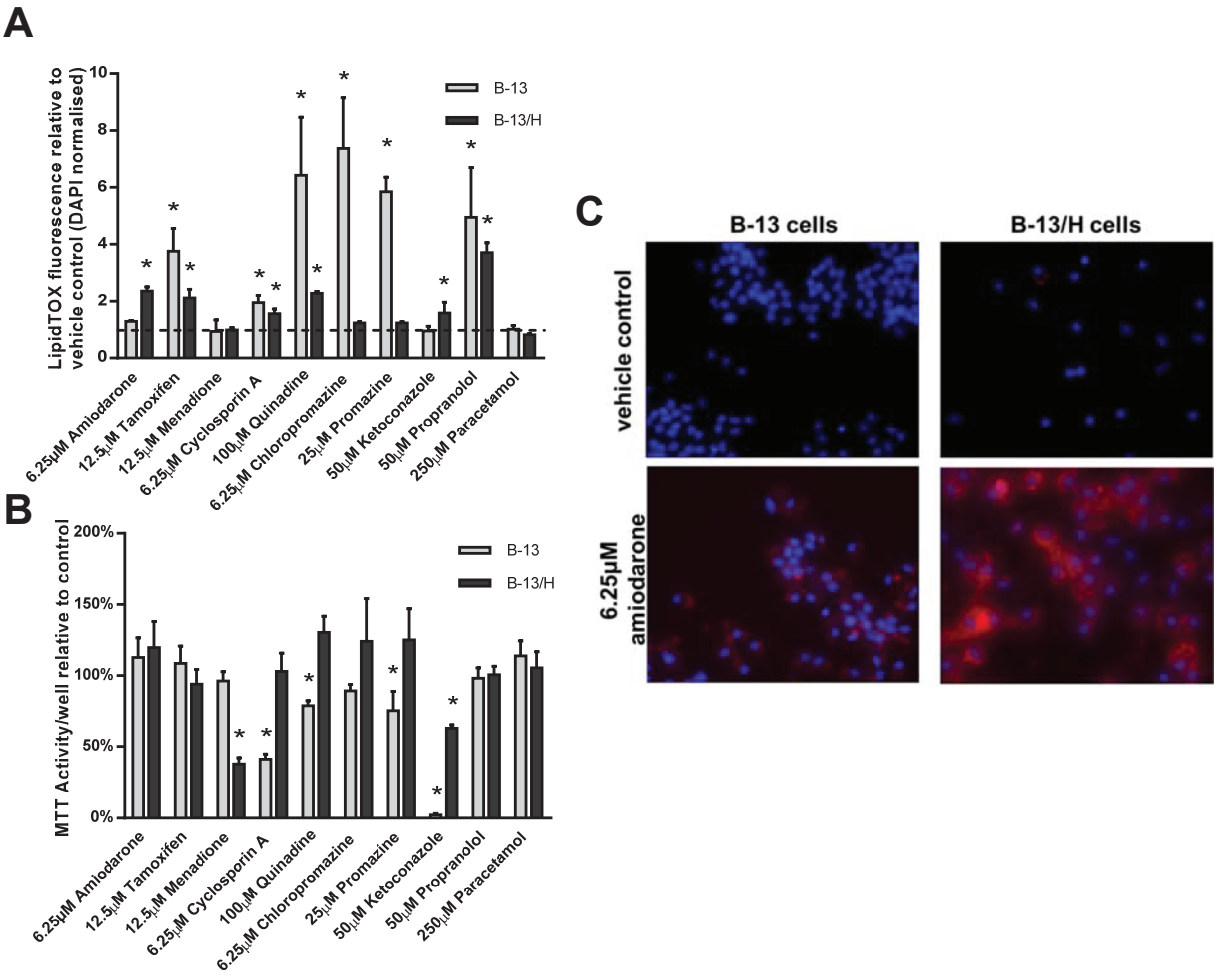

Figure 3.1: Exposure to cationic amphiphilic drugs results in phospholipidosis in B-13 and B-13/H cells. A, B-13 and B-13/H cells were treated for 48 hours with indicated chemicals in addition to the LipidTOX probe. Following treatment cells were fixed and DAPI stained. LipidTOX fluorescence was measured and normalised to DAPI fluorescence. Data are the mean and SD of 3 separate determinations from the same experiment, typical of 3 separate experiments. * significantly different phospholipidosis to control ($p<0.05$). **B,** B-13 and B-13/H cells treated as in A. Following treatment, cells were incubated with MTT for 2 hours and reduction determined. Data are the mean and SD of 6 separate determinations from the same experiment, typical of 2 separate experiments. * significantly different MTT activity to control ($p<0.05$). **C,** B-13 and B-13/H cells treated with amiodarone (and control) and LipidTOX (red), following treatment cells were fixed, stained with DAPI (blue) and analysed using fluorescence microscopy.

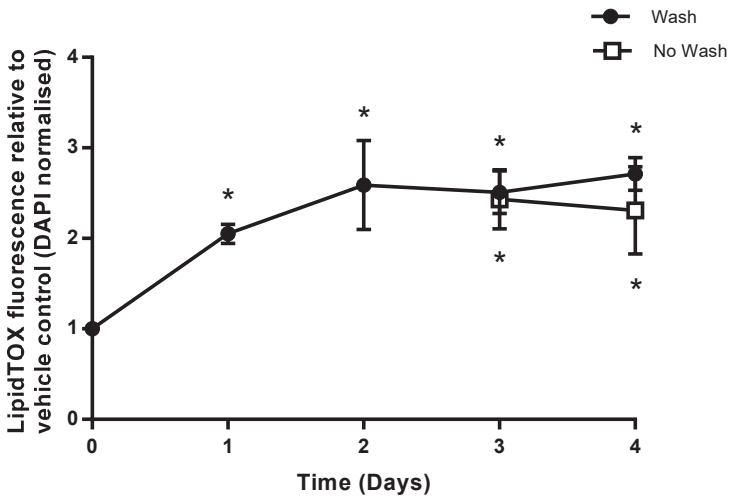

Figure 3.2: B-13/H cells accumulate phospholipids in a time dependent manner. B-13/H cells were treated daily with 5µM amiodarone. 24 hours prior to fixation and analysis, cells were also incubated with LipidTOX. Following treatment cells were fixed and DAPI stained. LipidTOX fluorescence was measured and normalised to DAPI fluorescence. Data are the mean and SD of 3 separate determinations from the same experiment, typical of 2 separate experiments. * significantly different phospholipidosis to control ($p<0.05$) tested by ANOVA followed by Bonferroni post-hoc test.

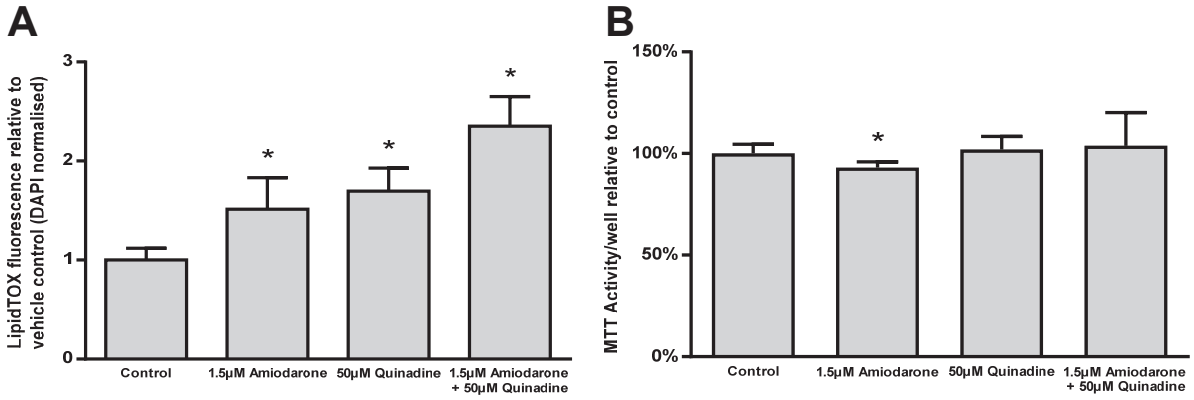

Figure 3.3: Co-incubation of CADs in B-13/H cells increases phospholipid accumulation. A, B-13/H cells were treated for 48 hours with indicated chemicals in addition to the LipidTOX probe. Following treatment, cells were fixed and DAPI stained, LipidTOX fluorescence was measured and normalised to DAPI fluorescence. Data are the mean and SD of 3 separate determinations from the same experiment, typical of 2 separate experiments. * significantly different phospholipidosis to control ($p<0.05$). **B,** B-13/H cells treated as in A. Following treatment, cells were incubated with MTT for 2 hours and reduction determined. Data are the mean and SD of 6 separate determinations from the same experiment, typical of 3 separate experiments. * significantly different MTT activity to control ($p<0.05$).

3.3 Methapyrilene induces phospholipid accumulation in B-13 and B-13/H cells.

Methapyrilene is a H1 antagonist that was withdrawn from the market due to its hepatic carcinogenicity (Habs *et al.*, 1986) and has been shown to be toxic to rat hepatocytes *in vitro* (Ratra *et al.*, 1998). Methapyrilene has a cationic amphiphilic structure (Figure 3.4A) but has not been investigated for its ability to induce PLD. Using LipidTOX staining, methapyrilene induced phospholipid accumulation in a dose-dependent manner in both B-13 and B-13/H cells (Figure 3.4B&C). Similar to many of the other CADs, methapyrilene induced PLD was greater in B-13 cells than B-13/H cells as B-13 cells showed significant accumulation at concentrations ranging from 25-200µM whereas accumulation occurred at 100-200µM in B-13/H cells. As previously demonstrated (Probert *et al.*, 2014) methapyrilene was only toxic to B-13/H cells and not to B-13 cells at 100 and 200µM (Figure 3.4D). This suggests that B-13/H cells metabolise methapyrilene from a PLD inducing drug into a toxic metabolite.

3.4 DTT inhibits the induction of phospholipid accumulation

Previous studies have found that methapyrilene hepatoxicity is inhibited by sulfhydryl reducing agents and the Ca^{2+} channel blocker nifedipine (Ratra *et al.*, 1998; Probert *et al.*, 2014). The effect of sulfhydryl reducing agent, dithiothreitol (DTT), and nifedipine were therefore investigated for any effect they may have on methapyrilene induced PLD. As previously shown, DTT and nifedipine inhibited methapyrilene hepatotoxicity, with a greater effect in the nifedipine treated cells (Figure 3.5B). 100µM nifedipine significantly increased induction of PLD 1.75-fold whereas DTT inhibited PLD almost back to control levels (Figure 3.5A).

Amiodarone and tamoxifen were selected to investigate whether the PLD inhibition observed with DTT co-incubation with methapyrilene could be replicated in other known CADs. Both drugs showed a significant inhibition of phospholipid accumulation to control levels or lower, despite displaying a greater induction of PLD than methapyrilene (Figure 3.5C). No significant change was detected in cell viability of cells treated with DTT and those without treatment (Figure 3.5D). This shows that DTT has an inhibitory effect on the development of phospholipid accumulation.

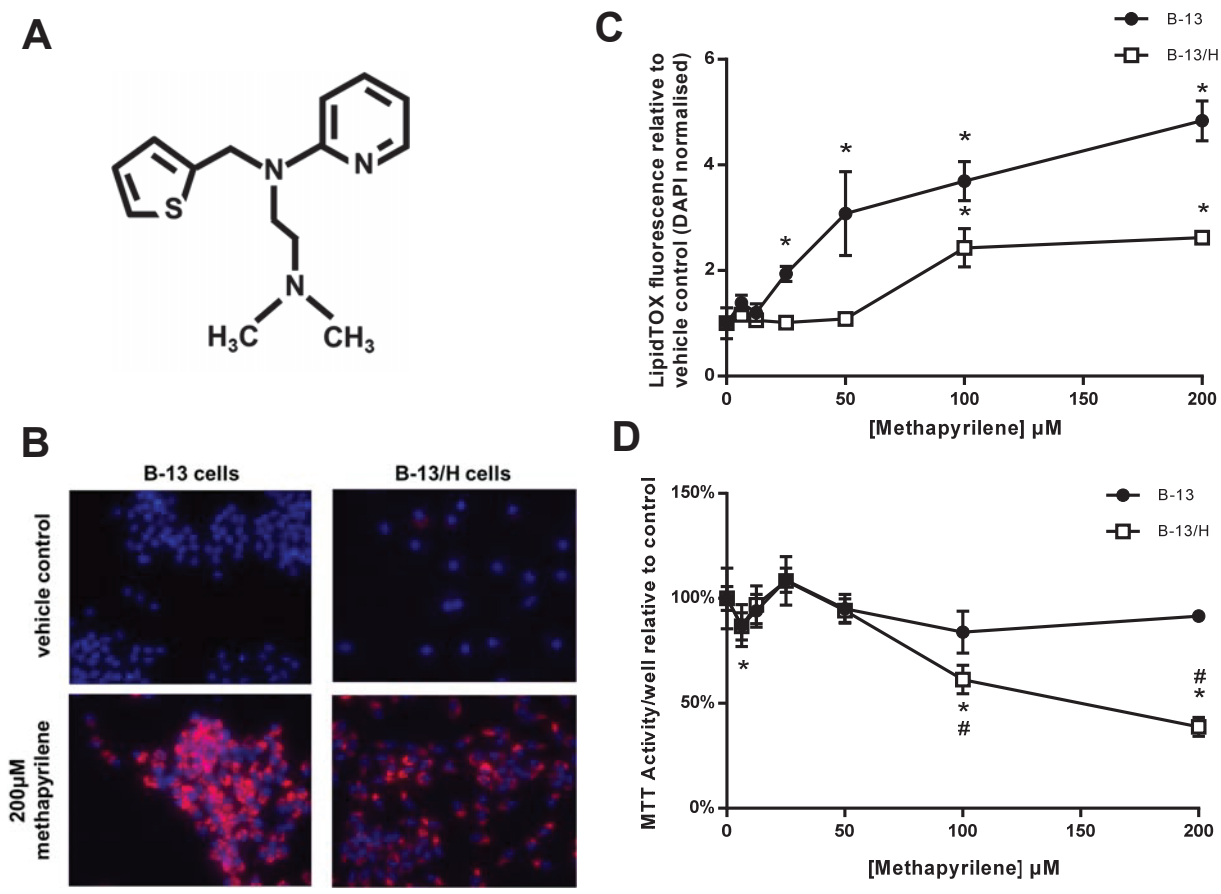

Figure 3.4: Methapyrilene exposure causes phospholipidosis in B-13, B-13/H cells. A, structure of methapyrilene. **B,** B-13 and B-13/H cells treated with 200µM methapyrilene and LipidTOX (red), following treatment cells were fixed, stained with DAPI (blue) and analysed using fluorescence microscopy. **C,** Cells were treated for 48 hours with indicated concentrations of methapyrilene in addition to the LipidTOX probe. Following treatment cells were fixed and DAPI stained. LipidTOX fluorescence was measured and normalised to DAPI fluorescence. Data and SD are of 3 separate experiments, typical of 3 experiments. * significantly different phospholipidosis to control ($p<0.05$) tested by ANOVA followed by Bonferroni post-hoc test. **D,** cells were treated as in A. Following treatment, cells were incubated with MTT for 2 hours and reduction determined. Data are the mean and SD of 5 separate determinations from the same experiment, typical of 3 separate experiments. * significantly different MTT activity to control ($p<0.05$) tested by ANOVA followed by Bonferroni post-hoc test.

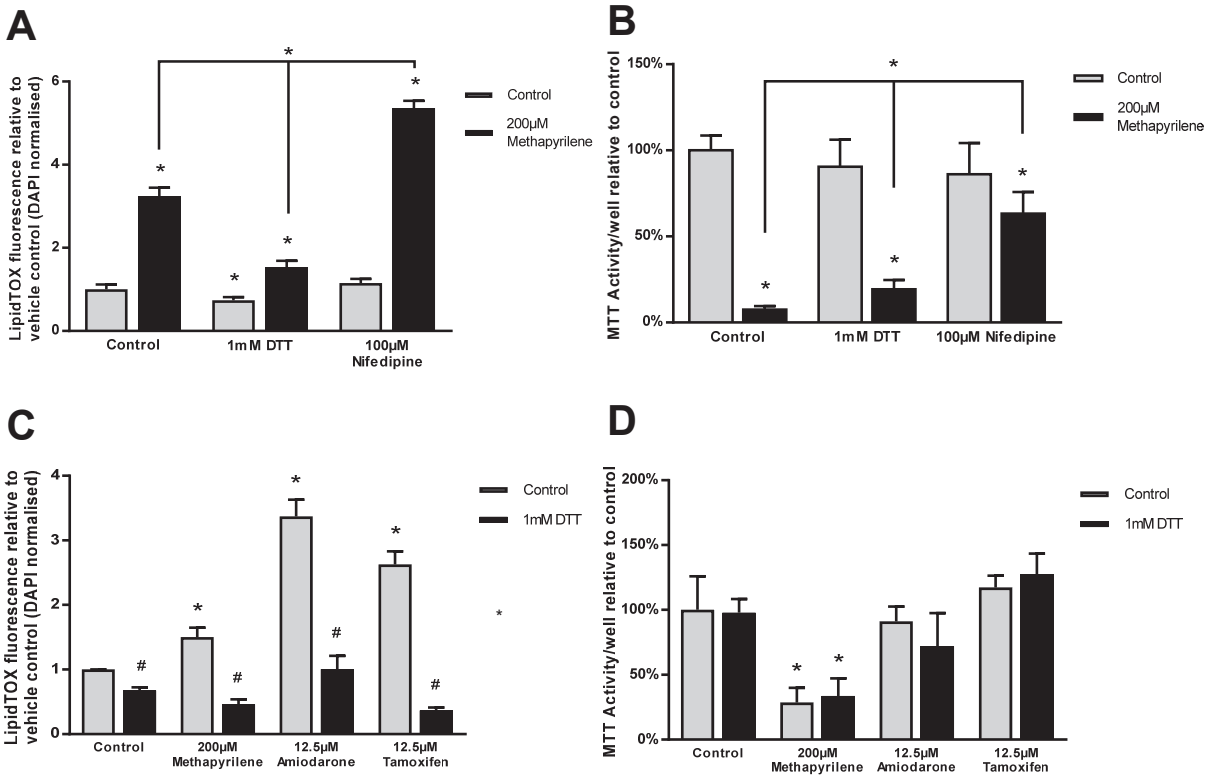

Figure 3.5: DTT treatment inhibits cationic amphiphilic drug-induced phospholipidosis in B-13/H cells. A, B-13/H cells were pre-incubated with DTT/nifedipine for 4 hours followed by treatment with methapyrilene and LipidTOX. Following treatment, cells were fixed and DAPI stained. LipidTOX fluorescence was measured and normalised to DAPI fluorescence. Data are the mean and SD of 3 separate determinations from the same experiment, typical of 3 separate experiments. * significantly different phospholipidosis to control ($p<0.05$). **B,** B-13/H cells treated as in A. Following treatment, cells were incubated with MTT for 2 hours and reduction determined. Data are the mean and SD of 6 separate determinations from the same experiment, typical of 3 separate experiments. * significantly different MTT activity to control ($p<0.05$). **C,** B-13/H cells were pre-incubated with 2mM DTT for 4 hours followed by treatment with the indicated phospholipidosis-inducing drugs. Following treatment cells were fixed and DAPI stained. LipidTOX fluorescence was measured and normalised to DAPI fluorescence. Data are the mean and SD of 3 separate determinations from the same experiment, typical of 3 separate experiments. * significantly different phospholipidosis to vehicle control ($p<0.05$). # significantly different phospholipidosis versus chemical control. **D,** B-13/H cells treated as in A. Following treatment, cells were incubated with MTT for 2 hours and reduction determined. Data are the mean and SD of 6 separate determinations from the same experiment, typical of 3 separate experiments. * significantly different MTT activity to control ($p<0.05$).

3.5 LPLA2 has a role in B-13 cell phospholipidosis

One of the potential mechanisms leading to the accumulation of phospholipids has been proposed to be due to CADs blocking of lysosomal phospholipase A2 (LPLA2) interaction with the lysosomal membrane and inhibition of phospholipid degradation. This leads to an inhibition of phospholipid turnover and therefore phospholipid accumulation (Shayman and Abe, 2013). It was hypothesised that transfection of a plasmid encoding LPLA2 would reduce the accumulation of phospholipids.

It was first confirmed that B-13 and B-13/H cells express LPLA2 transcripts to similar levels as rat liver (Figure 3.6A), assuming translation to protein, these cells are unlikely to be sensitised to PLD due to an absence of functional LPLA2. B-13 cells were selected to be used for transfection due to their greater susceptibility to CAD induced PLD. These were shown to be successfully transfected with HA-tagged LPLA2 (Figure 3.6B). Expression of human LPLA2 with phospholipidosis-inducing concentrations of tamoxifen in B-13 cells resulted in a statistically significant reduction of PLD (Figure 3.6C). Cells were transfected with increasing amounts of LPLA2-encoding plasmid. RL-TK was also added to make the total DNA per well 2µg. Increasing RL-TK (with decreasing LPLA2) increased renilla luminescence and increasing LPLA2 (with decreasing RL-TK) resulted in a dose dependent reduction in PLD (Figure 3.6D). This supports the hypothesis of a role of LPLA2 in the induction of PLD.

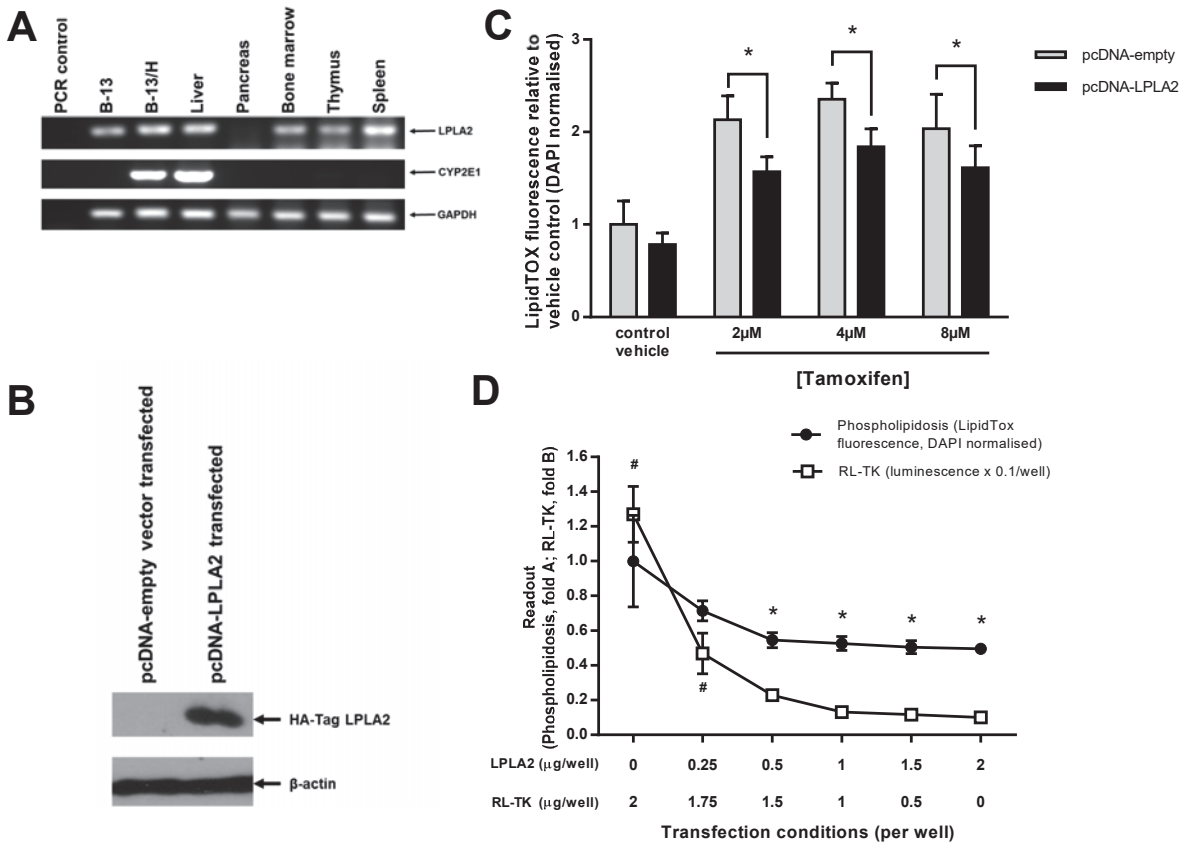

Figure 3.6: Human LPLA2 expression reduces tamoxifen induced phospholipidosis in B-13 cells. A, RT-PCR for indicated transcripts. **B,** Western Blot in extracts from B-13 cells transfected with indicated construct. Each lane contained 10μg protein/lane. **C,** B-13 cells were transfected as indicated for 24 hours. Cells were then treated with LipidTOX and indicated doses of tamoxifen for 24 hours. Following treatment cells were fixed and DAPI stained. LipidTOX fluorescence was measured and normalised to DAPI fluorescence. Data are the mean and SD of 3 separate experiments. * significantly different phospholipidosis to pcDNA-empty of each treatment ($p<0.05$). **D,** B-13 cells were transfected with indicated concentrations of pcDNA-LPLA2 and RL-TK to a final concentration of 2μg/well for 24 hours. Cells were then treated with 6μM tamoxifen. Following a further 24 hours treatment phospholipidosis and renilla activities were determined (separate samples). Data are the mean and SD of 3 separate experiments. Significantly different * phospholipidosis or # renilla versus cell transfected in absence of LPLA2 or RL-TK respectively ($p<0.05$) tested by ANOVA followed by Bonferroni post hoc test.

3.6 B-13/H cells accumulate lipids in response to exposure to fatty acids

Steatosis was also hypothesised to be able to be modelled in B-13/H cells. B-13 and B-13/H cells expressed a variety of transcripts associated with fatty acid uptake and synthesis including acetyl-CoA synthetases and carboxylases, mitochondrial pyruvate transporters, lipid droplet associated proteins and fatty acid synthase (Figure 3.7A). Expression of these transcripts was similar in both B-13 and B-13/H cells. However, B-13 cells had undetectable levels of CD36 (also known as fatty acid translocase). Transdifferentiation to B-13/H cells induced an increase in CD36 levels which suggests that there may be an increase in the functional uptake capacity in B-13/H cells compared to B-13 cells.

Previous studies have shown 2mM oleic acid and linoleic acid induce lipid accumulation in rat hepatocytes (Nativ *et al.*, 2013). This was therefore used to investigate whether B-13/H cells respond in the same manner as rat hepatocytes. Oil red staining showed that the incubation of these fatty acids for 72 hours increased lipid accumulation 11-fold (Figure 3.7B). Incubation with a higher concentration of glucose (25mM) and 100nM insulin had no effect on lipid accumulation in B-13/H cells alone, or when incubated separately with fatty acids. However, a combination of both insulin and glucose significantly increased the total accumulation of lipids 17-fold compared to control cells when incubated with fatty acids. Examination of oil red stained cells using bright field microscopy showed that large lipid droplets form when the cells were exposed to fatty acids (Figure 3.7C).

Incubation of B-13/H cells with hyperglycemic concentrations of glucose (25mM) for two weeks resulted in a 1.5-fold increase in lipid accumulation compared to normal glucose concentrations (Figure 3.8A&B). These data show that the B-13/H cells can be used as a model for lipid accumulation and steatosis.

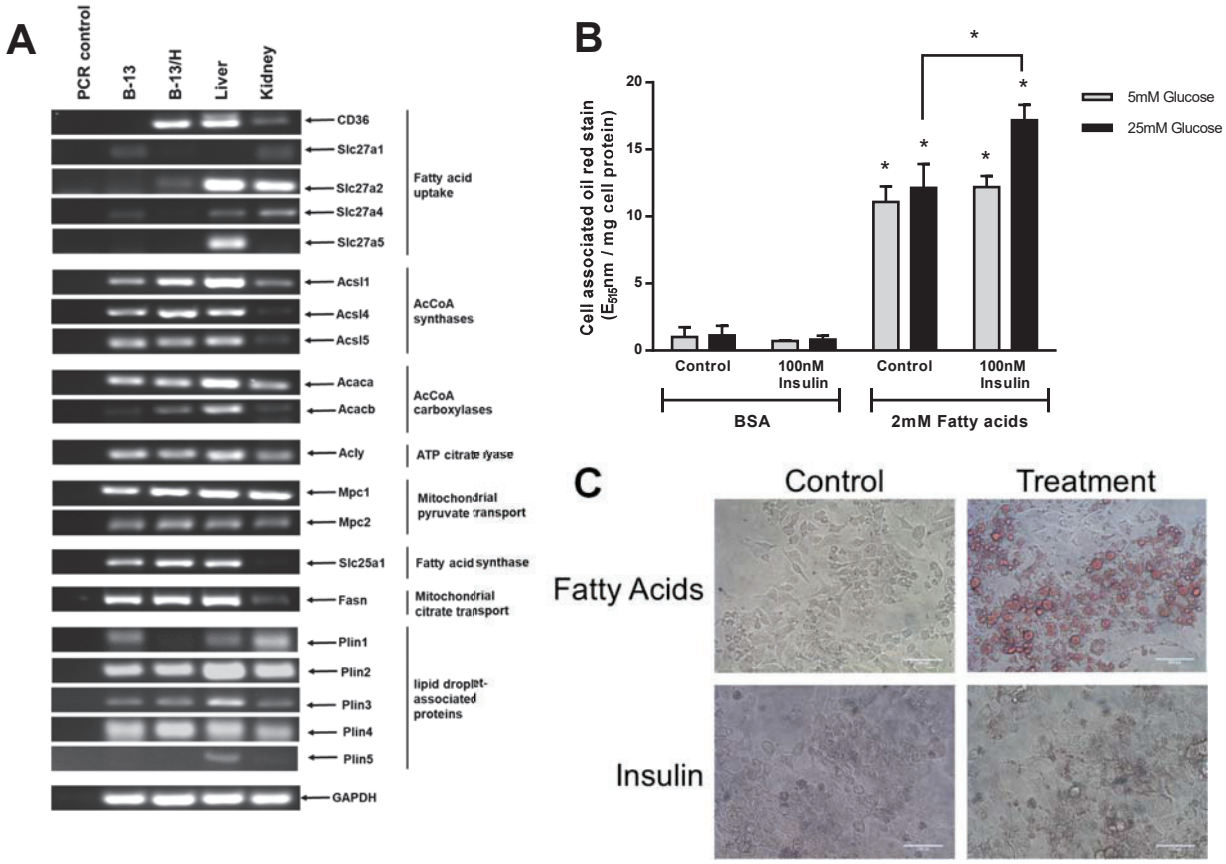

Figure 3.7: B-13/H cells exposed to fatty acids results in lipid accumulation. A, RT-PCR for the indicated transcripts in the indicated cell types and rat tissue. **B,** B-13/H cells were treated with medium supplemented with the indicated treatments for 72 hours. Following treatment, cells were fixed and stained with oil red. Lipid accumulation was quantified by the extraction of oil red from the cells and the absorbance was measured at 515nm. Data was normalised to protein concentration by Lowry protein determination. Data are the mean and SD of 3 separate determinations from the same experiment, typical of 3 separate experiments. * significantly different between treatments ($p<0.05$). **C,** B-13/H cells treated as described in B, prior to oil red extraction cells were imaged by bright-field microscopy (scale bar = 100µm).

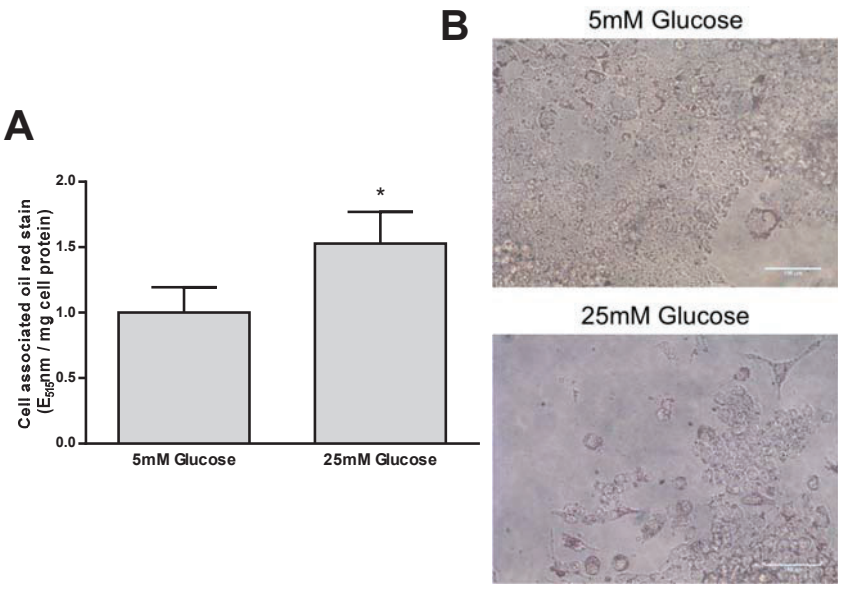

Figure 3.8: Prolonged exposure to elevated levels of glucose increase lipid accumulation. A, B-13/H cells were incubated with the indicated concentrations of glucose for 2 weeks, changing the media every 2-3 days. Following treatment cells were fixed and stained with oil red. Lipid accumulation was quantified by the extraction of oil red from the cells and absorbance was measured at 515nm. Data was normalised to protein concentration by Lowry protein determination. Data are the mean and SD of 3 separate determinations from the same experiment, typical of 3 separate experiments. * significantly different versus control cells ($p<0.05$). **B,** Cells were treated as in A, before extraction of oil red stain, cells were imaged by bright-field microscopy (scale bar = 100μm).

3.7 LipidTOX and oil red staining are specific to phospholipid and neutral lipids respectively

To ensure that LipidTOX was specific to phospholipid accumulation and oil red staining was specific to neutral lipid accumulation, B-13/H cells were treated with known inducers of each lipid storage disorder. Treatment with LipidTOX gave positive results for amiodarone and tamoxifen treated cells but not those treated with fatty acids (Figure 3.9A&C). Oil red stained cells were only stained in fatty acid treated cells and not CAD treated cells (Figure 3.9B&C). These results indicate that it is possible to differentiate between phospholipid and neutral lipid accumulation using these two assays.

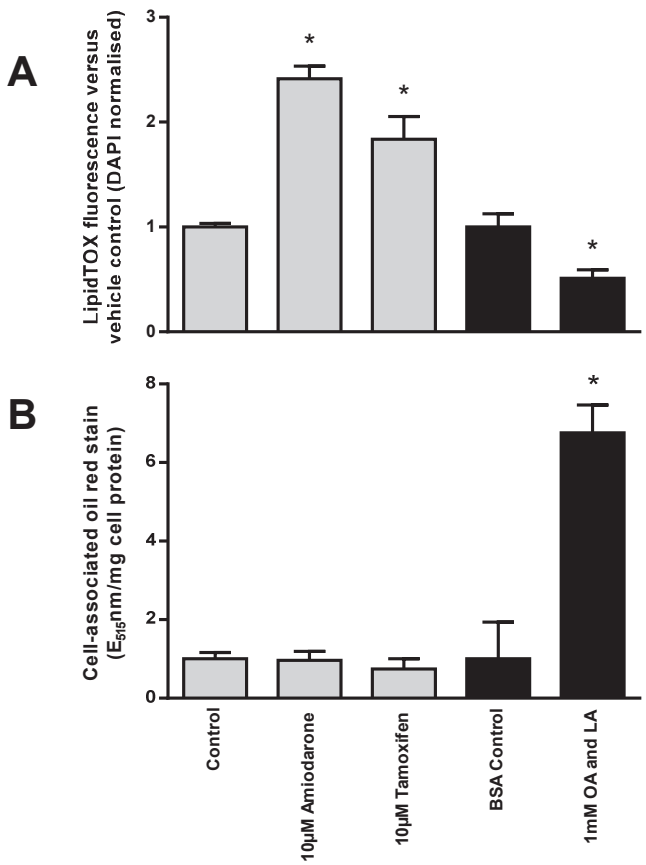

Figure 3.9: Specificity of LipidTOX and oil red staining. A, B-13/H cells were treated for 48 hours with indicated treatments in addition to the LipidTOX probe. Following treatment cells were fixed and DAPI stained. LipidTOX fluorescence was measured and normalised to DAPI fluorescence. Data are the mean and SD of 3 separate determinations from the same experiment, typical of 3 separate experiments. * significantly different phospholipidosis to control ($p<0.05$). **B,** Cells were treated with indicated treatments for 48 hours. Following treatment cells were fixed and stained using oil red. Lipid accumulation was determined by the extraction of oil red and the content was measured by absorbance at 515nm. Data was normalised to protein concentration by Lowry protein determination. Data are the mean and SD of 3 separate determinations from the same experiment, typical of 3 separate experiments. * significantly different to control ($p<0.05$). **C,** B-13/H cells were treated as described in A and B. Cells were then imaged using fluorescent microscopy or light microscopy for LipidTOX and neutral oil red staining respectively.

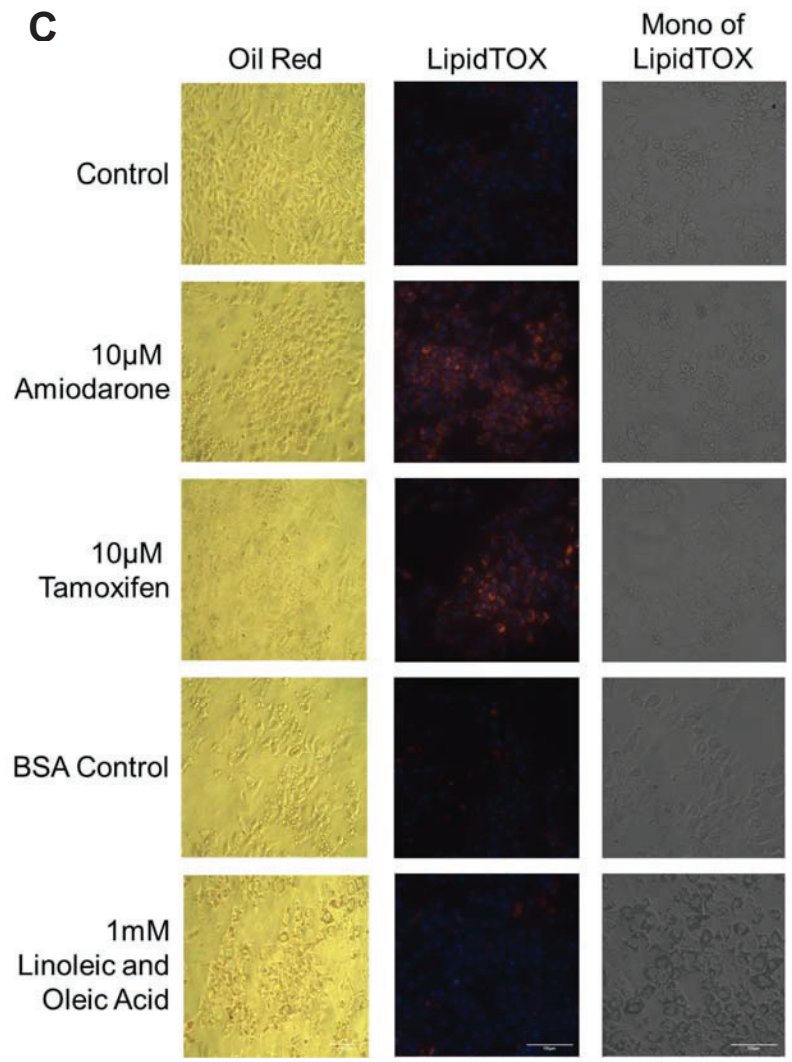

Figure 3.9. Specificity of LipidTOX and oil red staining. (Continued)

3.8 Lipid accumulation is dose- and time-dependent in B-13 and B-13/H cells

B-13 and B-13/H cells accumulated lipids in a dose-dependent manner (Figure 3.10A), reaching a max accumulation at 250μM. B-13/H cells showed a greater accumulation of lipid droplets compared to B-13s (15-fold and 5-fold increases respectively). Only microsteatosis was observed in B-13 cells (Figure 3.10C). However, at higher concentrations (1mM and 2mM) of fatty acids in B-13/H cells macrosteatosis as well as microsteatosis occurred (Figure 3.10D). At lower concentrations, such as 250μM, primarily microsteatosis was observed. Quantification of micro and macrosteaotic droplets within B-13/H cells suggested that microsteatosis remains approximately the same at 4 droplets per cell between 250μM and

2000µM of fatty acid treatment whereas macrosteatosis occurred at 1mM and 2mM (Figure 3.10B), suggesting development of micro or macrosteatosis is dependent on concentration.

Lipid accumulation in B-13/H cells increased with fatty acid incubation time over a 4-day period, resulting in a 13-fold increase compared to control cells (Figure 3.11A). However, they appeared to resist significant reversal for at least 2 days when the cells were washed and incubated in fresh medium free of fatty acids, however, lipid accumulation did not increase as much as the cells that were continually exposed to fatty acids. The increased variability of cell-associated oil red stain in un-washed cells after 3 days of exposure was likely due to stress associated with triglyceride accumulation (Figure 3.11B). It is therefore possible to investigate the effect of different concentrations and times of exposure to fatty acids in B-13/H cells.

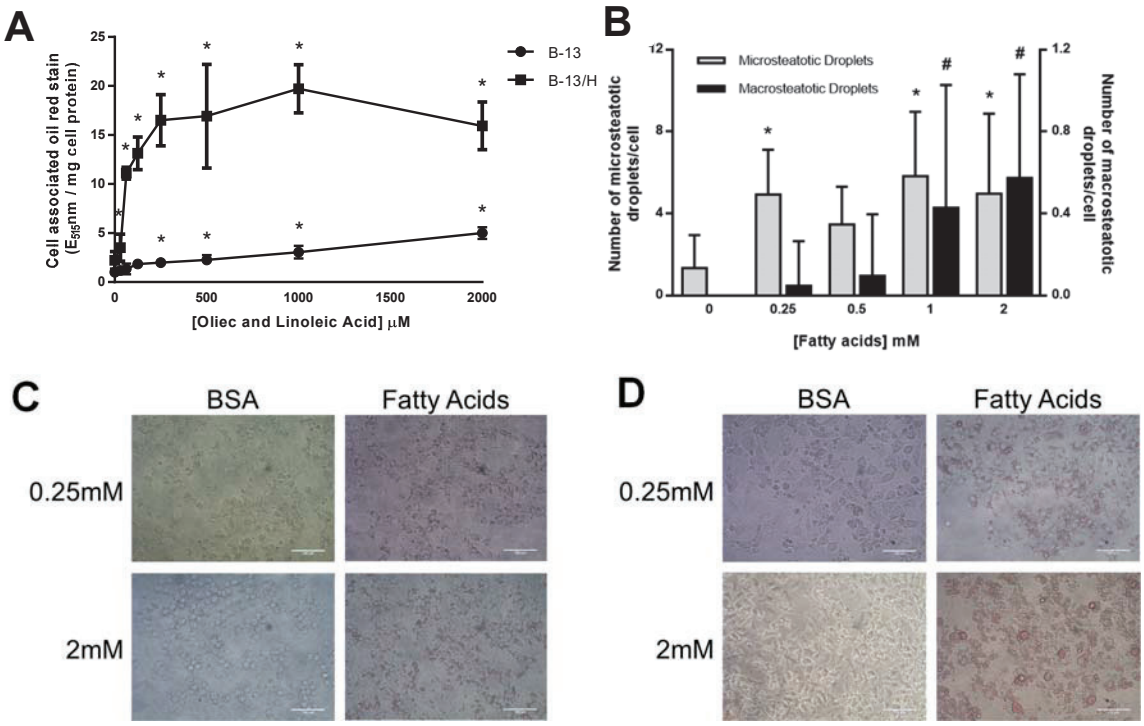

Figure 3.10: Exposing B-13 and B-13/H cells to fatty acids results in dose-dependent micro and macrosteatosis. A, B-13 and B-13/H cells were treated with fatty acids at indicated concentrations for 72 hours. Following treatment, cells were fixed and stained with oil red. Lipid accumulation was quantified by the extraction of oil red from the cells and the absorbance was measured at 515nm. Data was normalised to protein concentration by Lowry protein determination. Data are the mean and SD of 3 separate determinations from the same experiment, typical of 3 separate experiments. * significantly different to control treated cells ($p<0.05$) tested by ANOVA followed by Bonferroni post-hoc test. **B,** quantification of the number of micro and macrosteatotic droplets in cells. Data are the mean and SD of the number of droplets in 20 cells for each concentration. * significantly different to control treated cells ($p<0.05$) tested by ANOVA followed by Bonferroni post-hoc test. **C and D**, B-13 **(C)** and B-13/H **(D)** cells were treated as in A, before extraction of oil red stain, cells were imaged by bright-field microscopy (scale bar = 100µm).

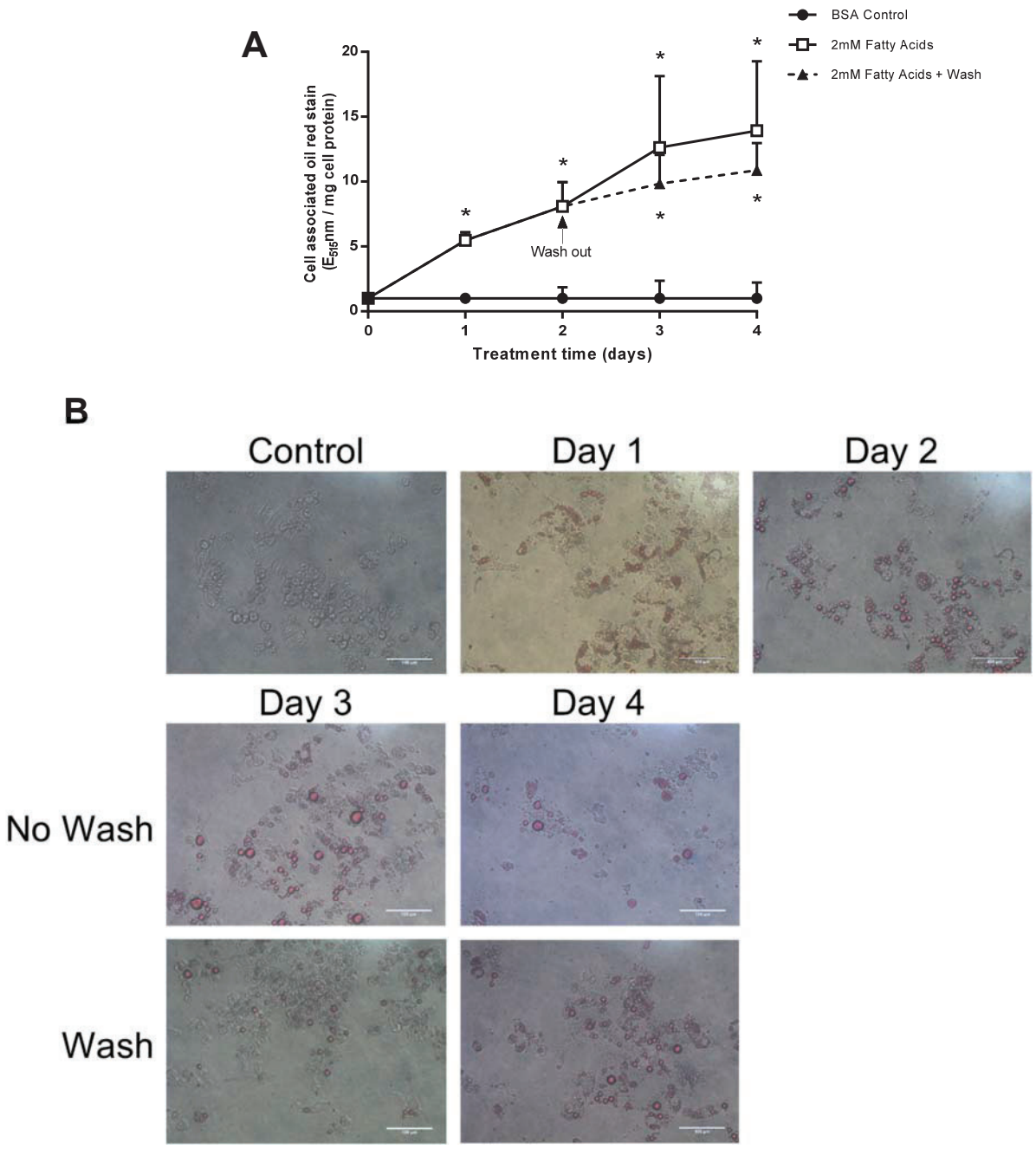

Figure 3.11: Exposure of B-13/H cells to fatty acids results in irreversible micro and macrosteatosis. A, Cells were treated with 2mM fatty acids for indicated time. Following treatment, cells were fixed and stained with oil red. Lipid accumulation was quantified by the extraction of oil red from the cells and the absorbance was measured at 515nm. Data was normalised to protein concentration by Lowry protein determination. Data are the mean and SD of 3 separate determinations from the same experiment, typical of 3 separate experiments. * significantly different to control treated cells ($p<0.05$) tested by ANOVA followed by Bonferroni post-hoc test. **B,** B-13/H cells were treated as in A, before extraction of oil red stain, cells were imaged by bright field microscopy (scale bar = 100µm).

3.9 B-13/H cells exposure to fatty acids accumulate triglycerides

Triglyceride (TG) determination and TLC were used to establish whether the lipid droplets observed in B-13/H cells exposed to fatty acids contained triglycerides. It was possible to identify cells likely to be accumulating triglycerides based on light microscopy (Figure 3.12A). Triglyceride determination showed that cells treated with 1mM fatty acids contained 73µg of TG/mg of protein compared to 5µg/ml in the control treated cells (Figure 3.12B). TLC of lipids extracted from B-13/H cells treated with 1mM fatty acids showed that the presence of triglycerides, as well as cholesterol and phospholipids, was greater than those without treatment (Figure 3.12C). This confirms that the observable lipid droplets contain triglycerides.

3.10 Fatty acid exposure to rat, mouse and human hepatocytes show an increase in lipid accumulation

Use of primary hepatocytes is considered the gold standard when investigating hepatocyte toxicity *in vitro*. Treatment of human hepatocytes with 1mM fatty acids showed a 2-fold increase in lipid accumulation (Figure 3.13A). However, the increase observed in B-13/H cells was much greater. This was likely due to the condition of the liver the hepatocytes were isolated from, as they were already steatotic (Figure 3.13B). Hepatocytes isolated from rats showed a greater increase of in lipid accumulation (7-fold increase compared to control cells) when exposure to fatty acids compared to their human counterparts (Figure 3.13C&D).

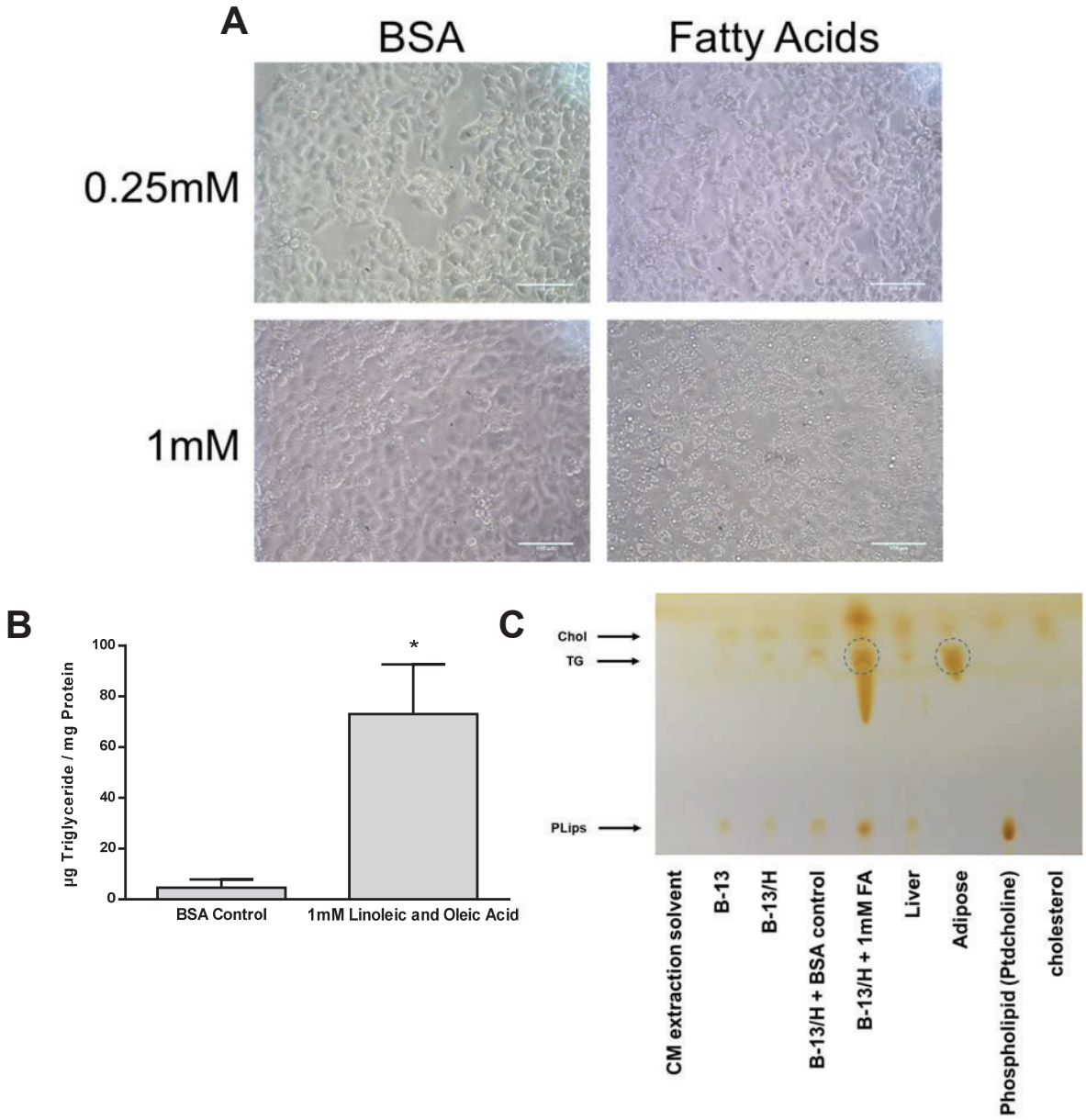

Figure 3.12: Droplet formation in B-13/H cells contain triglycerides. A, B-13/H cells were treated with indicated conditions of fatty acids for 72 hours and cells were imaged by bright-field microscopy (scale bar = 100µm). **B,** B-13/H cells were treated with indicated conditions of fatty acids for 72 hours, following treatment triglyceride content was determined. Data was normalised to protein concentration by Lowry protein determination. Data are the mean and SD of 3 separate experiments. * significantly different versus control cells ($p<0.05$). **C,** TLC analysis of lipids extracted from the indicated cells/tissue (triglycerides indicated by dotted circles; Chol = cholesterol; TG = triglycerides; PLips = phospholipids).

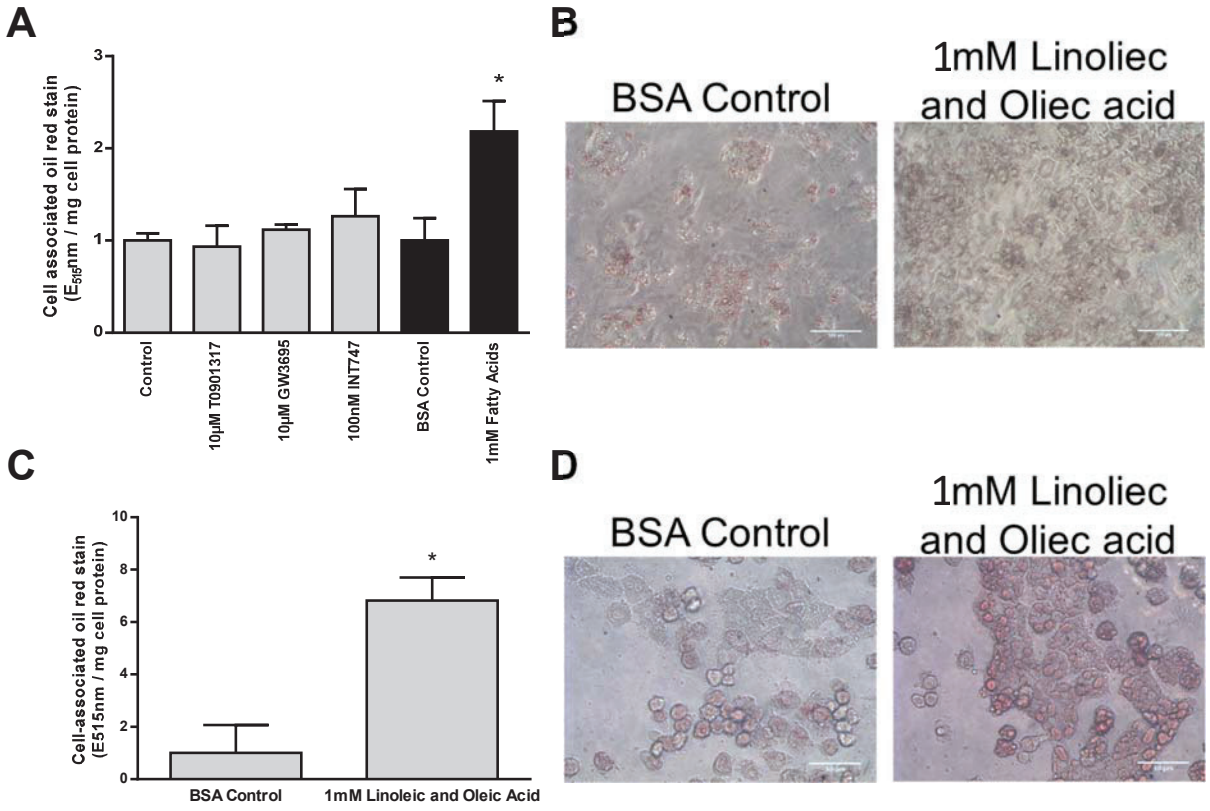

Figure 3.13: B-13/H exposure to fatty acids results in lipid accumulation similarly to primary cells. Primary hepatocytes (**A,** human. **C,** Rat) were treated with indicated conditions for 48 hours. Following treatment cells were fixed and stained with oil red. Lipid accumulation was quantified by extraction of oil red from the cells and absorbance was measured at 515nm. Data was normalised to protein concentration by Lowry protein determination. Data are the mean and SD of 3 separate determinations from the same experiment. * significantly different versus control cells ($p<0.05$). Cells were treated as in A, before extraction of oil red stain cells were imaged by light microscopy (**B,** human. **D,** Rat) (scale bars = 50μm and 100μm respectively).

3.11 Addition of insulin during transdifferentiation of B-13 cells to B-13/H cells increases lipid accumulation.

It was previously found that the differentiation of B-13 to B-13/H cells with the addition of 1X ITS solution (insulin, transferrin, selenium) resulted in lipid accumulation after 2 weeks in the absence of BSA and fatty acid loading. To investigate which of these components was important to this effect, each was individually added to medium with DEX during the transdifferentiation process. Treatment of B-13/H cells with these components during transdifferentiation showed that insulin treatment induced lipid accumulation at similar levels observed in those treated with ITS solution (Figure 3.14A). This effect was observed in all treatments that contain insulin. Selenium also significantly increased lipid accumulation on its own, but

not at the levels observed with insulin or ITS solution. Imaging of ITS and insulin treated cells showed that lipid accumulation occurs around the periphery of the cell (Figure 3.14B).

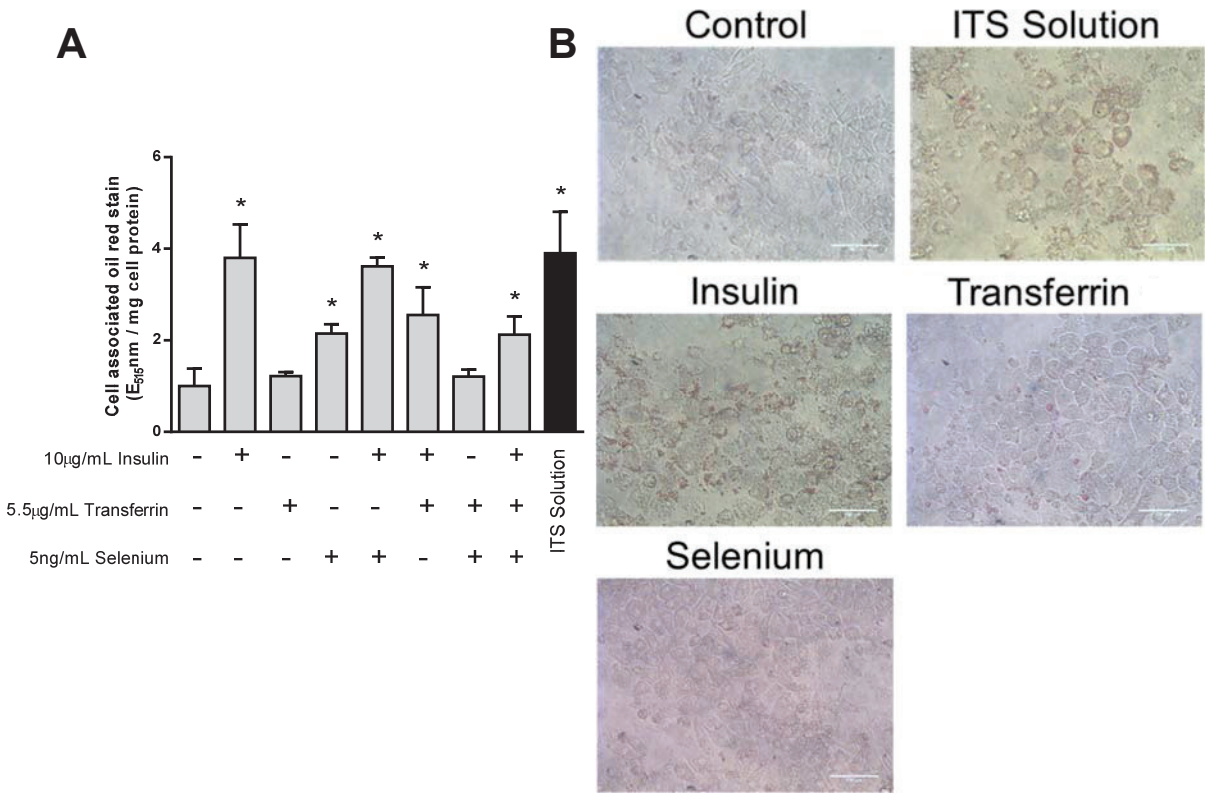

Figure 3.14: Transdifferentiation of B-13 cells to B-13/H cells in medium containing high insulin levels induces lipid accumulation. A, B-13/H cells were transdifferentiated from B-13 to B-13/H cells in indicated conditions for 2 weeks. Following treatment cells were fixed and stained with oil red. Lipid accumulation was quantified by the extraction of oil red from the cells and the absorbance was measured at 515nm. Data was normalised to protein concentration by Lowry protein determination. Data are the mean and SD of 4 separate determinations from the same experiment, typical of 3 separate experiments. * significantly different versus control cells ($p<0.05$). **B,** Cells were treated as in C, before extraction of oil red stain, cells were imaged by bright-field microscopy (scale bar = 100μm).

3.12 The B-13 cells is homozygous wild type for the PNPLA3 gene.

NAFLD in humans has been associated with a polymorphism in the Patatin-like phospholipase domaining-containing protein 3 (PNPLA3) gene. PNPLA3 is an enzyme that has both triacylglycerol lipase and acylglycerol O-acyltransferase activity (Liu *et al.*, 2014). B-13/H cells were therefore sequenced to investigate whether they were genetically susceptible to NAFLD via a mutation in PNPLA3. B-13 and B-13/H cells expressed the transcripts for PNPLA3 (Figure 3.15A). Since these cells expressed PNPLA3, the

human and rat PNPLA3 sequences were aligned (Figure 3.15B). Alignment showed that rodent and human PNPLA3 N-terminal amino acid sequences show high homology. The isoleucine at position 148 (which is replaced by methionine in individuals with increased susceptibility to NAFLD, I148M) is conserved.

A segment of the PNPLA3 transcript, in B-13/H cells was amplified by RT-PCR, cloned and sequenced. The segment was selected around the point of possible mutation (Figure 3.15C). Eleven clones were sequenced, and all were shown to encode a wild type PNPLA3 transcript, indicating with greater than 95% confidence, that if susceptibility to NAFLD in rat is similarly affected by this polymorphism, then B-13/H cells have a homozygous wild type phenotype (Figure 3.15D) and therefore do not have a greater susceptibility due to PNPLA3.

A

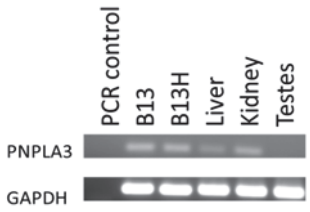

B

```
rPNPLA3      MYDPERRWSLSFAGCGFLGFYHIGATLCLSERAPHILREARTFFGCSAGALHAVTFVCSL
hPNPLA3      MYDAERGWSLSFAGCGFLGFYHVGATRCLSEHAPHLLRDARMLFGASAGALHCVGVLSGI
             *** ** ***************:*** ****:***:**:** :**.******.* .:..:

rPNPLA3      PLDHIMEILMDLVRKARSRNIGTLHPFFNINKCVRDGLQETLPDNVHQIISGKVYISLTR
hPNPLA3      PLEQTLQVLSDLVRKARSRNIGIFHPSFNLSKFLRQGLCKCLPANVHQLISGKIGISLTR
             **:: :::* ************ :** **:.* :*:** : ** ****:****: *****

rPNPLA3      VSDGENVLVSEFHSKDEVVDALVCSCFIPLFSGLIPPSFRGERYVDGGVSDNVPVLDAKT
hPNPLA3      VSDGENVLVSDFRSKDEVVDALVCSCFIPFYSGLIPPSFRGVRYVDGGVSDNVPFIDAKT
             **********:*:***************::********** ************.:****

rPNPLA3      TITVSPFYGEHDICPKVKSTNFLQVNITNLSLRLCTGNLHLLTRALFPSDVKVMGELCFQ
hPNPLA3      TITVSPFYGEYDICPKVKSTNFLHVDITKLSLRLCTGNLYLLSRAFVPPDLKVLGEICLR
             **********:************:*:**:**********:**:**:.* *:**:**:*::

rPNPLA3      GYLDAFRFLEENGICNGPQRSLSLSLEKEMAPETMIPCLENGHLVAGN----------K
hPNPLA3      GYLDAFRFLEEKGICNRPQPGLKSSSE-GMDPEVAMPSWANMSLDSSPESAALAVRLEGD
             ***********:**** ** .*. * *  * **. :*.  *  * :.           .

rPNPLA3      VPVSCVCLTAVPSDESIWEMLSPKLSTALTEAIKDRGGYLNKVCNLLPIRILSYILLPCT
hPNPLA3      ELLDHLRLSILPWDESILDTLSPRLATALSEEMKDKGGYMSKICNLLPIRIMSYVMLPCT
               :. : *: :* **** : ***:*:***:* :**:***:.*:********:**::****

rPNPLA3      LPVESAIAAVHRLVMWLPDIHEDIQWLQWATSQVCARMTMCLLPSTRSRASKDNHQTLKH
hPNPLA3      LPVESAIAIVQRLVTWLPDMPDDVLWLQWVTSQVFTRVLMCLLPASRSQMPVSSQQASPC
             ******** *:*** ****: :*: ****.**** :*: *****::**:   ..:*:

rPNPLA3      GYH---PS--LHKPQGSSAGL---------------------------------------
hPNPLA3      TPEQDWPCWTPCSPKGCPAETKAEATPRSILRSSLNFFLGNKVPAGAEGLSTFPSFSLEK
               .   *.    .*:*. *

rPNPLA3      --
hPNPLA3      SL
```

C

```
                 US primer site→
wtPnpla3         CTCACCAGAGTGTCCGATGGGGAGAACGTGCTGGTGTCTGAGTTCCATTCCAAAGACGAA
mutPnpla3        CTCACCAGAGTGTCCGATGGGGAGAACGTGCTGGTGTCTGAGTTCCATTCCAAAGACGAA
                 ************************************************************

wtPnpla3         GTGGTGGATGCCCTGGTGTGCTCCTGCTTCATTCCTCTCTTCTCTGGCCTAATCCCTCCT
mutPnpla3        GTGGTGGATGCCCTGGTGTGCTCCTGCTTCATGCCTCTCTTCTCTGGCCTAATCCCTCCT
                 ******************************** *************************
                                                  FatI

wtPnpla3         TCCTTCCGAGGTGAGCGGTACGTGGATGGAGGAGTGAGTGACAACGTCCCTGTG
mutPnpla3        TCCTTCCGAGGTGAGCGGTACGTGGATGGAGGAGTGAGTGACAACGTCCCTGTG
                 ********************************************************
                                                  ← DS primer site
```

D

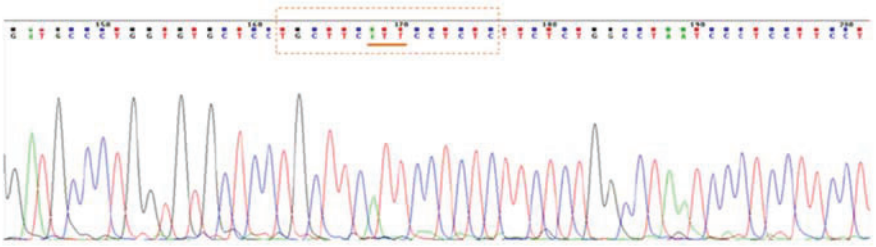

Figure 3.15: The B-13 cells is homozygous wild type for the patatin-like phospholipase domain-containing protein 3 (Pnpla3) gene. A, RT-PCR for indicated transcripts in indicated cell types and rat tissue. **B,** CLUSTAL O (1.2.1) multiple sequence alignment (http://www.ebi.ac.uk/Tools/msa/clustalo/) of rat (rPNPLA3) and human (hPNPLA3) amino acid sequences, with the wild type isoleucine residue at position 148 indicated in red. "*", a single, fully conserved residue; ":", conservation between groups of strongly similar properties; ".", conservation between groups of weakly similar properties; – no residue alignment. **C,** Alignment of CLUSTAL O (1.2.1) multiple sequence alignment of the wild type rat Pnpla3 cDNA sequence (wtPnpla3) and the predicted mutant Pnpla3 cDNA sequence (mutPnpla3) amplified by RT-PCR using the upstream (US) and downstream (DS) primers as indicated. **D,** Typical sequencing data from RT-PCR product amplifying the region of the B-13 patatin-like phospholipase domain-containing protein 3 (PNPLA3) cDNA sequence.

3.13 Polysorbate 80 induces lipid accumulation in B-13/H cells

Emulsifiers are commonly used in a variety of food have been shown to induce a gain in body weight (Cani and Everard, 2015; Chassaing *et al.*, 2015). Polysorbate 80 (P80) was therefore selected as an emulsifier to investigate if exposure of these compounds can induce lipid accumulation *in vitro* due to it containing oleic acid additions. Incubation with P80 caused an increase in lipid accumulation in a dose dependent manner (Figure 3.16A). 2mM P80 induced a 5-fold increase, however 4mM developed less lipid formation than control cells. MTT data showed that this was most likely due to toxicity induced at this concentration (Figure 3.16B). However, 2mM P80 also showed a reduced MTT activity to 48% compared to control cells.

Carboxymethyl cellulose (CMC) is a second emulsifier that has a different structure to P80, with no fatty acid addition, and was also investigated for its ability to induce lipid accumulation. At the highest concentration tested (30µM), there was no change in lipid formation (Figure 3.16C). There was also no change in MTT activity at these concentrations (Figure 3.16D) and higher concentrations were unable to be tested due to the inability of CMC to remain in solution. These data suggest that only emulsifiers with fatty acid chains like those of P80 could potentially induce steatosis.

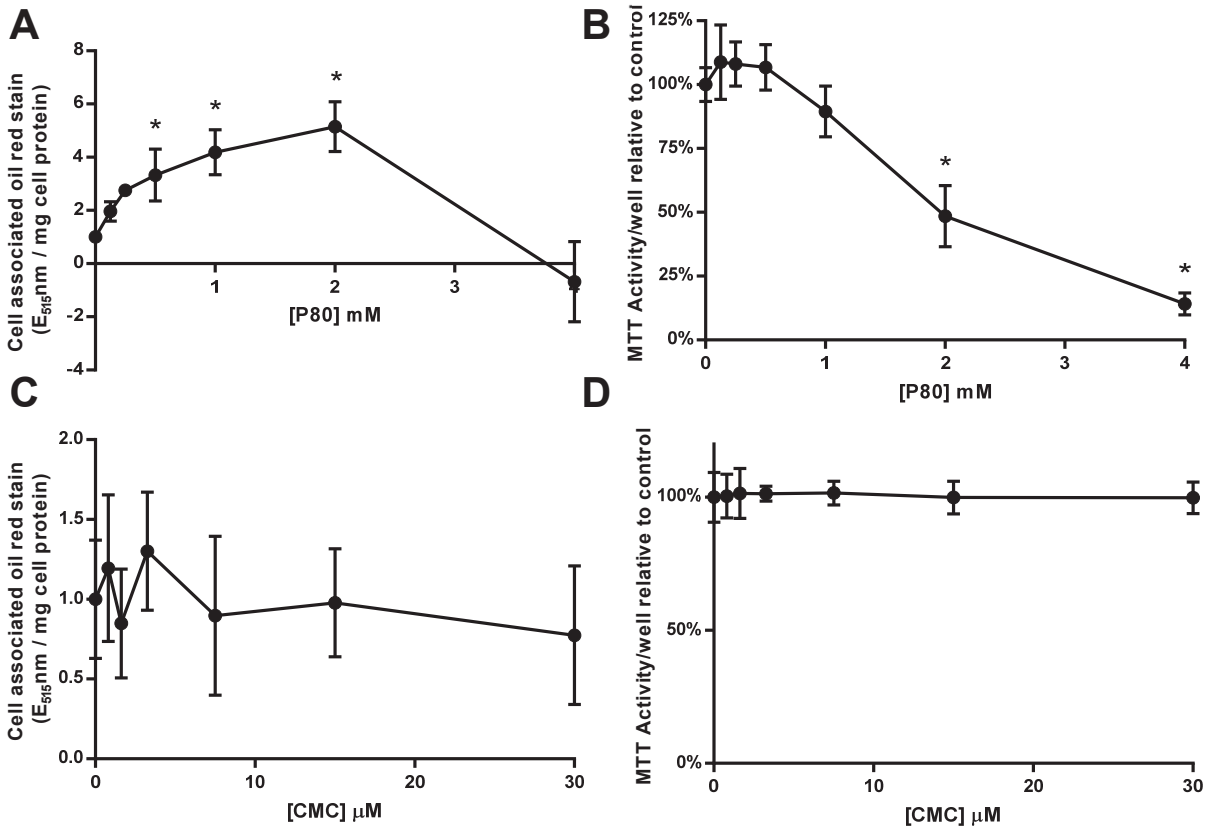

Figure 3.16: Emulsifiers induce lipid accumulation in B-13/H cells. A and C, B-13/H cells were treated with indicated chemicals **(A, P80. B, CMC.)** for 24 hours. Following treatment cells were fixed and stained with oil red. Lipid accumulation was quantified by the extraction of oil red from the cells and the absorbance was measured at 515nm. Data was normalised to protein concentration by Lowry protein determination. Data are the mean and SD of 3 separate determinations from the same experiment, typical of 3 separate experiments. * significantly different to control treated cells ($p<0.05$) tested by ANOVA followed by Bonferroni post-hoc test. **B and D,** cells treated as for A and C respectively. Following treatment, cells were incubated with MTT for 2 hours and reduction determined. Data are the mean and SD of 6 separate determinations from the same experiment, typical of 3 separate experiments. * significantly different to control ($p<0.05$) tested by ANOVA followed by Bonferroni post-hoc test.

3.14 Treatment with fatty acids does not alter the basal oxygen consumption rate of B-13/H cells

Steatotic cells are more susceptible to endoplasmic reticulum stress (Dara *et al.*, 2011). This and other forms of cellular stress could therefore be investigated in a steatotic B-13/H cell model. Mitochondrial function comparing steatotic and non-steatotic cells was selected to investigate. The functioning of the mitochondria in B-13/H cells pre-treated with fatty acids for 24 hours was compared to control cells using the seahorse flux analyser. The oxygen consumption rate (OCR) in fatty acid treated cells was similar to control cells (Figure 3.17A). However, when FCCP was added the OCR was lower than control cells. There

was no observed change in the extracellular acidification rate (ECAR) between treatments (Figure 3.17B). Fatty acid pre-treatment did not have any effect on the basal rate, proton leak, non-mitochondrial oxygen consumption or ATP production (Figure 3.17C). There was a reduction in maximal respiration (from 31.86 to 26.39pmol/min/µg) and the spare respiratory capacity (from 11.59 to 5.64pmol/min/µg), as observed with the addition of FCCP. Overall these data suggest that fatty acid treatment had an effect on the maximal respiration rate of the mitochondria with no basal effects.

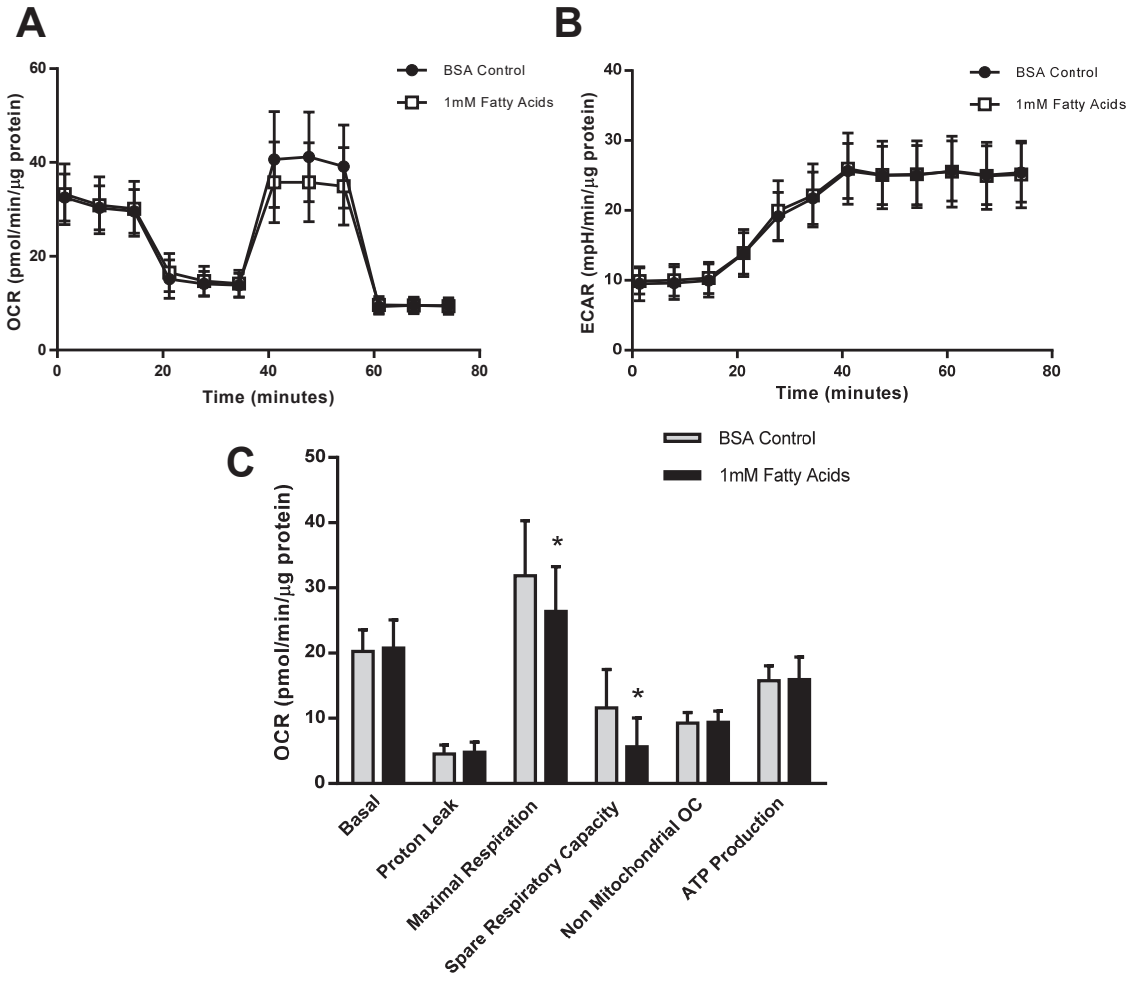

Figure 3.17: Treating B-13/H cells with fatty acids has no effect on mitochondrial oxygen consumption rate. A, time course plot of oxygen consumption rate (OCR) in B-13/H cells pre-treated with 1mM fatty acids (and control) for 24 hours. OCR was determined using a Seahorse flux analyser with injections as indicated. Readings are normalised to protein concentration determined using a Bradford assay. Data are mean and SD of at least 12 readings from the same experiment, typical of 3 experiments. **B,** Extracellular acidification rate (ECAR) of B-13/H cells treated as in A. Data are mean and SD of at least 12 readings from the same experiment, typical of 3 experiments. **C,** effects that indicated treatments have on B-13/H mitochondrial functions based on seahorse time course data. Data are mean and SD of at least 12 readings from the same experiment, typical of 3 experiments. * significantly different between treatments ($p<0.05$).

3.15 Fatty acid treated cells does not affect the toxicity of hepatotoxic drugs

It was hypothesised that steatotic cells would be more susceptible to hepatotoxins. Menadione was selected as the hepatotoxin to test whether this can be studied *in vitro* in B-13/H cells. Under standard conditions of glucose medium and 20% oxygen, menadione showed no change in cell viability between

fatty acid treated cells and control cells, indicated by MTT activity (Figure 3.18A). Oxygen percentage in the incubator was increased to 80% and cells were also treated in galactose supplemented media instead of glucose media. Increasing the oxygen to 80% had a protective effect on menadione toxicity, (Figure 3.18A), despite the mechanism of menadione toxicity being ROS production (Criddle *et al.*, 2006). Fatty acid treated cells were also more toxic at 15-20μM menadione than the BSA control cells. Menadione treatment in galactose had a similar effect to that of glucose media at 20% (Figure 3.18B). However, at 80% oxygen the protective effect observed in glucose media was lost.

To confirm the mitochondrial effects of menadione, analysis using the seahorse flux analyser was carried out. There was no change observed between fatty acid and control treated cells with menadione in the OCR (Figure 3.19A) or ECAR (Figure 3.19B). Menadione increased the OCR and the ECAR when exposed to the cells. This appeared the influence the effects of oligomycin and FCCP. When comparing the end points of the analysis, nearly all showed some change when incubated with menadione. For example, the increase in proton leak and decrease in coupling efficacy (Figure 3.19C).

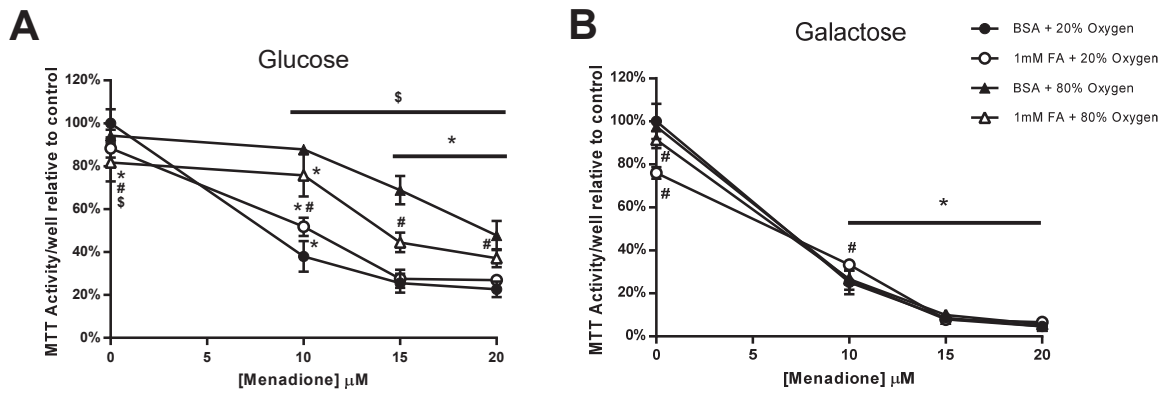

Figure 3.18: Pre-treatment of B-13/H cells with fatty acids does not affect the toxicity of menadione. B-13/H cells were pre-treated for 24 hours with 1mM linoleic and oleic acid (or vehicle control). After pre-treatment cells were treated for a further 24 hours with indicated doses of menadione in either 20% oxygen or 80% oxygen. These treatments were either in **A,** glucose or **B,** galactose medium. Following treatment, cells were incubated with MTT for 2 hours and reduction determined. Data are the mean and SD of 3 separate determinations from the same experiment, typical of 3 separate experiments. * significantly different to BSA 20% control treated cells, # significantly different between 20% and 80% oxygen of the same cell treatments, $ significantly different between BSA and 1mM FA of the same oxygen percentage ($p<0.05$) tested by two-way ANOVA followed by Bonferroni post-hoc test.

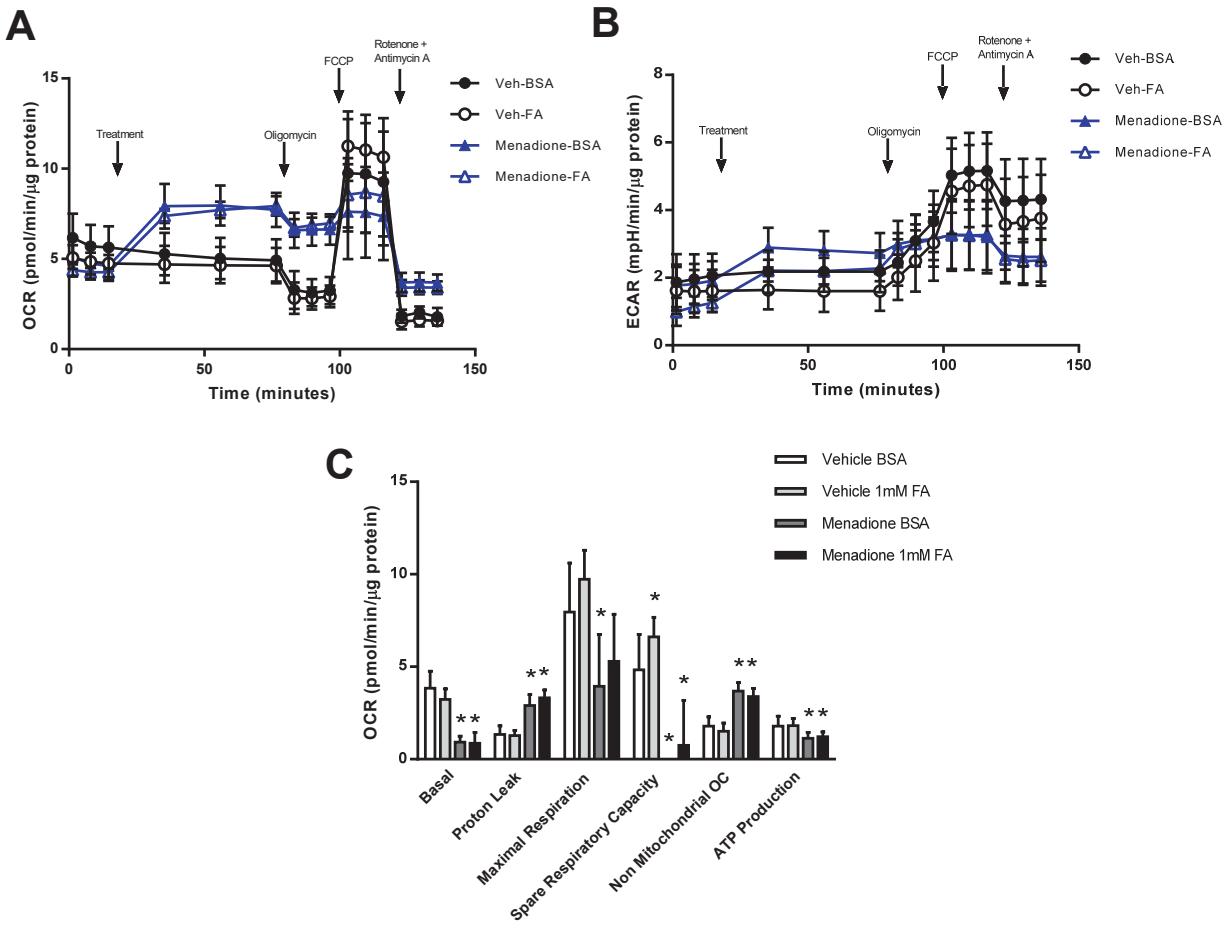

Figure 3.19: Preloading B-13/H cells with fatty acids causes no change in the effect of menadione on the cells OCR. A, time course plot of oxygen consumption rate (OCR) in B-13/H cells pre-treated with 1mM fatty acids for 24 hours. OCR was determined using a Seahorse flux analyser with injections as indicated. Reading are normalised to protein concentration determined using a Bradford assay. Data are mean and SD of at least 12 readings from the same experiment, typical of 3 experiments. **B,** Extracellular acidification rate (ECAR) of B-13/H cells treated as in A. Data are mean and SD of at least 12 readings from the same experiment, typical of 3 experiments. **C, D and E,** effects that indicated treatments have on B-13/H mitochondrial functions based on seahorse time course data. Data are mean and SD of at least 12 readings from the same experiment, typical of 3 experiments. * significantly different between treatments ($p<0.05$).

3.16 B-13/H cells have a functional LXR response

The LXR is a nuclear receptor that is activated by oxysterols and has been considered to be a potential drug target for the treatment of hypercholesterolemia (Bełtowski, 2008; Calkin and Tontonoz, 2012). LXR activators such as T0901317 (Houck *et al.*, 2004) and GW3965 (Kotokorpi *et al.*, 2007) promote steatosis in the liver (Repa *et al.*, 2000; Cha and Repa, 2007). It was therefore hypothesised that these LXR activators could be used to induce steatosis in B-13/H cells.

The LXR transcripts were present in B-13 and B-13/H cells with B-13/H cells expressing the transcripts at similar levels to rat liver (Figure 3.20A). However, the presence of the LXR protein in B-13 and B-13/H cells was low when compared to rat hepatocytes (Figure 3.20B). Despite low expression, T0901317 and GW3965 transactivated an LXR regulated luciferase reporter construct suggestive of functional LXR transcriptional activity. T0901317 was a more potent activator that GW3965 and the FXR agonist, INT747, had no effect (Figure 3.20D). Exposing B-13/H cells to T0901317 significantly induced lipid accumulation, whereas GW3965 (the weaker LXR activator) increased levels but not to a significant level (Figure 3.20C). These data suggest lipid accumulation via the activation of the LXR can be modelled in B-13/H cells.

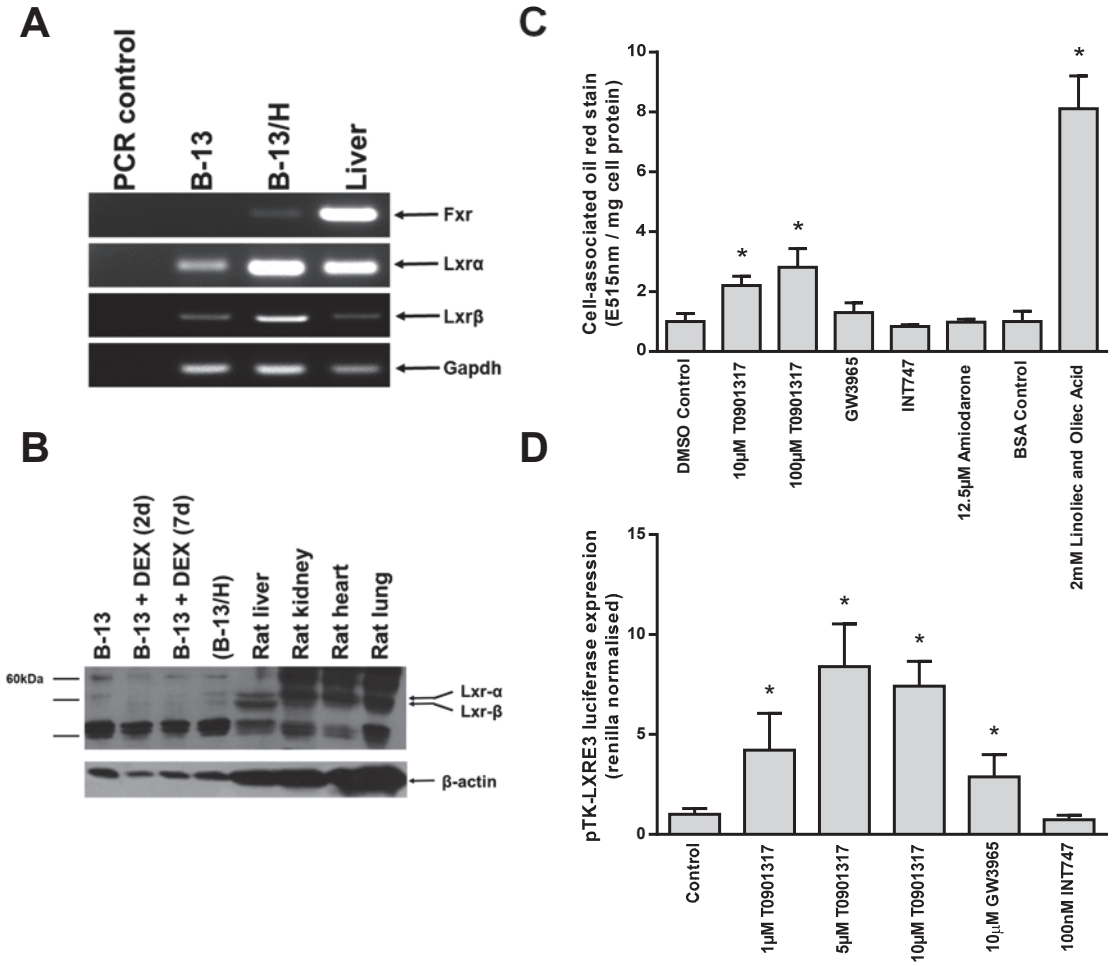

Figure 3.20: B-13/H cells express the LXR and accumulate lipids in response to treatment with LXR activator T0901317. A, RT-PCR for indicated transcripts. **B,** Western Blot for the indicated proteins in extracts from indicated cells/rat tissue. Each lane contains 10μg protein/lane. **C,** B-13/H cells were incubated with indicated treatments for 72 hours. Following treatment cells were fixed and stained with oil red. Lipid accumulation was quantified by the extraction of oil red from the cells and the absorbance was measured at 515nm. Data was normalised to protein concentration by Lowry protein determination. Data are the mean and SD of 3 separate determinations from the same experiment, typical of 3 separate experiments. * significantly different to control treated cells ($p<0.05$) **D,** B-13/H cells were transfected with pTK-LXRE3 luciferase and RL-TK constructs for 48 hours, cells were then treated with indicated compounds for 24 hours. Following treatment luciferase and renilla activities were determined. Data are the mean and SD of 6 separate determinations from the same experiment, typical of 3 experiments. * significantly different versus control ($p<0.05$).

3.17 Exposure of B-13/H cells to ethanol does not induce lipid accumulation

Alcoholic steatosis and steatohepatitis are on the spectrum of alcoholic liver disease caused by the excessive consumption of alcohol (Zhou *et al.*, 2003). Given that B-13/H cells could model steatosis when exposed to fatty acids, it was hypothesised that they could also model alcohol induced steatosis when exposed to ethanol. Ethanol is highly calorific, with energy being produced in the form of NADH from the production of acetate that enters the TCA cycle. The functional expression of alcohol dehydrogenase (ADH) and aldehyde dehydrogenase (ALDH) are required for cells to metabolise ethanol to aldehyde and acetate respectively. B-13 cells expressed alcohol dehydrogenases 1 and 2. When differentiated into B-13/H cells they expressed these transcripts at levels more similar to that of rat liver, with the addition of ADH4 (Figure 3.21A). However, they appeared to lack the transcript for ADH6 and 6a. B-13 cells expressed transcripts for aldehyde dehydrogenase 1a1, expression of this was lost in B-13/H cells. Both B-13 and B-13/H cells expressed ALDH1a2, 2 and 3a2, but not 3a1 (Figure 3.21A).

Exposure of B-13/H cells to ethanol up to 200mM did not result in any lipid accumulation (Figure 3.21B). As ethanol in hepatocytes is metabolised into acetaldehyde and then further to acetate, these were also examined for their ability to induce lipid accumulation. Acetaldehyde induced a non-significant increase, however 200mM sodium acetate induced a significant increase, with lipid accumulation beginning from 50mM. Small lipid droplets were seen to form around the periphery of the cell when observed using oil red staining (Figure 3.21C).

3.18 B-13/H cells do not have functional alcohol dehydrogenase activity

The reason why B-13/H cells do not accumulate lipid droplets was then investigated. While they did express ADHs at the mRNA level it was not known whether this resulted in functional ADH activity. This can be detected by measuring the conversion of NAD to NADH (Clemens *et al.*, 1995), a co-factor used by ADH and ALDH. Absorbance wavelength scans showed that when pure ADH and ethanol is added to NAD there is a change in absorbance at 340nm that is indicative of the conversion of NAD to NADH (Figure 3.22A). Therefore, by measuring a change in absorbance at 340nm it can be determined if cells express functional ADH activity.

Using this assay, it was shown that B-13/H cells do not convert NAD to NADH in the presence of ethanol. As a positive control, rat hepatocytes were used and successfully showed the conversion of NAD to NADH (Figure 3.22C). To confirm that this conversion was due to ethanol metabolism by ADH, the ADH inhibitor

pyrazole was added part way through the assay. The addition of pyrazole inhibited NADH conversion from 5.36nmol/mg protein/min to 1.25nmol/mg protein/min (Figure 3.22D) and therefore the effects observed can be attributed to ADH activity.

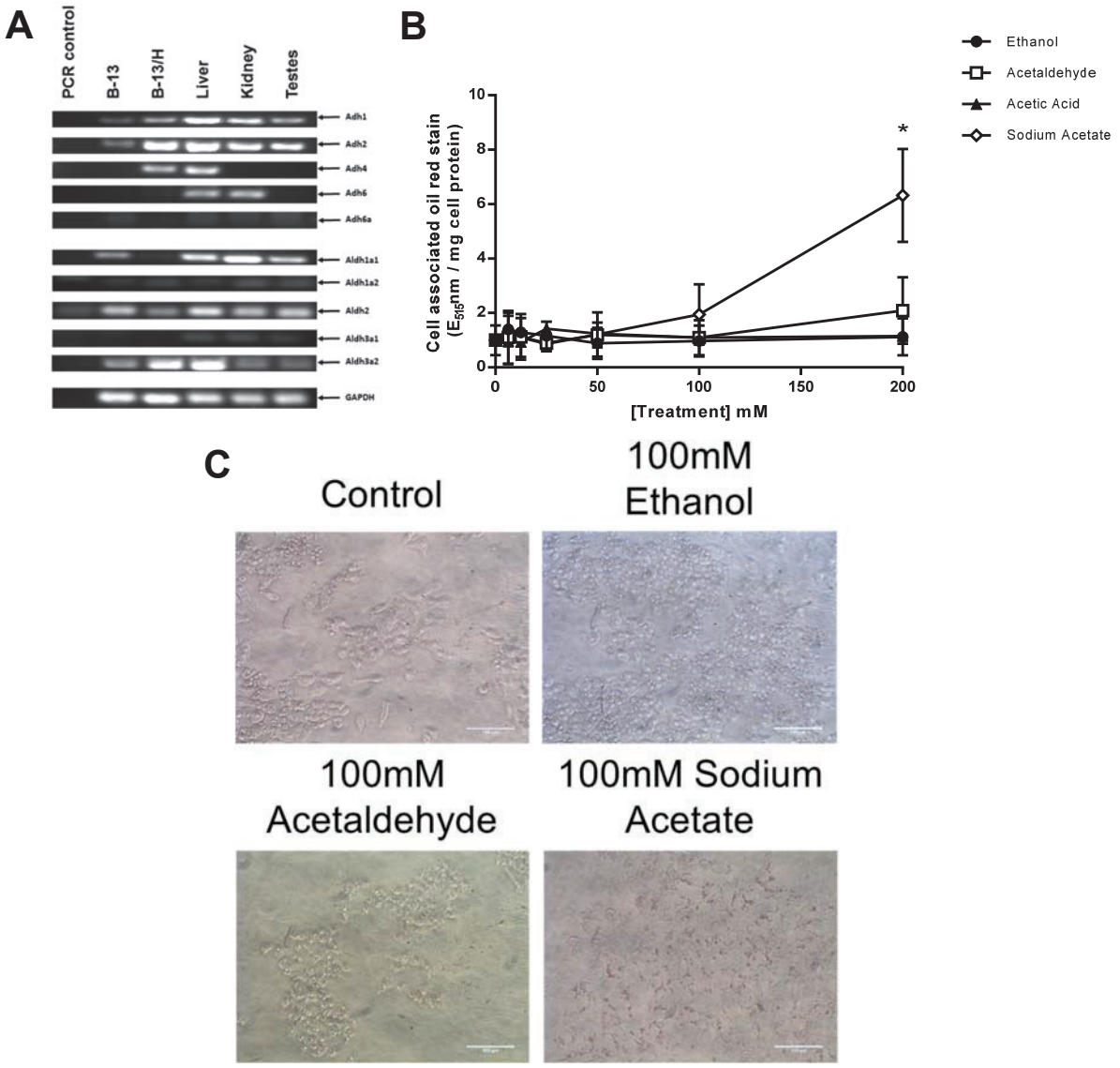

Figure 3.21: Exposure of B-13/H cells to ethanol does not result in lipid accumulation. A, RT-PCR of indicated transcripts in indicated cell types and rat tissue. **B,** B-13/H cells were incubated with indicated treatments for 72 hours. Following treatment cells were fixed and stained with oil red. Lipid accumulation was quantified by the extraction of oil red from the cells and the absorbance was measured at 515nm. Data was normalised to protein concentration by Lowry protein determination. Data are the mean and SD of 3 separate determinations from the same experiment, typical of 3 separate experiments. * significantly different to control treated cells ($p<0.05$) tested by ANOVA followed by Bonferroni post-hoc test. **C,** B-13/H cells were treated as in B, prior to extraction of oil red stain cells were imaged by bright-field microscopy (scale bar = 100µm).

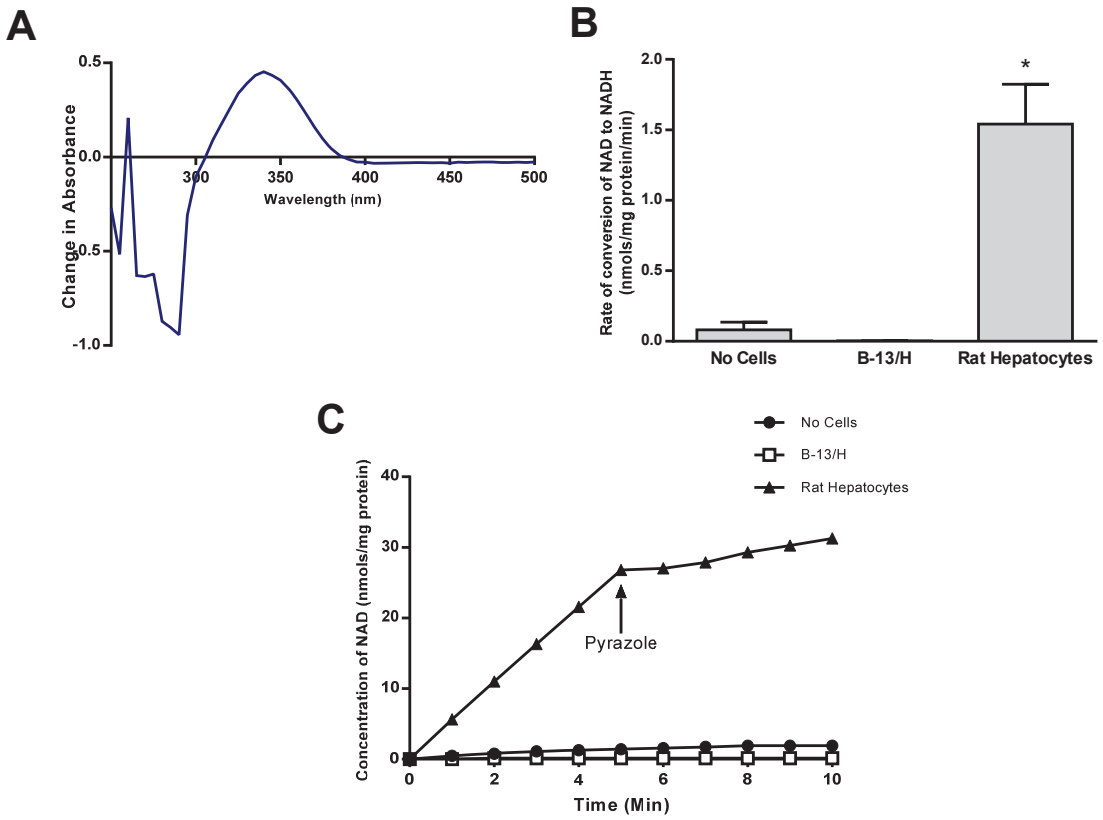

Figure 3.22: B-13/H cells do not have alcohol dehydrogenase activity. A, change in absorbance comparing NAD in absence and presence of alcohol dehydrogenase (ALD) and ethanol. In presence of ethanol and ALD, NAD is used as a cofactor and during the process is converted into NADH, producing a change in absorbance at 340nm **B,** alcohol dehydrogenase activity of cell lysates was determined by measuring conversion of NAD to NADH outlined in the methods section. Readings were normalised to protein concertation determined by Lowry assay. Data are the mean and SD of 3 separate experiments. * significantly different between treatments ($p<0.05$). **C,** alcohol dehydrogenase activity of cell lysates was determined by measuring conversion of NAD to NADH outlined in the methods section. 10mM pyrazole was added to the mixture after 5 minutes as conversion was continually measured.

3.19 Chapter Discussion

The B-13 cell line can be used as a simple, cost effective tool for generating the hepatocyte-like B-13/H cells. Previous work has shown these cells can be used in metabolism and toxicity studies (Probert *et al.*, 2014). It was therefore hypothesised that the B-13/H cells could be used to model steatosis and phospholipidosis.

Phospholipidosis was shown to be induced in B-13 and B-13/H cells when exposed to CADs. For most of the drugs tested there was a difference between these cell types. This is most likely due to the increased expression of functional cytochrome P450's in B-13/H cells. In most cases, B-13 cells showed more phospholipid accumulation compared to B-13/H cells. This suggests that the metabolism of these CADs removes the specific structural/chemical properties required to induce phospholipidosis. Methapyrilene was shown to be a potent inducer of phospholipidosis. However, this response is unlikely to play a role in necrosis since the induction is greater in B-13 cells, which were insensitive to methapyrilene toxicity. This is supported by the addition of nifedipine, that inhibits methapyrilene cell death in B-13/H cells (Ratra *et al.*, 1998; Probert *et al.*, 2014) but showed an increase in phospholipidosis.

Interestingly, the addition of DTT to B-13/H cells treated with methapyrilene (as well as amiodarone and tamoxifen) potently blocked the induction of phospholipidosis. This suggests that an oxidative redox status and/or protein thiol oxidation is required for CAD induction of phospholipidosis, however further experimentation is needed to confirm this hypothesis. The B-13 cells were also used to investigate the role of LPLA2 in the induction of phospholipidosis. LPLA2 has been proposed to interact with lysosomal membranes where it breaks down phospholipids (Shayman and Abe, 2013). CADs incorporate into the membrane where they reduce the surface charge, weakening the interaction between LPLA2 and the membrane. LPLA2 deficient mice (Lpla2 -/-) show an increase in phospholipid accumulation (Hiraoka *et al.*, 2006). Data from the transfection of LPLA2 in B-13 cells showed that an increase in LPLA2 expression reduced the accumulation of phospholipids, supporting the hypothesis that LPLA2 has a role in the mechanism of phospholipidosis. These data suggest that B-13 and B-13/H cells can be used to model PLD as well as used for investigating the possible mechanisms involved in PLD development.

B-13 and B-13/H cells expressed transcripts for fatty acid uptake and synthesis, however only B-13/H cells expressed CD36 which could explain why B-13/H cells displayed an increased capacity for fatty acid accumulation. B-13 cells were also shown to be homozygous wild type for the PNPLA3 gene, therefore are not as susceptible to NAFLD compared to if they had the I148M polymorphism (Liu *et al.*, 2014). The B-

13/H cells have been shown to accumulate intracellular triglycerides in the form of lipid droplets (steatosis) in response to the exposure of fatty acids (bound to albumin to reduce their toxicity). This response was both dose and time-dependent. These data were translatable to human hepatocytes that also showed an increase in lipid accumulation following exposure to fatty acids. One advantage the B-13/H cells had over the primary human hepatocytes was that they were not already steatotic prior to treatment, whereas the primary human hepatocytes had some lipid accumulation following isolation. Additionally, inter-experimental variation in B-13/H cells is much lower than human hepatocytes, since B-13 cells between experiments are derived from the same donor source and essentially genetically identical. In contrast, human donors are likely to be highly variable. Prolonged exposure to high concentrations of glucose and insulin also showed development of steatosis. However, the levels of insulin used (100nM) are not biologically relevant as levels normally around 100pM (Bonner-Weir *et al.*, 1983).

Steatosis induced by chemicals was also investigated in B-13/H cells using LXR activators and emulsifiers. The LXR is ligand-activated transcription factor, activators of which have been shown to induce steatosis in the liver (Cha and Repa, 2007). Treatment of B-13/H cells with LXR activators (T0901317) showed the accumulation of lipid droplets. Storage of neutral lipids is directly proportional to the abundance of adipocyte differentiation-related protein (ADFP), a protein at the surface of lipid droplets (Chang *et al.*, 2006). GW3965 induces ADFP in human but not rat hepatocytes. This may explain why GW3965 induces the LXR but does not show significant lipid droplet formation. Emulsifiers have been shown to have a negative alteration on gut microbiota and induce weight gain and inflammation (Cani and Everard, 2015; Chassaing *et al.*, 2015). Their use in food production could mean that there is a high exposure to these chemicals to the general population. P80 is an emulsifier used in many food products and showed a significant increase in lipid accumulation in B-13/H cells whereas CMC did not. This suggests that emulsifiers that contain fatty acids, such as P80, induce hepatic steatosis and should be further investigated.

These data suggest that the B-13/H cells can be used to model hepatic steatosis. This can be induced by fatty acids, LXR activation or by exposure to chemicals such as emulsifiers. A repeatable steatotic model could be used to compare steatotic and non-steatotic cells and how they respond to other stresses such as toxins. This was investigated in the B-13/H model to compare the effects of the hepatotoxin menadione, and mitochondrial effects in steatotic and non-steatotic cells. Seahorse analysis showed there was little change between the mitochondrial function between steatotic and non-steatotic cells, with and without menadione treatment. There was an increase in oxygen consumption in cells treated with menadione.

Menadione disrupts the mitochondrial membrane potential and induces the production of ROS, resulting in in oxidative stress and apoptosis of the cell (Criddle *et al.*, 2006; Loor *et al.*, 2010). While no significant effects were observed, other stresses/toxins should be investigated in steatotic cells.

The final inducer of steatosis investigated was ethanol. Results showed that exposure to ethanol did not induce lipid droplet formation. This was likely due to the lack of alcohol dehydrogenase activity (or aldehyde dehydrogenase when exposed to acetaldehyde). This means that ethanol and acetaldehyde are not metabolised to acetate. This results in extra acetate not being used in the TCA cycle, or the extra energy being produced during metabolism in the form of NADH. This is supported by the lipid accumulation observed when cells were exposed to acetate.

This chapter has demonstrated that the B-13 and B-13/H cells can be used to investigate two drug and chemical induced lipid storage disorders, phospholipidosis and steatosis. These can be used to investigate the effects that metabolism may have on phospholipidosis, as well as possible mechanisms. The B-13/H cells can be used to model non-alcoholic steatohepatitis induced by fatty acids and chemicals, without interference from alcoholic liver disease. These steatotic cells can then be used to investigate the effects other stresses may have on steatotic cells compare to normal cells.

Chapter 4. Toxicity of an ionic liquid, M8OI

4.1 Introduction

The aetiology of PBC is uncertain, however, it is generally considered that susceptibility is determined by an individual's genetics as well as some environmental factors. Studies have found uneven distribution of PBC incidence in cities in the north of England (Triger, 1980; Prince *et al.*, 2001) and in New York City (Ala *et al.*, 2006). Environmental triggers have been suggested in these cases, such as a water reservoir in Sheffield and a superfund waste site in New York. Xenobiotics used in cosmetics have also been identified as possible triggers in the general population (Rieger *et al.*, 2006). However, no infectious agent or xenobiotic has been identified in areas of high prevalence of PBC that could be described as a trigger and therefore explain why clustering is observed in these areas.

Prior research in the group has shown a xenobiotic in the environment that could potentially act as a trigger for PBC (Probert *et al.*, 2018). In the study, soil samples were taken from taken from around an urban landfill site in an area with a high PBC incidence as well as control sites. These samples were screened for receptor activation and cell toxicity. It was found that some of the samples from the landfill site were toxic to B-13 cells. An imidazolium based ionic liquid, 3-methyl-1-octyl-1H-imidazol-3-ium (M8OI), was identified in these samples and was considered to be the chemical responsible for the toxic effects observed in B-13 cells (Probert *et al.*, 2018).

Ionic liquids (ILs) are composed of an organic cation and inorganic anion, have melting temperatures below the boiling point of water and are often liquids at room temperature (Pernak *et al.*, 2016). They are considered environmentally friendly "green" solvents due to their low volatility and therefore a possible alternative to existing organic solvents (Pernak *et al.*, 2016). ILs have other properties that make them desirable for their use in industry and technology. These include the afore mentioned low volatility as well as low flammability, high thermal stability and conductivity (Pernak *et al.*, 2016). ILs are used/associated with lubricants, nanoparticle synthesis, bio-catalysts, industrial solvents, fuel cells, batteries and metal plating (Heckenbach *et al.*, 2016).

A meta-analysis of the IL and toxicology literature found that relatively few publications have focused on the toxicology of all ILs (Heckenbach *et al.*, 2016). Approximately 50% of all IL toxicity publications were based on imidazolium ILs and the publications that used *in vivo* models were limited (Heckenbach *et al.*, 2016). Therefore, the toxicity data available of M8OI specifically is limited. Thus, the aim of this chapter, with the use of several *in vitro* and *in vivo* models, is to investigate the toxicity of M8OI and potential

mechanisms and to compare any toxic effects to those observed in the soil samples extracted from the landfill site found close to a high incidence rate of PBC.

4.2 M8IO is toxic to the liver progenitor B-13 cells

To assess M8OI toxicity, several cell lines were treated with increasing concentrations of M8OI for 48 hours and cell viability was determined by an MTT assay. The B-13 and B-13/H cells were used to assess the difference between liver progenitor cells and hepatocyte-like cells. To model the effects in human hepatocytes and cholangiocytes, HepG2 and H69 cells were used. M8OI was significantly toxic to all cell lines used at 100µM, with the greatest effect in the B-13 and B-13/H cells where there was close to complete loss in cell viability. H69 cells were more resistant to M8OI induced toxicity, displaying ~50% cell death at 100µM (Figure 4.1). At 10µM M8OI, cell viability was reduced to approximately 75% for B-13/H, HepG2 and H69 cells. B-13 cells were more sensitive to M8OI and 10µM, showing a cell viability of ~25%.

Cell titre glo was used to measure ATP content and used as a second cell viability assay to confirm the results from the MTT and to investigate the difference between B-13 and B-13/H cells. At 24 hours and 48 hours a difference between B-13 and B-13/H cells was observed, with B-13 cells being more sensitive to M8OI induced toxicity and showing a reduced ATP content. The greatest difference was at 10 and 100µM (a difference of 50% and 43% respectively at 24 hours) while at 500µM and 1000µM there was no difference between the two cell lines (Figure 4.2A&B). There was a significant increase in ATP content in B-13/H cells treated with 0.1µM M8OI after 24 hours (Figure 4.2A). These data show that B-13 cells, liver progenitor cells, are more sensitive to M8OI than the hepatocyte-like B-13/H cells.

4.3 M8OI is less toxic to primary human hepatocytes than primary mouse hepatocytes

M8OI toxicity was measured in primary human and mouse hepatocytes. In primary mouse hepatocytes, 100µM M8OI significantly reduced cell viability to 25% of control. No cell death was observed at lower concentration (Figure 4.3A). Cell viability was then measured in primary human hepatocytes and showed a significant reduction in cell viability between 40 and 100µM (Figure 4.3B). At 100µM M8OI, human hepatocytes were less sensitive than mouse hepatocytes with cell viabilities of 59.5% and 25% respectively (Figure 4.3). M8OI toxicity was therefore observed in primary cells as well as immortalised cell lines.

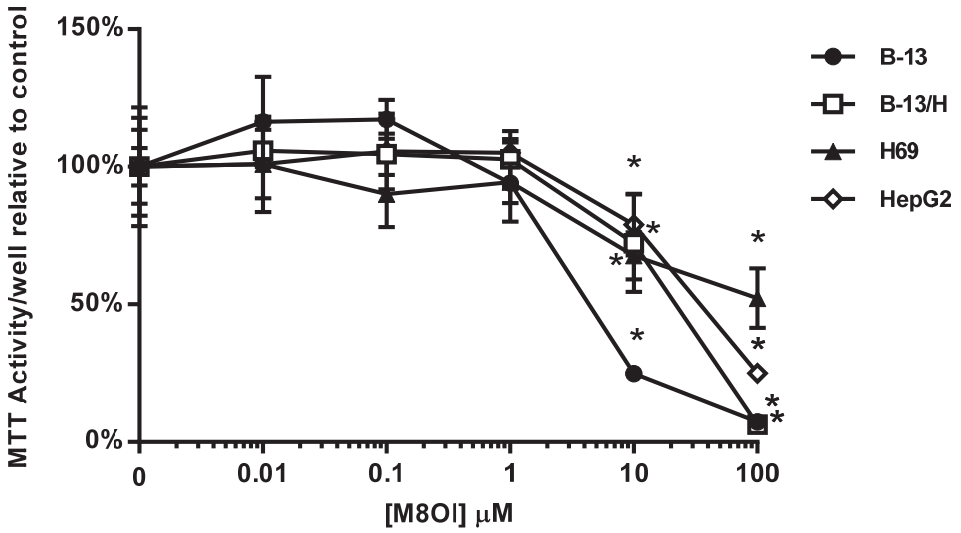

Figure 4.1: MTT activity is reduced by M8OI in immortalised cell lines. B-13, B-13/H, HepG2 and H69 cells were treated for 48 hours with indicated concentrations of M8OI. Following treatment, cells were incubated with MTT for 2 hours and reduction determined. Data are the mean and SD of 6 separate determinations from the same experiment, typical of 3 separate experiments. * significantly different to control ($p<0.05$) tested by ANOVA followed by Bonferroni post-hoc test.

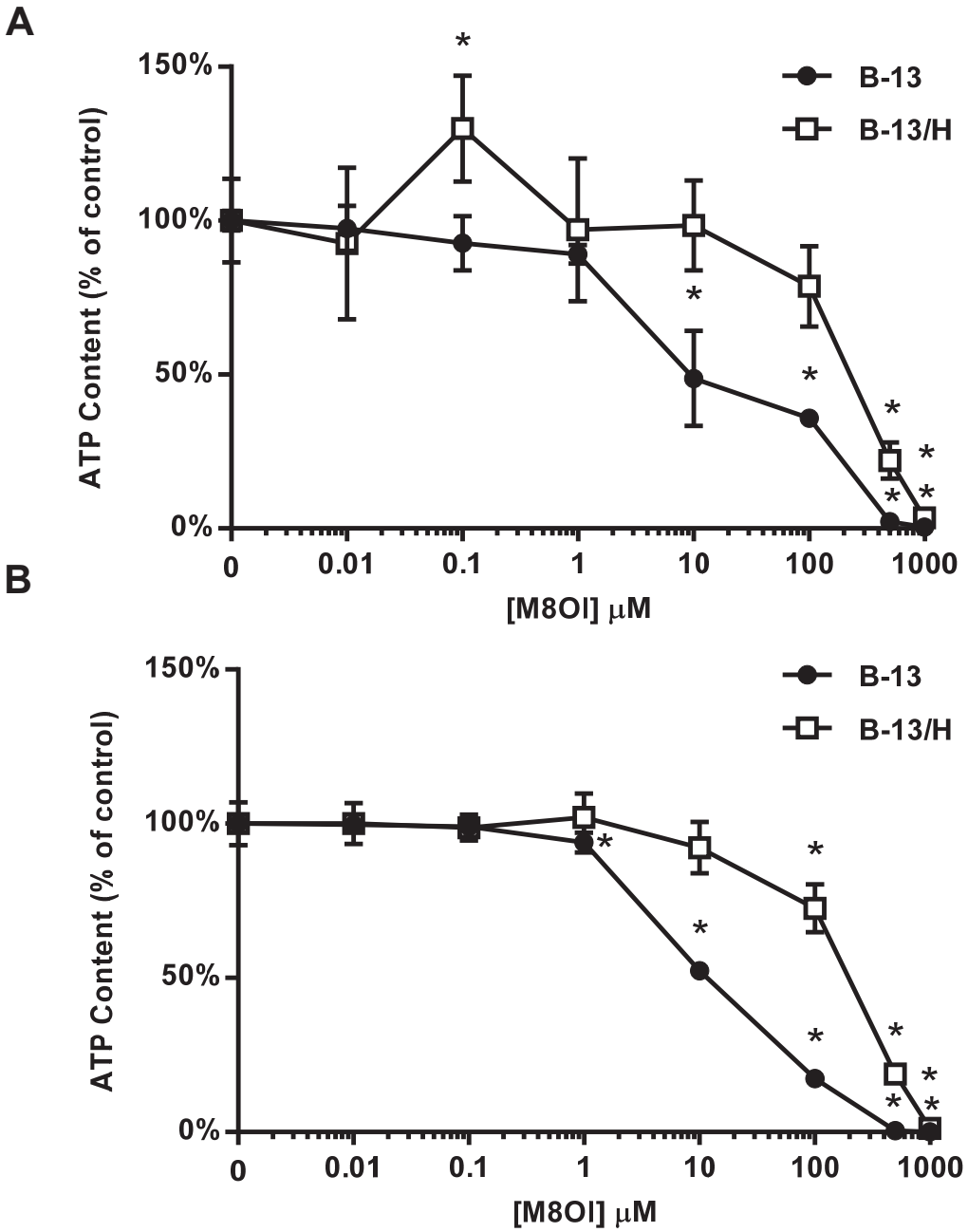

Figure 4.2: M8OI reduces ATP content in B-13 and B-13/H cells. B-13 and B-13/H cells were treated with indicated concentrations of M8OI for 24 hours **(A)** and 48 hours **(B)**. Following treatment, media was changed, and the cells were incubated with cell titre glo for 30 minutes and luminescence measured, and relative ATP content was determined. Data are the mean and SD of 5 separate determinations from the same experiment, typical of 2 separate experiments. * significantly different to control ($p<0.05$) tested by ANOVA followed by Bonferroni post-hoc test.

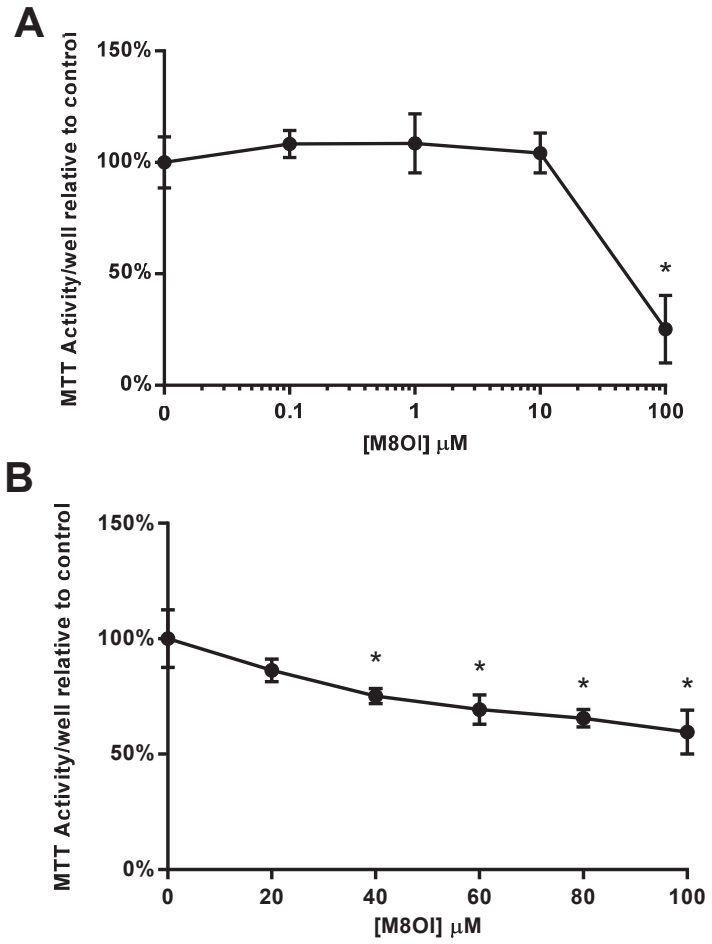

Figure 4.3: M8OI reduces MTT activity in primary hepatocytes. A, primary mouse hepatocytes and **B,** primary human hepatocytes (donor 2, see Table 5.1) were treated with indicated concentrations of M8OI for 24 hours. Following treatment, cells were incubated with MTT for 2 hours and reduction determined. Data are the mean and SD of 6 separate determinations from the same experiment, typical of 2 separate donors. * significantly different to control ($p<0.05$) tested by ANOVA followed by Bonferroni post-hoc test.

4.4 M8OI induces apoptosis in immortalised cell lines

To determine the mechanisms of cell death, necrosis and apoptosis was measured over a 48-hour period in HepG2, H69 and B-13 cells using the Realtime apoptosis and necrosis assay. In HepG2 cells treated with 1000µM of M8OI, luminescence (indicative of the levels of apoptosis) increased over time until it reached a peak at 15 hours (Figure 4.4B). After this peak, a decrease in luminescence was observed and was likely due to the sustainability of the luminescent signal. Overall, this trend was similar to that of the apoptotic positive control compound, 10µM staurosporine. In both 1000µM M8OI and 10µM staurosporine, the

greatest increase in levels of necrosis occurred between 12 and 24 hours, and 9 hours after levels of apoptosis reached a peak (Figure 4.4A). Apoptosis was 3.6-fold lower at 100µM M8OI at its peak compared to 1000µM (Figure 4.4B) and apoptosis levels plateaued at 15 hours. At 48 hours, necrosis levels of 100µM M8OI were 3.6-fold lower than that of 1000µM M8OI, similar to the fold difference with levels of apoptosis (Figure 4.4A). No apoptosis or necrosis was observed at 1µM or 10µM.

In H69 cells, apoptosis was observed at 1000µM, increasing up to 15 hours where peak levels were reached, similar to the response observed in HepG2 cells. However, unlike HepG2 cells, peak levels of apoptosis occurred 11 hours later than staurosporine (Figure 4.5B). Levels of necrosis increased at its greatest rate between 8 and 31 hours after which necrosis levels plateaued (Figure 4.5A). The difference between the peaks at apoptosis and necrosis was 13 hours, slower than HepG2 cells. No necrosis or apoptosis was observed at 1-100µM M8OI.

Apoptosis levels in B-13 cells treated with 1000µM increased between 7 and 15 hours and followed a similar trend to staurosporine (Figure 4.6B). 100µM M8OI increased levels of apoptosis between 15 and 22 hours and at its peak was 2-fold lower than 1000µM. No apoptosis was observed at 10µM M8OI, and low levels were detected at 1µM at 40 hours. Necrosis increased in a dose depended manner. Low levels of necrosis were detected at 1µM M8OI, this increases 3.9-, 7.2-, and 9.5-fold with 10, 100 and 1000µM treated cell respectively (Figure 4.6A). The peak levels of necrosis at 1000µM occurred after 31 hours and was 9 hours later than the peak apoptosis time (Figure 4.6A&B).

Comparing the different cell lines used, all cells showed a peak in luminescence (apoptosis) at 15 hours and fluorescence peaking 9-13 hours later, suggesting secondary necrosis. H69 cells were showed the weakest apoptotic response to M8OI, with only 1000µM producing an effect. B-13 cells were the most sensitive to M8OI induced apoptosis and necrosis with effects being observed at 10µM. These data support the cell viability data in 4.2, where B-13 cells were shown to be the most sensitive and H69 cells the most resistant to M8OI induced toxicity (Figure 4.1).

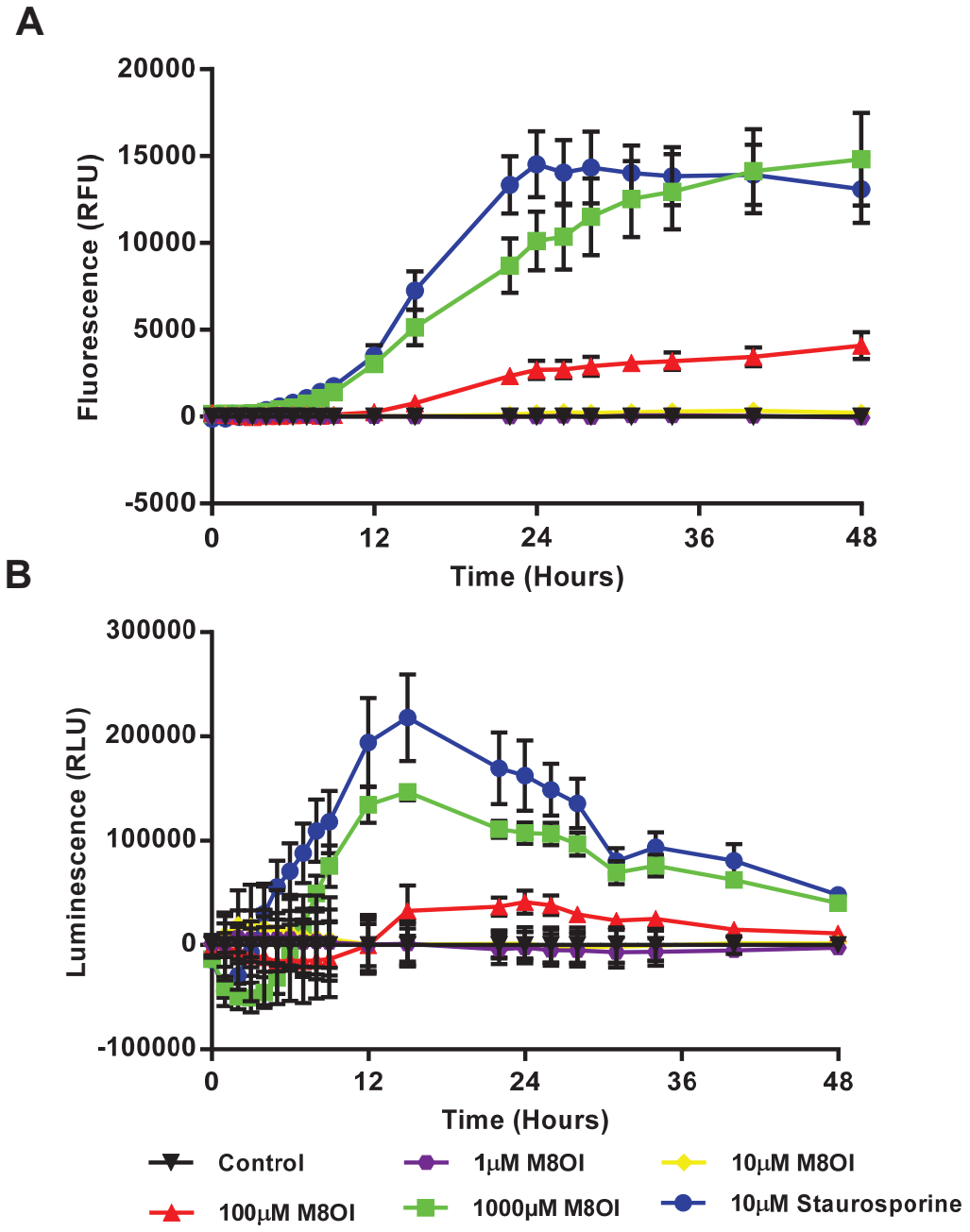

Figure 4.4: M8OI induces apoptosis followed by necrosis in HepG2 cells. HepG2 cells were treated with indicated concentrations of M8OI (and 10μM staurosporine as an apoptotic positive control) and incubated with Realtime-glo annexin V apoptosis and necrosis assay. Fluorescence **(A)** and luminescence **(B)** was measured every 1-8 hours over a 48-hour period to determine levels of necrosis and apoptosis respectively. Data are the mean and SD of 4 separate determinations from the same experiment, typical of 2 separate experiments. Statistics not determined.

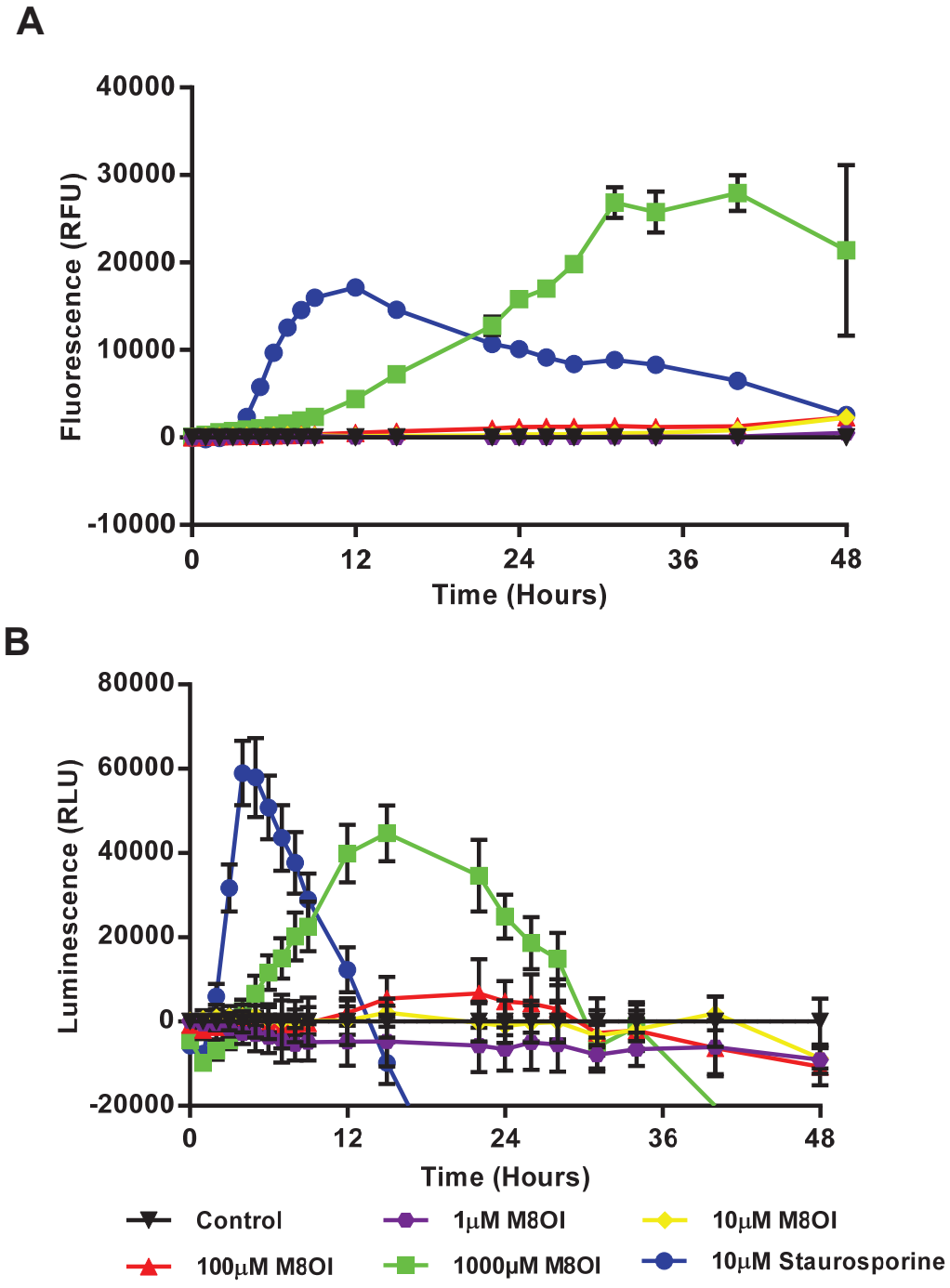

Figure 4.5: M8OI induces apoptosis followed by necrosis in H69 cells. H69 cells were treated with indicated concentrations of M8OI (and 10μM staurosporine as an apoptotic positive control) and incubated with Realtime-glo annexin V apoptosis and necrosis assay. Fluorescence **(A)** and luminescence **(B)** was measured every 1-8 hours over a 48-hour period to determine levels of necrosis and apoptosis respectively. Data are the mean and SD of 4 separate determinations from the same experiment, typical of 2 separate experiments. Statistics not determined.

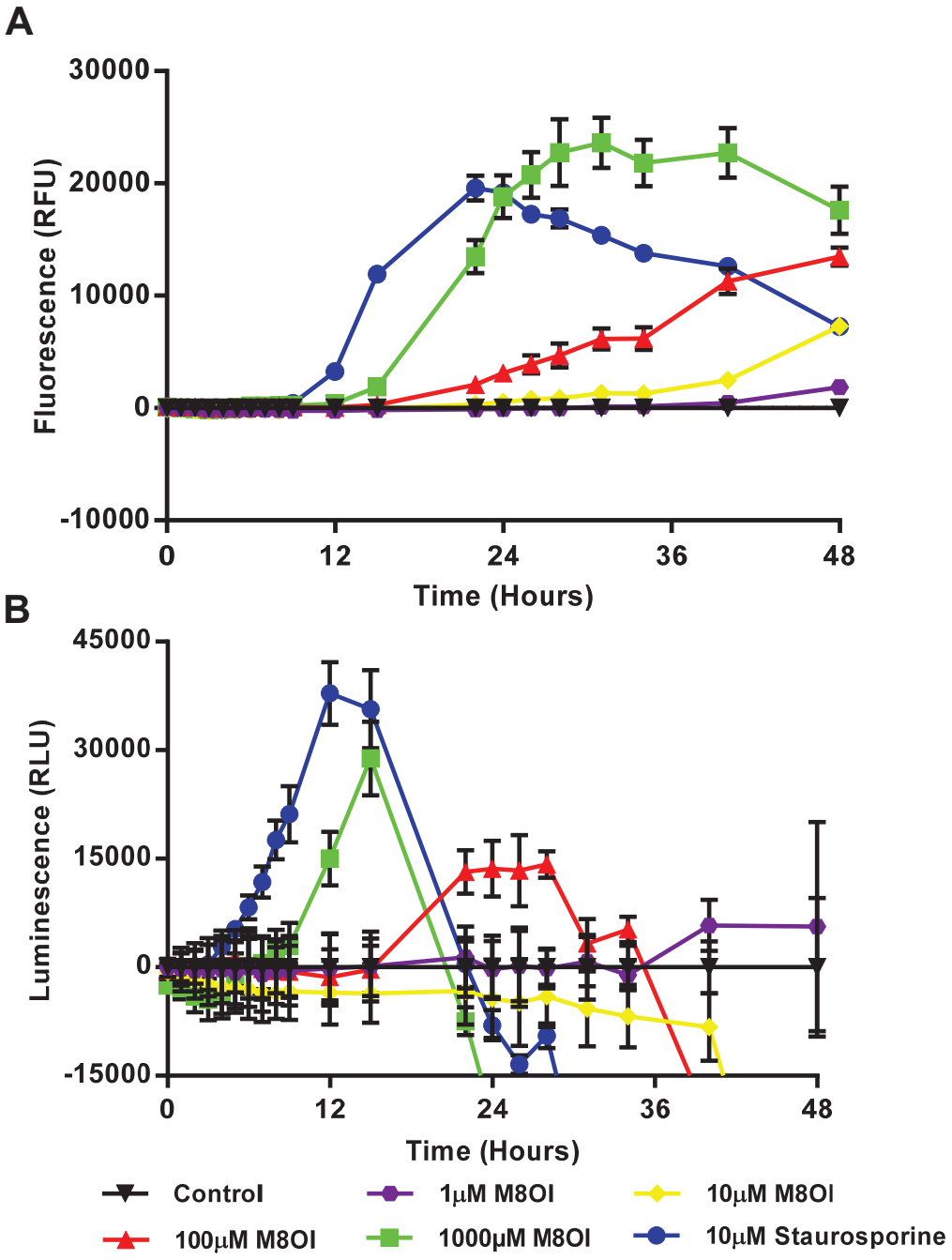

Figure 4.6: M8OI induces apoptosis followed by necrosis in B-13 cells. B-13 cells were treated with indicated concentrations of M8OI (and 10μM staurosporine as an apoptotic positive control) and incubated with Realtime-glo annexin V apoptosis and necrosis assay. Fluorescence **(A)** and luminescence **(B)** was measured every 1-8 hours over a 48-hour period to determine levels of necrosis and apoptosis respectively. Data are the mean and SD of 4 separate determinations from the same experiment, typical of 2 separate experiments. Statistics not determined.

4.5 Apoptotic DNA is observed in M8OI treated B-13 cells

B-13 cells were treated with M8OI for 24 and 48 hours, the DNA was then isolated and ran on an agarose get to visualise. Nucleosomal DNA fragmentation, classically observed in programmed cell death and apoptosis was observed in 10µM and 100µM after 24 hours, with 100µM M8OI showing a greater band intensity (Figure 4.7). At 48 hours, there was more apoptotic DNA in 100µM treated cells compared to 24 hours and at a similar intensity to cells treated with staurosporine for 24 hours. Weak bands were also observed at 1µM. 1000µM M8OI treated cells showed no apoptotic DNA (not shown), suggesting the DNA had been completely degraded or that there was no apoptosis.

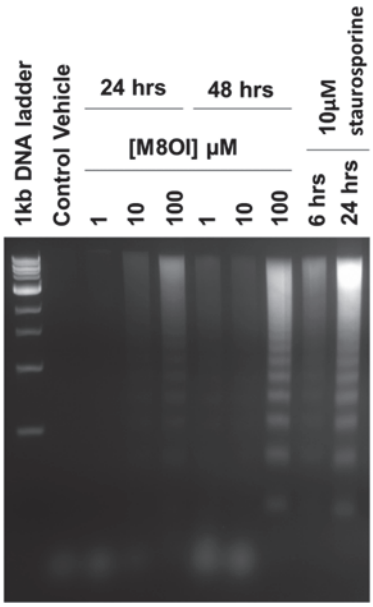

Figure 4.7: M8OI induces nucleosomal ladder formation in B-13 cells. B-13 cells were treated with indicated concentrations of M8OI and staurosporine for 24 and 48 hours. DNA was isolated and ran out on an agarose gel and the apoptotic DNA was visualised using UV light.

4.6 The mitochondria of B-13 cells swell when exposed to M8OI

B-13 cells were treated with 200µM of M8OI for 24 hours and 10µM staurosporine for 6 hours and fixed before being processed for electron microscopy to visualise any cell structure abnormalities. Control treated B-13 cells showed that the nucleus accounts for the majority of the cell, with the mitochondria and other components around the periphery of the cell (Figure 4.8A). The mitochondria of the 24 hour, 200µM M8OI treated cells were swollen and the cristae were not as visible in comparison to control cells

(Figure 4.8B). This is an observable feature of late stage apoptosis (Sun 2007). This effect was also seen at 6 hours, 10µM staurosporine, along with a condensing nucleus (Figure 4.8C).

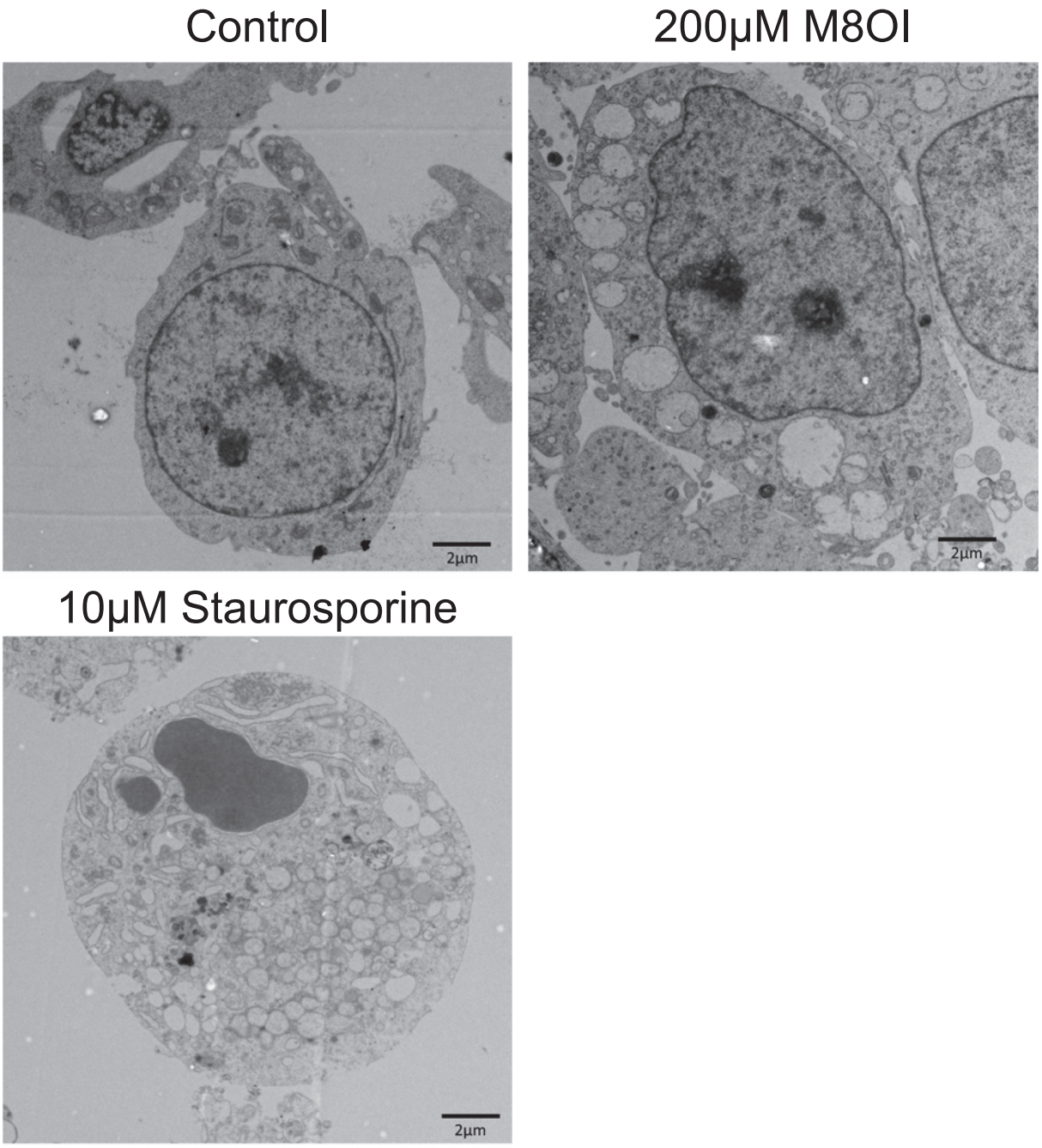

Figure 4.8: M8OI induces mitochondrial swelling in B-13 cells. B-13 cells were treated with 200µM M8OI (and vehicle control) for 24 hours, and staurosporine for 6 hours. Cells were then fixed and processed for TEM. Images are at 5800X magnification.

4.7 M8OI inhibits mitochondrial oxygen consumption rate in intact B-13 and B-13/H cells.

As cells treated with M8OI were shown to undergo apoptosis and induced mitochondrial swelling, the mitochondrial function of cells treated with M8OI was investigated. B-13 cells were treated with 50µM M8OI and the OCR and ECAR measured using the seahorse flux analyser. M8OI caused a rapid reduction in the OCR after 15 minutes of treatment and after 30 minutes the OCR was inhibited to near 100% (Figure 4.10A). This decrease in the OCR was accompanied with an increase in the ECAR that is suggestive of a shift to glycolysis as compensation (Figure 4.10C). Injection of the F1FO ATP synthase inhibitor, oligomycin (sites of substrates and inhibitors summarised in Figure 4.9) reduced oxygen consumption in vehicle treated cells but not in M8OI treated cells due mitochondrial respiration being inhibited by M8OI (Figure 4.10A). Following exposure to the uncoupler, FCCP, the OCR was increased to its maximal capacity in vehicle treated cells. There was also an increase in oxygen consumption of the M8OI treated cells, however this was lower than control cells and did not recover the basal level OCR. Finally, oxygen consumption was inhibited to near completion when treated with rotenone and antimycin A as the ETC becomes inhibited. A significant difference was observed in proton leak, as M8OI inhibited the OCR more efficiently than oligomycin (Figure 4.10E) whereas non-mitochondrial OCR after the antimycin A addition was not different. ATP production was also decreased compared to control, due to the decrease in the OCR. Finally, maximal respiration rate was decreased when treated with FCCP (Figure 4.10E).

B-13/H cells were also tested and showed that the basal OCR was higher than in B-13 cells (Figure 4.10B). Exposure to 50µM of M8OI had a similar response as B-13 cells in that there was a decrease in the OCR and an increase in the ECAR (Figure 4.10B&D). However, the decrease in the OCR and increase in the ECAR was more gradual than in the B-13 cells. Oligomycin reduced OCR slower in vehicle control B-13/H cells compared to B-13 cells. The other trends observed in B-13 cells were similar in B-13/H cells. Oligomycin had no response in M8OI treated cells, FCCP partially recovered the OCR, and rotenone/antimycin A inhibited oxygen consumption (Figure 4.10B). A significant difference in the OCR accounting for proton leak, spare respiratory capacity, non-mitochondrial consumption maximal respiration and ATP production was observed (Figure 4.10F). These data suggest that there are mitochondrial effects when B-13 and B-13/H cells are exposure to M8OI, inhibiting one or more components involved in mitochondrial respiration.

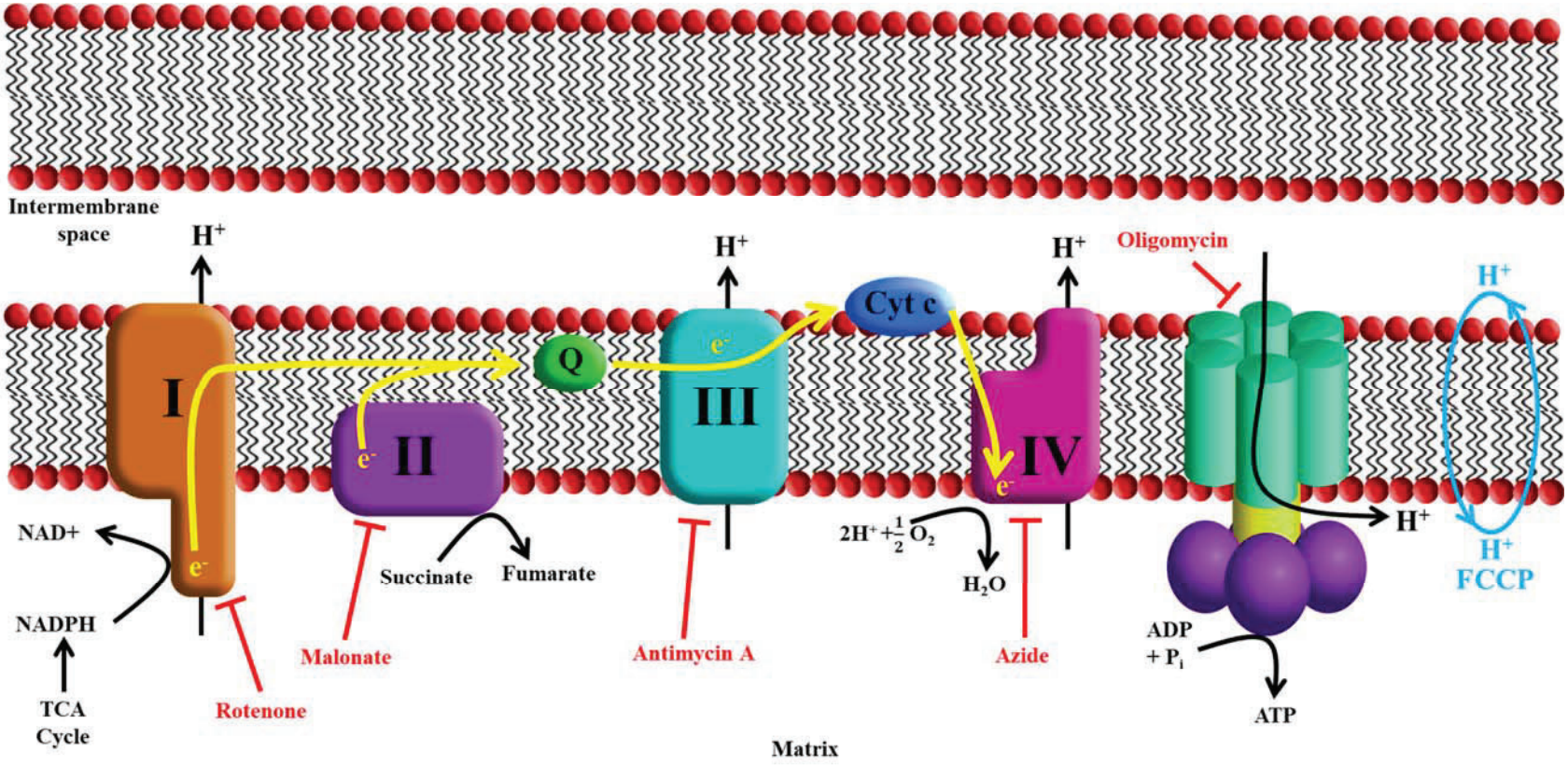

Figure 4.9: The electron transport chain and inhibitors.

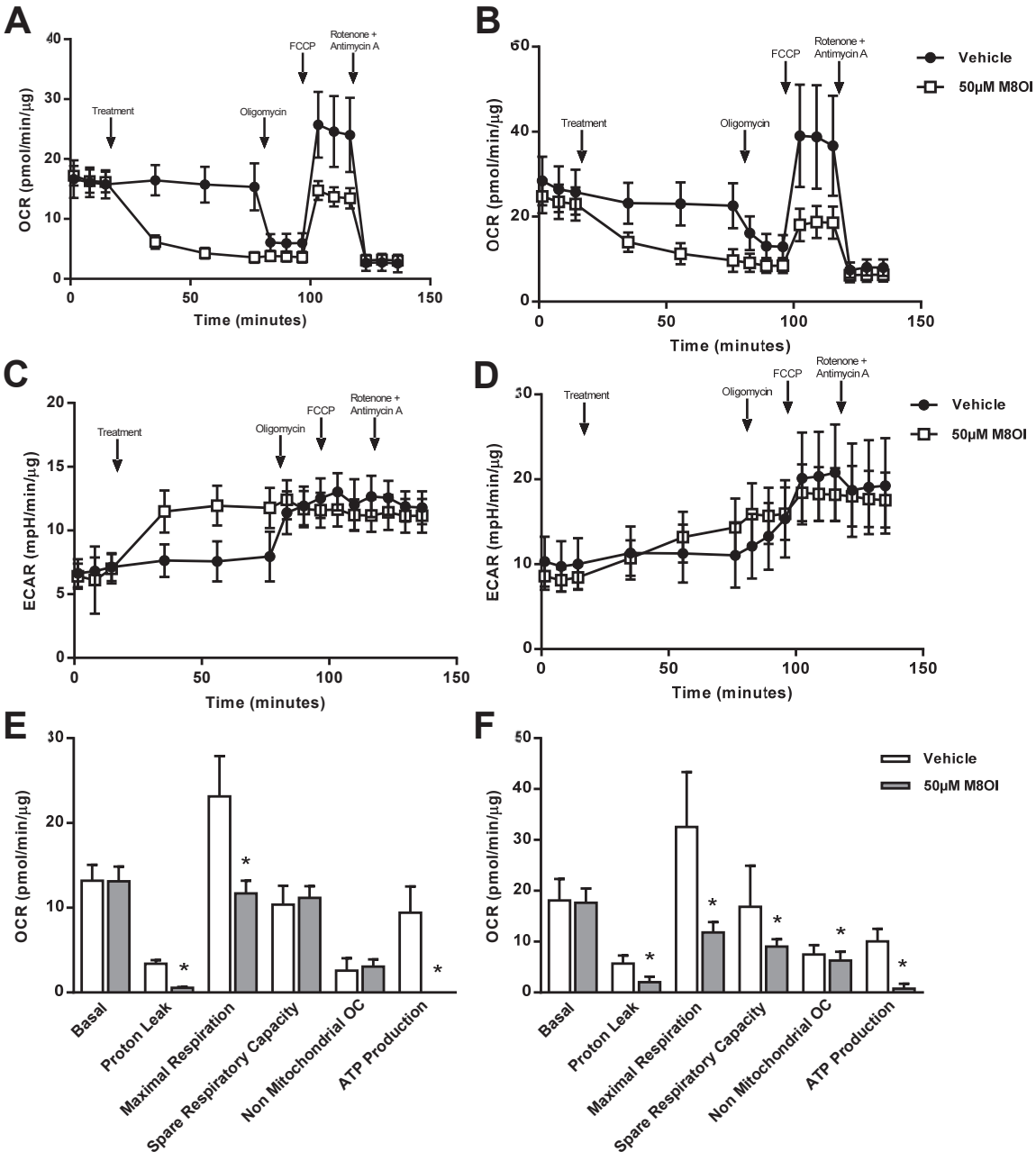

Figure 4.10: OCR is inhibited when intact B-13 and B-13/H cells are exposure to M8OI. The mitochondrial function of B-13 **(A, C, E),** and B-13/H cells **(B, D, F)** were analysed with the seahorse flux analyser using the mito stress test as described in the methods (2.15.1). Data was normalised to protein concentration calculated using a Bradford assay. **A-B,** OCR (mitochondrial respiration) and **C-D,** ECAR (glycolysis). Arrows indicate the injection of indicated compounds. **E-F,** Key parameters of mitochondrial respiration. Data are the mean and SD of at least 10 separate determinations from the same experiment, typical of 3 experiments. * significantly different to control of each parameter ($p<0.05$) tested by students t-test.

4.8 M8OI reduces the OCR and increases the ECAR in a dose dependent manner in intact B-13 cells.

Intact B-13 cells were treated with a dose response of M8OI and showed a dose dependent decrease in the OCR (Figure 4.11A). Oxygen consumption was not affected when the cells were treated with 0.1 and 1µM of M8OI throughout the mito stress test. 50 and 100µM of M8OI rapidly reduced the OCR to levels below that which oligomycin inhibited the OCR. 10µM inhibited oxygen consumption gradually over the treatment time and inhibited OCR to approximately 50% of the basal rate. Oligomycin further reduced the OCR in 10µM M8OI treated cells and reduced it below 0-1µM M8OI treated cells. No effect of oligomycin was observed at 50 and 100µM. FCCP increased the OCR in all treatments, an increase that was dose dependent, as the higher the concentration of M8OI exposed to the cells, the lower the oxygen consumption rate observed after FCCP treatment. Rotenone and antimycin A reduced the OCR to near completion (Figure 4.11A). The ECAR similarly increased in a dose dependent manner, 50 and 100µM M8OI rapidly increased whereas 10µM showed a more gradual increase but unlike the OCR, the ECAR reached similar levels at 50 and 100µM whereas 0.1 and 1µM showed no effect. (Figure 4.11B). Statistically significant dose dependent decreases were observed in proton leak, maximal respiration, spare respiratory capacity, mitochondrial oxygen consumption and ATP production (Figure 4.11C).

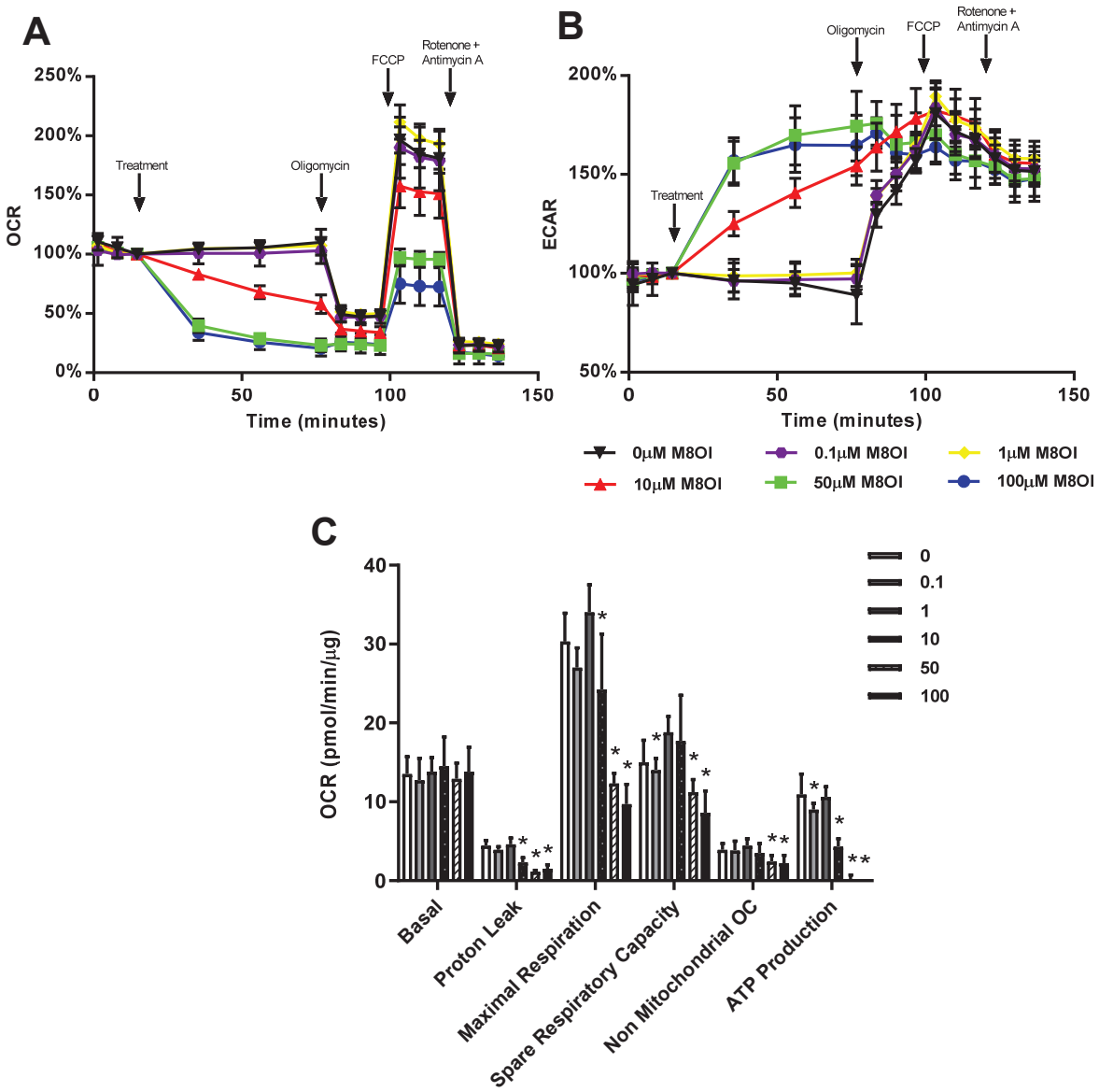

Figure 4.11: M8OI mitochondrial effects are dose dependent in B-13 cells. The mitochondrial function of B-13 cells was analysed with the seahorse flux analyser using the mito stress test as described in the methods (2.15.1). Data was normalised to protein concentration calculated using a Bradford assay. **A,** OCR (mitochondrial respiration) and **B,** ECAR (glycolysis). Arrows indicate the injection of indicated compounds. **C,** Key parameters of mitochondrial respiration. Data are the mean and SD of at least 8 separate determinations from the same experiment, typical of 3 separate experiments. * significantly different to control of each parameter ($p<0.05$) tested by ANOVA followed by Bonferroni post-hoc test.

4.9 M8OI acts on two sites in the ETC

Plasma membrane permeabilizer (PMP) experiments were used to identify the sites of action and mechanisms of M8OI within the mitochondria. Firstly, the direct effects of M8OI on the OCR of mitochondria (via PMP treated cells) was measured. Cells were permeabilised using PMP and preincubated with an increasing dose of M8OI ranging from 10pM-10μM, cells were then injected adenosine diphosphate (ADP) giving a final concentration of 4mM using the seahorse flux analyser and the resulting OCR was measured. Cells treated with 1 and 10μM M8OI had a lower OCR compared to control cells, no significant effects were observed at lower concentrations (Figure 4.12A).

Effects of complex I were then investigated using the PMP complex I assay (Salabei *et al.*, 2014). Cells were treated with 100μM M8OI and 5μM rotenone as a positive control for complex I inhibition. Control vehicle treated cells showed an increase OCR when ADP was added to the cells and this increase was reduced back to basal levels following oligomycin treatment (Figure 4.12B). FCCP then recovered the OCR from oligomycin inhibition back to similar levels seen when treated with ADP before being inhibited once again by the complex III inhibitor antimycin A. Rotenone had no response to any of the compounds injected, including ADP and FCCP, therefore successfully inhibiting complex I.

100μM of M8OI inhibited the increase in oxygen consumption induced by ADP, and therefore there was no effect induced by oligomycin. (Figure 4.12B). The addition of FCCP increased the OCR but to lower levels compared to vehicle treated cells. Finally, as with the control treated cells, antimycin A inhibited the OCR back to basal levels. These data combined with the data from the mito stress test suggest that M8OI inhibits ATP synthase (complex V) as there is some recovery of the OCR when FCCP is added. However, there may be effects elsewhere in the ETC as FCCP does not completely recover the OCR at similar levels to control cells.

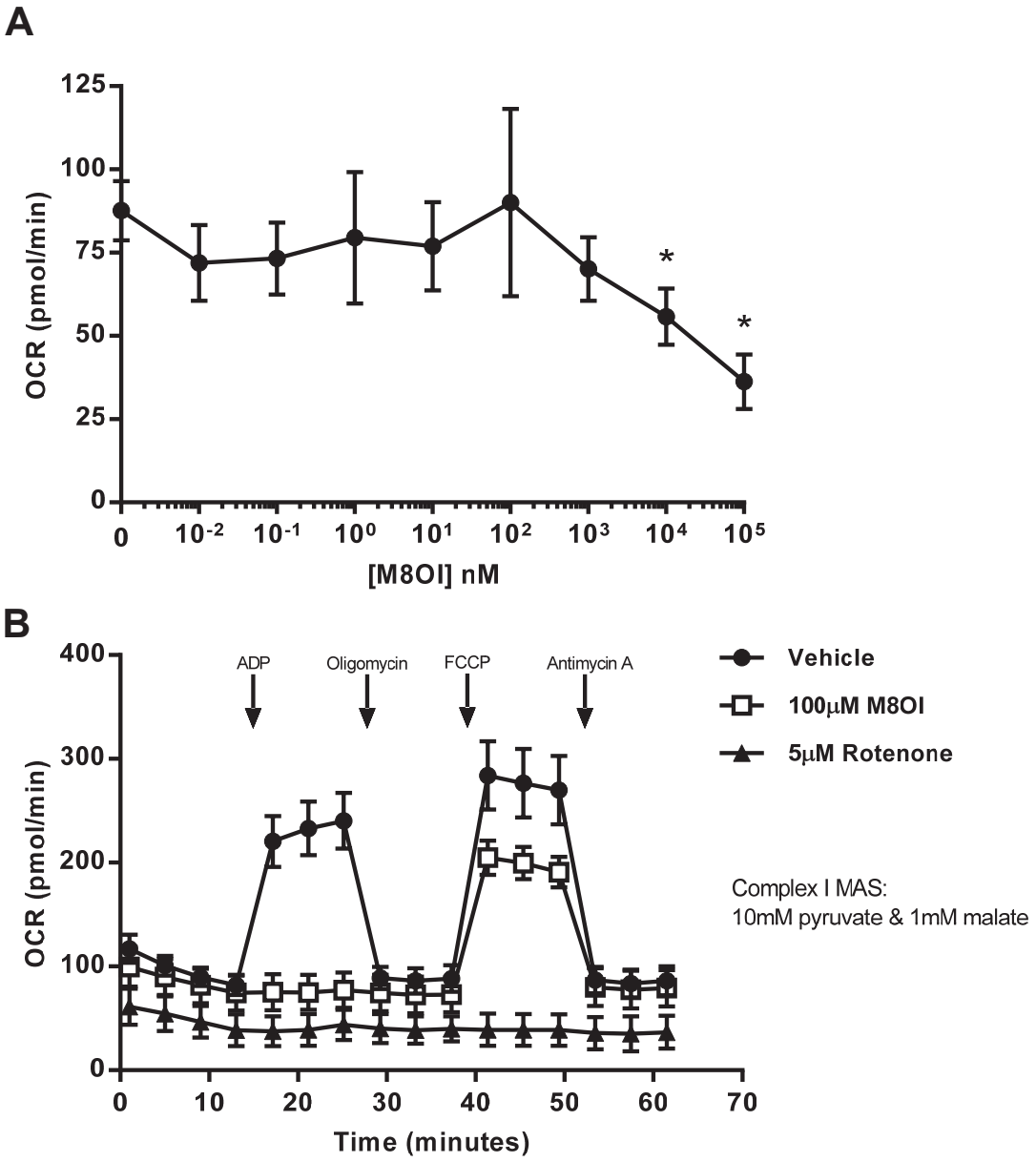

Figure 4.12: M8OI has a direct effect on the mitochondria of B-13 cells. A, B-13 cells were permeabilised using PMP and incubated in complex I assay MAS and indicated concentrations of M8OI. After 14 minutes in the seahorse flux analyser ADP was injected into the well (giving a final concentration of 4mM) and after a further 10.5 minutes of incubation OCR was measured. Data are the mean and SD of at least 6 separate determinations from the same experiment, typical of 2 separate experiments. * significantly different to control ($p<0.05$) tested by ANOVA followed by Bonferroni post-hoc test. **B,** B-13 cells were permeabilised using PMP and incubated in complex I assay buffer and indicated compounds. OCR was then measured using the PMP assay described in the methods sections (2.15.2). Arrows indicate the injection of indicated compounds. Data are the mean and SD of at least 6 separate determinations from the same experiment, typical of 2 separate experiments.

4.10 M8OI interacts with complex II in B-13 cells

The interactions of complex II and M8OI was investigated using PMP experiments by inhibiting complex I using rotenone and providing the substrate, succinate, for complex II. Control cells followed a similar trend to that observed in complex I as previously described in Figure 4.10. 1mM malonate, a complex II inhibitor, inhibited the response from any of the injected compounds. However, pre-treatment with 100µM M8OI caused an increase in the OCR compared to vehicle treated cells (Figure 4.13A). This increase was greater than the effect of ADP on control cells and was unaffected by oligomycin treatment. FCCP further increased the OCR and antimycin A inhibited oxygen consumption as normal.

These effects were then monitored by pre-treating the cells for a complex I assay and once a baseline was established the cells were injected with succinate, rotenone and 10µM M8OI (or vehicle). Cells treated with M8OI showed an increase in oxygen consumption compared to control cells. 10µM M8OI was not sufficient enough to increase the OCR above ADP addition and was inhibited by oligomycin (Figure 4.13B). Finally, these effects of M8OI required the presence of the complex II substrate, succinate, for this increase in the OCR to occur (Figure 4.13C). These data demonstrate that M8OI interacts with complex II in some capacity in which an increase in oxygen consumption occurs.

4.11 M8OI produces mitochondrial ROS

As M8OI had a mitochondrial effect, the production of mitochondrial ROS was measured using the MitoSOX fluorescent probe. Cells were treated for 2 hours post MitoSOX incubation and fluorescence measured. M8OI induced the production of mitochondrial ROS in a dose dependent manner, with 1000µM of M8OI producing a response similar to that of 10µM of oligomycin and other inhibitors of mitochondrial respiration that are known to produce ROS (Figure 4.14) (Miwa *et al.*, 2003; Quinlan *et al.*, 2013).

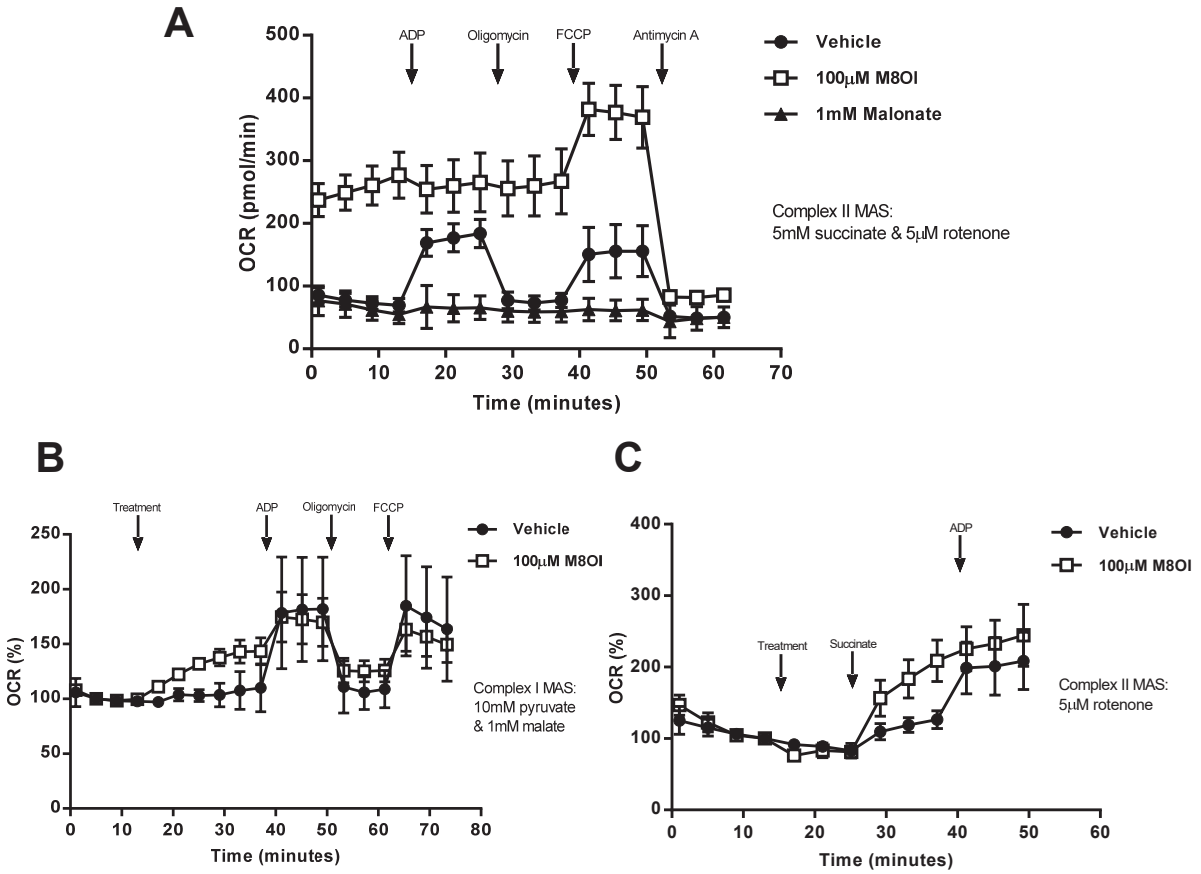

Figure 4.13: M8OI interacts with complex II of the ETC. A, B-13 cells were permeabilised using PMP and incubated in complex II assay MAS and indicated compounds. OCR was then measured using the PMP assay described in the methods sections (2.15.2). Arrows indicate the injection of indicated compounds. Data are the mean and SD of at least 6 separate determinations from the same experiment, typical of 3 separate experiments. **B,** B-13 cells were permeabilised using PMP and incubated with complex I MAS. OCR was then measured using the PMP assay described in the methods sections (2.15.2). The first injection contained succinate, rotenone and indicated treatment giving a final concentraions of 5mM, 5μM and indicated concentration respectively. Arrows indicate the injection of indicated compounds. Data are the mean and SD of at least 6 separate determinations from the same experiment, typical of 3 separate experiments. **C,** B-13 cells were permeabilised using PMP and incubated with complex II MAS without succinate. OCR was then measured using the PMP assay described in the methods sections (2.15.2). Arrows indicate the injection of indicated compounds. Data are the mean and SD of at least 6 separate determinations from the same experiment, typical of 2 separate experiments.

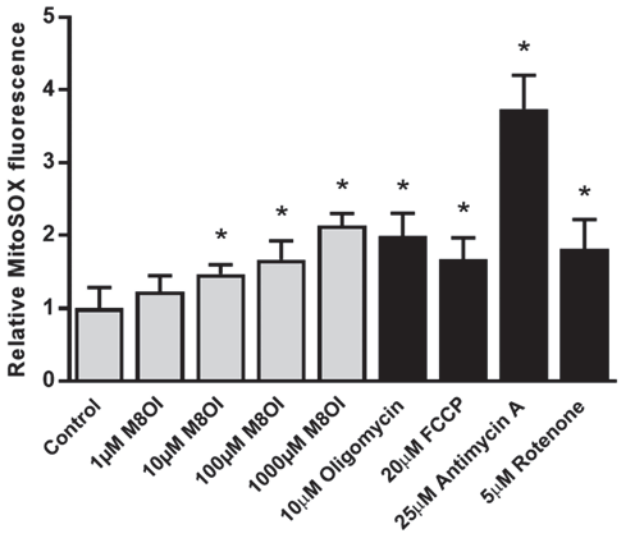

Figure 4.14: Mitochondrial ROS production is observed in M8OI treated B-13 cells. B-13 cells were preincubated with MitoSOX, the cells were then washed in PBS and incubated with chemicals indicated for 2 hours and fluorescence was measured. Data are the mean and SD of at least 6 separate determinations from the same experiment, typical of 3 separate experiments.
* significantly different MitoSOX fluorescence to control of each parameter ($p<0.05$) tested by ANOVA followed by Bonferroni post-hoc test.

4.12 Human hepatic progenitor cells are EpCAM positive

As B-13 cells are considered rat hepatic progenitor cells and sensitive to M8OI toxicity, it was hypothesised that human hepatic progenitors would be sensitive to M8OI induced toxicity. There is no human B-13 equivalent, therefore human progenitor cells derived from human liver (Huch *et al.*, 2015) were used to examine the effects in a human equivalent model, and therefore provide an *in vitro* model more relevant to man. Epithelial cell adhesion molecule (EpCAM) is a transmembrane glycoprotein involved in cell adhesion, proliferation and maintenance of pluripotent state and is expressed in hepatic progenitor cells (Dolle 2015). Thus, EpCAM was used to confirm the cells used were hepatic progenitor cells as previously described (Huch *et al.*, 2015). EpCAM was present at RNA level in the induced pluripotent stem cells and hepatic progenitor cells but not present in human hepatocytes as expression is lost during the maturation of hepatocytes (Figure 4.15A). HNF4α and albumin were used as mature hepatocyte markers and were present in human hepatocytes and not hepatic progenitors.

4.13 Organoid formation is reduced in M8OI treated hepatic progenitors

Hepatic progenitor cells form organoids in Matrigel. Individual cell/small colonies were exposed to M8OI for 48 hours and left for a further 48 hours in normal medium, the number of organoids formed were then counted in randomly selected fields. The number of organoids formed was reduced in cells treated with 200-1000μM M8OI in a dose dependent manner (Figure 4.15B). Chlorpromazine was used as a positive control as a known cytotoxin and showed a reduced number of organoids compared to control and similar to 1000μM M8OI.

Individual cell/small colonies were treated for 48 hours with M8OI, after treatment the cells were fixed, and cell morphology was then examined. It was observed that small spherical structures appeared to form at the periphery of the cells at 100-1000μM (Figure 4.16). The number of these structures appeared to increase as the concentration of M8OI increased. These structures are believed to be apoptotic blebs, a structure formed during the apoptosis of cells.

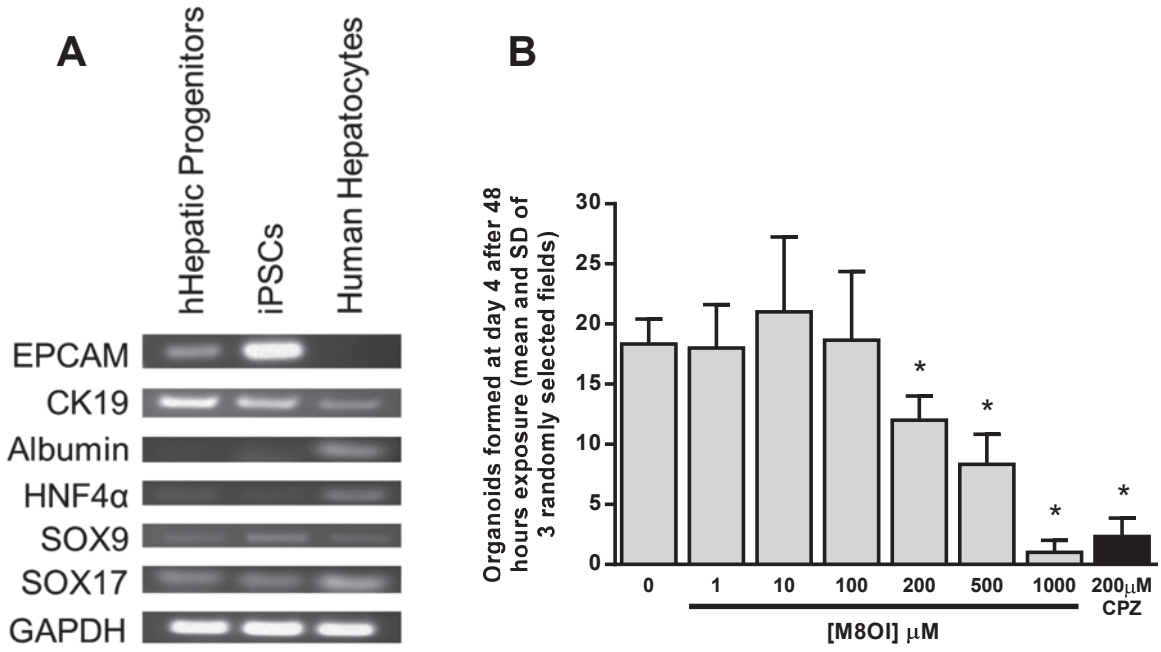

Figure 4.15: Human hepatic progenitor organoid formation is inhibited by M8OI. A, RT-PCR for indicated transcripts. **B,** hepatic progenitor cells were treated for 48 hours with indicated concentrations of M8OI and chlorpromazine and treated for a further 2 days in expansion medium. Cells were then fixed, and the number of organoids formed were counted from 3 randomly selected fields. Data are the mean and SD of 3 separate determinations from the same experiment, typical of 2 separate experiments. * significantly different to control ($p<0.05$) tested by ANOVA followed by Bonferroni post-hoc test. For chlorpromazine * significantly different to control ($p<0.05$) tested by students t-test.

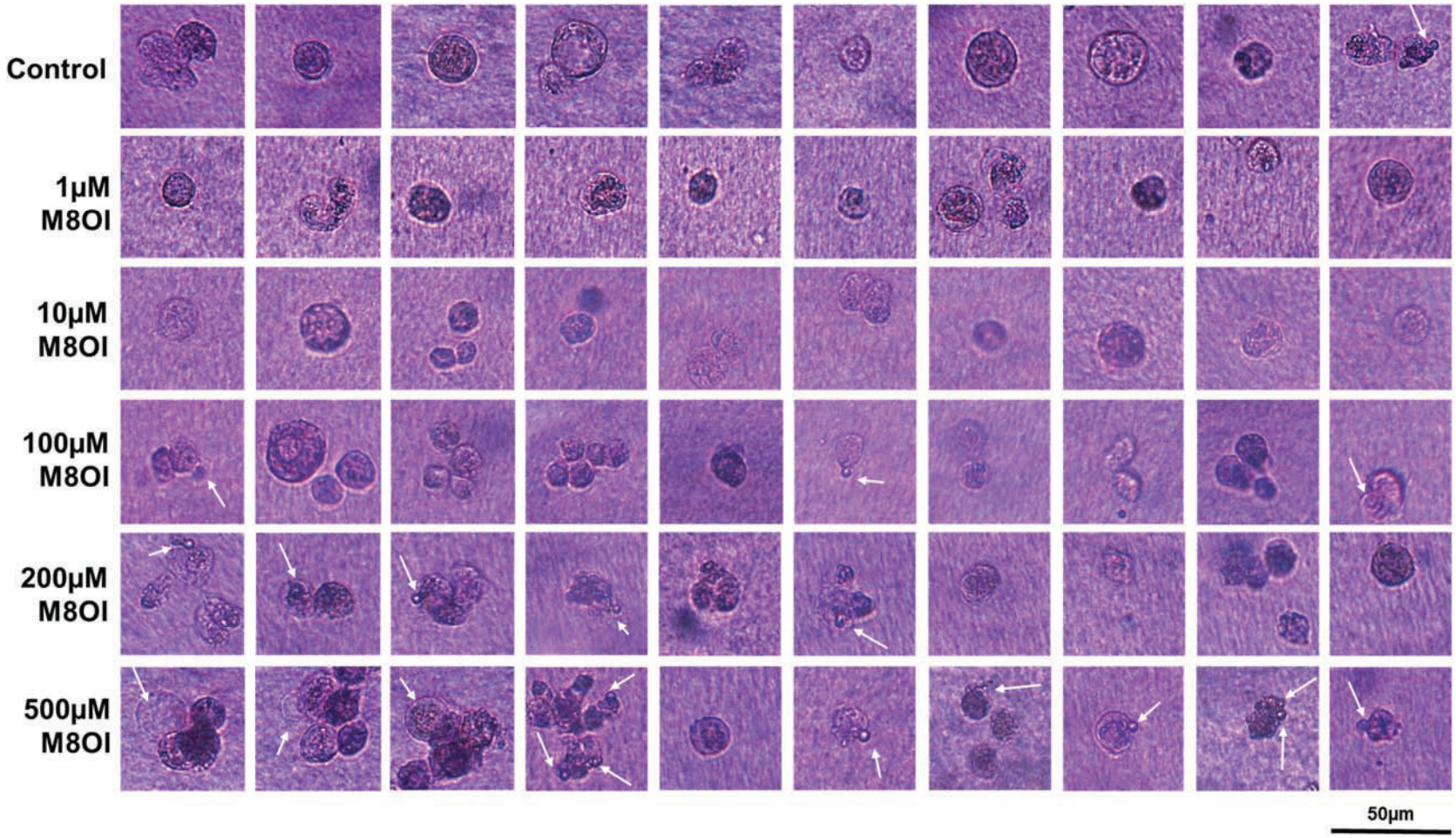

Figure 4.16: Apoptotic blebs are formed in human hepatic progenitors in response to exposure to M8OI. Human hepatic progenitor cells were incubated with indicated concentrations of M8OI for 48 hours. 10 Images of individual/clusters of cells were taken. White arrows indicate apoptotic blebs.

4.14 M8OI is toxic to hepatic progenitor organoids

Hepatic progenitors were cultured to form organoids and then treated with M8OI for 48 hours and cell viability was assessed using trypan blue staining and MTT assays. Trypan blue staining showed that there was a significant increase in cell death at 500 and 1000µM of M8OI (Figure 4.17A). 200µM chlorpromazine was used as a positive control for cytotoxicity and induced cell death at similar levels to 1000µM M8OI. Staurosporine was used as an apoptosis control and 20% of cell area was trypan blue stained. Images showed that organoids maintain their structure at 500µM but 'burst' at 1000µM M8OI, whereas chlorpromazine treated organoids 'shrink' (Figure 4.17B). However, MTT assays showed that only chlorpromazine treated organoids displayed a reduction in MTT activity (Figure 4.18A). As with the trypan blue stained organoids, it was observed that the organoids treated with 1000µM M8OI lost their structure (Figure 4.18B). These results suggest that there may be some cell death and at 1000µM M8OI the organoids lose their structure.

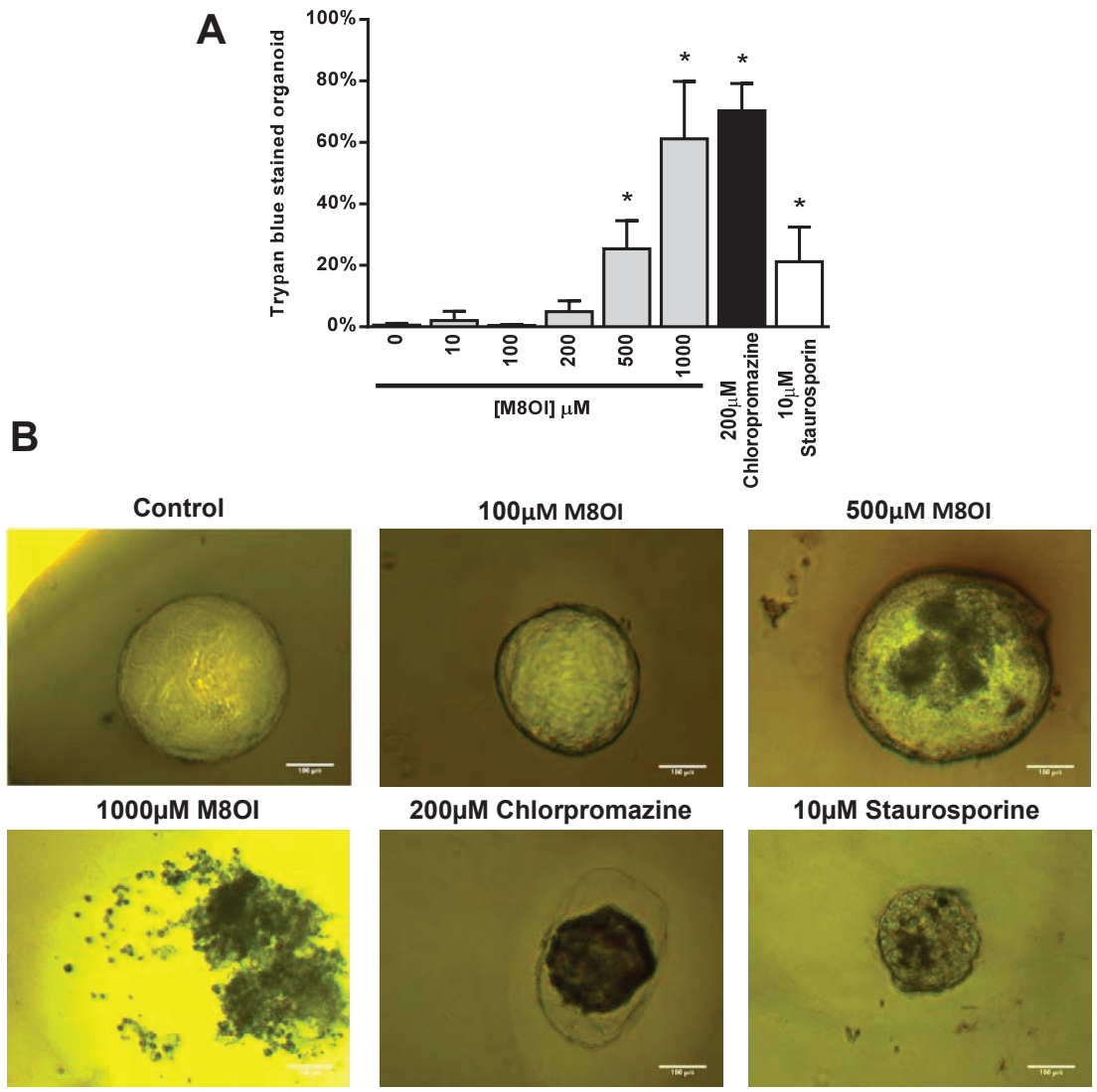

Figure 4.17: M8OI increases trypan blue staining of organoids. A, Human hepatic progenitor organoids were treated with indicated concentrations of M8OI, chlorpromazine, and staurosporine for 48 hours. Following treatment, cells were incubated with trypan blue for 5 minutes and images taken of the organoids. Using ImageJ, the threshold command was used to convert images to black and white based on staining, analyse particles was then used to calculate the black pixels (trypan blue stained), the percentage of the organoid stained with trypan blue was then determined. Data are the mean and SD of 5 separate organoids from the same experiment, typical of 2 separate experiments. * significantly different to control ($p<0.05$) tested by ANOVA followed by Bonferroni post-hoc test. For chlorpromazine and staurosporine * significantly different to control ($p<0.05$) tested by students t-test. **B,** Human hepatic progenitor organoids were treated as described in A and were imaged by bright-field microscopy (scale bar = 100µm).

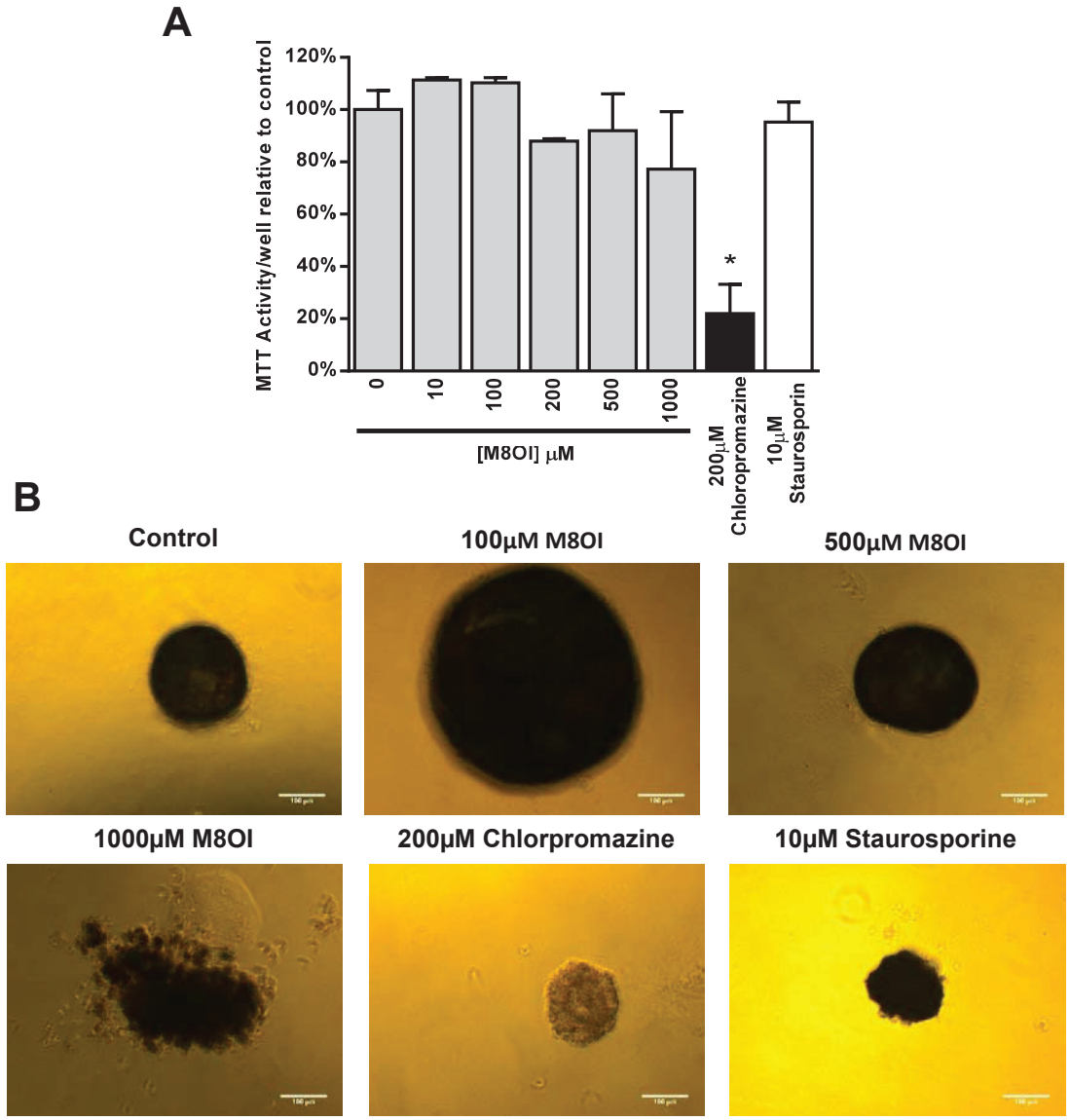

Figure 4.18: MTT activity was not reduced with M8OI treatment. A, Human hepatic progenitor organoids were treated with indicated concentrations of M8OI, chlorpromazine, and staurosporine for 48 hours. Following treatment, cells were incubated with MTT for 2 hours and images taken of the organoids. Using ImageJ, the threshold command was used to convert images to black and white based on staining, analyse particles was then used to calculate the black pixels (formazan conversion), the percentage of the organoid converted formazan was determined. Data are the mean and SD of 5 separate organoids from the same experiment, typical of 2 separate experiments. * significantly different to control ($p<0.05$) tested by ANOVA followed by Bonferroni post-hoc test. For chlorpromazine and staurosporine * significantly different to control ($p<0.05$) tested by students t-test. **B,** Human hepatic progenitor organoids were treated as described in A and were imaged by bright-field microscopy (scale bar = 100μm).

4.15 M8OI caused the swelling of hepatic progenitor organoid mitochondria

Organoids were treated for 48 hours with M8OI, fixed, and visualised using electron microscopy. Control organoids appeared to be hollow in structure (i.e. cysts), that when sectioned for electron microscopy appeared as a ring of cells (Figure 4.19A). Cellular components including the nuclear and mitochondria were easily visualised (Figure 4.19C).

The organoids treated with 500µM M8OI had a compromised structure compared to control organoids. In some organoids the structure was nearly completely lost, and cells appeared to be dead (Figure 4.19B). Cells that appeared to have maintained some structure, appeared abnormal in comparison to control organoids. As with the B-13 cells, one of the most observable features of the cells was that the mitochondria appeared to swell, and they also appeared to be darker in colour and the cristae were not as visible as the control mitochondria (Figure 4.19D). These images suggest that the mitochondria of the cells that make the organoids are affected in response to M8OI treatment.

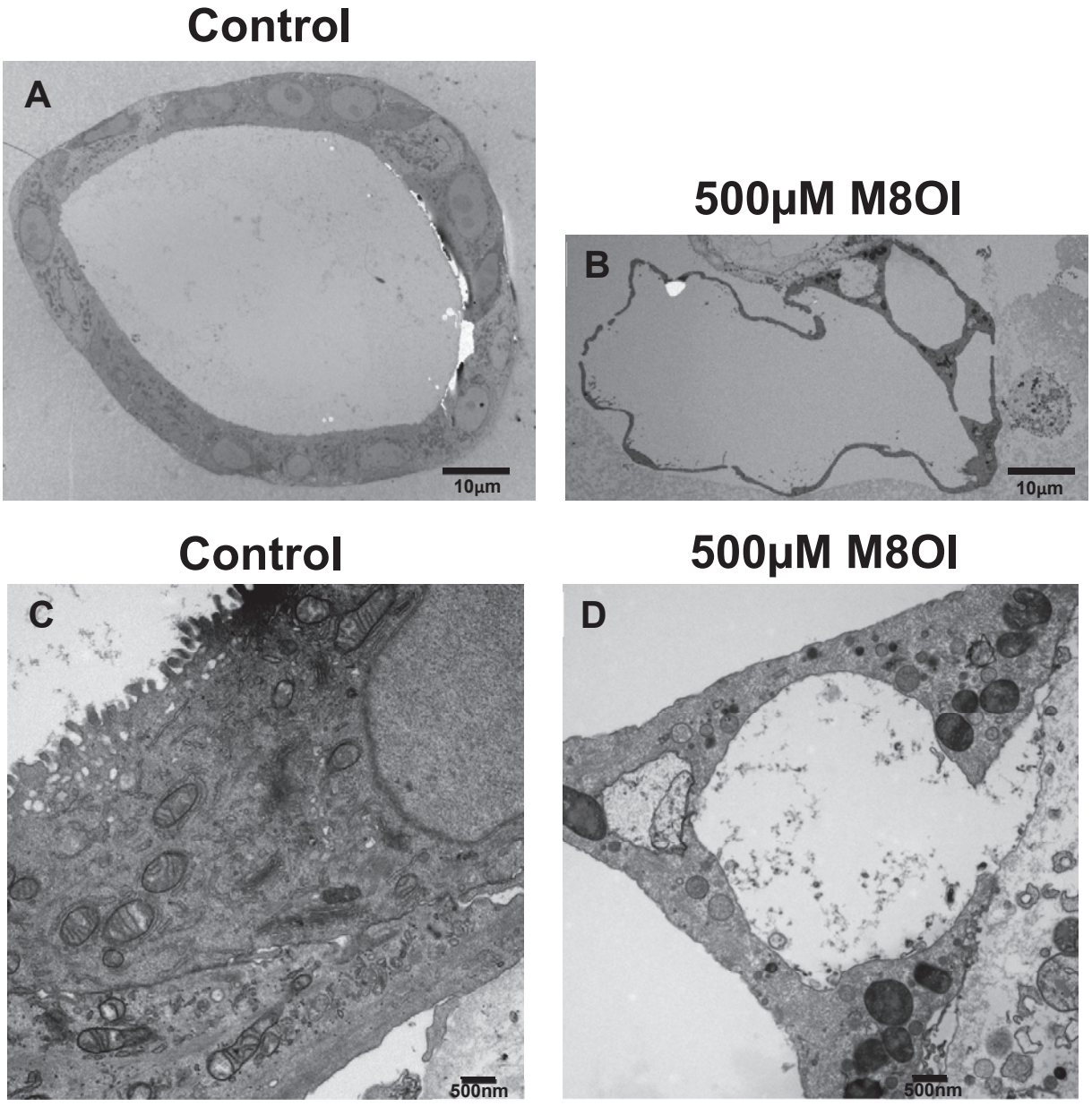

Figure 4.19: Human hepatic organoid mitochondria swell in response to M8OI exposure. Human hepatic progenitors were treated with 500µM M8OI and a vehicle control for 48 hours. Organoids were fixed and processed for TEM. Images show organoids at **A&B,** 800x and **C&D,** 13500x magnification.

4.16 45 day, low level, oral exposure to M8OI does not cause any detectable inflammatory response.

Transgenic NK-κB-luc female mice of at least 52 weeks of age were administered a daily dose of 1mg/kg body weight (bw) M8OI via their drinking water. This dose was calculated from the EFSA (European food safety authority) recommendations of the administration of chemical substances in drinking water for sub chronic studies (EFSA, 2012). Older female mice were selected due PBC generally being considered a disease predominantly affecting postmenopausal women. Inflammation was regularly monitored by IVIS imaging. On day 27 mice were administered 50mg/kg bw α-naphthylisothiocyanate (ANIT) (or olive oil vehicle control) by oral gavage. On day 45 mice were terminated by cervical dislocation and the tissue and serum were collected. Mice that died or were terminated before the end of the experiment were not included in the final analysis, as their termination was due to age related issues.

IVIS imaging showed that M8OI did not result in an increase in an inflammatory response suggestive of injury in M8OI treatment over the course of the experiment. ANIT induced a significant response 2 days post administration in both ANIT groups, however, there was no significant difference between mice treat with ANIT and M8OI compared to those treated with ANIT alone (Figure 3.20A&B). Additionally, there was no significant difference between groups in hepatic glycogen content or ALP (Figure 4.20C&D). Finally, the only significant response observed in serum ALT was a reduction in the control/M8OI treated mice (Figure 4.20E).

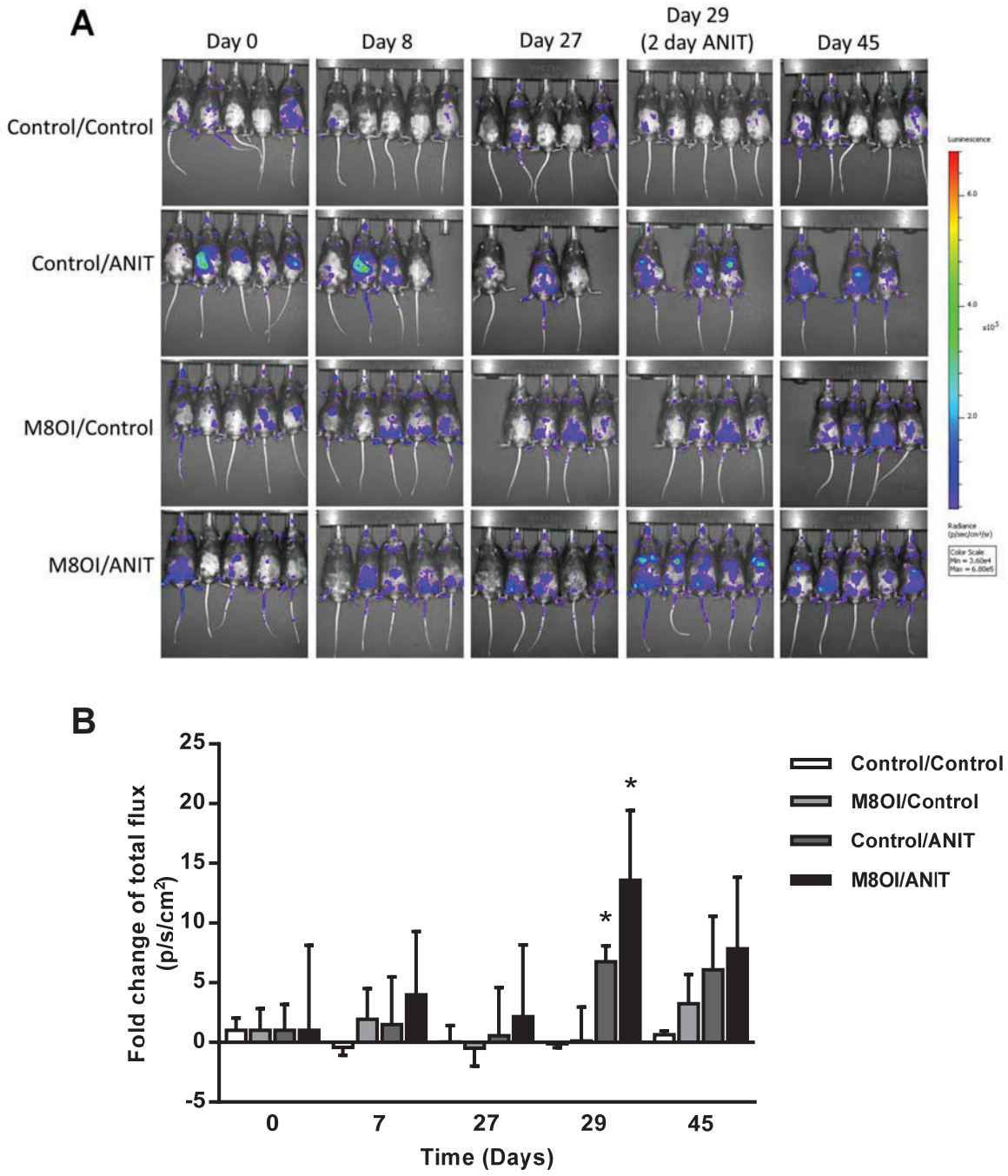

Figure 4.20: Long-term exposure to M8OI does not cause any detectable inflammatory response. (Legend on next page)

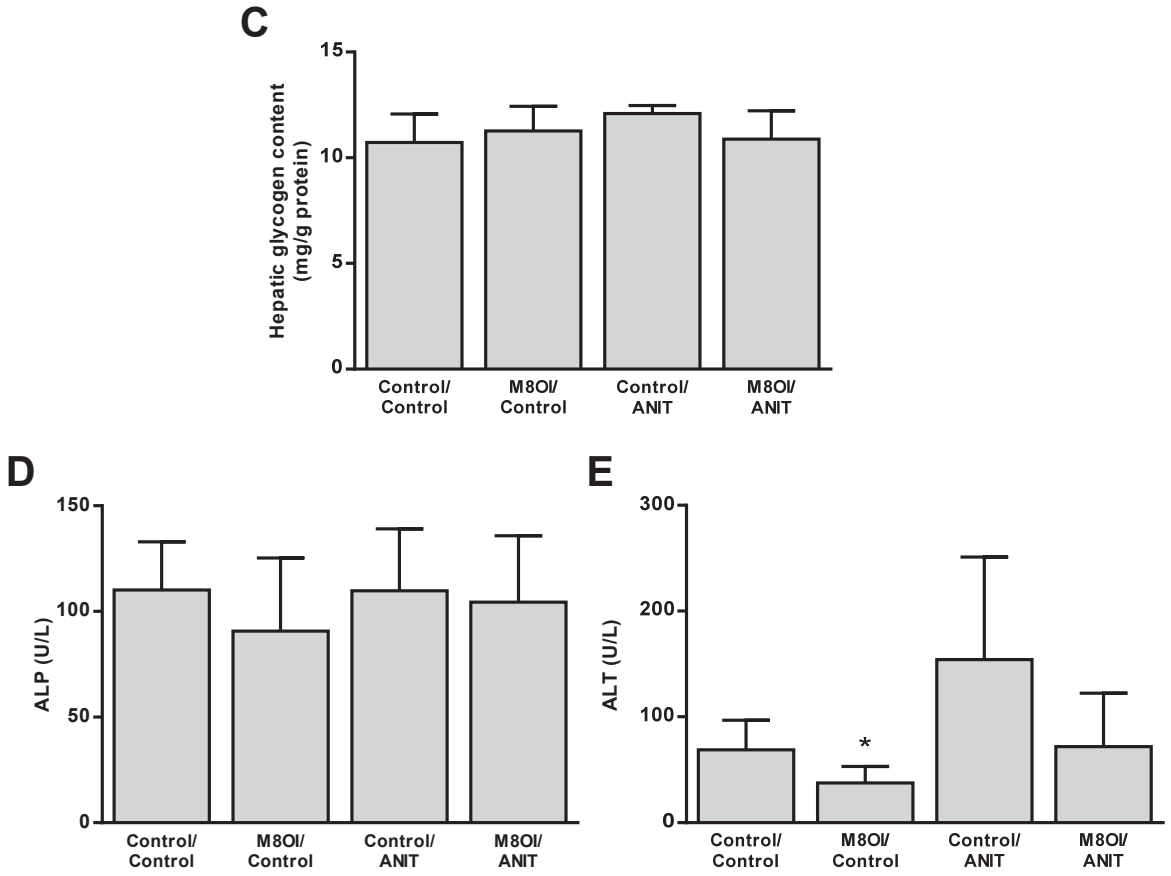

Figure 4.20: Long-term exposure to M8OI does not cause any detectable inflammatory response (Continued). Transgenic NK-κB-luc female mice were administered a daily dose of 1mg/kg bw M8OI via their drinking water. On day 27 mice were administered 50mg/kg bw ANIT (or olive oil vehicle control) by oral gavage. On day 45 mice were terminated by cervical dislocation and tissue and serum collected. **A,** IVIS images of treated mice at time indicated as described in the methods (2.2.4). **B,** Quantified abdominal luminescence of treated mice. IVIS data are the mean and SD of the following animal numbers Control/Control = 5, Control/ANIT = 3, M8OI/Control = 4, M8OI/ANIT = 5. * significantly different to control ($p<0.05$) tested by students t-test. **C,** Hepatic glycogen determination. **D,** ALP. **E,** ALT. * significantly different to control ($p<0.05$) tested by students t-test.

4.17 M8OI induced glycogen depletion in mice when administered by intraperitoneal injection.

To study the acute effects of M8OI *in vivo*, male C57B6 mice of at least 12 weeks of age were intraperitoneally or orally administered with M8OI ranging from 0-40mg/kg bw. The mice were given two doses, the second dose given 18 hours after the first dose. 24 hours after the first dose was administered, the mice were terminated by cervical dislocation and tissue, serum, bile and urine were collected. Oral administration of M8OI at the concentrations implemented showed no evidence of weight loss (Figure 4.21A) or hepatic injury as there was no significant change in serum ALP (Figure 4.21C) or ALT (Figure

4.21D) compared to vehicle treated mice, and there was no widespread histological evidence of hepatic injury (Figure 4.22A). Pilot study data suggested that M8OI may induce hepatic glycogen depletion. Therefore, hepatic glycogen content was determined but showed no change compared to vehicle treated mice (Figure 4.21B). Additionally, PAS stained liver sections showed no change in glycogen content (Figure 4.22B).

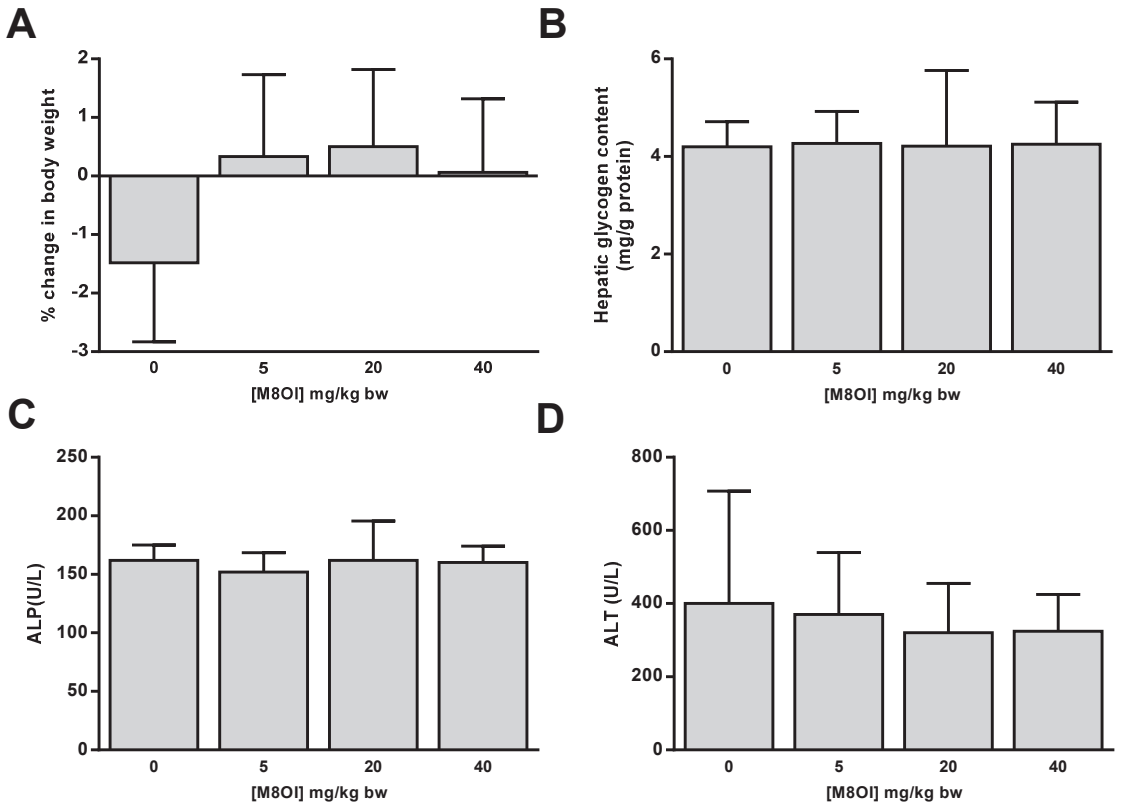

Figure 4.21: Oral administration of M8OI does not have any hepatic effects. Male C57B6 mice were administered with indicated doses of M8OI by oral gavage twice, the second dose was given 18 hours after the first. 24 hours after the first dose was administered, the animals were terminated by cervical dislocation and serum and tissue collected. **A,** change in body weight. **B,** sections of liver were homogenised and glycogen content was determined as described in section 2.14, data was normalised to protein by Lowry determination. **C,** serum ALP. **D,** serum ALT. Data are mean and SD of 5 separate animals. No statistical significance.

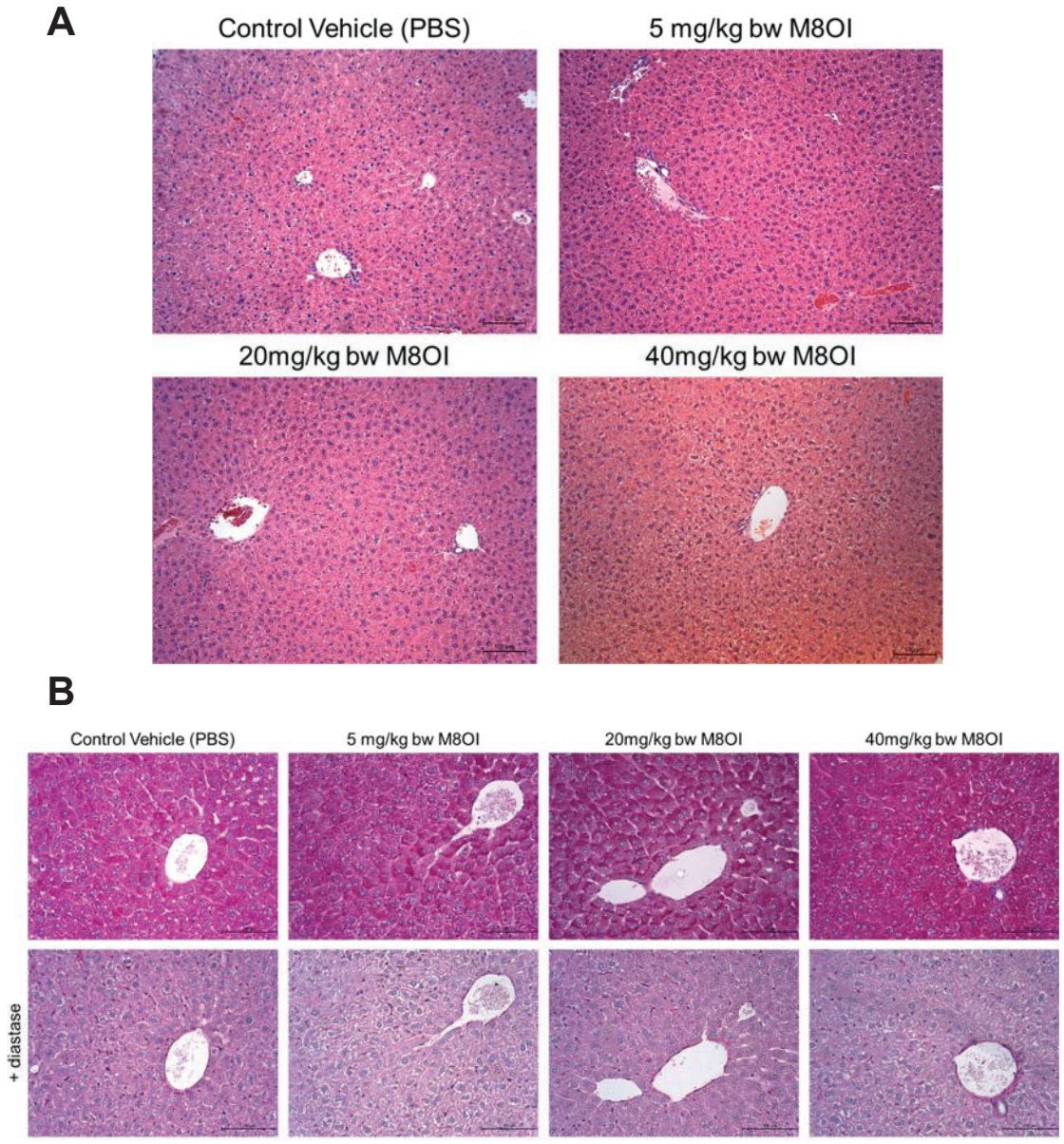

Figure 4.22: Histological examination of the liver in mice administered with M8OI orally does not display any hepatic injury. C57B6 mice were administered with indicated doses of M8OI by oral gavage twice, the second dose was given 18 hours after the first. 24 hours after the first dose was administered, the animals were terminated by cervical dislocation and serum and tissue collected. **A,** H&E stained sections of liver from animals treated as indicated, typical views chosen. **B,** PAS stained sections of liver from animals treated as indicated, typical views chosen. (scale bar = 100µm).

Administration of M8OI intraperitoneally did induce a toxic response. During a pilot study, mice administered with 20mg/kg bw and 40mg/kg bw had to be terminated before severity was exceeded, with the 40mg/kg bw mouse needing to be terminated almost immediately. A lower dose range was therefore selected for i.p. administration of M8OI, ranging from 0-10mg/kg bw. There was a decrease in body weight after 24 hours in mice treated with 5mg/kg bw and 10mg/kg bw, however this was not statistically significant (Figure 4.23A). No change in serum ALP (Figure 4.23C) and ALT (Figure 4.23D) compared to vehicle treated mice was observed. i.p. administration of M8OI at 5mg/kg bw and 10mg/kg bw did have hepatic effects. The liver weight decreased in M8OI treated mice in a dose-dependent manner, however this was not statistically significant, (Figure 4.23B) and some inflammation was observed when the liver was histologically examined (Figure 4.24 & Figure 4.25A). However, this inflammation was patchy and not observered throughout the liver. Additionally, parts of the liver displayed unstained areas of the cytoplasm that were not observed in the livers of control treated mice and like inflammation, this was not observed throughout the liver (Figure 4.24A). The most prominent hepatic effect was the depletion of glycogen in 10mg/kg bw M8OI treated mice (Figure 4.23E). This was supported by PAS staining of liver sections which showed that there was some glycogen depletion in 5mg/kg bw treated mice and that in 10mg/kg bw treated mice the glycogen was depleted to similar levels as the diastase negative controls (Figure 4.25B). Histological examination of the heart showed no overt change in the heart compared to control treated mice. However, in the kidneys of 10mg/kg bw M8OI treated mice there was evidence of disruption to the renal architecture similar to acute tubular necrosis and an increase in the number of nuclei in the glomerulus suggesting the infiltration of inflammatory cells (Figure 4.24).

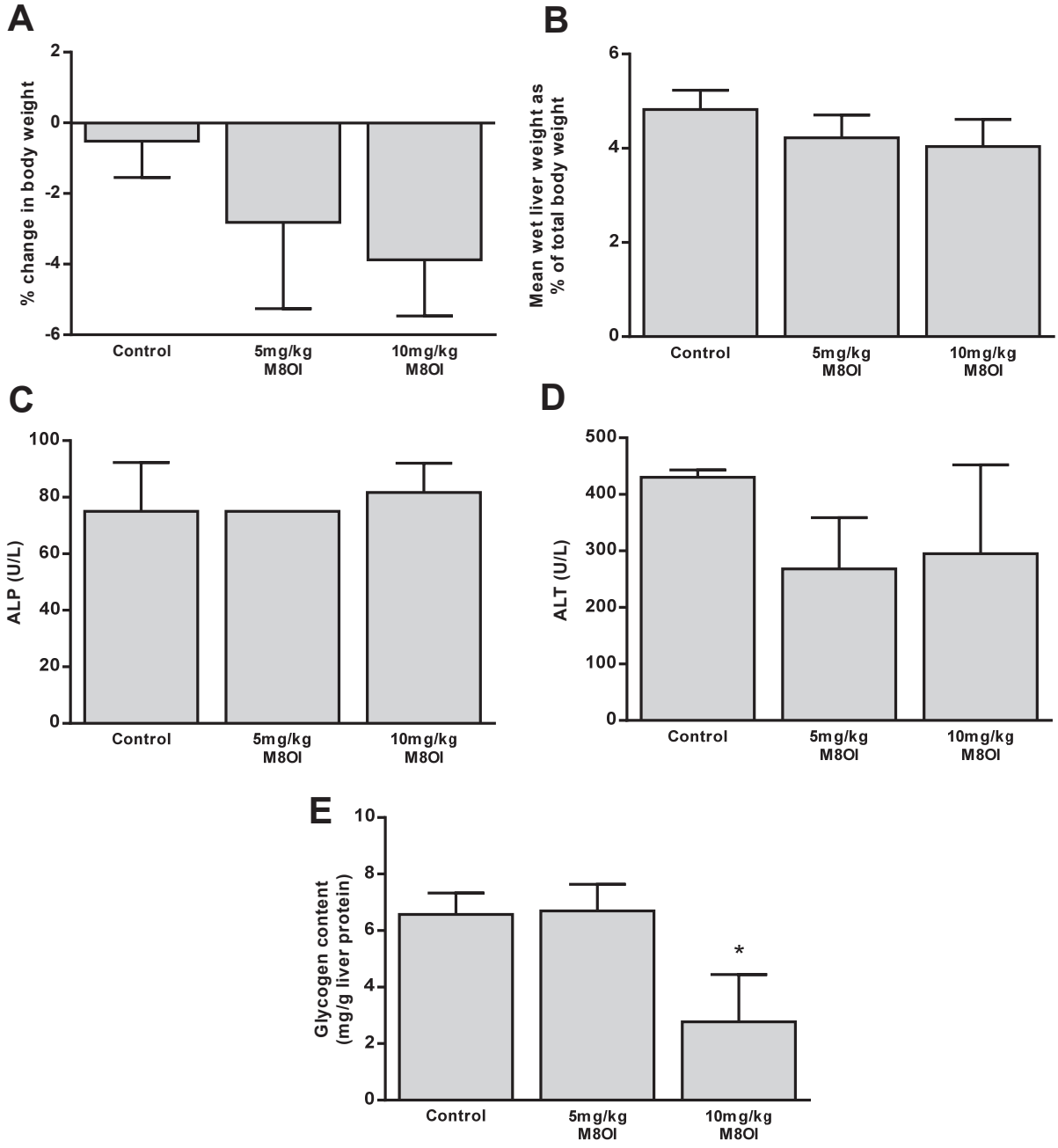

Figure 4.23: Intraperitoneal administration of M8OI reduces hepatic glycogen content in mice. Male C57B6 mice were administered with indicated doses of M8OI by i.p. injection twice over 24 hours, the second dose was given 18 hours after the first. 24 hours after the first dose was administered, the animals were terminated by cervical dislocation and serum and tissue collected. **A,** change in body weight. **B,** wet liver wright as % of total body weight. **C,** serum ALP. **D,** Serum ALT. **E,** sections of liver were homogenised and glycogen content was determined as described in section 2.14, data was normalised to protein by Lowry determination. Data are mean and SD of 3 separate animals. * significantly different to control ($p<0.05$) tested by one-way ANOVA followed by Bonferroni post-hoc test.

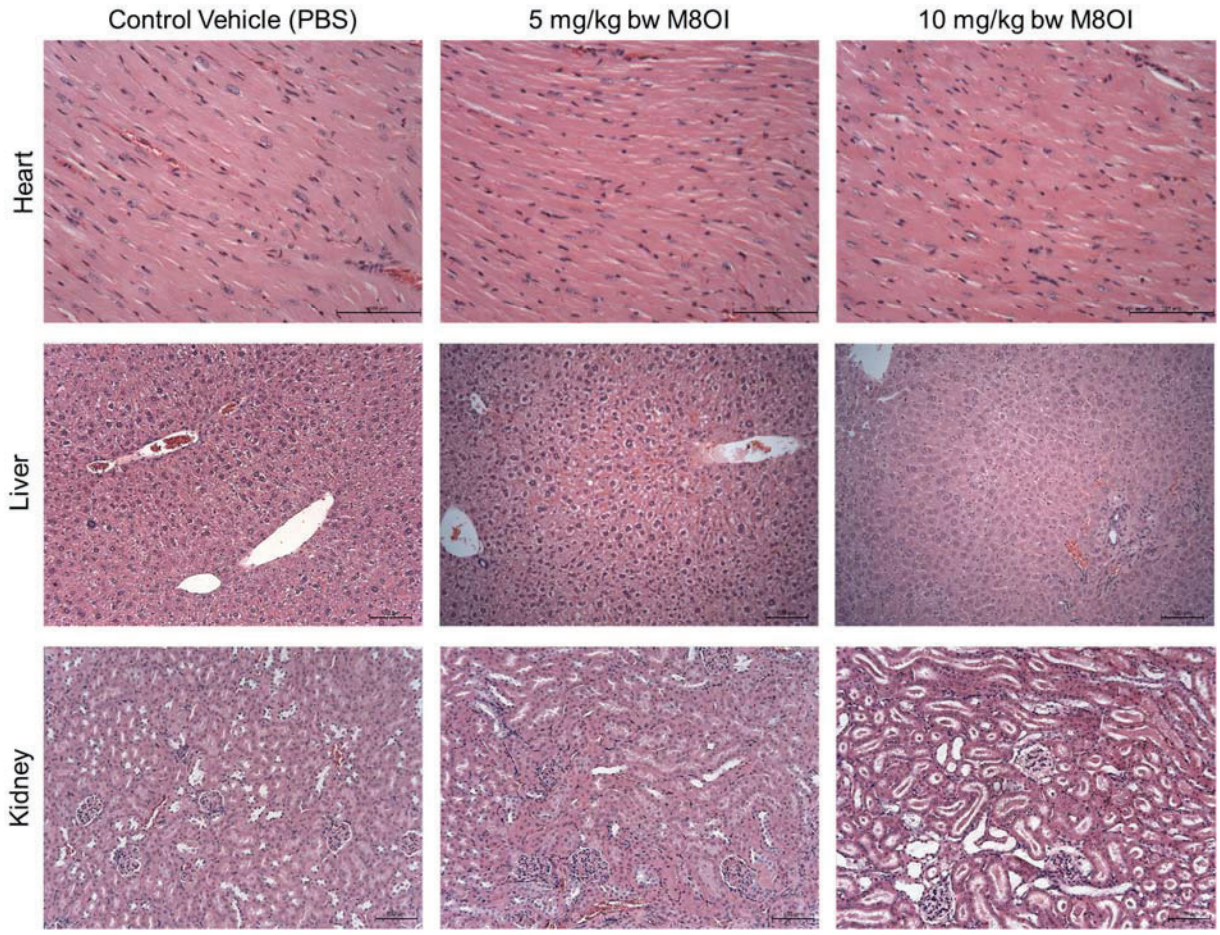

Figure 4.24: Intraperitoneal administration of M8OI results in kidney damage. Male C57B6 mice were administered with indicated doses of M8OI by i.p. injection twice over 24 hours, the second dose was given 18 hours after the first. 24 hours after the first dose was administered, the animals were terminated by cervical dislocation and serum and tissue collected. H&E stained sections of heart liver and kidney from animals treated as indicated, typical views chosen. (scale bar = 100µm).

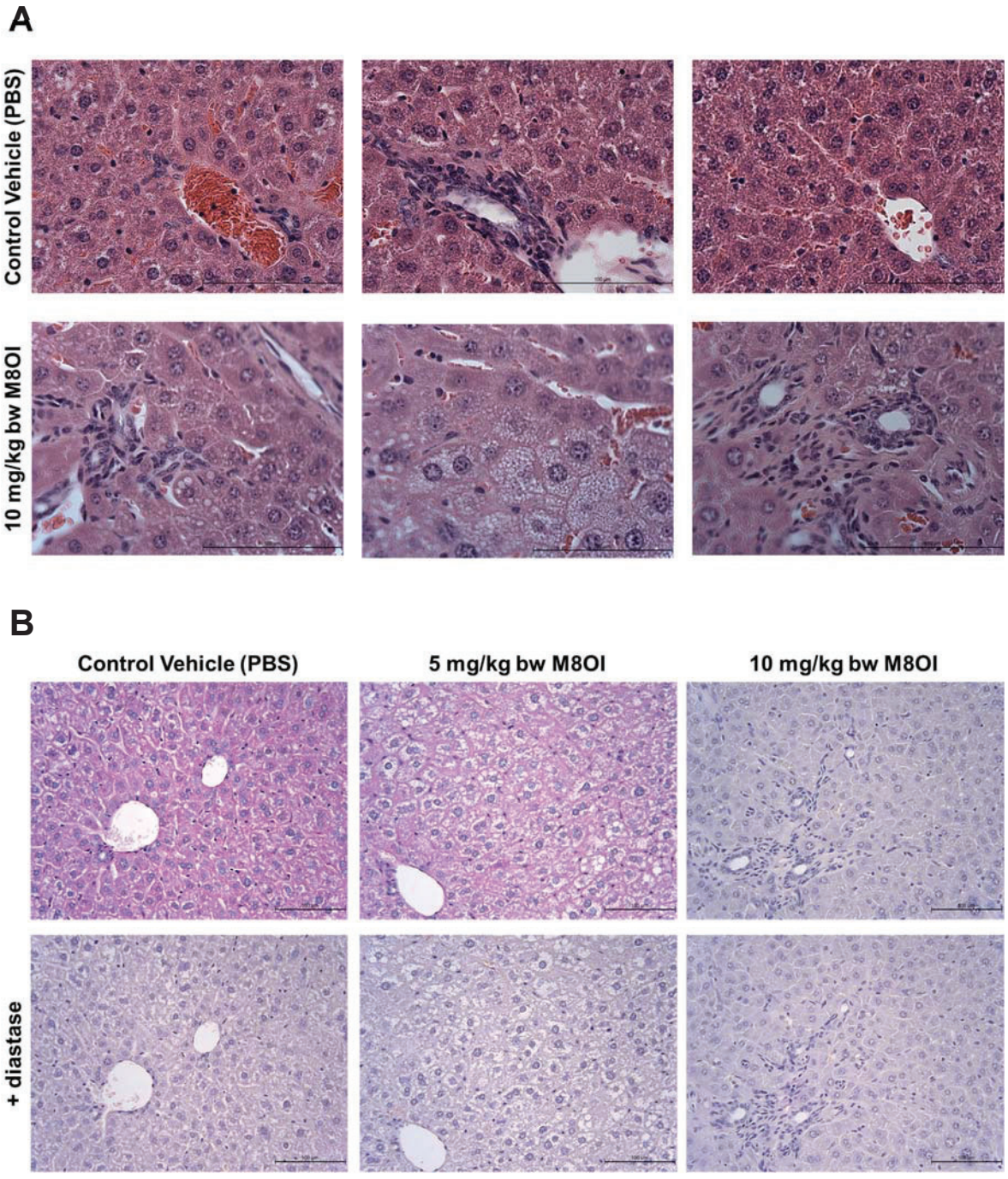

Figure 4.25: Intraperitoneal administration of M8OI depletes hepatic glycogen. Male C57B6 mice were administered with indicated doses of M8OI by i.p. injection twice over 24 hours, the second dose was given 18 hours after the first. 24 hours after the first dose was administered, the animals were terminated by cervical dislocation and serum and tissue collected. **A,** H&E stained sections of liver from animals treated as indicated, 3 typical views chosen. **B,** PAS stained sections of liver from animals treated as indicated, typical views chosen. (scale bar = 100µm)

4.18 Chapter Discussion

Xenobiotics that can act as triggers for PBC have been searched for since environmental factors have been linked to the disease (Probert *et al.*, 2018). Some chemicals such as those found in cosmetics and hair dyes have been suggested to be a reason why there appears to be a female predominance of PBC. However, a chemical had not been found in the environment where there is a clustering of PBC cases that could explain possible geographical prevalence until the identification of M8OI in the north east of England (Probert *et al.*, 2018). M8OI is an imidazolium-based IL that has limited toxicological data. Therefore, the aim of this chapter was to investigate the toxicity of M8OI in *in vitro* and *in vivo* models.

The cell lines used as models to investigate M8OI toxicity have been focused on liver cell lines, such as hepatocytes (HepG2, B-13/H and primary cells), cholangiocytes (H69 cells) and liver progenitor cells (B-13 and human hepatic progenitors). Liver cell models were used as this is the most likely target for xenobiotic toxicity and PBC is a liver-based disease characterised by the destruction of intrahepatic bile ducts. Progenitor cells are important to model because in a diseased liver (including PBC), the damage and removal of hepatocytes and cholangiocytes is greater than the ability of progenitor cells to replace them and one factor for this could be the death of progenitor cells.

Data in this chapter demonstrates that M8OI is toxic to all cell types tested to some degree. Of the cell lines tested, B-13 cells were the most susceptible to M8OI toxicity and in H69 cells there was a reduced sensitivity (Figure 4.1). B-13/H cells were less susceptible to M8OI toxicity than B-13 cells, an effect that was also observed in the toxic soil samples where M8OI was identified (Probert *et al.*, 2018). As B-13 cells were the most susceptible, they were used to investigate the mechanism of toxicity.

Data from the soil sample extracts suggested a mitochondrial effect and the induction of apoptosis (Probert *et al.*, 2018), therefore, real-time apoptosis and necrosis assays and apoptotic DNA laddering experiments were carried out with M8OI. Apoptosis was observed in B-13, H69 and HepG2 cells before switching to necrosis several hours later. Apoptosis assessment was based on the expression of phosphatidylserine on the surface of apoptotic cells and thus the binding of annexin V. This along with the cleavage of genomic DNA generating nucleosomal ladders (Figure 4.7) supports the role of apoptosis in M8OI induced toxicity. Finally, M8OI induces mitochondrial swelling (Figure 4.8). Mitochondrial swelling is induced by the opening of the mitochondrial permeability transition pore (MPTP), which causes cell death by necrosis (though calcium overload and oxidative stress) and is believed to be involved in apoptosis (Rasola and Bernardi, 2007; Crichton *et al.*, 2009) as it has been shown that MPTP-induced mitochondrial

swelling induces cytochrome c release (Petit *et al.*, 1998). The induction of apoptosis is important in PBC as the cholangiocytes undergo apoptosis and present the PDC-E2 antigen in the apotope formed (Odin *et al.*, 2001). Therefore, M8OI induced apoptosis could contribute to the degradation of the bile ducts and the presentation of the PDC-E2 antigen. However, further work using primary human cholangiocytes is required to confirm M8OI induced apoptosis in humans.

The model used for human progenitor cells cannot be cultured in basic medium or using standard plastics and must be cultured in matrigel to form organoids. Additionally, small amounts of material were sourced and expanded, therefore the number of experiments were limited. This meant studying cell viability was difficult and it was not possible to use certain analytical tools such as the seahorse flux analyser. Trypan blue staining showed a loss of cell viability in organoids treated with M8OI, however MTT assays showed active reduction to formazan suggesting the mitochondrial reductases are still functioning but the cell membrane has become permeable (Figure 4.17 & Figure 4.18). The human progenitor cells showed evidence of apoptosis in the form of apoptotic blebs (Figure 4.16) and TEM analysis showed mitochondrial swelling (Figure 4.19), indicative of MPTP opening, cytochrome c and apoptosis inducing factor release and therefore suggest late-apoptosis (Petit *et al.*, 1998; Sun *et al.*, 2007). As assays using these cells are limited, Western Blot analysis of cleaved caspase PARP and cleaved caspase 3 could be used to confirm the apoptotic mechanism.

There is little literature on M8OI toxicity *in vitro* for comparison. One study found M8OI induced toxicity in rat pheochromocytoma (PC12) cell line (Li *et al.*, 2012). The authors concluded that M8OI induced apoptosis in PC12 cells, as well as increasing ROS and decreasing ATP content. Finally, they suggested that M8OI caused mitochondrial dysfunction. All these findings support to the findings in liver cells presented in this chapter.

The mitochondrial effects of M8OI were studied using the seahorse flux analyser as the mitochondria play a vital role in apoptotic cell death. It took longer for M8OI to fully inhibit mitochondrial oxygen consumption/µg protein in B-13/H cells compared to B-13 cells (Figure 4.10). It has previously been noted in this lab that B-13/H cells have a greater number of mitochondria and a decrease in glucose consumption compared to B-13 cells. This could be one explanation why there is a difference in cell viability between B-13 and B-13/H cells as M8OI inhibits oxidative phosphorylation and increases glycolysis and therefore requires glucose.

A 50% inhibition of the OCR was achieved at 10µM of M8OI and no effects were observed at 1µM or lower (Figure 4.11). The maximal respiration and spare respiratory capacity of M8OI treated cells was inhibited when the cells were exposed to FCCP, which under normal conditions results in uncoupling (Brand and Nicholls, 2011). This effect was also observed in PMP experiments with complex I, M8OI inhibited the OCR when ADP was added and partially inhibited the OCR when FCCP was added. PMP experiments with complex II showed that M8OI increases oxygen consumption when in the presence of succinate.

These data could be used to draw a hypothesis of the mechanism of action of M8OI on the ETC. M8OI is likely to interact with multiple sites involved in oxidative phosphorylation. Firstly, M8OI appears to inhibit ATP synthase (Complex V) as M8OI inhibits the OCR in a similar manner to oligomycin as FCCP can rescue OCR by uncoupling, although to a limited extent. If M8OI inhibited via different complex in the ETC then FCCP would not increase oxygen consumption upon uncoupling, as seen when rotenone and antimycin A (complex I and III inhibitors respectively) inhibited the OCR post-FCCP treatment. This effect is also observed in the PMP experiments for complex I. Additionally, rotenone induced inhibition is not recovered by FCCP in complex I PMP experiments showing that this blocks the electron flow beyond complex I, suggesting M8OI does not act at the same site as rotenone. However, the increase in oxygen consumption induced by FCCP is significantly less than control cells, suggesting that M8OI may have an effect elsewhere, either on complex I or elsewhere on the ETC. Substrate oxidation is a limiting factor during uncoupling (Brand and Nicholls, 2011), M8OI could therefore inhibit substrate supply, cause electron leakage or inhibit substrate oxidation that is not through the inhibition of complexes I-IV. In complex II PMP experiments, M8OI induced a large increase in the OCR in the presence of succinate. This suggests the activation of complex II, an effect that has been shown with 5-Aminoimidazole-4-carboxamide 1-beta-D-ribofuranoside (AICAR). AICAR contains an imidazole structure similar to M8OI and increases complex II activity through AMP- activated protein kinase (AMPK) (Pfleger *et al.*, 2015). The mechanism of M8OI induced effects on the mitochondria require further study. However, data thus far suggests the involvement of complex V inhibition and activation of complex II.

Given that the mitochondria are generally considered to be highly conserved between species it is likely that the effects observed in the cell lines tested will translate to humans as evidenced by the toxicity induced by M8OI in primary human hepatocytes. Yet it is difficult to determine whether the concentrations examined reflect potential human exposure as it is not known. Route of exposure, the concentration at which an individual could be exposure and the metabolism of M8OI are determining factors that are unknown and therefore further data is required to validate any potential risk.

Mice dosed intraperitoneally above 10mg/kg bw M8OI in a pilot study were culled within an hour of dosing to prevent exceeding severity. These effects are highly unlikely to be hepatic due to the rapid onset of effects. 10mg/kg bw M8OI showed evidence renal injury and is similar to acute tubular necrosis observed in rats with renal ischemic injury (Ferreyra *et al.*, 2013; Narayan *et al.*, 2016), suggesting that the kidney is the target organ of toxicity. Further studies would need to be carried out to confirm inflammation and damage in the kidney as well as measuring serum creatinine and urea as well as urinary protein. Some hepatic effects were observed, including an increase in the presence inflammatory cells in parts of the liver and depletion in hepatic glycogen content throughout the liver. This glycogen depletion supports the mitochondrial effects seen *in vitro*, as the inhibition of oxidative phosphorylation and the shift to glycolysis would increase glucose consumption by the mitochondrial for anaerobic respiration, and therefore the catabolism of glycogen to glucose. Additionally, it has been shown that AICAR increases myocardial glycogen degradation in rats via AMPK activation (Longnus *et al.*, 2003). Oral dosing of M8OI up to 40mg/kg body weight had no adverse effects suggesting that the bioavailability of M8OI is low and it is either excreted or metabolised to a non-toxic metabolite. The only toxicity study using a mouse model provides very limited data and only administered M8OI intraperitoneally for 10 hours and reports an LD_{50} of 35.7mg/kg bw (Yu *et al.*, 2008). It is therefore difficult to compare the *in vivo* results with the literature other than at 20mg/kg bw mice were culled to ensure severity was not exceeded.

In this chapter it has therefore been demonstrated that M8OI induces toxicity *in vitro*. Additionally, intraperitoneal administration of M8OI suggested that the kidney is the primary target organ for M8OI. Like the soil samples from the waste tip site where M8OI was identified, M8OI induced apoptosis caused by mitochondrial dysfunction, possibly via combination of ATP synthase inhibition and other mitochondrial interactions. These mitochondrial effects could also explain why glycogen depletion is observed in mice administered with M8OI. The induction of apoptosis is also important in the mechanism of PBC, as cholangiocytes undergo apoptosis to present the PDC-E2 antigen.

Chapter 5. An investigation of the metabolism of M8OI

5.1 Introduction

Lipoic acid is an endogenously synthesised cofactor that covalently binds to the E2 subunit of pyruvate dehydrogenase and is essential for function to reduce flavin adenine dinucleotide (FAD) to $FADH_2$ (Kaplan and Gershwin, 2005). The carboxylic acid moiety of lipoic acid covalently binds to the lysine residue in two lipoyl domains. It is these lipoyl domains that contain the amino acid residues that are recognised by immune cells in patients with PBC, specifically residues 170 (glutamic acid), 172 (aspartic acid) and 173 (lysine). The lysine residue at 173 is the lysine that binds to lipoic acid, and the conjugated form is considered responsible for the breakdown of self-tolerance (Bruggraber *et al.*, 2003).

This lipoyl domain is also of interest in PBC as during the apoptosis of the cholangiocyte, the lysine residue is not bound to glutathione as is the case with other cells (Odin *et al.*, 2001). Xenobiotic modification of PDC-E2 occurs within the lipoyl domain and it has been shown that xenobiotics can be incorporated in PDC-E2 via the exogenous lipoylation pathway (Walden *et al.*, 2008). Xenobiotics conjugated to BSA are immunoreactive *in vivo* (Leung *et al.*, 2003) and xenobiotically modified PDC-E2 is reactive against PBC patient sera (Amano *et al.*, 2005; Rieger *et al.*, 2006). The chemical structure of these xenobiotics is important. Currently known xenobiotics that modify PDC-E2 all contain a carboxyl moiety at the end of a short chain of around 4-10 carbons and thus have a similar structure to lipoic acid (Rieger *et al.*, 2006).

The structure of M8OI is similar to lipoic acid in that it has a 5-carbon cyclic ring with a long carbon chain attached (Figure 5.1). However, it does not have the carboxylic acid moiety required for it to conjugate to PDC-E2. While M8OI is persistent in the environment, it has been shown to be biodegraded through the oxidation of the terminal carbon to form a carboxylic acid - 1-(7-carboxyheptyl)-3-methyl-1H-imidazol-3-ium (COOH7IM) (Markiewicz *et al.*, 2015) and is therefore more structurally similar to lipoic acid than M8OI and has the potential for incorporation into PDC-E2. COOH7IM was synthesised and shown to covalently incorporate into an unlipoylated fragment of PDC-E2, whereas neither M8OI or the intermediate hydroxyl-M8OI (HO8IM, 3-(8-hydroxyoctyl)-1-methyl-1H-imidazol-3-ium) were incorporated (Probert *et al.*, 2018). It is therefore possible that COOH7IM could modify the lipoyl domain of PDC-E2 that is recognised by immune cells and produce AMAs.

While the previous chapter demonstrated that M8OI was toxic to liver cells, it is unknown whether the two metabolites HO8IM and COOH7IM are also toxic. Additionally, HO8IM and COOH7IM have been shown to be products of the biodegradation of M8OI yet it has not been shown as to if M8OI is metabolised by the human (or other mammalian) liver. Metabolism of M8OI is the most likely route of exposure to

COOH7IM as levels of the metabolite were negligible in the soil samples that contained M8OI (unpublished data), and therefore environmental exposure to COOH7IM is unlikely. Finally, it is unknown how likely M8OI is to reach systemic circulation if an individual were to be exposure to the chemical.

Therefore, the aims of this chapter were to determine the toxicity of the two metabolites and to investigate whether M8OI is metabolised by hepatocytes *in vitro* and *in vivo* in human and murine models, and if so, what metabolites are produced. The final aim was to investigate possible routes of exposure (via oral administration), bioavailability and excretion. These aims will aid in the understanding of the M8OI exposure risk and the likelihood of exposure to the COOH7IM metabolite and the potential risk of an immune response.

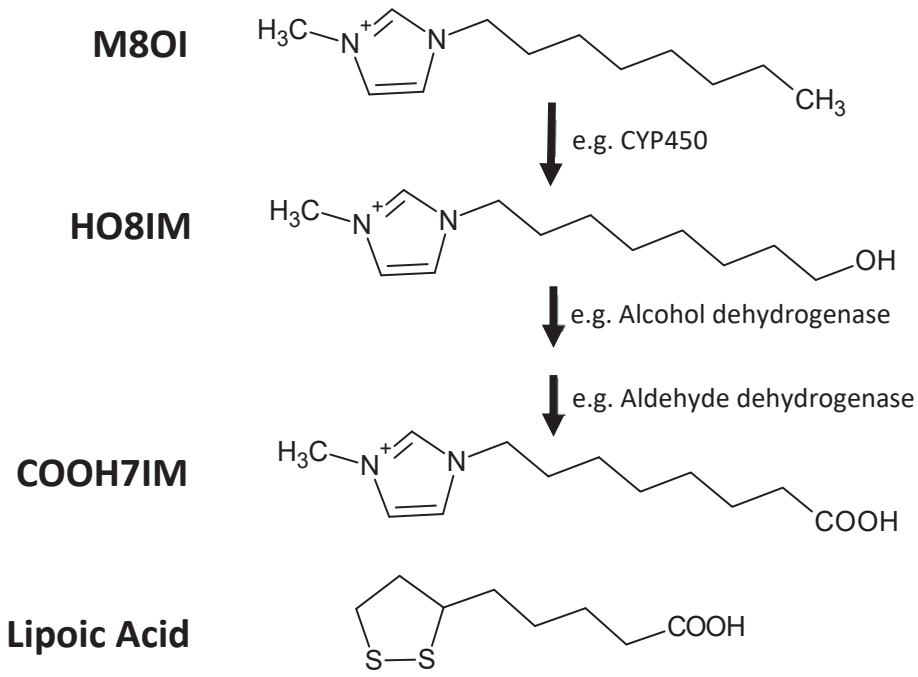

Figure 5.1: Proposed metabolic pathway of M8OI to a carboxylic acid and structural comparison to lipoic acid. Abbreviations: M8OI, 3-methyl-1-octyl-1H-imidazol-3-ium; HO8IM, 1-(8-hydroxyoctyl)-3-methyl-imidazolium; COOH7IM, 1-(7-carboxyheptyl)-3-methyl-1H-imidazol-3-ium. Structures for each compound were drawn using ChemSketch (ACDLabs).

5.2 COOH7IM is not toxic to liver cells *in vitro*

M8OI was previously shown to be toxic to hepatic progenitors and hepatocytes, it was therefore hypothesised that the metabolism of M8OI to HO8IM and COOH7IM would reduce toxicity. To assess the toxicity of the potential M8OI metabolites, HO8IM and COOH7IM, liver cells were exposed to a dose

response of all three compounds and cell viability was determined using MTT assays. B-13 and B-13/H cells were used to detect changes between hepatic progenitors and hepatocytes. As seen in chapter 4, M8OI was more toxic to B-13 than B-13/H cells (Figure 5.2A-D). In B-13 cells at 24 hours, HO8IM showed a statistically significant reduction in cell viability from 1µM to 1000µM (Figure 5.2A). Cell viability at 500µM and 1000µM was 29.73% and 23.55% respectively. The toxicity of HO8IM was greater after 48 hours with a significant reduction in MTT activity observed from 0.1µM and higher (Figure 5.2B). However, B-13/H cells were less susceptible to HO8IM induced toxicity, similarly to M8OI. At both 24 and 48 hours, a significant reduction in MTT activity was only observed at 500µM and 1000µM with the response at 24 hours showing a reduction of cell viability to 83.02% and 81.76% respectively (Figure 5.2C). This is a difference of 53.29% and 58.21% compared to B-13 cells. No such decrease in cell viability was observed in either cell type after 48 hours of exposure of COOH7IM at the concentrations tested (Figure 5.2A-D).

The effects in HepG2 cells and H69 cells were also investigated. M8OI was toxic to both cell lines as seen in chapter 4, with H69 cells being more resistant. HO8IM was toxic to HepG2 cells at 500 and 1000µM, evidenced by the reduction of MTT activity at 24 hours (Figure 5.3A). The effect was further exacerbated after 48 hours, but this effect was not as great in HepG2 cells (Figure 5.3B). As with M8OI, HO8IM appeared less toxic in H69 cells. At 24 hours of exposure of 500µM and 1000µM there was a significant reduction in MTT activity compared to control cells (Figure 5.3C). There was a greater reduction after 48 hours exposure but similarly not as toxic in HepG2 cells (Figure 5.3D). As observed in B-13 and B-13/H cells, COOH7IM did not induce any toxicity in either cells type at the concentrations implemented after 24 or 48 hours (Figure 5.3A-D). These data show that if M8OI was metabolised via the pathway hypothesised then it would be metabolised to the less toxic intermediate compound of HO8IM and further metabolised to the non-toxic COOH7IM. As previously described with M8OI, HO8IM showed variation in toxicity between cell types with B-13 cells being the most susceptible and H69 and B-13/H cells being the most resistant.

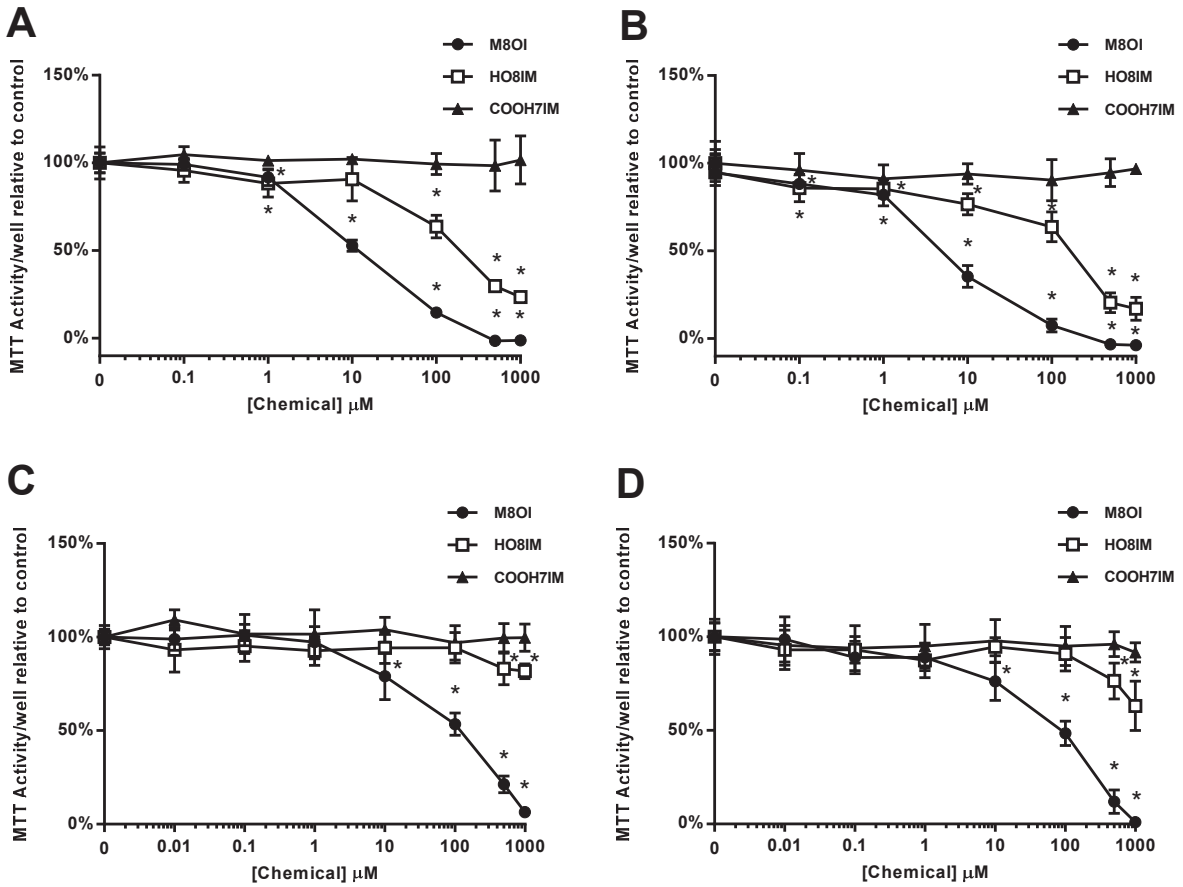

Figure 5.2: HO8IM is toxic whereas COOH7IM is not toxic to B-13 and B-13/H cells. B-13 **(A&B)** and B-13/H cells **(C&D)** were treated with indicated compounds for 24 hours **(A&C)** and 48 hours **(B&D)**. Following treatment, cells were incubated with MTT for 2 hours and reduction determined. Data are the mean and SD of 6 separate determinations from the same experiment, typical of 3 separate experiments. * significantly different cell viability to 0μM ($p<0.05$) tested by one-way ANOVA followed by Bonferroni post-hoc test.

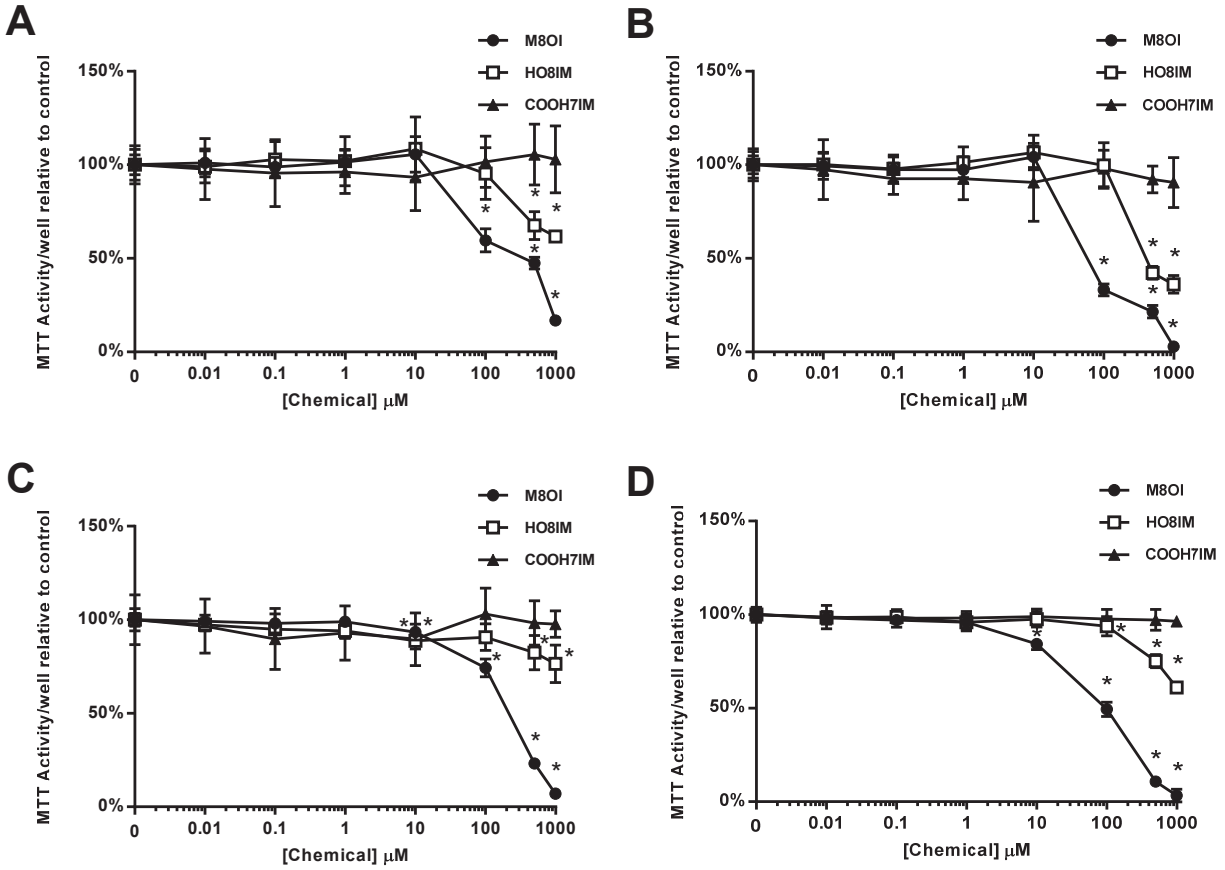

Figure 5.3: HO8IM is toxic, and COOH7IM is not toxic to HepG2 and H69 cells. HepG2 cells **(A&B)** and H69 cells **(C&D)** were treated with indicated compounds for 24 hours **(A&C)** and 48 hours **(B&D)**. Following treatment, cells were incubated with MTT for 2 hours and reduction determined. Data are the mean and SD of 6 separate determinations from the same experiment, typical of 3 separate experiments. * significantly different cell viability to 0μM ($p<0.05$) tested by one-way ANOVA followed by Bonferroni post-hoc test.

5.3 HO8IM and COOH7IM are not toxic in primary hepatocytes

The cell viability of primary hepatocytes from mouse and human hepatocytes exposed to HO8IM and COOH7IM was tested at 24 and 48 hours. Mouse hepatocytes were susceptible to M8OI induced toxicity at low concentrations of 0.1μM in at 24 and 48 hours. At 100μM after 24 hours cell viability was 8.6% compared to control, demonstrating that mouse hepatocytes are highly susceptible to M8OI induced toxicity. However, unlike the immortalised cell lines used in 5.2, HO8IM did not induce cell toxicity after 24 hours up to 1000μM (Figure 5.4A). After 48 hours of exposure there was some statistically significant

reduction in MTT activity, yet this did not fall below 85% (Figure 5.4B). COOH7IM was not toxic at the concentrations implemented at either 24 or 48 hours of exposure.

Primary human hepatocytes exposed to M8OI showed less susceptibility to this compound than mouse hepatocytes (Figure 5.5). Chlorpromazine was used as a hepatotoxic control and showed significant toxicity from 100µM to 1000µM. Human hepatocytes treated with HO8IM and COOH7IM showed no reduction in cell viability compared to control cells up to 1000µM (Figure 5.5). These observations support the data from using immortalised cell lines that COOH7IM is not toxic to liver cells. However, unlike the immortalised cells, little toxicity was observed in mouse hepatocytes and no toxicity was detected in human hepatocytes treated with HO8IM. The difference between the primary hepatocytes and the other cells lines used is likely to be the metabolic capacity of human and mouse hepatocytes. Therefore, primary cells may be capable of metabolising HO8IM before it can induce its toxic effects.

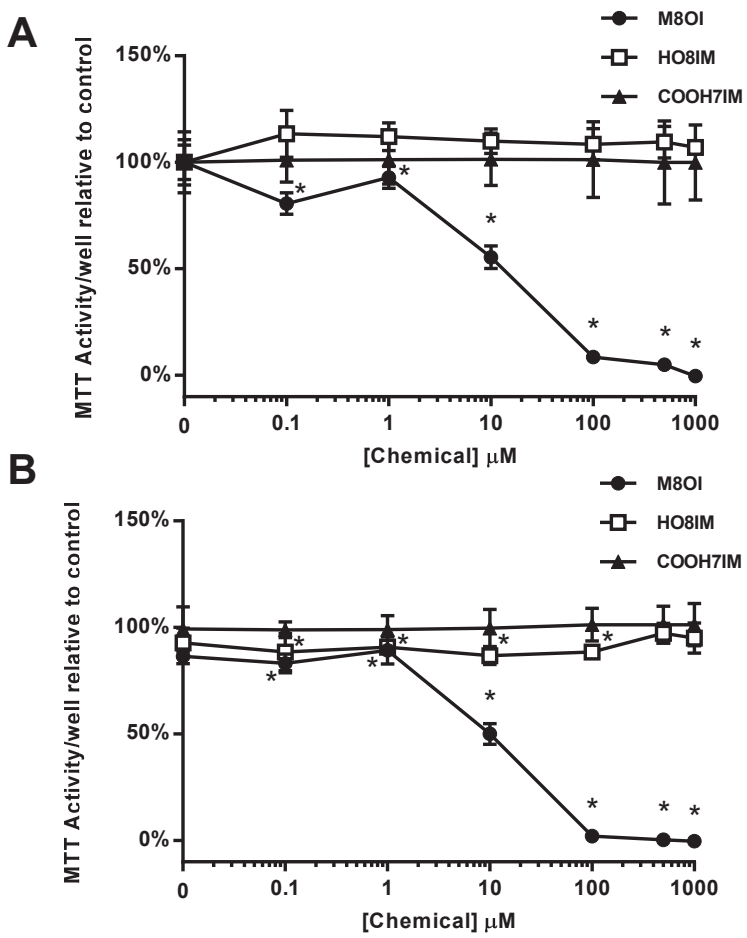

Figure 5.4: HO8IM and COOHIM are not toxic to primary mouse hepatocytes. Primary mouse hepatocytes were treated with indicated compounds for 24 hours (A) and 48 hours (B). Following treatment, cells were incubated with MTT for 2 hours and reduction determined. Data are the mean and SD of 6 separate determinations from the same experiment, typical of 3 separate experiments. * significantly different cell viability to 0μM ($p<0.05$) tested by one-way ANOVA followed by Bonferroni post-hoc test.

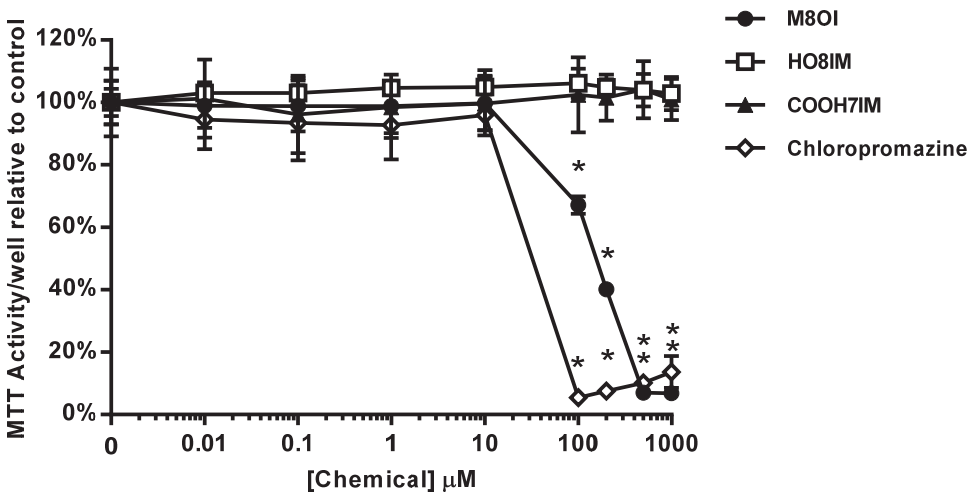

Figure 5.5: HO8IM and COOHIM are not toxic to primary human hepatocytes. Primary human hepatocytes (Donor 1, see table 5.1) were treated with indicated compounds for 24 hours. Following treatment, cells were incubated with MTT for 2 hours and reduction determined. Data are the mean and SD of 6 separate determinations from the same experiment, typical of 3 separate donors. * significantly different cell viability to 0μM ($p<0.05$) tested by one-way ANOVA followed by Bonferroni post-hoc test.

5.4 HO8IM induced toxicity does not affect the mitochondria.

As M8OI toxicity was induced by interactions with the mitochondria, the potential of a mitochondrial mechanism of HO8IM induced toxicity in B-13 cells was investigated using the seahorse flux analyser to see if HO8IM acted in a similar manner as M8OI. Neither HO8IM or COOH7IM at 100μM induced any effect on the OCR or the ECAR and throughout the experiment the effects were similar to controls cells when oligomycin, FCCP and rotenone/antimycin A were added. As previously observed, 100μM of M8OI inhibited mitochondrial oxygen consumption (that was partially recoverable with the addition of FCCP) and increased the ECAR (Figure 5.6). This suggests that HO8IM mechanism of toxicity differs to M8OI and does not interact with the mitochondria. However, higher concentrations of HO8IM and COOH7IM should be investigated.

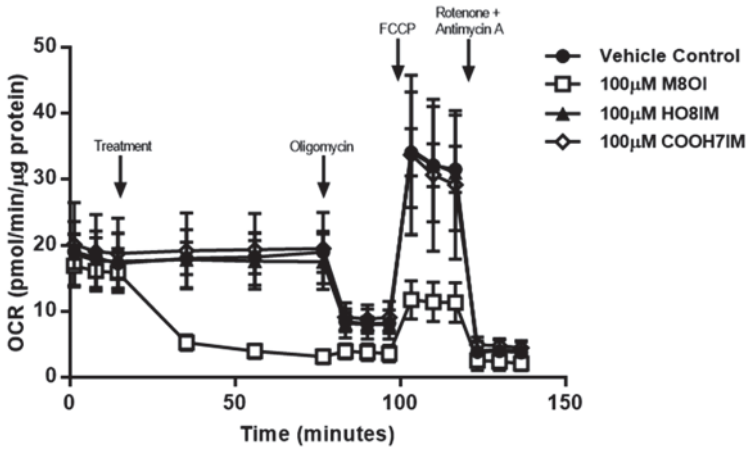

Figure 5.6: HO8IM and COOH7IM do not have any effect on the mitochondria. The effect of the indicated chemicals on mitochondrial function in B-13 cells was analysed with the seahorse flux analyser using the mito stress test as described in the methods (2.15.1). Data was normalised to protein concentration calculated using a Bradford assay and OCR determined. Arrows indicate the injection of indicated compounds. Data are the mean and SD of at least 8 separate determinations. Statistics not determined

5.5 High concentrations of M8OI form micelles

It has previously been shown that M8OI can form micelles (Markiewicz *et al.*, 2013) to confirm this, increasing concentrations of M8OI was made up using the buffer to be used for HPLC (STIM buffer + 0.1% phosphoric acid, see 2.17.1) containing 100nM of Nile red and SDS was used as a positive control for micelle formation. M8OI formed micelles at 1M only whereas SDS showed a dose dependent increase in micelle formation from 10mM to 1M (Figure 5.7A). The formation of micelles during HPLC could be different however as both temperature and pressure have an effect on the critical micelle concentration (Kato 1997).

To determine whether M8OI was metabolised by hepatocytes and if the metabolites produced were the hypothesised HO8IM and COOH7IM, HPLC was used to analyse the medium of cells treated with M8OI. UV/Vis was to be used for detection, and so absorbance wavelength was to be determined so M8OI, HO8IM and COOH7IM could be quantified. All three compounds produced a peak absorbance at 212nm (Figure 5.7B). This meant one wavelength at 212nm could be used to detect all compounds of interest.

STIM buffer with the three compounds (M8OI, HO8IM and COOH7IM) were analysed using the HPLC to produce chromatograms to make it possible to identify the compounds. STIM buffer containing a water

vehicle produced a peak likely made up of several components (from the STIM buffer) at 2 minutes (Figure 5.8). 100µM M8OI produced a peak retention time at 13.5 minutes (Figure 5.8). This peak had a long peak tail compared to the peak front. HO8IM and COOH7IM had retention times close to each other of 3.2 and 2.9 minutes (Figure 5.8) respectively. The shape and intensity were different with HO8IM displaying a peak tail and greater intensity.

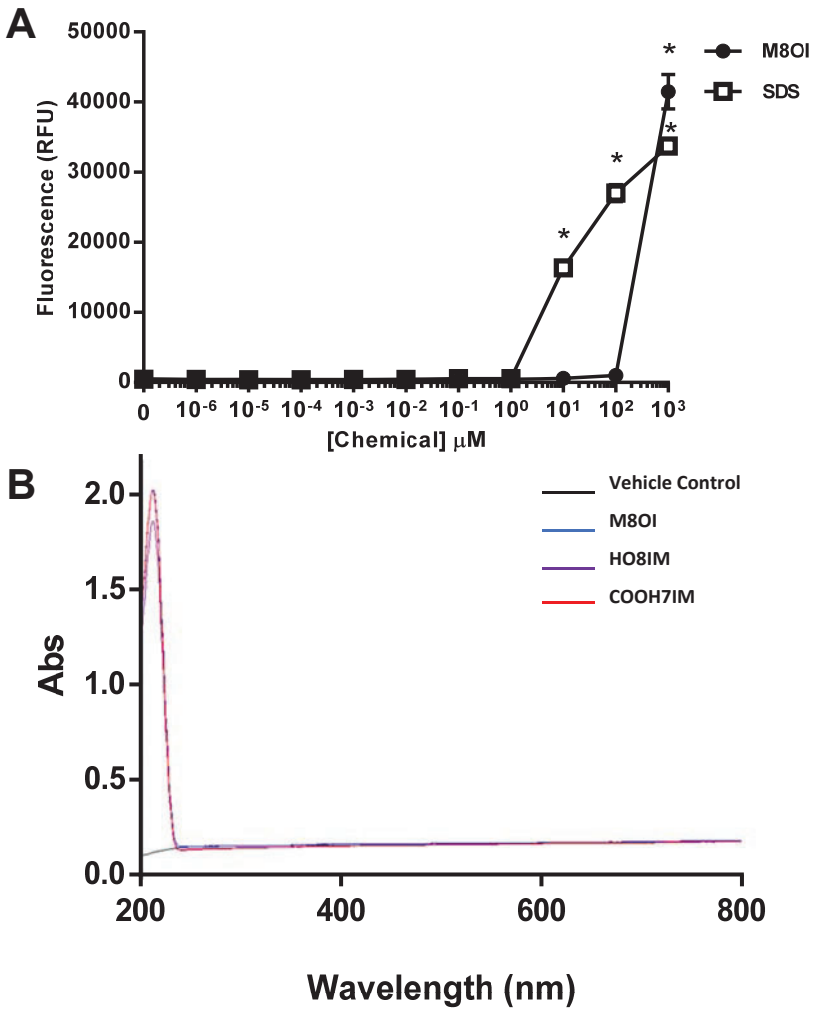

Figure 5.7: M8OI forms micelles in STIM buffer and M8OI, HO8IM and COOH7IM absorb at 212nm. A, a 500µM of M8OI solution was made in STIM buffer plus 0.1% phosphoric acid. Absorbance wavelength was determined using a duel-beam spectrophotometer. **B,** M8OI and SDS solutions were made up at indicated concentrations in STIM buffer containing 0.1% phosphoric acid and Nile red at a final concertation of 100nM. The formation of micelles was determined by measuring the fluorescence of Nile red ($552nm_{Ex}/636nm_{Em}$). Data are the mean and SD of 4 separate determinations from the same experiment, typical of 3 separate experiments. * significantly different Nile red fluorescence to control ($p<0.05$) tested by one-way ANOVA followed by Bonferroni post-hoc test.

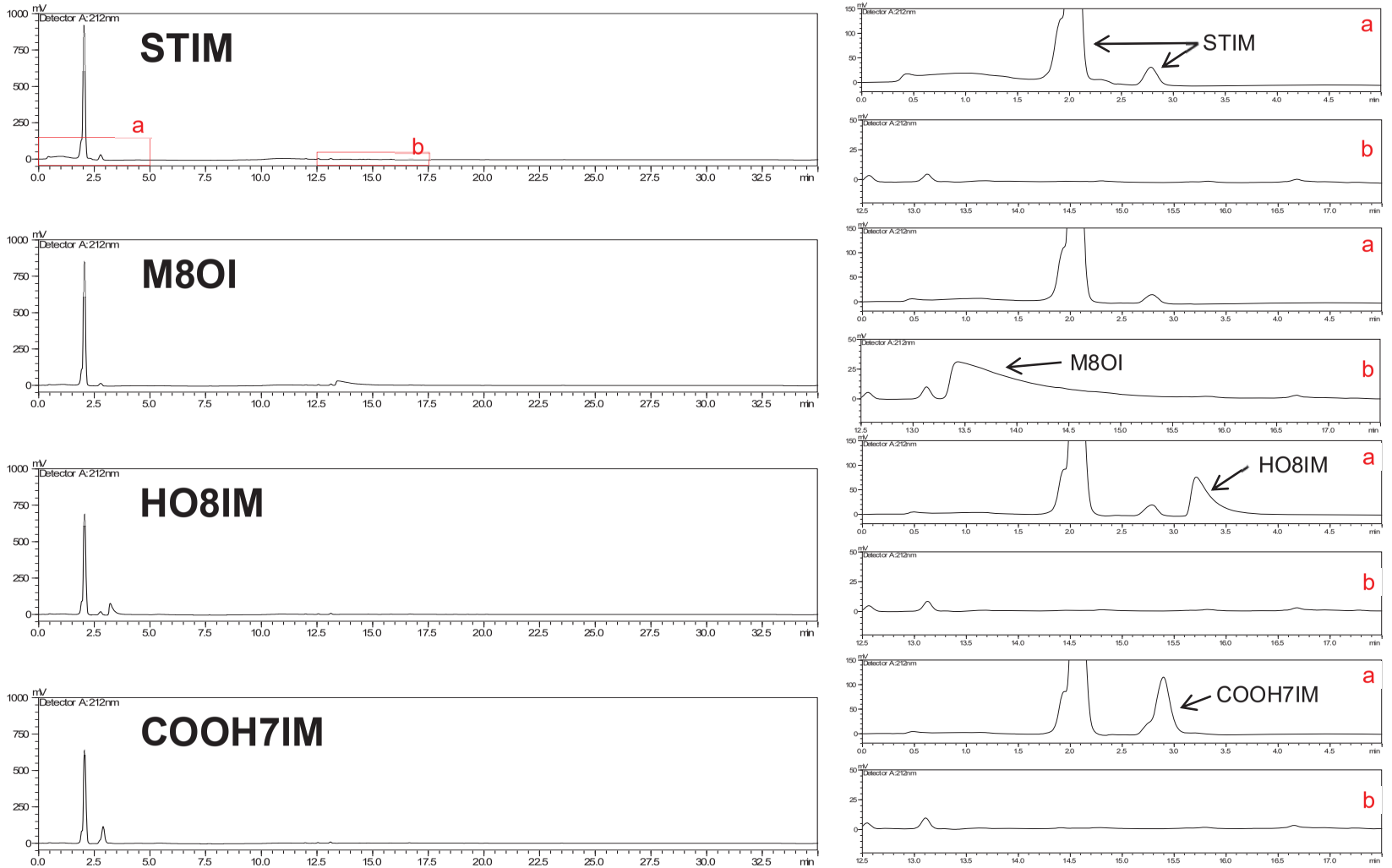

Figure 5.8: HPLC chromatograms for M8OI, HO8IM and COOH7IM. 100µM of M8OI, HO8IM and COOH7IM, along with a vehicle control were prepared in STIM buffer plus 0.1% phosphoric acid. Samples were then separated by HPLC and absorbance detected at 212nm (see methods, 2.17) and full chromatograms of each chemical were produced (left panels). Right panels are zoomed in chromatograms of red boxes of **a,** 0-5 minutes and **b,** 12.5-17.5 minutes. arrows indicative of peaks for each chemical.

5.6 M8OI is metabolised by human hepatocytes and metabolism is inhibited by ketoconazole.

The metabolism of M8OI was determined by culturing the cells in STIM buffer containing M8OI and taking samples from the medium and analysing them by HPLC to detect any depletion in the M8OI peak as well as the production of any new peaks that appear that would indicate a UV absorbing metabolite. Primary human hepatocytes were cultured with STIM buffer and 100µM M8OI. At 0, 4, 8 and 24 hours, a sample of the medium was taken from the culture, treated with phosphoric acid before HPLC analysis. M8OI was rapidly metabolised by human hepatocytes (donor 2, see Table 5.1). The concentration in the medium was reduced from 111.91µM to 23.92µM after 8 hours of incubation and this was further reduced to 2.70µM after 24 hours (Figure 5.9A). A new peak was formed at 4 and 8 hours that appeared at the same retention time as the pure COOH7IM standard, suggesting M8OI is metabolised into COOH7IM. The concentration of COOH7IM in the culture medium increased linearly over 8 hours (Figure 5.9B). It was not possible to determine the concentration of COOH7IM at 24 hours as the STIM buffer peak at 1.8 minutes widened, masking any COOH7IM peak being produced.

Human hepatocytes were also pre-treated with known CYP450 inhibitors; metyrapone (non-specific, CYP11B1, CYP3A4), ketoconazole (CYP3A4), SKF525a (non-specific), and methimazole (FMO inhibitor). Hepatocytes pre-treated with ketoconazole and incubated with M8OI for 24 hours had a higher concentration of M8OI in the medium at 59.93µM compared to 2.70µM of the control cells (Figure 5.9A). There was no difference between the other inhibitors and vehicle control cells after 24 hours. However, after 8 hours there was a significant difference between vehicle cells and metyrapone and SKF525a pre-treated cells. This suggests that ketoconazole strongly inhibits M8OI metabolism whereas metyrapone and SKF525a weakly inhibit metabolism. Similar results were observed with the production of the COOH7IM metabolite. Ketoconazole treated cells only produced 5.06µM of metabolite compared to 37.58µM in vehicle treated cells. SKF525a treated cells showed a decrease in the amount of COOH7IM produced and methimazole treated cells showed an increase in COOH7IM production (Figure 5.9B). It was not possible to determine the concentration of COOH7IM produced in metyrapone treated cells as the retention time of the two compounds overlapped. To ensure the reason M8OI concentration did not decrease in ketoconazole treated cells was due to cell toxicity, cells were treated with the same concentration of ketoconazole for 24 hours and cell viability was determined and showed that 10µM ketoconazole was not toxic to primary human hepatocytes (Figure 5.9C). These data suggest as ketoconazole is a CYP3A4 inhibitor, that CYP3A4 is one of the enzymes responsible for some of the metabolism of M8OI.

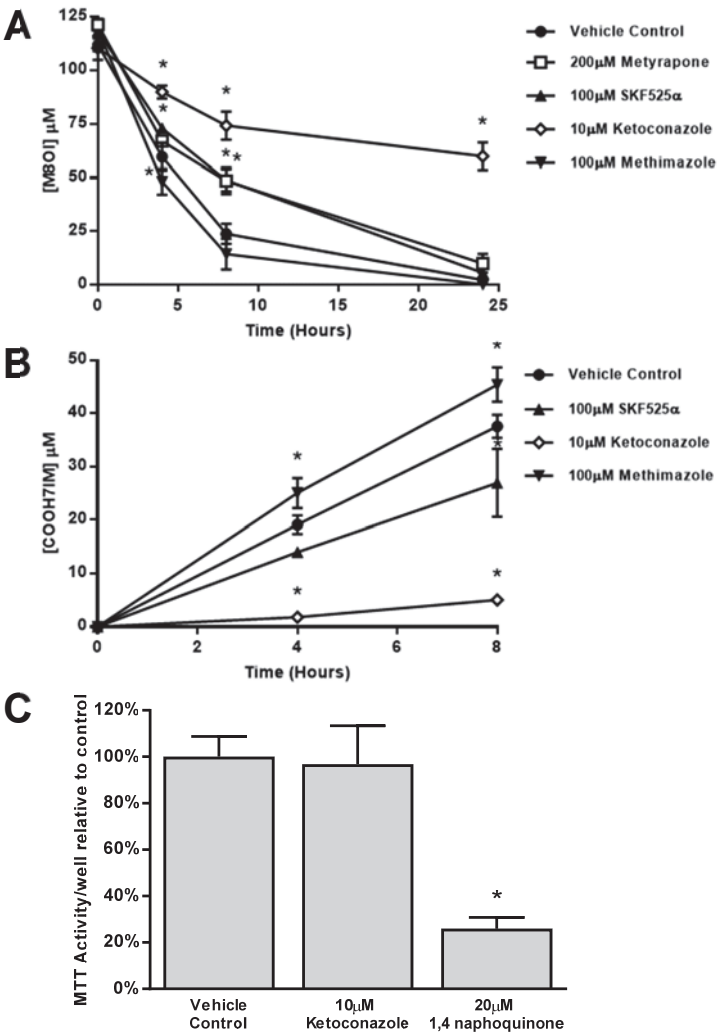

Figure 5.9: Ketoconazole reduces M8OI depletion and COOH7IM production on in metabolising human hepatocytes. A, Primary human hepatocytes (donor 2, see table 2.1) were pre-incubated with STIM buffer and indicated chemicals for 2 hours. Cells were then retreated with these chemicals plus 100µM of M8OI. 200-500µl of STIM buffer was then taken from the culture at 0, 4, 8 and 24 hours. The samples were treated with phosphoric acid, separated by HPLC and absorbance detected at 212nm. The area under the curve of the peak at 15 minutes was calculated and the concentration of M8OI in the sample was determined from the M8OI standard curve. Data are the mean and SD of 3 separate determinations from the same donor. * significantly different M8OI concentration to control treatment of the same timepoint ($p<0.05$). **B,** Primary human hepatocytes were treated, and the sampled buffer was treated as described in A. The area under the curve of the peak at 3.1 minutes was calculated and the concentration of COOH7IM in the sample was determined from the COOH7IM standard curve. * significantly different COOH7IM concentration to control treatment of the same timepoint ($p<0.05$). **C,** Primary human hepatocytes were indicated with indicated chemicals for 26 hours. Following treatment, cells were incubated with MTT for 2 hours and reduction determined. Data are the mean and SD of 3 separate determinations from the same experiment. * significantly different cell viability to control ($p<0.05$).

5.7 CYP3A4 deficient hepatocytes do not metabolise M8OI

The comparison of two hepatocyte preparations from two separate donors (Table 5.1) showed that one preparation contained hepatocytes capable of metabolising M8OI over 24 hours where as another could not metabolise M8OI enough to be detectable using HPLC determination (Figure 5.10A). qRT-PCR of these two hepatocyte preparations was therefore used to examine their differences in CYP450 expression. The largest difference was CYP3A4, mRNA expression was 277-fold higher in the M8OI metabolising preparation compared to the non-metabolising preparation (Figure 5.10B). The next greatest difference was a 64.5-fold increase in CYP2D6 expression in the non-metabolising hepatocytes. Other significant differences in expression that were higher in the M8OI metabolising hepatocytes and included CYP1A1 (51.7-fold), CYP1A2 (13.2-fold), CYP2A6 (17.4-fold), CYP2B6 (9.5-fold) and CYP3A34 (5.6-fold). Those higher in the non-metabolising hepatocytes included CYP4A11 and ACOX1 which showed a 4.6-fold and 2.4-fold increase respectively (Figure 5.10B).

Hepatocyte Prep Number	Age	Sex	Drugs
1	23	Male	Propofol, fentanyl, midazolam, sertraline, fluoxetine, citalopram, lansoprazole, gentamicin, metronidazole, teicoplanin, naproxen, co-codamol.
2	64	Female	Dexamethasone, meropenem, levetiracetam.

Table 5.1: Hepatocyte donor information.

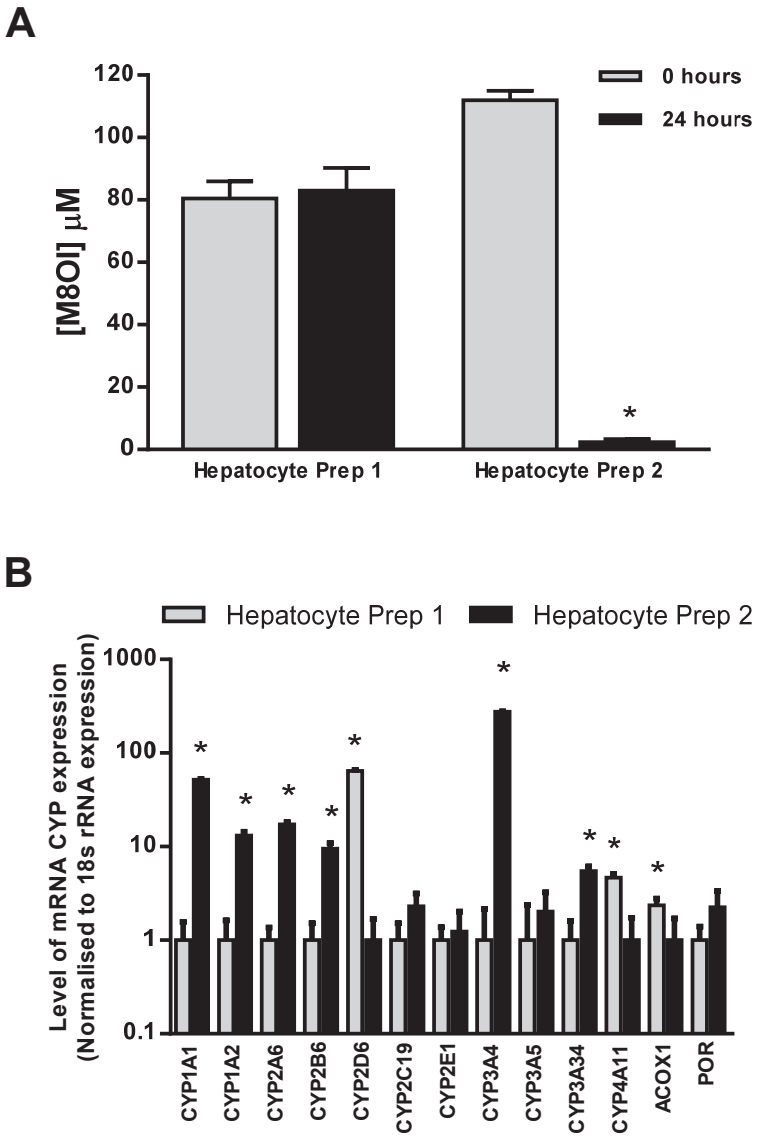

Figure 5.10: Interindividual variation between donor hepatocyte cultures. A, Primary human hepatocytes were incubated with 100µM of M8OI in STIM buffer for 24 hours. The samples were treated with phosphoric acid, separated by HPLC and absorbance detected at 212nm. The area under the curve of the peak at 15 minutes was calculated and the concentration of M8OI in the sample was determined from the M8OI standard curve. Data are the mean and SD of 3 separate determinations from the same experiment. * significantly different M8OI concentration to time = 0 hours ($p<0.05$). **B,** Total RNA was extracted from primary human hepatocytes from the two donors and reverse transcribed. The cDNA was used as template for qPCR to measure the expression of the indicated transcripts. Readings were normalised to 18S rRNA expression and fold change expressed relative to the donor with the lowest expression. Bars are the mean and SD of 3 separate determinations of each donor *significantly different expression ($p<0.05$).

As CYP3A4 levels were greater in the M8OI metabolising hepatocytes, protein levels and enzyme activity of CYP3A4 were measured in the two hepatocytes cultures. Firstly, the concentration of p450 present in each donor was determined by duel beam-spectroscopy (chapter 2.11). A peak at 450nm was not detectable, but there was a peak 420nm. It is generally considered that p420 represents the biologically inactive conformations of p450. It was therefore assumed that values for p420 were derived from p450 as hepatocytes were frozen and p450 levels were retrospectively determined likely leading to the transition from p450 to p420. The concentration of p420 was 4.45 times greater in the M8OI metabolising hepatocytes compared to the non-metabolising cells (Figure 5.11A). Western blot analysis showed that CYP3A4 was not detectable in hepatocytes incapable of metabolising M8OI, whereas it was expressed in the metabolising hepatocytes (Figure 5.11B). CYP2E1 and P450 reductase were both expressed at similar levels in both hepatocyte preparations. Finally, CYP3A4 activity was greater in the M8OI metabolising hepatocytes compared to the non-metabolising hepatocytes (Figure 5.11C). CYP2D6 activity was also measured and found to be greater in hepatocytes from donor 2, however the difference was not as great as the difference observed in CYP3A4 activity between the donors. These data compared two different hepatocyte donors with differing M8OI metabolising capabilities and show that CYP3A4 is involved in the metabolism of M8OI. These observations support the data that showed that ketoconazole, a CYP3A4 inhibitor, inhibits M8OI metabolism in culture.

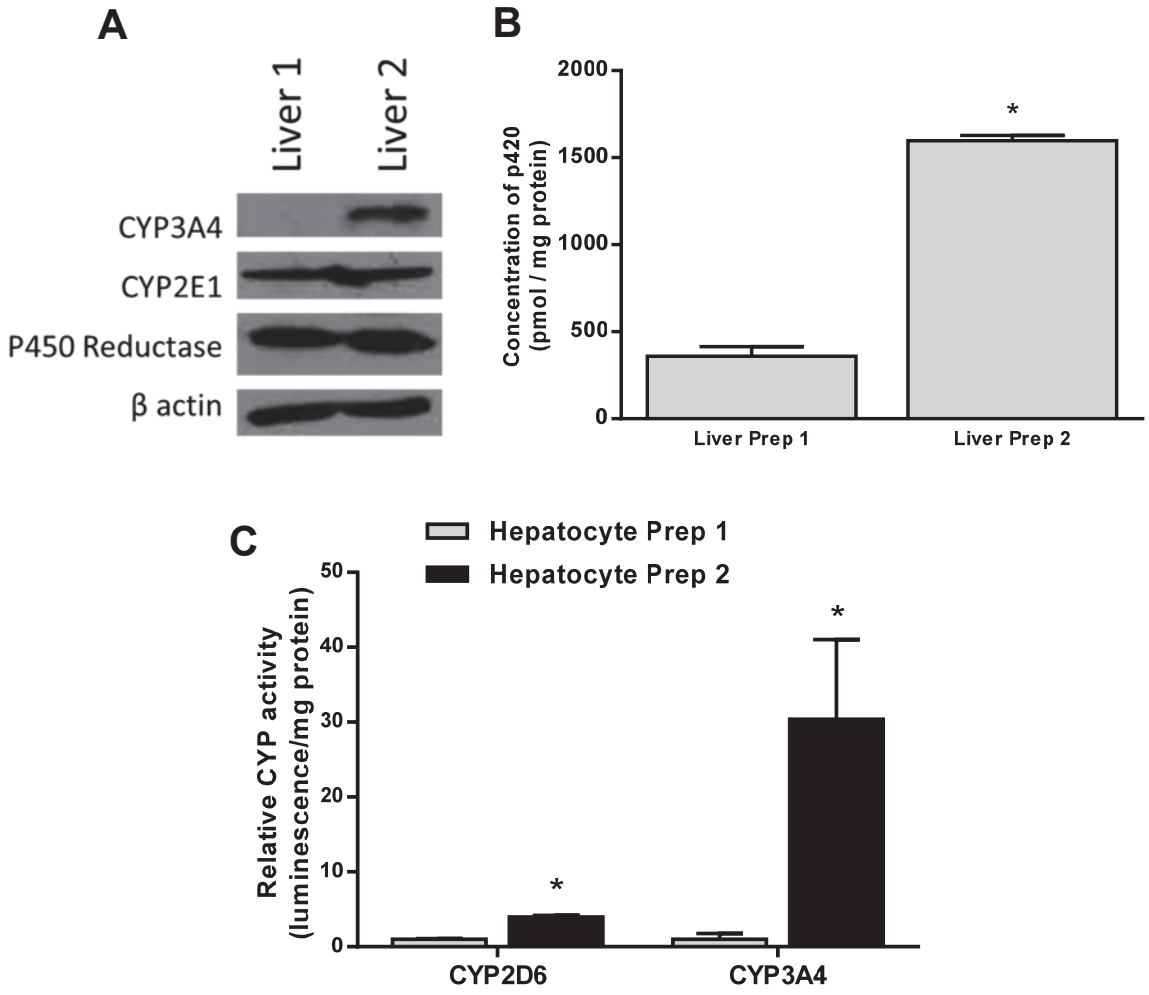

Figure 5.11: CYP3A4 expression and activity is greater in M8OI metabolising hepatocytes. A, Western Blot for the indicated proteins in extracts from indicated hepatocyte donor. Each lane contains 10µg protein/lane. **B,** Total p420 for indicated hepatocyte donors. Data was normalised to protein concentration determined by Lowry protein determination. Data are the mean and SD of 3 separate determinations from the same hepatocyte isolation. * significantly different p420 concentration between hepatocyte isolations ($p<0.05$). **C,** CYP450 enzyme activity was determined using the Promega enzyme assays for indicated CYP450s. Data was normalised to protein concentration determined by Lowry protein determination. Data are the means and SD of 3 separate determinations from the same hepatocyte isolation. * significantly different P450 activity between hepatocyte isolations ($p<0.05$).

5.8 Mass spectroscopy confirms the metabolism of M8OI to COOH7IM

Mass spectroscopy was used to confirm the structure of the metabolites produced and identify any other structures undetectable by the previously used HPLC method. Figure 5.12 and Figure 5.13 show the HPLC-

MS analysis on the medium of hepatocytes treated with M8OI for 4 hours. Mass spectroscopy confirmed the identity of both hypothesised metabolites HO8IM and COOH7IM. Three other metabolites were also identified in low quantities; dehydro-M8OI, M8OI-carbonyl and dihydroxyl-M8OI. The most abundant of these metabolites was COOH7IM followed by HO8IM. Additionally, no phase II metabolites were detected (Dr Michael Dunn, Newcastle University, personal communication).

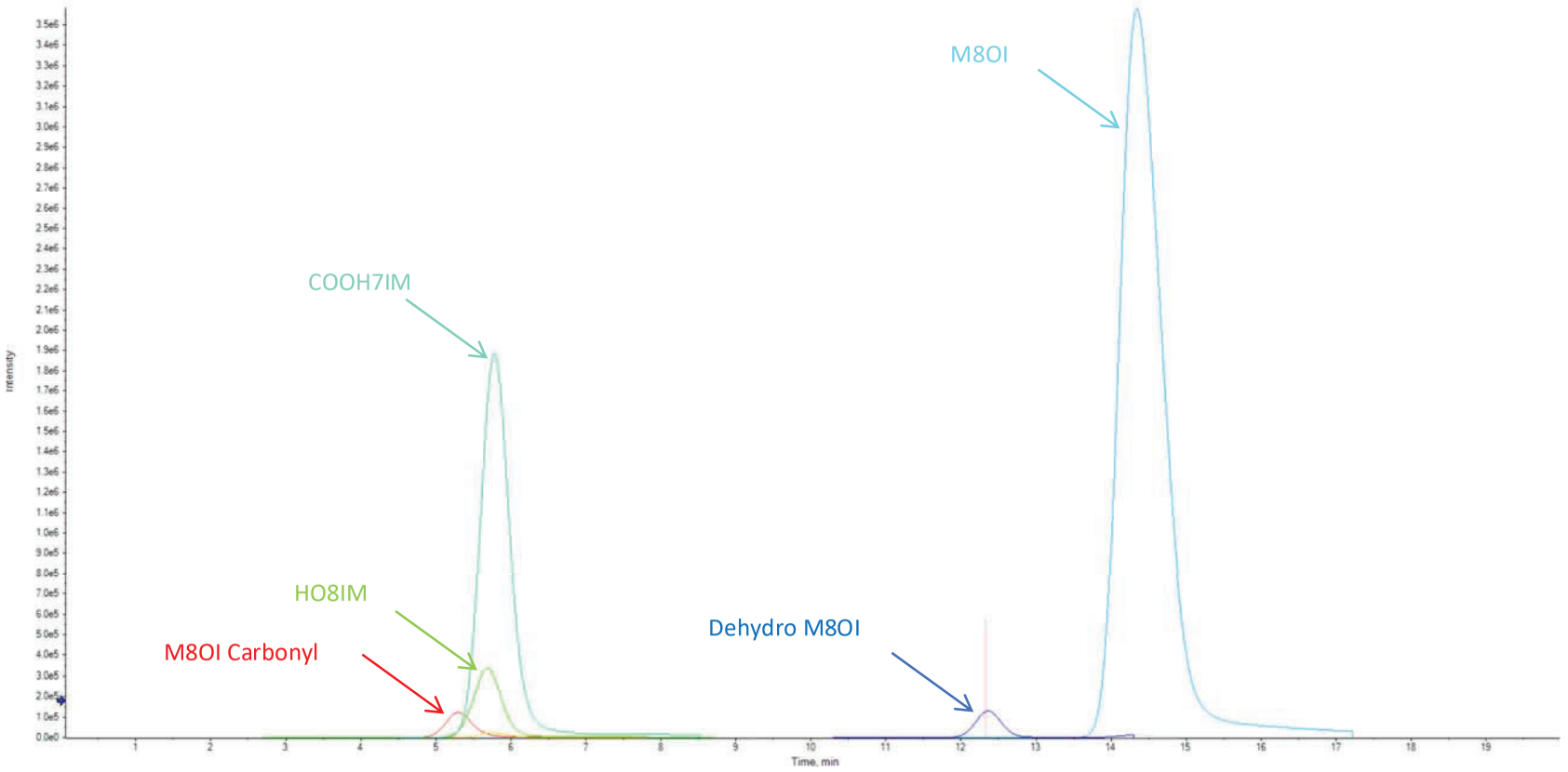

Figure 5.12: HPLC-MS chromatogram of M8OI and metabolites from hepatocyte culture buffer. Primary human hepatocytes were exposure to 100µM of M8OI in STIM buffer for 4 hours. The sample was then treated with phosphoric acid, and analysed using an LC-HR-MS/MS. Data processing for the identification of M8OI and metabolites was performed using MasterView software version 1.1 incorporated within PeakView Software version 2.2 (Sciex). Data provided by Dr Michael Dunn.

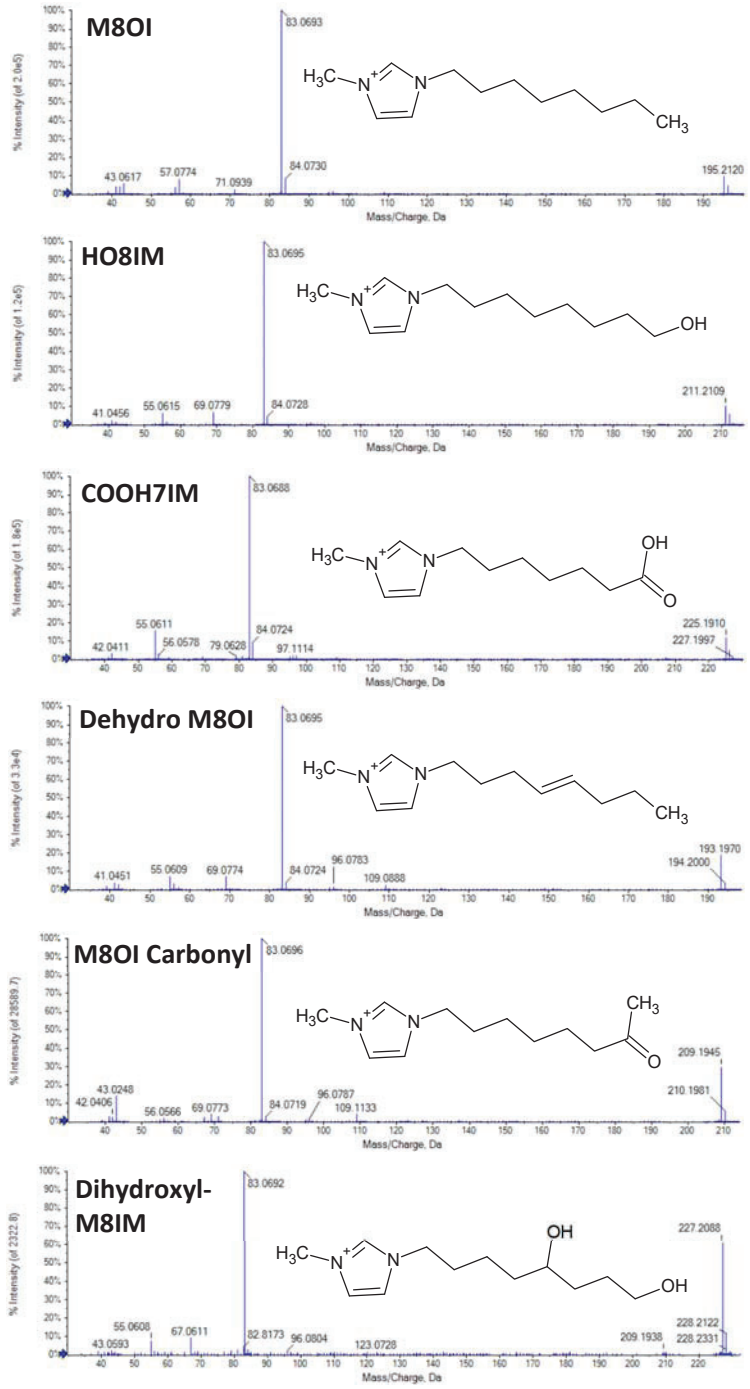

Figure 5.13: Mass spectrum of M8OI and metabolites, including structures. Primary human hepatocytes were exposure to 100µM of M8OI in STIM buffer for 4 hours. The sample was then treated with phosphoric acid, and analysed using an LC-HR-MS/MS. Data processing for the identification of M8OI and metabolites was performed using MasterView software version 1.1 incorporated within PeakView Software version 2.2(Sciex). Structures for each compound were drawn using ChemSketch (ACDLabs). Data provided by Dr Michael Dunn.

5.9 HO8IM, but not M8OI, is efficiently metabolised by mouse hepatocytes

As human hepatocytes metabolise M8OI, other more readily available models were tested for their ability to metabolise the ionic liquid. B-13 and B-13/H cells as well as primary mouse hepatocytes were tested. B-13 and B-13/H cells were not capable of M8OI metabolism. Mouse hepatocytes reduce the concentration of M8OI in the medium by 15%, but this decrease is not statistically significant (Figure 5.14A). These models were also tested for their ability to metabolise HO8IM. B-13 cells were shown to not reduce the concentration of HO8IM in the medium over 8 hours (Figure 5.14B). B-13/H cells reduced 14.5% of HO8IM in the medium and mouse hepatocytes reduced the concentration by 76.4%. The tested models were therefore not efficient at metabolising M8OI, with the exception of mouse hepatocytes that rapidly metabolised HO8IM suggesting that the primary cells express some metabolising enzymes that the immortalised cell lines tested do not.

5.10 M8OI induces CYP1A1 and CYP2A6 expression.

To investigate if M8OI activates CYP inducing receptors, M8OI was incubated with primary human hepatocytes for 24 hours and the relative level of CYP450 mRNA expression was measured by real-time PCR. Hepatocytes were treated with M8OI at 20 and 100µM M8OI as well as a positive control for each receptor; the PXR (rifampicin, CYP3A), AhR (βNF, CYP1A) and CAR (PB, CYP2). Two of the P450 enzymes tested, CYP1A1 and CYP2A6 showed a 7.8-fold and 10.9-fold increase in mRNA expression when exposure to 100µM of M8OI (Figure 5.15A). There was no increase in the expression of CYP1A2, CYP2B6 or any of the CYP3A family. The majority of enzymes were induced by the known receptor inducers. Rifampicin induced CYP3A4 and CYP3A34, however did not seem to induce CYP3A5. βNF induced CYP1A1, CYP1A2 and CYP2A6 to highly significant levels. It was not possible to determine whether M8OI activated the CAR and induced an increase in CYP2B6 as PB, a CAR activator, did not induced CYP2B6 expression.

CYP1A1 is regulated by the LXR that is activated by βNF, T0901317 and GW3965. M8OI increased CYP1A1 expression in human hepatocytes, therefore LXR activation was determined by transfecting the LXR responsive reporter gene construct (TK-LXRE-LUC) into HepG2 cells. 24 hours of M8OI exposure demonstrated an increase in LXR activation in a dose dependent manner (Figure 5.15B). 10µM T091517 induced a greater response than GW3965 as seen in chapter 3, as well as the concentrations of M8OI implemented. M8OI has therefore been shown to activate the LXR *in vitro*.

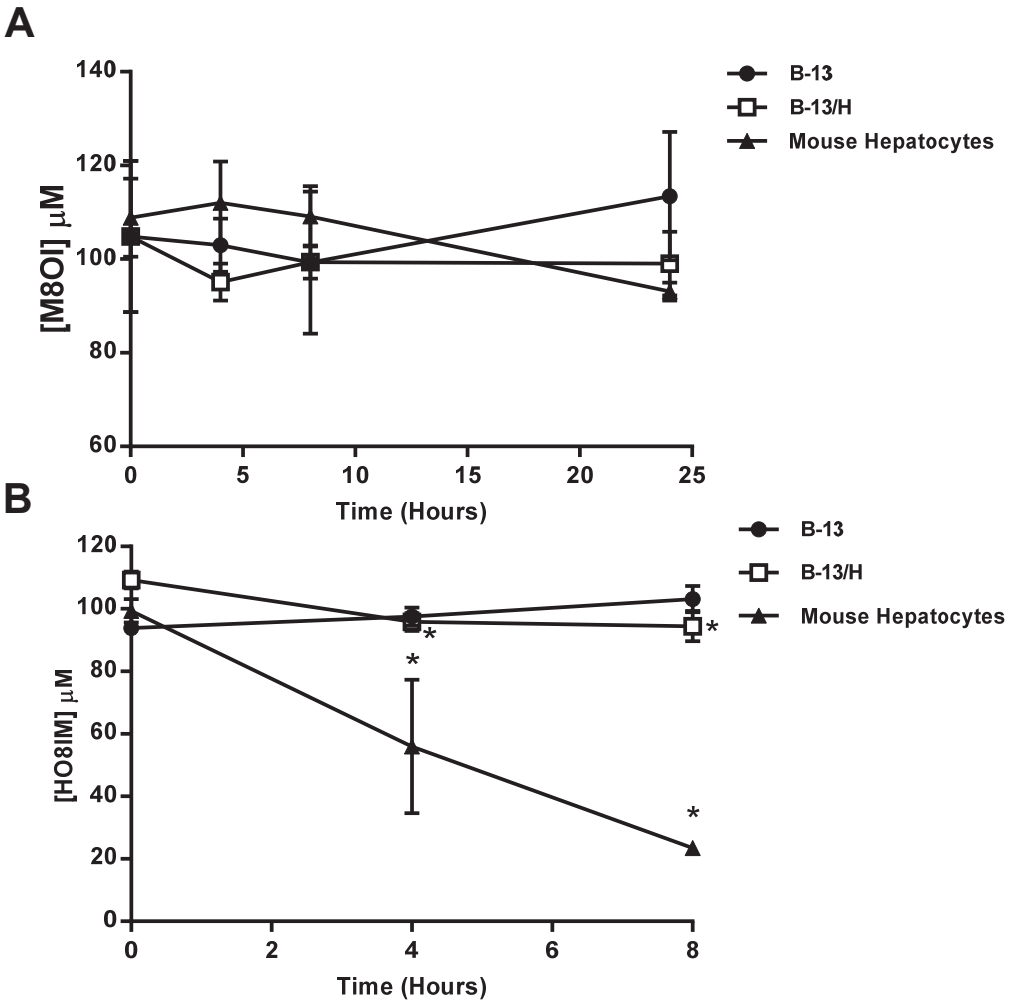

Figure 5.14: Primary mouse hepatocytes efficiently metabolise HO8IM but not M8OI. A, indicated cells were incubated with 100µM of M8OI in STIM buffer for 24 hours. 200-500µl of STIM buffer was then taken from the culture at 0, 4, 8 and 24 hours. The samples were treated with phosphoric acid, separated by HPLC and absorbance detected at 212nm. The area under the curve of the peak at 15 minutes was calculated and the concentration of M8OI in the sample was determined from the M8OI standard curve. Data are the mean and SD of 3 separate determinations from the same experiment. Typical of 2 separate experiments tested by ANOVA followed by Bonferroni post-hoc test. **B,** indicated cells were incubated with 100µM of HO8IM in STIM buffer for 24 hours. 200-500µl of STIM buffer was then taken from the culture at 0, 4, 8 hours. The samples were treated with phosphoric acid, separated by HPLC and absorbance detected at 212nm. The area under the curve of the peak at 2.9 minutes was calculated and the concentration of M8OI in the sample was determined from the HO8IM standard curve. Data are the mean and SD of 3 separate determinations from the same experiment. Typical of 2 separate experiments. * significantly different HO8IM concentration to time = 0 hours ($p<0.05$) tested by ANOVA followed by Bonferroni post-hoc test.

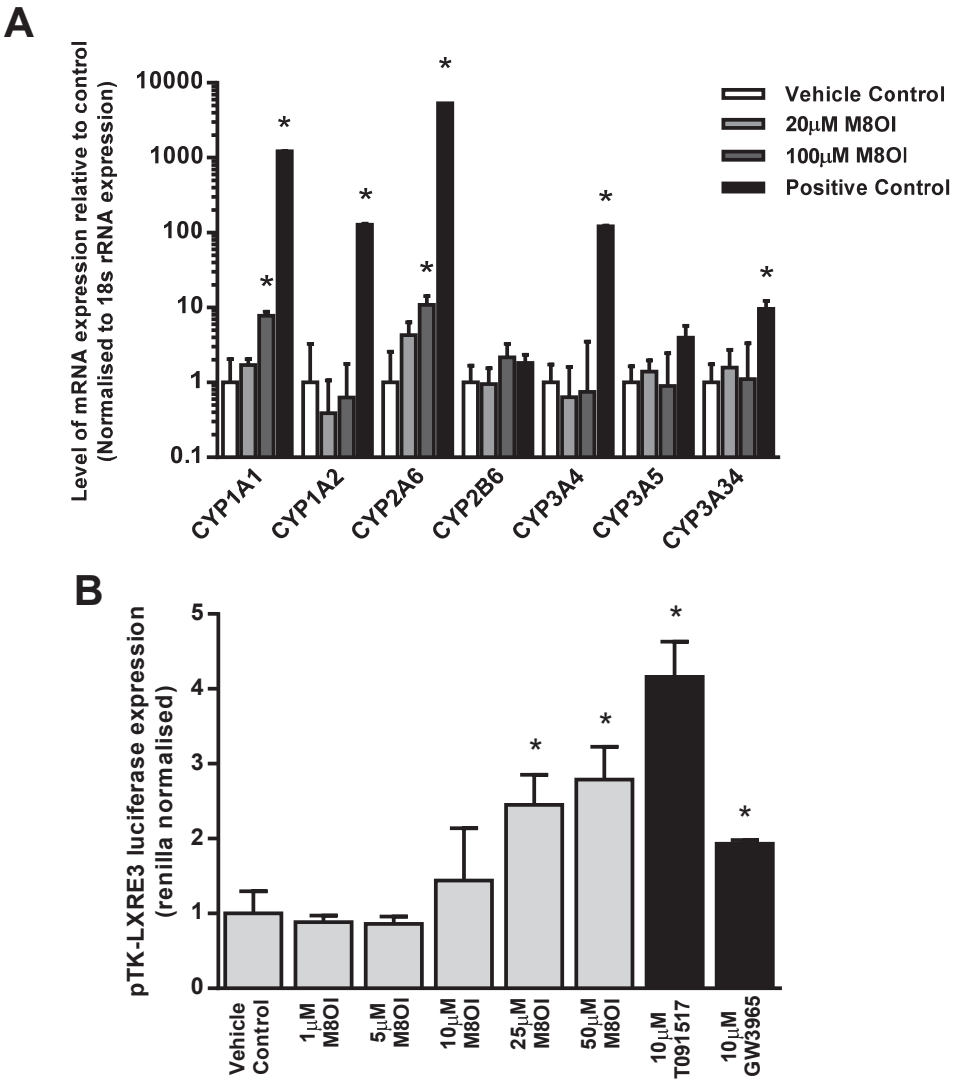

Figure 5.15: M8OI activates the human LXR. A, Primary human hepatocytes (Donor 1, see Table 5.1) were incubated with indicated chemicals for 24 hours. Positive control includes: CYP1 = 20μM βNF; CYP2 = 1mM phenobarbital; CYP3 = 20 μM rifampicin. Total RNA was extracted from primary human hepatocytes following treatment. The cDNA was used as template for qPCR to measure the expression of the indicated transcripts. Readings were normalised to 18S rRNA expression and fold change expressed relative to vehicle control treated cells. Bars are the mean and SD of 3 separate determinations from the same experiment *significantly different expression ($p<0.05$). **B,** HepG2 cells were transfected with pTK-LXRE3 luciferase and RL-TK constructs for 48 hours, cells were then treated with indicated compounds for 24 hours. Following treatment luciferase and renilla activities were determined. Data are the mean and SD of 3 separate determinations from the same experiment, typical of 3 experiments. * significantly different versus control ($p<0.05$).

5.11 M8OI and metabolites are detectable in murine serum after 45 days, oral exposure.

Transgenic NK-κB-luc female mice of at least 52 weeks of age were administered a daily dose of 1mg/kg body weight M8OI via their drinking water for 45 days as in chapter 4.17 (from the same mice). Serum from control mice and those treated with 1mg/kg body weight in the drinking water was collected following termination and analysed by HPLC-MS. Figure 5.16 shows that mice administered with M8OI via the drinking water contain M8OI, HO8IM and COOH7IM in the serum. M8OI retention time was at 9.4 minutes, HO8IM at 5.2 minutes and COOH7IM at 5.5 minutes. The intensity was HO8IM was the lowest of the 3 chemicals and COOH7IM was the most abundant, suggesting that M8OI was metabolised to HO8IM and rapidly converted to COOH7IM and that this is more likely to reach systemic circulation.

5.12 M8OI and metabolites are renally and biliary excreted after oral exposure.

Female C56B6 mice were administered with M8OI at concentrations ranging from 0-40mg/kg body weight by oral gavage, twice over 24 hours. Following treatment, mice were terminated, and serum, urine and bile were collected and analysed by HPLC-MS. The concentration of M8OI in the serum, bile and urine increased as the concentration of administered dose increased (Figure 5.17A). At 40mg/kg body weight, M8OI levels were low (180nM) in the serum, compared to in the bile and urine (4459nM and 8736nM respectively, Figure 5.17A) suggesting that little of M8OI that was not metabolised reaches systemic circulation and was excreted via the urine or bile. The concentration of HO8IM was greater at all time points and concentrations compared to M8OI (Figure 5.17B). As observed with M8OI, levels of HO8IM were lowest in the serum. The concentration in the bile increased as the concentration of M8OI dosed increased. The greatest increase was in the urine. Mice treated with 5mg/kg body weight M8OI had concentration of 8736nM in the urine, and this only slightly increased at 20mg/kg bodyweight and fell at 40mg/kg body weight. The concentration of COOH7IM in the serum and bile was relatively the same at approximately 2500nM (Figure 5.17C). The majority of COOH7IM was found in the urine, and as with HO8IM, there was a larger increase in COOH7IM at 5mg/kg bodyweight compared to M8OI and the concentration slightly increased as the dosing concentration increased.

These data support the metabolism of M8OI to HO8IM and to COOH7IM and indicate how these chemicals are excreted. The presence of M8OI in the serum is negligible and it is excreted via the bile and urine. There was more HO8IM and COOH7IM present in the serum but still at lower levels than elsewhere. However, this was only determined at termination and therefore the amount metabolised and excreted

before termination is unknown. HO8IM was excreted in both the urine and the bile whereas COOH7IM was predominantly excreted in the urine with not much in the bile. The concentration of HO8IM and COOH7IM in the urine did not increase linearly with the dosed concentration one possible reason for this is that there may be a limiting step possibly during metabolism or transport.

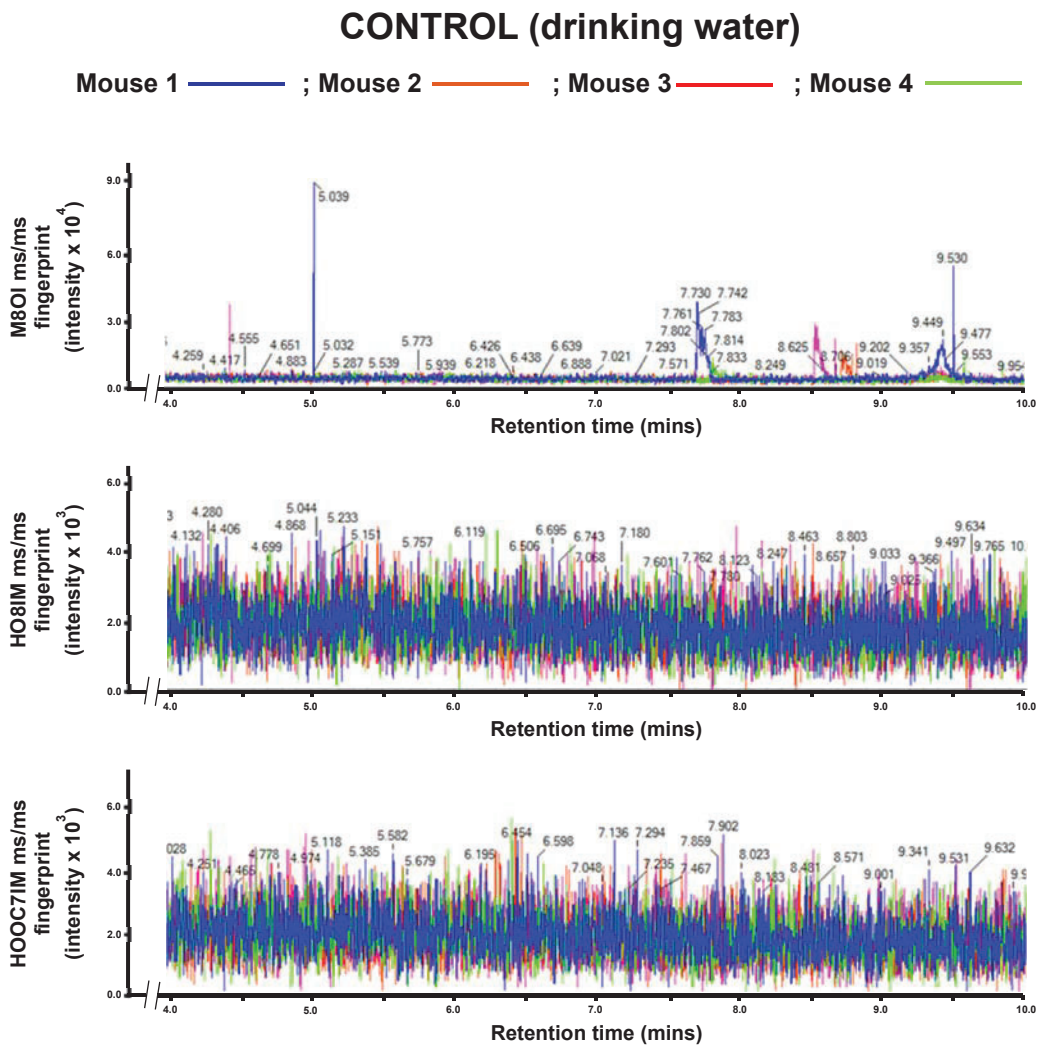

Figure 5.16: M8OI, HO8IM and COOH7IM are detectable in the serum of mice exposed to M8OI for 45 days via their drinking water. (Legend on next page)

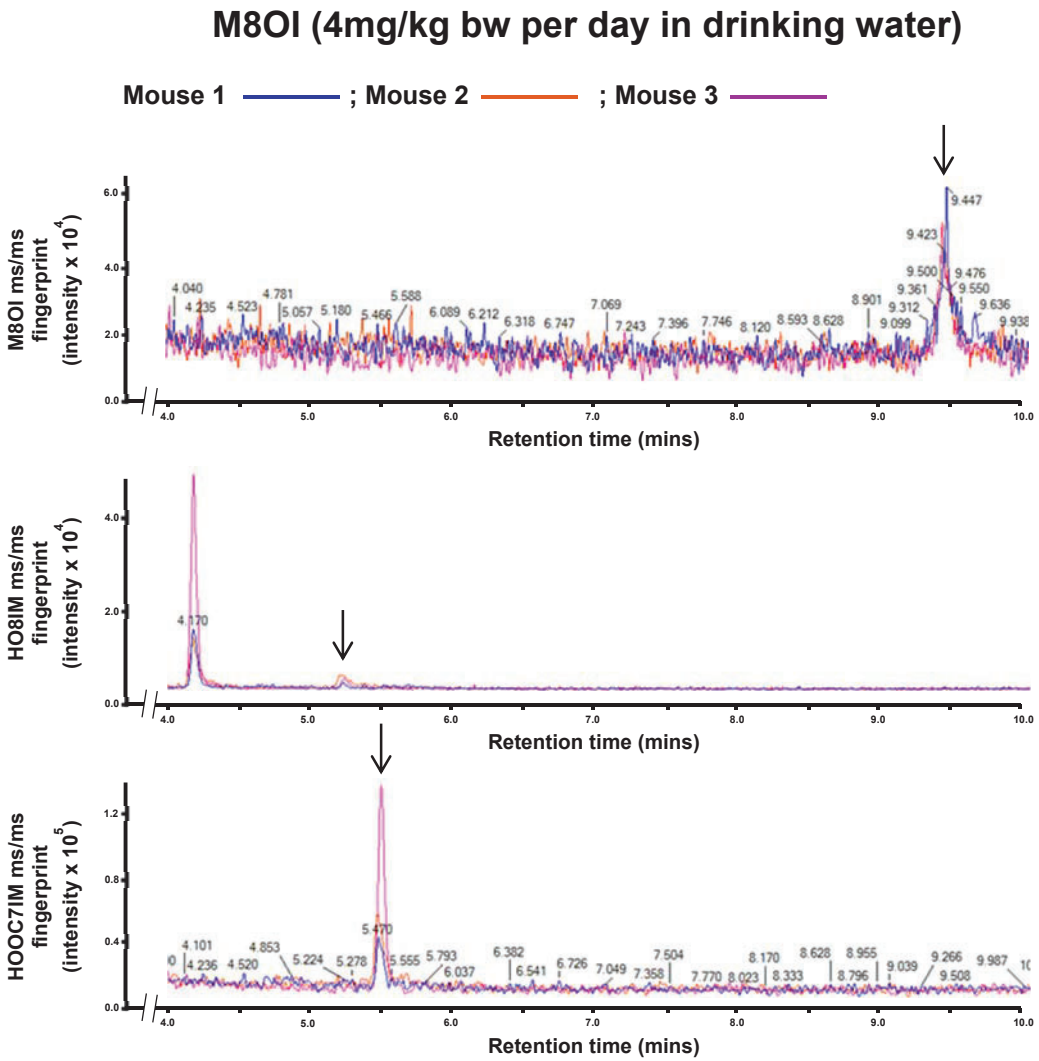

Figure 5.16: M8OI, HO8IM and COOH7IM are detectable in the serum of mice exposed to M8OI for 45 days via their drinking water. Transgenic NK-κB-luc mice were administered a daily dose of 1mg/kg body weight M8OI via their drinking water. On day 27 mice were administered 50mg/kg body weight ANIT (or olive oil vehicle control) by oral gavage. On day 45 mice were terminated by cervical dislocation and the tissue and the serum were collected. Serum samples were then sent for mass spectroscopy to identify the presence of M8OI and its metabolites within the serum. Data provided by Dr Michael Dunn.

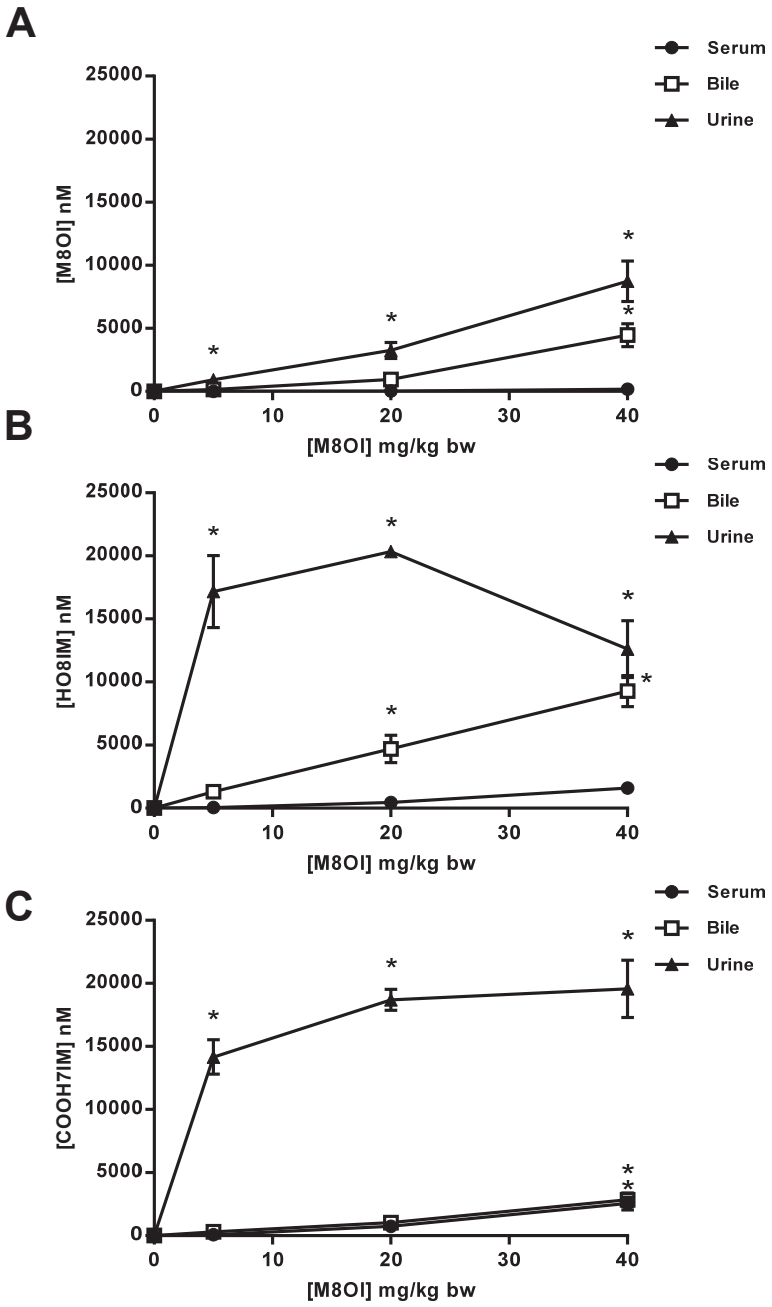

Figure 5.17: HO8IM accumulates in the urine and bile, COO7HIM accumulates in the urine. C57B6 mice were administered with indicated doses of M8OI by oral gavage twice in 24 hours. After 24 hours animals were terminated by cervical dislocation and serum, bile and urine were collected. Samples were sent for mass spectroscopy to quantify the presence of **A,** M8OI; **B,** HO8IM; **C,** COOH7IM in the serum, bile and urine. Data are the mean and SD of a minimum of 4 separate mice. * significantly different versus time = 0 ($p<0.05$) tested by ANOVA followed by Bonferroni post-hoc test.

5.13 Chapter discussion

The metabolism of M8OI in humans is currently not known. Therefore, the potential metabolites of M8OI could be more toxic or just as toxic as the parent compound. This is also of importance as this chemical has been discovered in the environment therefore the exposure to humans is feasible. Additionally, one of the hypothesised metabolites, COOH7IM, has a structural similarity to lipoic acid and has been shown to incorporate into PDC-E2 (Probert *et al.*, 2018). This response has been suggested as a possible trigger for the development of PBC in susceptible individuals.

Thus, M8OI metabolism was investigated in multiple cell lines, primary cells and in *in vivo* models. The data presented in this chapter showed that M8OI is efficiently metabolised by human hepatocytes and metabolised by mice *in vivo* and *in vitro*. M8OI was hypothesised to be metabolised to an intermediate metabolite of HO8IM by mono-oxygenation possibly by CYP450s and further metabolised to COOH7IM by alcohol dehydrogenase and aldehyde dehydrogenase. HPLC and mass spec data proved that M8OI was metabolised to these products with COOH7IM being the major metabolite suggesting HO8IM is rapidly metabolised. Other metabolites were detected and likely occur through M8OI metabolism via different pathways, but none were as abundant as COOH7IM or HO8IM.

The two main metabolites, HO8IM and COOH7IM, were tested for their toxicity to liver cells. COOH7IM was shown to be non-toxic in all cells lines tested. However, HO8IM was toxic to all immortalised cell lines utilised with B-13 cells being the most susceptible to HO8IM induced toxicity. Seahorse mito stress test data suggested that HO8IM toxicity does not act via the same mechanism as M8OI at the concentrations tested. The mechanism of HO8IM induced toxicity should be further investigated.

The metabolism of M8OI to HO8IM was shown to be predominantly carried out by CYP3A4, evidenced by the data from the inhibition studies and interindividual differences between donors of primary human hepatocytes. Inhibition studies showed that ketoconazole inhibited M8OI depletion and COOH7IM production. Ketoconazole incubation did not have any effects on cell viability, it was therefore assumed that the observed effects were due to inhibition of metabolism. Ketoconazole is a well-known CYP3A4 inhibitor and therefore it was concluded that the oxidation of M8OI to HO8IM involves CYP3A4 activity. The other compounds that had an effect on M8OI depletion were SKF525a and metyrapone. SKF525a (proadifen) is a non-specific CYP450 inhibitor (Ono *et al.*, 1996; Franklin and Hathaway, 2008), confirming the role of CYP450 in the mono-oxygenation of M8OI. SKF525a and its metabolites primarily inhibit CYP2D6, CYP2C19 and CYP3A, the enzymes responsible for the majority of drug metabolism (Ono *et al.*,

1996; Franklin and Hathaway, 2008). Metyrapone is a steroid 11β-hydroxylase inhibitor (CYP11B1) used clinically to test for pituitary function and used to treat Cushing's Syndrome (Wright *et al.*, 1994; Daniel *et al.*, 2015). It is a non-specific CYP inhibitor that has been shown to bind to the active site of CYP3A4 (Williams *et al.*, 2004). Therefore, the reduction of M8OI metabolism could be due to CYP3A4 inhibition however the inhibition of other CYP450s could contribute.

The comparison of two sperate donors of hepatocytes revealed a interindividual variation in the metabolism of M8OI. One hepatocyte culture metabolised M8OI to near completion whereas another did not metabolise M8OI sufficiently enough to be detected by HPLC analysis. One major difference between the two isolations was the level of CYP3A4, the mRNA and protein of which was expressed more highly in the M8OI metabolising hepatocytes. CYP3A4 protein was not detectible by Western blot analysis in the M8OI non-metabolising hepatocytes. This supports the role of CYP3A4 in the metabolism of M8OI. While CYP3A4 levels are likely to be a major contributor to the difference observed between the two hepatocyte cultures, other factors could be involved. One of these factors is that P450 levels were greater in the metabolising hepatocytes, therefore they could have a greater metabolising capability. Additionally, donor information showed that the donor of the M8OI non-metabolising hepatocytes was on many different drugs, including those known to be metabolised by CYP3A4 such as citalopram. The cocktail of these drugs would likely affect the efficiency of drug metabolising enzymes. The donor of the M8OI metabolising hepatocytes was on dexamethasone, a drug that has been shown to increase CYP3A4 expression through the PXR (Pascussi *et al.*, 2000) and would therefore induce the metabolism of M8OI to HO8IM.

Primary mouse hepatocytes and B-13/H cells (rat derived cells) displayed minimum depletion of M8OI over 24 hours. This suggests that these B-13/H cells and mouse hepatocytes in culture lack the metabolising enzymes for M8OI and are therefore not a suitable model for M8OI metabolism. Data using human hepatocytes suggest a role of CYP3A4 in M8OI metabolism, a CYP450 that rats and mice lack (van Herwaarden *et al.*, 2007). CYP3A11 in mouse could be further investigated as it is considered the most homologous to human CYP3A4 (Hasegawa *et al.*, 2011). As mouse hepatocytes and B-13/H cells have limited M8OI metabolising capabilities, they could be used as a model for the mechanism of M8OI induced hepatotoxicity without the interference of metabolism. HO8IM was efficiently metabolised by mouse hepatocytes but not by B-13/H cells. While the pathway of HO8IM metabolism to COOH7IM is yet to be studied, the pathway that has been hypothesised involves alcohol dehydrogenase and aldehyde dehydrogenase as these enzymes metabolise alcohols to aldehydes and carboxylic acids respectively. As seen in chapter 3, B-13/H cells do not express active, ethanol metabolising, alcohol dehydrogenases and

if the hypothesised HO8IM metabolism pathway is true then this lack of activity would explain why B-13/H cells were not able to metabolise HO8IM.

Further confirmation of CYP3A4 involvement and studies into the metabolism of HO8IM still need to be carried out. CYP3A4 induction in human hepatocytes using rifampicin (Rae *et al.*, 2001) could be used to increase CYP3A enzyme levels and therefore induce a more rapid decrease in M8OI concentration in culture. Alternatively, HepaRG cells could be utilised as they express functional CYP3A4 as well as other CYP450s. HO8IM metabolism could be studied by the inhibition of alcohol dehydrogenase by pyrazole in mouse or human hepatocytes (Li and Theorell, 1969). HepaRG cells could also be utilised as alcohol dehydrogenases have been shown to be expressed at protein level, however activity has not been shown (Attignon *et al.*, 2017). HO8IM could be incubated in a mixture containing human or mouse hepatocytes as previously shown using ethanol in chapter 3 and the method described in chapter 2.10.1 (Clemens *et al.*, 1995) and the solution analysed by mass spectroscopy to detect any production of COOH7IM.

M8OI was shown to be metabolised in vitro, additional studies *in vivo* provided an insight into the metabolism (supporting the *in vitro* data) and excretion of M8OI, however, serum, bile and urine were only collected upon termination. This limitation could be overcome using metabowls to collect all waste and more accurately determine M8OI metabolism and excretion. Mice orally administered with M8OI showed that the parent compound and both hypothesised metabolites were detected in the serum. When comparing the concentrations in serum, bile and urine, levels of M8OI were lowest in serum, and were detectable in the bile and urine. The greater concentration of M8OI in the bile is relevant PBC as it has previously been shown that M8OI induces apoptosis (Probert *et al.*, 2018), therefore apoptosis could be induced by M8OI in cholangiocytes leading to the destruction of the bile duct. HO8IM was also detectable in serum, bile and urine at higher concentrations than M8OI. The concentration of HO8IM reaches a maximum concentration at 5mg/kg body weight, and concentrations do not increase despite increasing the administered dose. This could be due to a limitation in the transport of HO8IM or that the majority is excreted via other routes. The accumulation in the bile could also lead to the degradation of the bile duct as HO8IM has been shown to be toxic to H69 cells and B-13 cells, yet the mechanism of cell death is unknown and studies in primary human cholangiocytes should be carried out to assess the toxicity of HO8IM as well as M8OI. COOH7IM was primarily found in the urine, but it was also detectable in the bile and serum. COOH7IM does not appear to be toxic so would not contribute to any cholangiocytes damage yet the presence in the bile and serum means that COOH7IM could potentially bind to PDC-E2 in place of lipoic acid, modifying it and inducing the breakdown of tolerance. As COOH7IM can be detected in the

urine, this could be used to go back to the area in the Northeast of England where M8OI was found in the landfill sites and test individuals living near these sites for the presence of COOH7IM in their urine. This would provide more insight into the potential exposure to M8OI, using a non-invasive method.

Given that human hepatocytes have been shown to be capable of metabolising M8OI and mouse modelling of the oral exposure of M8OI suggest some degree of metabolism in vivo, it could be suggested that M8OI would be readily metabolised by humans. Further studies in whole liver (connected to the perfusion system, section 2.3.4) could determine the M8OI metabolising capabilities of a whole liver and indicate whether M8OI and its metabolites are excreted in the bile as observed in the mouse model.

Finally, Realtime PCR analysis showed that M8OI induced CYP1A1 and CYP1A2 in human hepatocytes. This suggests the role of the LXR as the CYP1A family is regulated by this nuclear receptor (Beischlag *et al.*, 2008). This was supported by the LXR reporter assay in HepG2 cells, which showed that M8OI did activate the LXR. Additionally, the upregulation of CYP1A1 by M8OI in mouse mammary carcinoma cells has been reported (Li *et al.*, 2013). However, the AhR is also responsible for CYP1A1 regulation and therefore should also be investigated.

The data in this chapter show that M8OI is metabolised by the hypothesised pathway to HO8IM and to COOH7IM and that metabolism detoxifies the compound. It has also been shown that the oxidation of M8OI is primarily carried out by CYP3A4. The bioavailability of M8OI appears to be low with low levels of M8OI being detected in the serum this is supported by the ACD/Percepta data predicting a bioavailability in mammals of 2.02% at a 10mg dose. There are other routes of exposure to be investigated, one of these is through skin absorption, pilot data for which suggests that M8OI is readily absorbed through the skin (data not shown). Presence of M8OI and its metabolites in the bile could be a potential risk for individuals that have a genetic predisposition for PBC and live in close proximity of sites where M8OI has been found, such as the landfill site in the northeast of England (Probert *et al.*, 2018).

Chapter 6. M8OI is an activator of estrogen receptors

6.1 Introduction

Many chemicals in products used as food and cosmetics, as well as man-made chemicals released into the environment such as pesticides have been shown to be endocrine disrupting chemicals (Diamanti-Kandarakis *et al.*, 2009; Zoeller *et al.*, 2012). This results in numerous adverse effects in man and wildlife such as reproductive, neuroendocrinological, behavioural and metabolic effects (Alonso-Magdalena *et al.*, 2011; Mattison *et al.*, 2014). Xenoestrogens are endocrine disrupting chemicals that affect endogenous estrogen signalling via the estrogen receptor (ER), biosynthesis, metabolism and for transport (Shanle and Xu, 2011).

One hormonal target of estrogens is the liver where they play a role in the modulation of circulating levels of estrogens via their conversion to inactive products. They are also involved in insulin sensitivity and lipid homeostasis (Mauvais-Jarvis *et al.*, 2013). The main hormonal target in the liver is the estrogen receptor α (ERα). ERα is a nuclear receptor and one of two ER genes present in the human genome (the other being ERβ). The classical signalling pathway of the ER begins with ligand activation that form ER homo- or heterodimers (Cowley *et al.*, 1997). These ER dimers interact with specific DNA sequences (EREs, estrogen response elements). Following ER binding, co-activators and regulators are recruited and regulate changes in gene expression (Tsai and O'Malley, 1994; Hammes and Levin, 2007).

High levels of estrogens induce toxic effects in the liver through the disruption of bile flow and/or the alteration of the bile constituents (cholestasis) resulting in an accumulation of bile acids that induce necrosis and apoptosis (Woolbright and Jaeschke, 2012). It has been shown that estrogen activation of ERα transcriptionally repress bile acid and drug transporters (Yamamoto *et al.*, 2006), supporting a role for ERα in cholestasis.

Elevated estrogen levels and/or presence of xenoestrogens could be involved in the pathogenesis of PBC and indicate why there is a female bias. It has previously been shown that ERα is expressed in hepatocytes whereas ERα and ERβ are expressed in cholangiocytes and that expression of these receptors is upregulated in diseased states (Alvaro *et al.*, 2006). It has been suggested that estrogens modulate the proliferative response of cholangiocytes to damage via the expression of growth factors and cytokines (Alvaro *et al.*, 2004; Alvaro *et al.*, 2006). Estrogens have been shown to be cholestatic and induce periportal injury and inflammation (Axon *et al.*, 2012; Meyer *et al.*, 2017a). Therefore, it has been proposed that xenoestrogens could induce similar cholestatic effects.

Recently it was discovered that ethanol extracts from the environment around a landfill site contained higher levels of xenoestrogens (Meyer *et al.*, 2017a). Samples taken from the landfill site activated the murine and human ERα whereas the control site samples did not. This response was inhibited by the ER inhibitor ICI182780. Mice have two variants of ERβ (ERβv1 and ERβv2). It was shown that the samples from the landfill site activated both of these receptors. ICI182780 inhibited ERβv1, however it did not inhibit xenoestrogen activation of ERβv2, whereas E2 activation was inhibited suggesting the xenoestrogens present in the landfill site were "super activators" (Meyer *et al.*, 2017a). The landfill site where these "super-activating" xenoestrogens were found was the same site as where M8OI was identified (Probert *et al.*, 2018).

As M8OI was identified in these samples it was hypothesised that the xenoestrogenic activity in the samples from the landfill site was due to the presence of M8OI. To test this hypothesis, established ER reporter gene assays for murine ERα, ERβv1 and ERβv2 as well as human ERα were used to see if M8OI activated these receptors. A reporter gene assay was also developed for the activation of human ERβ. Evidence of M8OI inducing ER activation would mean that M8OI may have the potential to induce apoptosis, activate the ER and become metabolised to a compound capable of incorporating into PDC-E2. This trinity of effects could suggest M8OI as a potential trigger for PBC as all three effects are seen individually as potential triggers or are involved in the pathogenesis of the disease.

6.2 M8OI is toxic to LTPA and 603B cells.

Cells lines that were to be used for ER activation reporter assays were first tested for their viability in response to M8OI exposure to determine what concentrations of M8OI should be used for the receptor activation studies. For murine ER activation, 603B cells were used as these are biliary epithelial cells and therefore more relevant to the study of estrogenic response and PBC. However, 603B cells were resistant to ERα expression (Meyer *et al.*, 2017a). For ERα transfections LTPA cells were used. LTPA cells are a mouse ductal pancreatic cell line, while not a biliary cell line themselves, biliary and pancreatic ducts are physiologically linked (Probert *et al.*, 2015). Cell viability studies showed that LTPA cells were not as susceptible to M8OI induced toxicity as previously observed in other cell lines such as B-13 cells (Figure 6.1). A decrease in cell viability occurred at 10μM and 100μM after 24 hours however these data were not statistically significant. 603B cells were less resistant to M8OI induced toxicity with a significant decrease in cell viability occurring at 1-100μM, with exception of 0.1μM. Cell viability in 603B cells was similar to H69 cells (human biliary epithelial cells, chapter 4.2) and was reduced to 49.9% at 100μM after 24 hours.

These data show that, M8OI induces toxicity in LTPA and 603B cells, similarly to the effects observed in other cells studied in previous chapters and is likely to occur via the same mechanism of interfering with the cell's mitochondria.

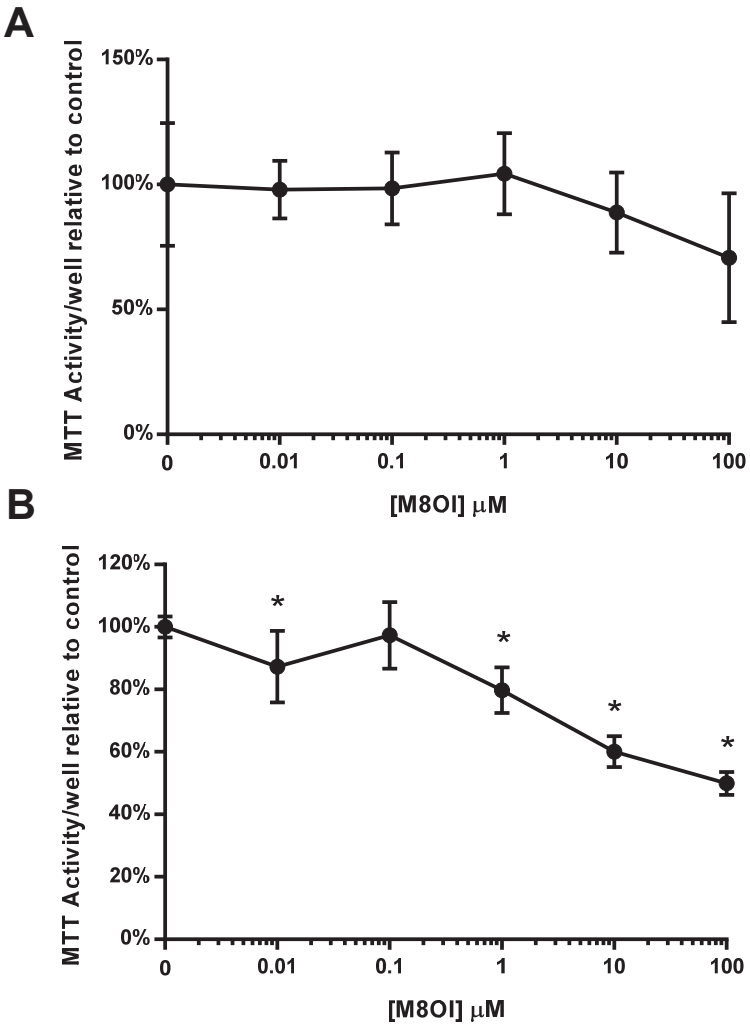

Figure 6.1: M8OI reduces MTT activity in LTPA and 603B cells. LTPA **(A)** and 603B cells **(B)** were treated for 24 hours with indicated concentrations of M8OI. Following treatment, cells were incubated with MTT for 2 hours and reduction determined. Data are the mean and SD of 6 separate determinations from the same experiment, typical of 3 separate experiments.
* significantly different MTT activity to control ($p<0.05$) tested by ANOVA followed by Bonferroni post-hoc test.

6.3 M8OI activate the murine ERα

The ability of M8OI to activate the murine ERα (mERα) was tested using an established reporter gene assay in which LTPA cells were transiently transfected with mERα and the reporter gene construct 3XERE TATA

Luc that is transactivated in cells expressing mERα (Meyer *et al.*, 2017a). Cells were transfected for 24 hours before being treated with M8OI, 17β oestradiol (E2) or ethinyloestradiol (EE) for a further 24 hours in the presence or absence of the ER inhibitor ICI182780 (Wardell *et al.*, 2011). M8OI activated the mERα at the concentrations implemented, and this activation was inhibited by ICI182780 (Figure 6.2A). The two estrogenic controls, 10nM E2 and 10nM EE, both activated the mERα at levels previously demonstrated using this reporter assay (Meyer *et al.*, 2017a). ICI182780 significantly reduced luciferase gene expression in the vehicle control treated cells. This effect was also observed in a previous study (Meyer *et al.*, 2017a) and suggests that mERα expression in LTPA cells transactivated the reporter gene constitutively, likely to be caused by estrogens present in the cell media such as phenol red (Berthois *et al.*, 1986). The two major metabolites of M8OI, HO8IM and COOH7IM, were also tested for their mERα activity (Figure 6.2B). The results showed that neither metabolite activated the mERα at the same concentrations tested for M8OI suggesting that M8OI metabolism reduces the xenoestrogenic activity.

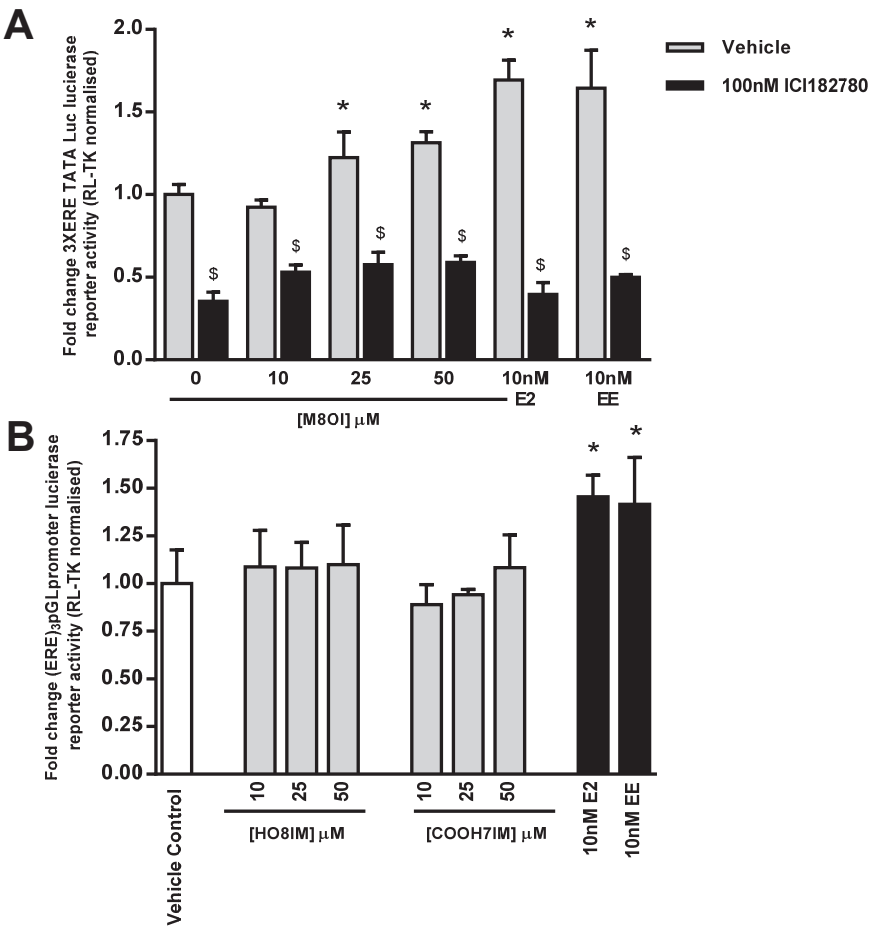

Figure 6.2: M8OI, but not it's metabolites, is an activator of the mERα. A, LTPA cells were transiently transfected with pcDNA3.1 expression constructs coding for mERα, 3XERE TATA luc and RL-TK control vector (at a ratio of 6:6:1) for 24 hours. Following transfection, cells were pre-treated with 100nM ICI182780 or DMSO vehicle (0.1% v/v) as indicated for 6 hours followed by the treatment of indicated compounds in the continued presence of ICI182780 or vehicle for a further 24 hours. Cells were then washed in PBS, lysed in passive lysis buffer and luciferase and renilla luminescence was determined by the dual luciferase assay. Data are the mean and SD of 3 separate determinations from the same experiment, typical of 3 separate experiments. *Significantly different increase ($p<0.05$) versus 0μM (DMSO vehicle) treated cells using two-way ANOVA followed by Bonferroni post-hoc test. $ Significantly different ($p<0.05$) versus equivalent treatments in the absence of ICI182780 using Student's t-test (two-tailed). **B,** LTPA cells were transiently transfected with pcDNA3.1 expression constructs coding for mERα, 3XERE TATA luc and RL-TK control vector (at a ratio of 6:6:1) for 24 hours. Following transfection, cells were treated with indicated compounds for 24 hours. Cells were then washed in PBS, lysed in passive lysis buffer luciferase and renilla luminescence was determined by the dual luciferase assay. Data are the mean and SD of 3 separate determinations from the same experiment, typical of 3 separate experiments. *Significantly different ($p<0.05$) versus 0μM (DMSO vehicle) treated cells using one-way ANOVA followed by Bonferroni post-hoc test.

6.4 M8OI 'super-activates' the mouse ERβ variant 1 and variant 2

Mice have two variants of ERβ variant 1 (mERβv1) and variant 2 (mERβv2). Both of these have been cloned and when transfected into 603B cells transactivate the $(ERE)_3$-pGL3promoter reporter gene construct (Meyer *et al.*, 2017a). M8OI activated the mERβv1 significantly at 5μM and 10μM (1.96-fold and 2.04-fold respectively) (Figure 6.3A). Reporter activity decreased at higher concentrations. 10nM E2 and EE were more potent activators, inducing approximately a 4-fold increase in reporter activity. This response was inhibited by ICI182780, however the M8OI induced receptor activation was not inhibited by ICI182780 and significantly increased the response observed at 25μM of M8OI, inducing a 2.2-fold increase compared to a 1.5-fold increase in the absence of ICI182780. As with mERα, the metabolites HO8IM and COOH7IM did not activate the mERβv1 (Figure 6.3B).

mERβv2 was activated by M8OI in a dose dependent manner and the response induced was greater than variant 1 (Figure 6.4A). The maximum response observed at 25μM activated the mERβv2 at similar levels to that of 10nM E2 and EE positive controls. As seen with mERβv1, ICI182780 inhibited E2 and EE induced activation but was unable to inhibit the M8OI induced response at any of the concentrations tested. HO8IM and COOH7IM did not activate the mERβv2, however, at cells exposed to 50μM of HO8IM showed a significant reduction in reporter activity (Figure 6.4B). These data indicate that M8OI is a super activator of both variants for the murine ER as ICI182780 failed to inhibit the reporter activation induced by the ionic liquid. Additionally, it has been shown that neither variants of ERβ or the ERα in mouse are activated by the major metabolites of M8OI.

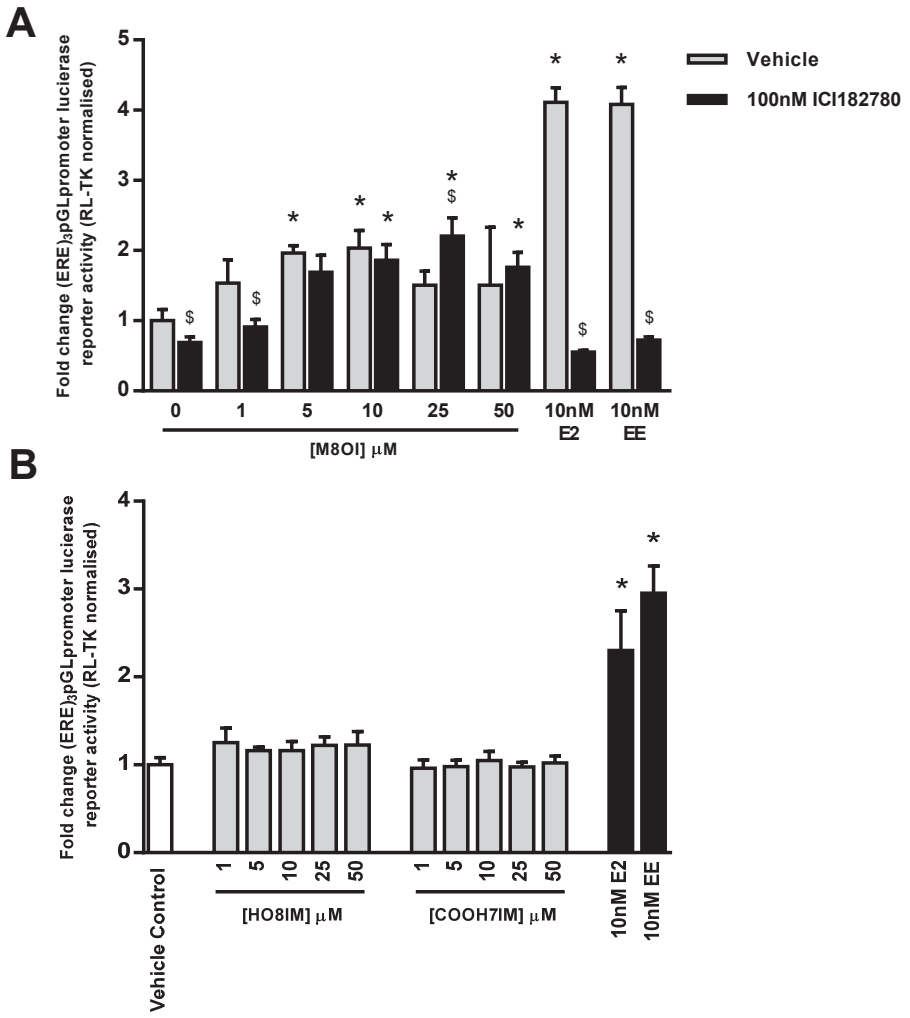

Figure 6.3: M8OI, but not it's metabolites, is an activator of the mERβv1. A, 603B cells were transiently transfected with pcDNA3.1 expression constructs coding for mERβv1, $(ERE)_3$-pGL3promotor and RL-TK control vector (at a ratio of 6:6:1) for 24 hours. Following transfection, cells were pre-treated with 100nM ICI182780 or DMSO vehicle (0.1% v/v) as indicated for 6 hours followed by the treatment of indicated compounds in the continued presence of ICI182780 or vehicle for a further 24 hours. Cells were then washed in PBS, lysed in passive lysis buffer and luciferase and renilla luminescence was determined by the dual luciferase assay. Data are the mean and SD of 3 separate determinations from the same experiment, typical of 3 separate experiments. *Significantly different ($p<0.05$) versus 0μM (DMSO vehicle) treated cells using two-way ANOVA followed by Bonferroni post-hoc test. $ Significantly different ($p<0.05$) versus equivalent treatments in the absence of ICI182780 using Student's t-test (two-tailed). **B,** 603B cells were transiently transfected with pcDNA3.1 expression constructs coding for mERβv1, $(ERE)_3$-pGL3promotor and RL-TK control vector (at a ratio of 6:6:1) for 24 hours. Following transfection, cells were treated with indicated compounds for 24 hours. Cells were then washed in PBS, lysed in passive lysis buffer and luciferase and renilla luminescence was determined by the dual luciferase assay. Data are the mean and SD of 3 separate determinations from the same experiment, typical of 3 separate experiments. *Significantly different ($p<0.05$) versus 0μM (DMSO vehicle) treated cells using one-way ANOVA followed by Bonferroni post-hoc test.

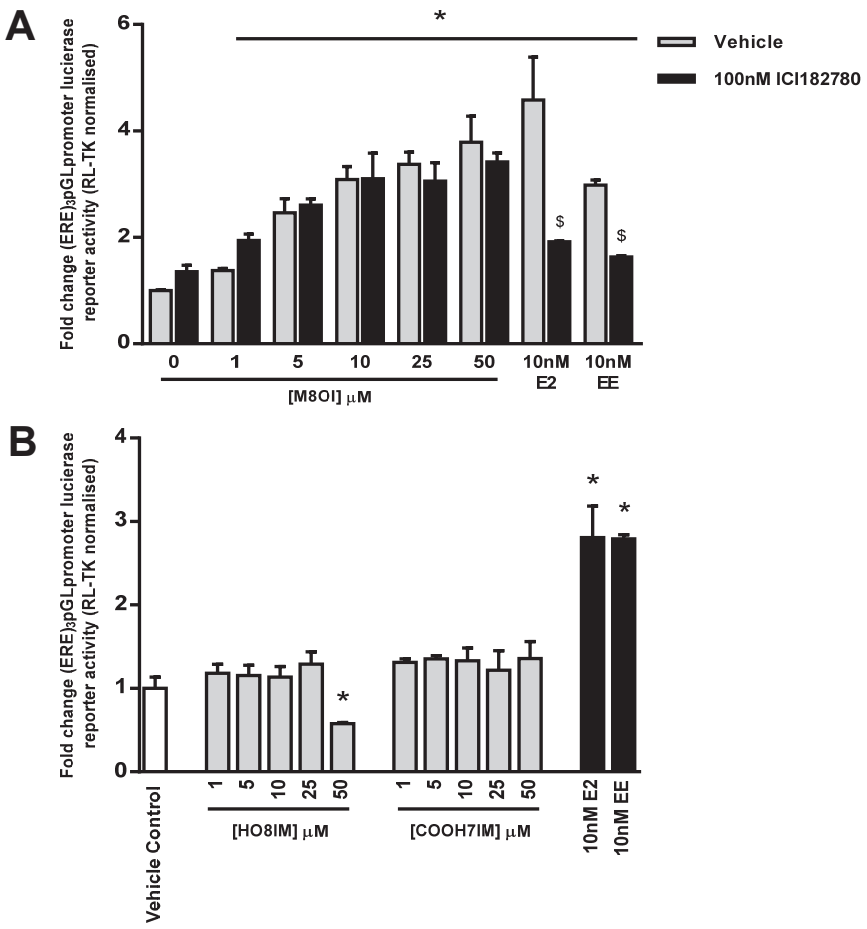

Figure 6.4: M8OI, but not it's metabolites, is an activator of the mERβv2. A, 603B cells were transiently transfected with pcDNA3.1 expression constructs coding for mERβv2, $(ERE)_3$-pGL3promotor and RL-TK control vector (at a ratio of 6:6:1) for 24 hours. Following transfection, cells were pre-treated with 100nM ICI182780 for 6 hours to de-activate constitutively active mERβv2. Cells were then washed twice in PBS followed by the treatment of indicated compounds in the presence of ICI182780 or DMSO vehicle (0.1% v/v) as indicated for a further 24 hours. Cells were then washed in PBS, lysed in passive lysis buffer and luciferase and renilla luminescence was determined by the dual luciferase assay. Data are the mean and SD of 3 separate determinations from the same experiment, typical of 3 separate experiments. *Significantly different ($p<0.05$) versus 0μM (DMSO vehicle) treated cells using two-way ANOVA followed by Bonferroni post-hoc test. $ Significantly different ($p<0.05$) versus equivalent treatments in the absence of ICI182780 using Student's t-test (two-tailed). **B,** 603B cells were transiently transfected with pcDNA3.1 expression constructs coding for mERβv2, $(ERE)_3$-pGL3promotor and RL-TK control vector (at a ratio of 6:6:1) for 24 hours. Following transfection, cells were pre-treated with 100nM ICI182780 for 6 hours to de-activate constitutively active mERβv2. Cells were then washed twice in PBS followed by the treatment of indicated compounds for a further 24 hours. Cells were then washed in PBS, lysed in passive lysis buffer and luciferase and renilla luminescence was determined by the dual luciferase assay. Data are the mean and SD of 3 separate determinations from the same experiment, typical of 3 separate experiments. *Significantly different ($p<0.05$) versus 0μM (DMSO vehicle) treated cells using one-way ANOVA followed by Bonferroni post-hoc test.

6.5 The human ERα is activated by M8OI

To examine the effect of M8OI on the human ERα receptor (hERα), MCF7 cells were transiently transfected with the $(ERE)_3$-pGLpromotor using a previously established method (Axon 2012, Meyer 2017). MCF7s were used as they express ERα that transactivates the promotor and therefore transfection of mERα into the cell would not be required. MTT assays were used to examine the effect of M8OI induced toxicity on MCF7 cells. Data showed a significant reduction in cell viability from 5µM to 1000µM with approximately a 50% reduction at 100µM of M8OI (Figure 6.5A). From this it was determined a range of 0.1µM to 50µM was to be tested for hERα activity. Figure 6.5B shows that M8OI induced a dose dependent increase in hERα activation with a max response at 50µM inducing a 2.63-fold increase in activation compared to vehicle control cells. This response was similar to that observed in 10nM E2 and EE treated cells. All activation observed in MCF7 cells treated with M8OI, E2 or EE was inhibited by the co-incubation with ICI182780 (Figure 6.5B).

Trefoil factor 1 (TFF1) is a small secretory protein first found to be expressed in MCF7 cells (Pelden *et al.*, 2013). The TFF1 gene contains an ERE and is therefore regulated by the activation of the estrogen receptor and it has been shown that in MCF7 cells, 1 hour of exposure to 10nM of E2 is sufficient to increase TTF1 RNA levels (Sun *et al.*, 2005). Real-time PCR analysis was therefore used to measure TFF1 RNA levels in MCF7 cells exposed to M8OI to confirm the activation of hERα. As previously shown, 10nM of E2 treatment increased TFF1 RNA expression (Figure 6.6). After 24 hours of exposure to E2 there was a 30-fold increase in expression that was reduced to 4.5-fold in cells co-incubated with ICI182780. M8OI induced a dose-dependent increase in TFF1 expression up to 10µM at greater levels than that which 10nM E2 induced TFF1 expression. 25µM of M8OI displayed a reduction in TFF1 expression compared to 10µM. At all concentrations of M8OI treatment and the vehicle control there was an inhibition of TFF1 expression when additionally exposed to ICI182780. Receptor activation and TFF1 expression suggest that M8OI activates the hERα and increase the expression of genes containing EREs *in vitro* and this response was inhibited by the ER inhibitor ICI182780.

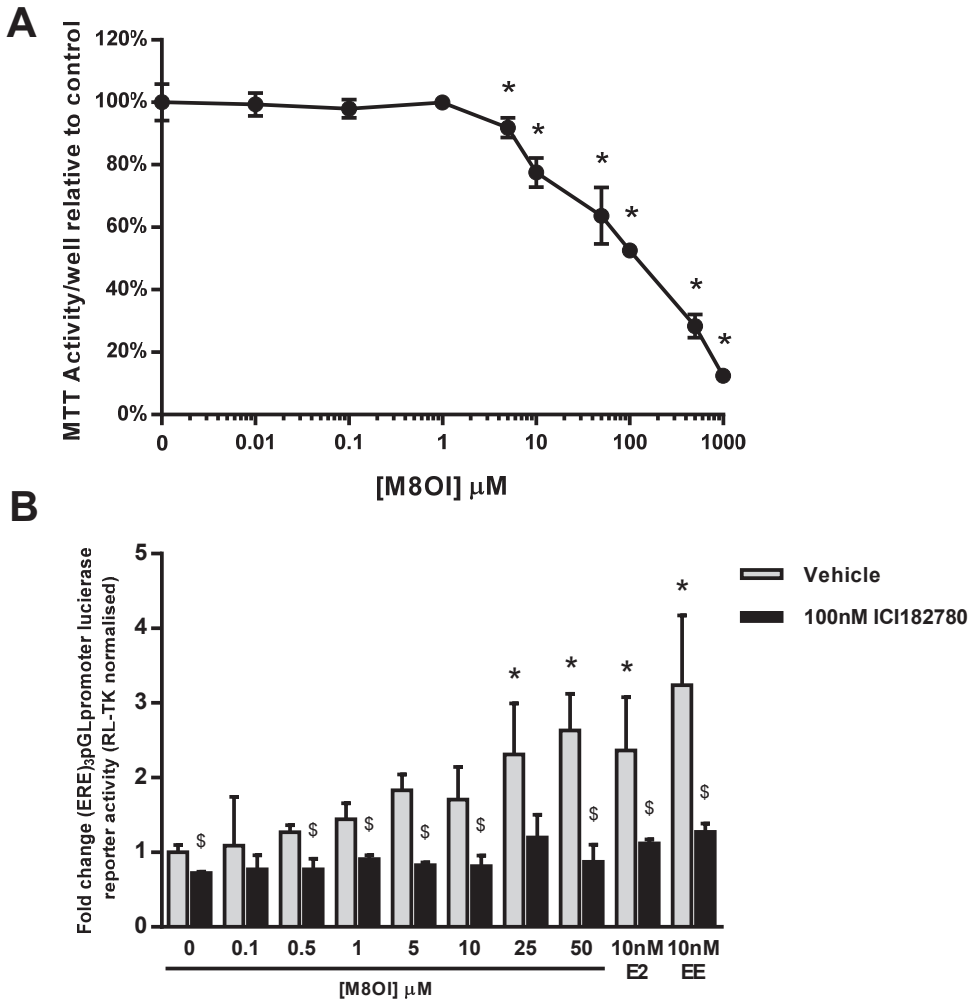

Figure 6.5: M8OI activates the hERα in MCF7 cells. A, MCF7 cells were treated for 24 hours with indicated concentrations of M8OI. Following treatment, cells were incubated with MTT for 2 hours and reduction determined. Data are the mean and SD of 6 separate determinations from the same experiment, typical of 3 separate experiments. * significantly different MTT activity to control ($p<0.05$) tested by one-way ANOVA followed by Bonferroni post-hoc test. **B,** MCF7 cells were transiently transfected with pcDNA3.1 expression constructs coding for (ERE)3-pGL3promotor and RL-TK control vector (at a ratio of 9:1) for 24 hours. Following transfection, cells were pre-treated with 100nM ICI182780 or DMSO vehicle (0.1% v/v) as indicated for 6 hours followed by the treatment of indicated compounds in the continued presence of ICI182780 or vehicle for a further 24 hours. Cells were then washed in PBS, lysed in passive lysis buffer and luciferase and renilla luminescence was determined by the dual luciferase assay. Data are the mean and SD of 3 separate determinations from the same experiment, typical of 3 separate experiments. *Significantly different ($p<0.05$) versus 0μM (DMSO vehicle) treated cells using two-way ANOVA followed by Bonferroni post-hoc test. $ Significantly different ($p<0.05$) versus equivalent treatments in the absence of ICI182780 using Student's t-test (two-tailed).

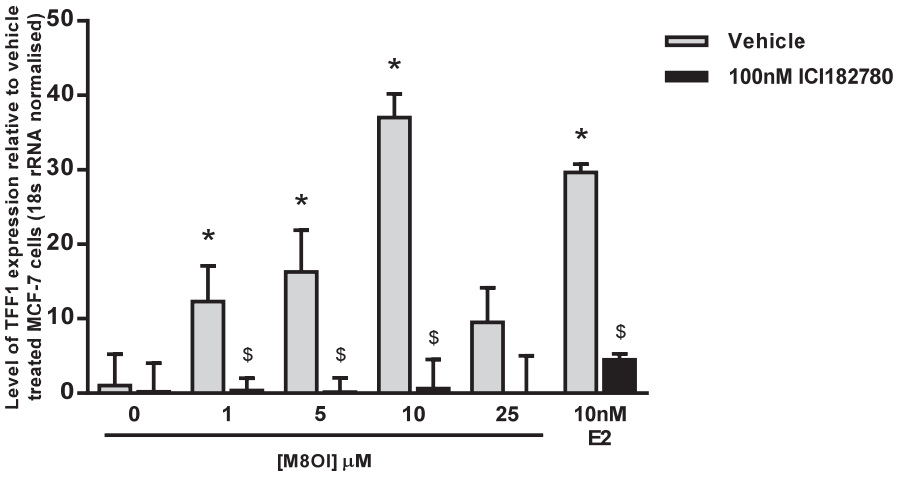

Figure 6.6: TFF1 expression is increased following M8OI treatment. MCF7 cells were pre-treated with 100nM ICI182780 or DMSO vehicle (0.1% v/v) as indicated for 6 hours followed by the treatment of indicated compounds in the continued presence of ICI182780 or vehicle for a further 24 hours. Total RNA was extracted from cells following treatment. The cDNA was used as template for qPCR to measure the expression of the indicated transcripts using the SYBR green master mix. Readings were normalised to 18S rRNA expression and fold change expressed relative to vehicle control treated cells. Bars are the mean and SD of 3 separate determinations * significantly different TFF1 expression ($p<0.05$) versus 0μM (DMSO vehicle) treated cells using two-way ANOVA followed by Bonferroni post-hoc test. $ Significantly different ($p<0.05$) versus equivalent treatments in the absence of ICI182780 using Student's t-test (two-tailed).

6.6 HO8IM activates the hERα

HO8IM and COOH7IM were tested for their ability to activate the hERα in MCF7 cells. Exposure to HO8IM induced an increase in the activation of hERα after 24 hours (Figure 6.7A). This increase in reporter activity was similar to that of 10nM E2 exposure. As seen with M8OI, HO8IM activation was inhibited by 100nM ICI182780. COOH7IM displayed no evidence for activation of the hERα receptor at the concentrations implemented (Figure 6.7B).

The capability of MCF7 cells to metabolise M8OI was examined using the same HPLC methods implemented in chapter 5. HPLC chromatograms suggested that M8OI is not metabolised by MCF7 cells (Figure 6.8). This suggests that the receptor activation observed in M8OI treated cells is not due to M8OI being metabolised to HO8IM and activating the reporter in this way. The data therefore implies that both M8OI and HO8IM are hERα activators.

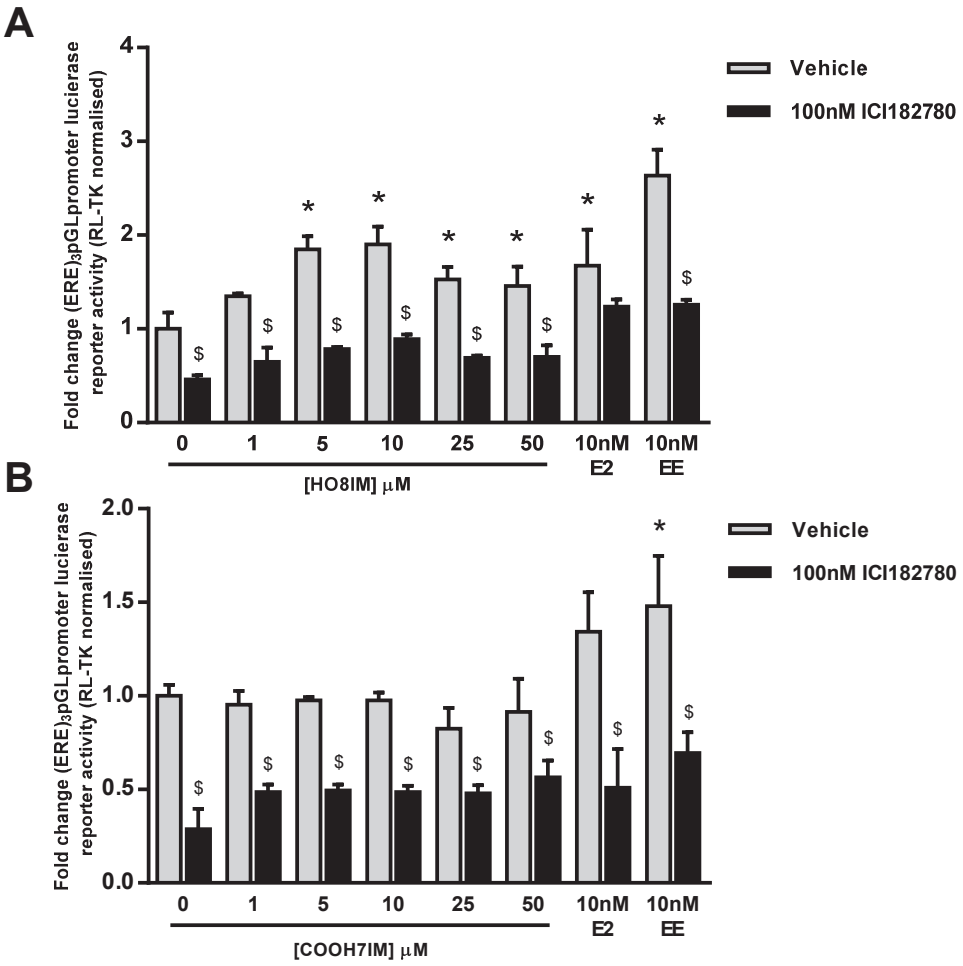

Figure 6.7: HO8IM activate the hERα. MCF7 cells were transiently transfected with pcDNA3.1 expression constructs coding for $(ERE)_3$-pGL3promotor and RL-TK control vector (at a ratio of 9:1) for 24 hours. Following transfection, cells were pre-treated with 100nM ICI182780 or DMSO vehicle (0.1% v/v) as indicated for 6 hours followed by the treatment of indicated compounds **(A, HO8IM. B, COOH7IM)** in the continued presence of ICI182780 or vehicle for a further 24 hours. Cells were then washed in PBS, lysed in passive lysis buffer and luciferase and renilla luminescence was determined by the dual luciferase assay. Data are the mean and SD of 3 separate determinations from the same experiment, typical of 3 separate experiments. *Significantly different ($p<0.05$) versus 0μM (DMSO vehicle) treated cells using two-way ANOVA followed by Bonferroni post-hoc test. $ Significantly different ($p<0.05$) versus equivalent treatments in the absence of ICI182780 using Student's t-test (two-tailed).

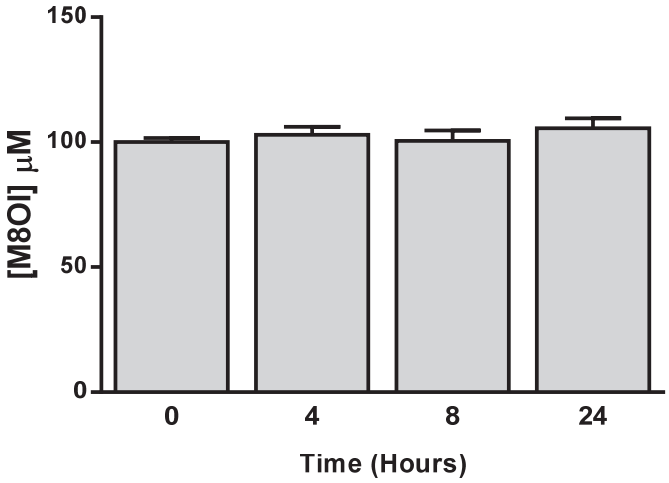

Figure 6.8: M8OI is not metabolised by MCF7 cells. MCF7 cells were incubated with 100μM of M8OI in STIM buffer for 24 hours. 200-500μl of STIM buffer was then taken from the culture at 0, 4, 8 and 24 hours. The samples were treated with phosphoric acid, separated by HPLC and absorbance detected at 212nm. The area under the curve of the peak at 15 minutes was calculated and the concertation of M8OI in the sample was determined from the M8OI standard curve. Data are the mean and SD of 3 separate determinations from the same experiment. No statistical significance.

6.7 Development of a model for the activation of human ERβ

The reporter assay for the human ERβ was generated by transiently transfecting human ERβ (hERβ) along with $(ERE)_3$-pGL3promotor and RL-TK into HEK293 cells. This reporter assay was tested using a dose response of E2 and EE treatment for 24 hours. Figure 6.9A shows that both EE and E2 induced an increase in the $(ERE)_3$-pGL3promotor activity suggesting the activation of the hERβ. The data showed that the concentration used in the other reporter assays of 10nM induced a 2.2-fold and 1.9-fold increase in promoter activity in cells exposed to E2 and EE respectively and therefore 10nM was continued to be used as a positive control for future assays.

To test whether the hERβ is constitutively active in the same way as previously described with mERβv2 (Meyer *et al.*, 2017a), transfected HEK293 cells were treated with 100nM ICI182780 for 6 hours prior to 10nM E2 and vehicle control treatment. Pre-treatment with ICI182780 showed a significant activation of the receptor and it could therefore not be determined if the hERβ was constitutively active in HEK293 cells (Figure 6.9B). However, ICI182780 did significantly inhibit 10nM E2 induced activation.

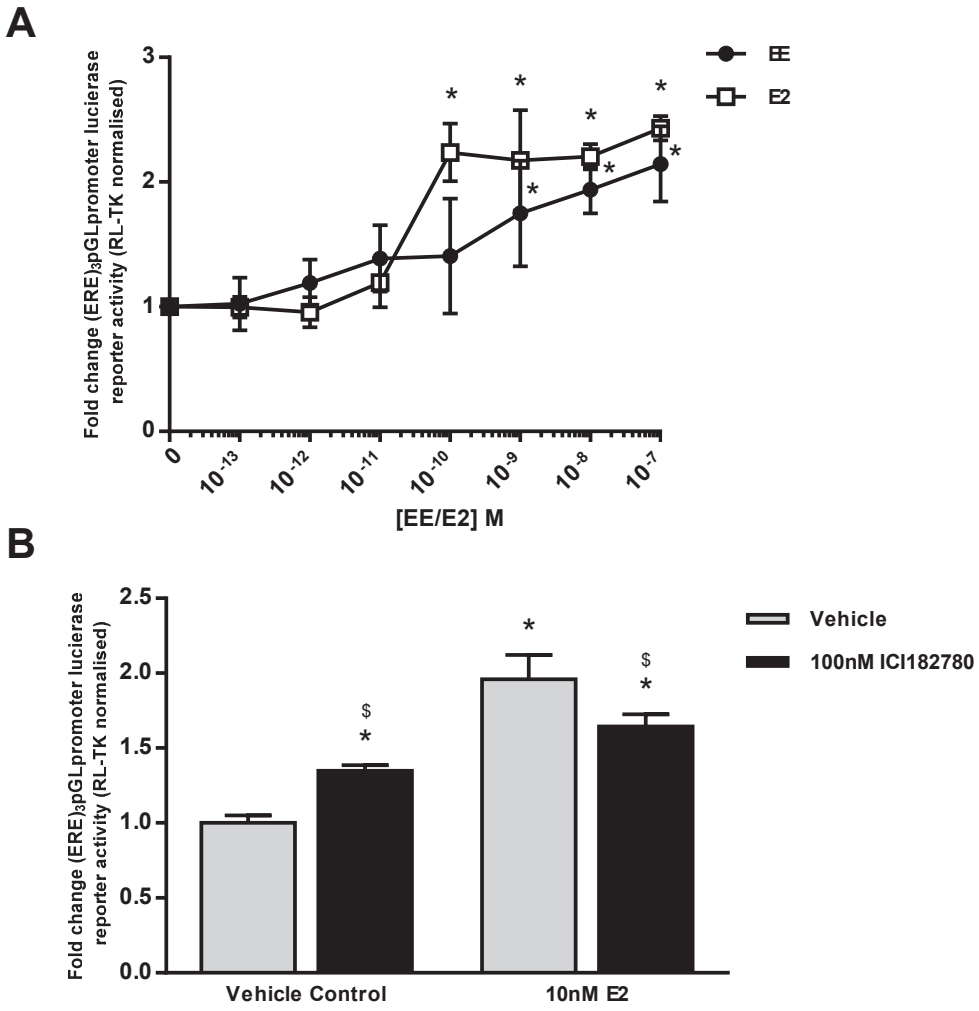

Figure 6.9: pcDNA-Flag-Erβ can be used with the (ERE)3-pGL3promotor to measure estrogen induced activation of the hERβ. **A,** HEK293 cells were transfected with expression constructs coding Flag-Erβ, $(ERE)_3$-pGL3promotor and RL-TK control vector (at a ratio of 6:6:1) using PEI. Following transfection, the cells were treated with indicated doses of E2 and EE for 24 hours. Cells were then washed in PBS, lysed in passive lysis buffer luciferase and renilla luminescence was determined by the dual luciferase assay. Data are the mean and SD of 3 separate determinations from the same experiment, typical of 3 separate experiments. *Significantly different ($p<0.05$) versus 0μM (DMSO vehicle) treated cells using one-way ANOVA followed by Bonferroni post-hoc test. **B,** HEK293 cells were transfected with expression constructs coding Flag-Erβ, $(ERE)_3$-pGL3promotor and RL-TK control vector (at a ratio of 6:6:1) using PEI. Following transfection, cells were pre-treated with 100nM ICI182780 or DMSO vehicle (0.1% v/v) as indicated for 6 hours. The cells were then washed twice in PBS before being treated with 10nM E2 or DMSO control. *Significantly different ($p<0.05$) versus vehicle treated cells using Student's t-test (two-tailed). $ Significantly different ($p<0.05$) versus equivalent treatments not given ICI182780 pre-treatment using Student's t-test (two-tailed).

6.8 M8OI, HO8IM and COOH7IM does not activate the hERβ in HEK293 cells

As previously described, MTT assays were carried out to determine the cell viability of HEK293 cells treated with M8OI. 24 hour incubation of M8OI in HEK293 cells induced a decrease in cell viability in a dose dependent manner (Figure 6.10). HEK293 cells appeared to be most resistant to M8OI induced toxicity compared to other cell lines with 53% of cells treated with 500μM M8OI being viable after 24 hours of treatment. Therefore, the same concentrations implemented in the other reporter assays were used.

M8OI did not induce reporter activity at any of the concentrations tested in HEK293 cells (Figure 6.11A). The addition of 100nM ICI182780 further induced luciferase expression in all cells treated with M8OI as well as the vehicle control treated cells. The cells treated with E2 and EE in the presence of ICI182780 showed an inhibitory effect compared to those treated with E2 and EE with the vehicle control. This inhibition reduced the activation to similar levels observed in the vehicle treated and M8OI treated cells, displaying a slight increase in luciferase expression compared to non-ICI182780 treated control cells. These results suggest that ICI182780 could weakly activate the hERβ in some capacity, yet it is still able to inhibit estrogen induced activity.

Additionally, HO8IM and COOH7IM did not appear to activate the hERβ in the HEK293 cell reporter assay (Figure 6.11B). These data therefore showed that neither M8OI nor it's metabolites activated the hERβ and the ERE reporter in this reporter gene assay, yet there could be weak agonistic effects induced by ICI182780 in this model.

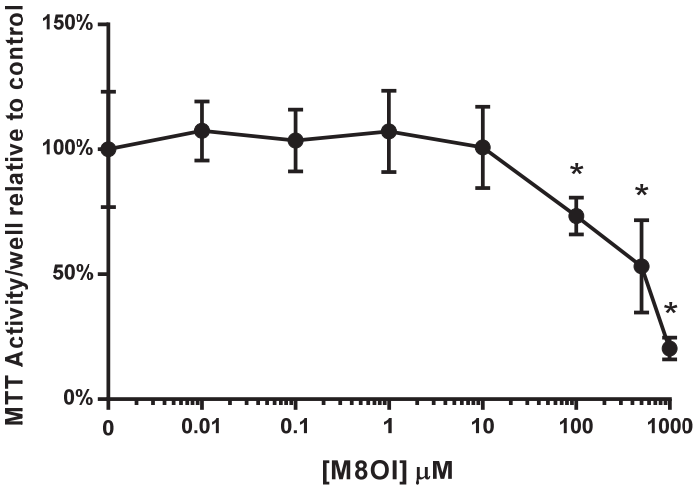

Figure 6.10: MTT activity is reduced in cells treated with M8OI for 24 hours. HEK293 cells were treated for 24 hours with indicated concentrations of M8OI. Following treatment, cells were incubated with MTT for 2 hours and reduction determined. Data are the mean and SD of 6 separate determinations from the same experiment, typical of 3 separate experiments.

* significantly different MTT activity to control ($p<0.05$) tested by one-way ANOVA followed by Bonferroni post-hoc test.

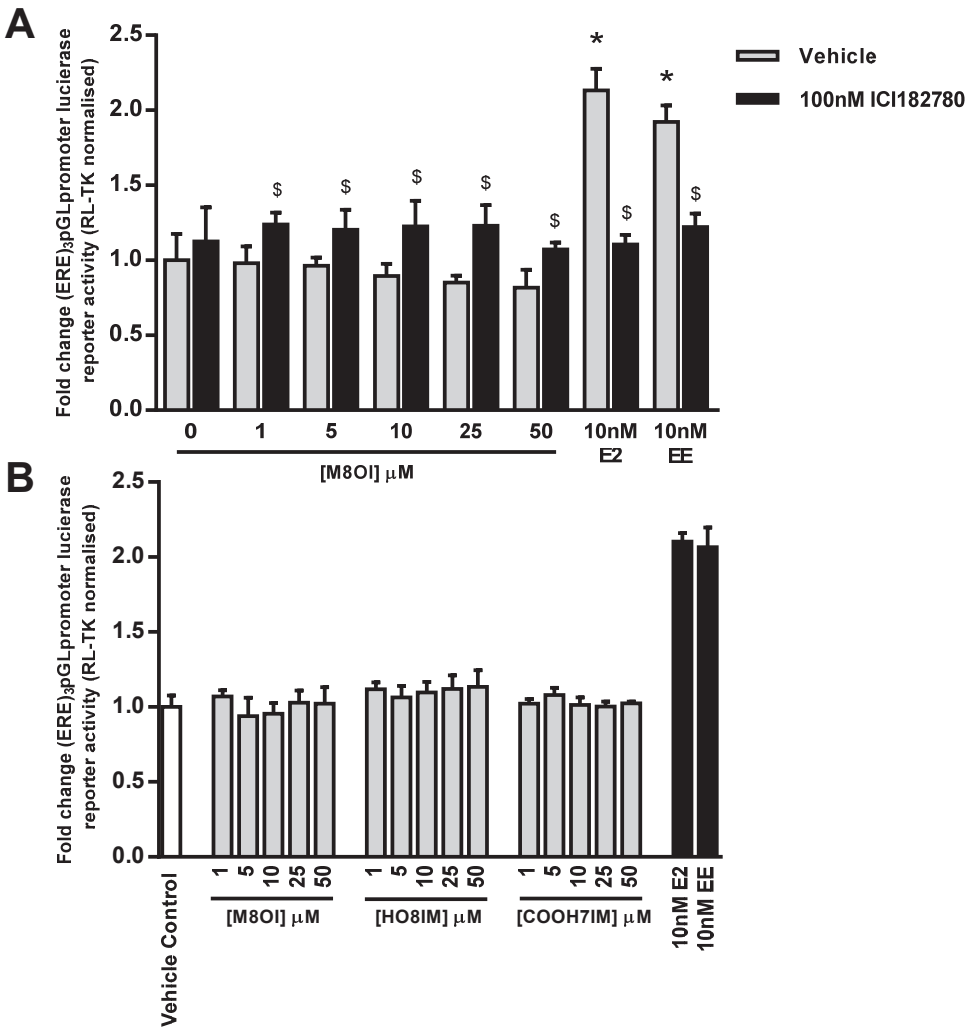

Figure 6.11: Neither M8OI nor its metabolites activate the hERβ in the (ERE)3-pGL3promotor assay in HEK293 cells. A, HEK293 cells were transfected with expression constructs coding Flag-Erβ, $(ERE)_3$-pGL3promotor and RL-TK control vector (at a ratio of 6:6:1) using PEI. Following transfection, cells were pre-treated with 100nM ICI182780 or DMSO vehicle (0.1% v/v) as indicated for 6 hours followed by the treatment of indicated compounds in the continued presence of ICI182780 or vehicle for a further 24 hours. Cells were then washed in PBS, lysed in passive lysis buffer and luciferase and renilla luminescence was determined by the dual luciferase assay. Data are the mean and SD of 3 separate determinations from the same experiment, typical of 3 separate experiments. *Significantly different ($p<0.05$) versus 0μM (DMSO vehicle) treated cells using two-way ANOVA followed by Bonferroni post-hoc test. $ Significantly different ($p<0.05$) versus equivalent treatments in the absence of ICI182780 using Student's t-test (two-tailed). **B,** HEK293 cells were transfected with expression constructs coding Flag-Erβ, $(ERE)_3$-pGL3promotor and RL-TK control vector (at a ratio of 6:6:1) using PEI. Following transfection, cells were treated with indicated compounds for 24 hours. Cells were then washed in PBS, lysed in passive lysis buffer and luciferase and renilla luminescence was determined by the dual luciferase assay. Data are the mean and SD of 3 separate determinations from the same experiment, typical of 3 separate experiments. *Significantly different ($p<0.05$) versus 0μM (DMSO vehicle) treated cells using one-way ANOVA followed by Bonferroni post-hoc test.

6.9 M8OI does not activate the hERβ in H69 cells

HEK293 cells were initially used to study the effects of M8OI on the hERβ due to their high transfection rate (Thomas and Smart, 2005). Yet as M8OI was being considered as a potential trigger for PBC (Probert *et al.*, 2018) and the cholangiocytes reportedly display an increase in ERβ in diseased states (Alvaro *et al.*, 2006), H69 cells were transfected using the same constructs as HEK293 cells to investigate if there were any changes in activity in the H69 cholangiocyte cell line. Figure 6.12 demonstrates that M8OI did not induce an increase in luciferase gene expression and therefore does not activate the hERβ in H69 cells.

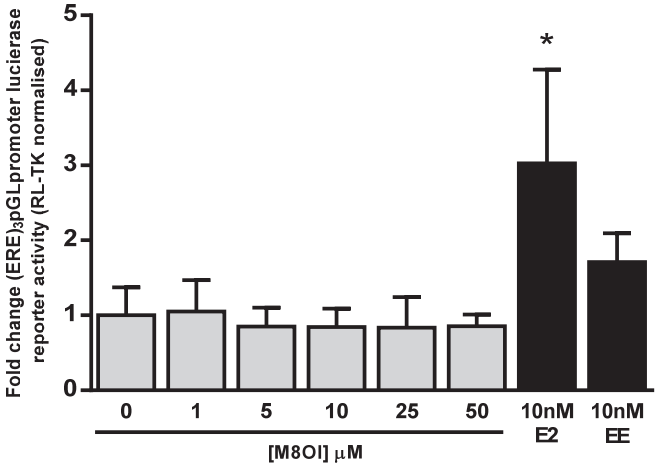

Figure 6.12: M8OI does not activate the hERβ in the (ERE)3-pGL3promotor assay in H69 cells. H69 cells were transfected with expression constructs coding Flag-Erβ, $(ERE)_3$-pGL3promotor and RL-TK control vector (at a ratio of 6:6:1) using Lipofectamine. Following transfection, cells were treated with indicated compounds for 24 hours. Cells were then washed in PBS, lysed in passive lysis buffer and luciferase and renilla luminescence was determined by the dual luciferase assay. Data are the mean and SD of 3 separate determinations from the same experiment, typical of 3 separate experiments. *Significantly different ($p<0.05$) versus 0μM (DMSO vehicle) treated cells using one-way ANOVA followed by Bonferroni post-hoc test.

6.10 Chapter discussion

The aim of this chapter was to investigate the capability of M8OI to activate the human and murine ERs. This was achieved through the use of previously established *in vitro* gene reporter assays in several different cell lines. Given that it had previously been shown that extracts from soil samples taken from around a landfill site contained xenoestrogens (Meyer *et al.*, 2017a) and that these landfill samples contained M8OI (Probert *et al.*, 2018), it was hypothesised that M8OI was the cause, at least in part, of the xenoestrogen activity of the landfill site samples.

Mouse cell lines were selected to investigate as these cell lines had previously been shown to respond to environmental xenoestrogens and mouse models had been used for *in vivo* studies in chapter 4. 603B and LTPA cells were selected due being biliary epithelial and ductal pancreatic cells lines respectively and therefore relevant to the study of ERs in the liver as biliary epithelial cells are considered to express both ERα and ERβ in diseased states (Alvaro *et al.*, 2006). The 3XERE TATA luc gene reporter assay in LTPA cells demonstrated that M8OI activates the mERα and the subsequent association with ERE promotors (Figure 6.2). This activation was effectively antagonised by ICI182780 to levels similar to vehicle control cells incubated with the antagonist. The decrease in the luciferase gene activity in vehicle cells treated with ICI182780 compared to those in absence of antagonist had been previously observed (Meyer *et al.*, 2017a). This indicates that the receptor is partially activated in standard culture medium and it is therefore likely that there are estrogens present in the cell media. Partial receptor activation in control conditions is also observed in mERβv1 but not in mERβv2 as the receptor appears to be fully activated and required the deactivation of ICI182780 pre-treatment before a response can be observed (Meyer *et al.*, 2017a). The two variants of the mERβ were both examined for the capability of M8OI to activate these receptors in the 603B cells using the $(ERE)_3$-pGLpromotor reporter gene. Both mERβv1 and mERβv2 were shown to be activated by M8OI in a dose dependent manner(Figure 6.3 & Figure 6.4), however unlike the mERα, ICI182780 was unable to antagonise the increase in luciferase activity induce by M8OI yet it was able to antagonise E2 and EE activation, indicating that M8OI has "super-activating" characteristics of both mERβv1 and mERβv2. This was previously observed with the landfill soil sample extracts in mERβv2 (Meyer *et al.*, 2017a), suggesting that M8OI could be the xenoestrogen present in the soil samples as both the landfill samples and M8OI induced the "super-activating" response in mERβv2. However, this effect was not seen in the mERβv1 reporter assay, and ICI182780 was shown to inhibit the landfill site extracts (Meyer *et al.*, 2017a). As to how M8OI may induce these "super-activating" effects, it has been hypothesised that the rate of dissociation of M8OI from the ligand binding domain is reduced compared to estrogens such as E2. Another proposed reason is that M8OI may activate the mERβ via a different mechanism such as via a different binding site resulting in ICI182780 unable to antagonise the response (Meyer *et al.*, 2017a). No increase in luciferase gene expression was observed following treatment of either of the major metabolites HO8IM or COOH7IM, therefore it could be assumed that once metabolised, M8OI loses in xenoestrogenic activity in mice.

To investigate whether the xenoestrogenic effects on the murine estrogen receptors translated to the human estrogen receptors, human ERα and ERβ gene reporter assays were utilised. The MCF7 cells were transiently transfected with the $(ERE)_3$-pGL3promotor reporter construct (as well as RL-TK control vector)

to generate the hERα-$(ERE)_3$-pGLpromotor reporter gene assay. While the murine cell lines were selected for the reasons stated above, MCF7 cells are not a biliary epithelial cell line and were selected as they express the hERα (Axon *et al.*, 2012). As seen with the mERα, the hERα was partially active in control cells, as evidenced by the reduction of luciferase gene expression in ICI182780 treated cells and as with the mERα, this could be due to estrogenic components of the cell media. M8OI was shown to activate the hERα to levels similar to that of 10nM E2 and was effectively antagonised by ICI182780 (Figure 6.5). This effect was also observed in the landfill tip sample extracts where M8OI was identified (Meyer *et al.*, 2017a; Probert *et al.*, 2018), supporting the hypothesis that M8OI was the xenoestrogen within these samples. To confirm the activation of hERα, TFF1 expression following M8OI treatment was investigated. TFF1 is a small secretory protein that contains an ERE and can therefore be regulated by estrogens (Sun *et al.*, 2005). TFF1 was first found in the MCF7 cells and been reported to be involved in the protection against apoptosis in various cell types *in vitro* and has been used to investigate the mechanisms of drug resistance of breast cancer treatment (Pelden *et al.*, 2013). Expression has been shown to increase when MCF7 cells are exposed to E2 after 1 hour (Sun *et al.*, 2005). Results in this chapter confirm that E2 induces an increase in TFF1, as well as indicate that M8OI also induces TFF1 (Figure 6.6), likely through the ERE and therefore activation of the hERα. This is supported by the antagonistic effect of ICI182780 on the M8OI induced expression of TFF1.

HO8IM induced an increase in luciferase gene reporter activity in MCF7 cells (Figure 6.7), and was antagonised by ICI182780, whereas no such increase was observed with COOH7IM treated cells. Further studies should investigate TFF1 expression as carried out with M8OI to confirm the activation of the hERα by HO8IM. As seen in chapter 5, M8OI was metabolised to HO8IM by CYP3A4 (Figure 5.9). It has been reported that MCF7 cells express CYP3A4 at low levels and display CYP3A4 activity, however the levels of activity are unknown as no comparison to cells known to express CYP3A4 at high levels such as primary hepatocyte was made (Thuy Phuong *et al.*, 2017). It was therefore decided to investigate whether MCF7 cells can metabolise M8OI. Data showed that MCF7 were unable to metabolise M8OI (Figure 6.8), it can therefore be concluded that both M8OI and HO8IM activate the hERα and the activation observed in M8OI treated cells is not a product of the metabolism to HO8IM and activation by the metabolite.

The final ER to be studied was the hERβ. The hERβ has several variants that have been previously described in humans (Green *et al.*, 1986). The NCBI database indicates 7 splice variants, leading to 5 variant proteins. The clustal alignment of these variants to mERβv1 and mERβv2 revealed that all the hERβ proteins lack an 18 amino acid insertion present in mERβv1 that effects the type and affinity of ligand binding and therefore

would more likely respond to ligands similarly to the mERβv2 (Meyer *et al.*, 2017a). The hERβ-(ERE)3-pGL3promotor gene reporter assay was first validated in HEK293 cells using E2 and EE and constitutive activation of the receptor was then investigated. It was noted that ICI182780 appeared to weakly activate the mERβ, an effect that was observed in other experiments. Interestingly, ICI182780 inhibited further activation by E2 and EE but luciferase gene activity remained higher than vehicle control cells in absence of the antagonist. This effect can also be seen in the mERv2 experiments. The reason for this could be that ICI182780 does mildly activate the hERβ or could be because ICI182780 stabilises the ERβ protein (Peekhaus *et al.*, 2004).

When exposed to M8OI, HO8IM and COOH7IM, the luciferase activity was not affected (Figure 6.11). Suggesting that neither M8OI or its metabolites activates the hERβ in HEK293 cells. HEK293 cells were selected due to their high transfection rate (Thomas and Smart, 2005), however, HEK293 cells are human embryonic kidney cells and thus not as relevant to the expression of ERs in the liver as other hepatocyte or biliary epithelial cell lines. Therefore, the biliary epithelial cell line, H69 cells, were transfected with the same constructs as used in HEK293 cells. While more difficult to achieve a high transfection rate compared to HEK293 cells, it was possible to successfully generate the hERβ-(ERE)3-pGL3promotor gene reporter assay and show that M8OI did not activate the hERβ in H69 cells (Figure 6.12). The ability of M8OI to activate hERα and not hERβ maybe be due to the amino acid differences in the ligand binding domain (LBD), or because the ligand-binding cavity is approximately 20% smaller in the ERβ, meaning it is more selective (Zhao *et al.*, 2008).

While M8OI does not appear to activate the hERβ in this gene reporter assay, there are several limitations that mean it could not be concluded that M8OI has no effect on the receptor. One is that there are differences in co-activators and adaptor proteins required depending on the conformation of the ER (Yi *et al.*, 2002). These conformational changes are ligand specific, therefore different cofactors are required for transcriptional induction depending on the ligand bound. It has been shown in the ERα that transcriptional activation from the same ERE differs between cell line, suggesting the availability of cofactors could contribute to ER transcriptional activation (Klinge, 2001). Additionally, the ERE sequence found in the promotor region of estrogen responsive genes have different binding affinities to the DNA binding domain of the ER despite these regions being highly homologous (Yi *et al.*, 2002). Therefore, the ERE can determine ER transcriptional activation. Only the hERβ-(ERE)3-pGL3promotor gene reporter was examined and it is possible that 3XERE TATA luc gene reporter could generate a different result. Alternatively, a downstream target of ERβ could be examined by real-time PCR such as that observed with hERα and TFF1. This would

ideally be carried out in primary human cholangiocytes as mouse cholangiocytes have been shown to express ERβ after several days of culture (Meyer *et al.*, 2017a).

As discussed in chapter 4, it is difficult to determine whether the effects observed (xenoestrogenic activity) following the exposure of M8OI are likely to be observed in humans as the potential human exposure of M8OI is unknown. Uterine growth could be investigated in mice administered with M8OI orally for a prolonged period as an increase in uterine growth has been linked to the exposure of estrogens (Reel *et al.*, 1996).

Elevated levels of estrogens or inhibition of transporters lead to cholestasis, believed to be caused by ERα dependent suppression of bile acid transporter expression (Yamamoto *et al.*, 2006). BSEP expression has been shown to be repressed in the late stages of pregnancy in mice (Song *et al.*, 2014) and bile acid and drug transporter repression induced by ERα has been shown to be lost in ERα knockout mice (Yamamoto *et al.*, 2006). Additionally, ERα and ERβ have been shown to be expressed in cholangiocytes in diseased state (Alvaro *et al.*, 2006). It is believed that ERα and ERβ play a role in the proliferative response in the liver (Alvaro *et al.*, 2006) with several studies showing that the ER plays a role in liver regeneration after rats and mice undergo partial hepatectomy (Francavilla *et al.*, 1989; Umeda *et al.*, 2015; Kao *et al.*, 2018). ERα is believed to bring about pro-proliferative effects where as ERβ antagonises these effects (Alvaro *et al.*, 2006). Additionally, selective ERβ agonists induce apoptosis in cholangiocarcinoma (Marzioni *et al.*, 2012).

Therefore, as M8OI has been shown to induce the activation of different ERs it could be hypothesised that M8OI could induce cholestatic effects. In humans these effects would be mediated by the ERα, potentially through the repression on bile transporters, yet further studies would be required to confirm this. The data presented in this chapter suggests that M8OI would have no effect on the ERβ, however in mice the activation of ERβ could antagonise proliferative effects and induce apoptosis in cholangiocytes in diseased states. *In vivo* studies with the landfill site extracts showed an increase in ALP yet no histological evidence of cholestatic injury. Additionally, *in vivo* data in chapter 4 showed some evidence of liver injury but no increase in ALP levels when mice were subjected to M8OI. Any cholestatic injury induced by the activation of the ERs could therefore play a role in the development of PBC, with the destruction of the bile duct being the major pathological hallmark in the disease. As M8OI activates the hERα, potentially inducing ER-mediated cholestasis, it is possible this could factor into a mechanism of M8OI as a trigger for PBC.

Chapter 7. General discussion

Hepatocytes are the main cell of the liver and perform the majority of its unique functions, such as the metabolism of clearance of xenobiotics. Therefore, the liver is a primary target for the majority of drug- and chemical-induced toxicity. The general population is exposed to many natural and man-made chemicals daily. These include pharmaceutical drugs as well as chemicals in food consumed, cosmetics, and chemicals released into the environment such as pesticides. As hepatocytes are a major target for drug and chemical toxicity, *in vivo* and *in vitro* models have been developed to study the effects of these compounds in hepatocytes. The gold standard for toxicity screening is the use of primary human hepatocytes. However, these are limited in availability and rapidly dedifferentiate within a few days of culture and lose their liver specific functions. The B-13/H cell line is an alternative to primary hepatocytes that express liver specific genes and can maintain their phenotype for several weeks (Probert *et al.*, 2015). The initial primary aims of this thesis was to investigate lipid dysregulation using the B-13/H model and to examine their response to fatty acids, alcohol and xenobiotics. Additionally, the potential toxic effects of an ionic liquid found in the environment, M8OI, was to be investigated using *in vitro* and *in vivo* models.

Exposure of B-13/H cells to fatty acids resulted in the accumulation of lipids in a dose dependent manner, as demonstrated by oil red staining. This response in B-13/H cells, being rat derived, was comparable to primary rat hepatocyte exposure to fatty acids which also showed the formation of both microsteaotic and macrosteaotic lipid droplets at high concentrations of 1mM. On the other hand, B-13 cells, a rat acinar cell line accumulated less lipids and did not display any evidence of macrosteatosis. This suggests that B-13/H cells, a simple model to generate without the sacrificing of animals, are just as an effective model for fatty acid induced lipid accumulation as primary rat hepatocytes. The LXR is a nuclear receptor that regulates SREBP-1c and ChREBP that are involved in *de novo* lipogenesis. The activation of the LXR by the LXR ligands T0901317 and GW3965 promoted lipid accumulation in the B-13/H cells. This demonstrates drug induced lipid accumulation in the B-13/H model. This model could be used to investigate new potential therapies for NAFLD, such as the recent drugs targeting the PPARδ (Staels *et al.*, 2013; Lee *et al.*, 2015).

Phospholipid accumulation was modelled in B-13/H cells by exposing them to known cationic amphiphilic drugs. PLD in B-13 cells was greater than in B-13/H cells. This is likely due to B-13/H cell expressing functional drug metabolising enzymes and therefore the CADs exposed to the cells could be being metabolised to a structure that is no longer cationic amphiphilic and lose their ability to incorporate into the lysosome and induce phospholipid accumulation. Data in this thesis has also demonstrated that methapyrilene induces PLD and as with other CADs phospholipid accumulation was greater in B-13 cells.

Methapyrilene induced toxicity in B-13/H cells but not B-13 cells. Additionally, nifedipine inhibited methapyrilene induced cell death but increased PLD accumulation. These data suggest that PLD is not a critical event in methapyrilene-induced hepatotoxicity. The addition of DTT to B-13/H cells blocked the induction of PLD by methapyrilene, amiodarone and tamoxifen, suggesting that an oxidative redox status and/or protein thiol oxidation is necessary for phospholipid accumulation. Finally, LYPLA2, an enzyme responsible for the metabolism of phospholipids, was over expressed in B-13 cells through transfection and reduced phospholipid accumulation. The data presented in this thesis has therefore shown that B-13/H cells are an effective model for lipid dysregulation in response to several drugs and chemicals, including fatty acid- and LXR activator-induced steatosis and CAD-induced phospholipidosis. Data has also shown it is possible to regulate CAD induced phospholipid accumulation chemically and through the over expression of LYPLA2.

PBC is a chronic cholestatic liver disease that is characterised by the destruction of intrahepatic bile ducts and occurs in individuals who are genetically predisposed and is generally considered to be triggered through the exposure to an environmental chemical(s)/toxins(s). Soil extracts from a landfill site in close proximity of an area with a high prevalence of PBC was found to be toxic to the B-13 liver progenitor cell line (Probert *et al.*, 2018) and activate estrogen receptors (Meyer *et al.*, 2017a). The ionic liquid, M8OI, was identified in these toxic/xenoestrogenic samples. Data on the toxicity of M8OI is limited, it was therefore hypothesised that M8OI was the chemical in the soil that induced toxicity in B-13 cells and induced xenoestrogenic effects.

Data in this thesis demonstrates that M8OI is toxic to several hepatic cell lines and primary human and mouse hepatocytes (The effects of M8OI are summarised in Figure 7.1). The toxicity observed was variable between cell lines with B-13 cells being the most susceptible to M8OI induced toxicity. Interindividual variability was also observed between hepatocyte preparations. M8OI induced apoptosis in these cells as shown using a annexin V luminescent assay. Mitochondrial swelling suggested that M8OI has a mitochondrial effect and this was confirmed using the seahorse mito stress test that revealed M8OI inhibited oxygen consumption and induced a shift to glycolysis. The exact target of M8OI inhibition of the ETC is yet to be determined however data presented in this thesis suggests that it inhibits ATP synthase (complex V) as FCCP partially recovered M8OI induced inhibition of oxygen consumption. However, as this recovery was only partial, it suggests that M8OI could also be acting elsewhere. M8OI appeared to stimulate the oxygen consumption rate in PMP experiments of complex II. Yet this effect is not observed in intact cell experiments and so the relevance of this effect to the overall mechanism is not yet known.

In vivo studies investigating the effects of M8OI in mice revealed toxic effects in the liver and kidney. Histological examination of the kidney showed evidence of renal tubule necrosis. Further studies should expand and examine serum creatine and urea levels as well as examining the urine for protein and glucose. Examination of the liver revealed evidence of periportal inflammation, however the predominant effect was complete glycogen depletion in mice treated with 10mg/kg bw M8OI. These data support the inhibition of oxidative phosphorylation and a shift to glycolysis as glycolysis requires glucose to generate ATP and therefore glycogen would need to be catabolised to generate glucose to provide energy via glycolysis.

M8OI has been shown to be acutely toxic in frogs during early embryonic development (Li 2009), genotoxic to planarians (flatworms) (Zhang 2016), toxic to fish (Nan 2016) and affects growth of algae (Deng 2016) and wheat (Liu 2009). However, data on toxicity in mammalian models is limited. M8OI has been shown to induce apoptosis in HepG2 cells (Li 2015) and to be acutely hepatotoxic to mice administered M8OI intra-peritoneally. Data in this thesis has therefore shown for the first time toxic effects in primary human hepatocytes and have demonstrate a mechanism of toxicity via the inhibition of oxidative phosphorylation.

The physiochemical properties of M8OI were also investigated. Based on the structure of M8OI, it is likely that it is readily able to cross the cell membrane. The ability of M8OI to form micelles was investigated as micelle formation could influence the properties and toxicity of M8OI. However, data presented in this thesis showed that M8OI only formed micelles at 1M. One study investigating the micelle formation of imidazolium based ionic liquids of differing alkyl chain length suggested that M8OI has a critical micelle concentration of 220mM (Jungnickel *et al.*, 2008). This concentration is over 200-fold higher than the highest concentration implemented in any experiment in this thesis and it is therefore unlikely that micelle formation could explain any of the effects observed.

Studies in M8OI metabolism in primary human hepatocyte revealed that M8OI is metabolised to hydroxyl (HO8IM) and carboxyl (COOH7IM) metabolites. COOH7IM was not toxic and HO8IM was toxic but its toxic effects were not as great as M8OI and did not inhibit oxidative phosphorylation and the concentrations examined. It has also been shown in this thesis that the metabolism of M8OI in human hepatocytes involves CYP3A4, and there is interindividual variability in M8OI metabolising capability. *In vivo* studies showed that M8OI, HO8IM and COOH7IM were present in the serum, bile and urine. These data demonstrated that M8OI is metabolised by the mouse *in vivo* and that HO8IM and COOH7IM are excreted via the bile and serum.

These data suggest M8OI could act as a trigger for PBC, as it is possible for COOH7IM to incorporate into PDC-E2, the enzyme that is targeted by AMAs and induce an autoimmune response (Probert *et al.*, 2018). COOH7IM has been shown to be present in the bile and therefore is exposed to cholangiocytes, the cells that make up the bile duct. M8OI is also present in the bile, and therefore could potentially induce the apoptosis of cholangiocytes. Apoptosis of the cholangiocytes is a characteristic of PBC as it results in the degradation of the bile duct leading to the increase of bile acids in the liver and cholestatic injury. Additionally, cholangiocytes are generally considered unique as when they undergo apoptosis, PDC-E2 remains intact. It is possible that M8OI induced apoptosis of the cholangiocyte could present COOH7IM modified PDC-E2 to AMAs and trigger an autoimmune response and further damage to the bile duct.

Finally, data in this thesis has demonstrated through the use of *in vitro* reporter assays that M8OI is xenoestrogenic. Murine ERβ variants 1 and 2 were both "super-activated" in 603B cells by M8OI and were not antagonised by the ER inhibitor ICI182780. M8OI activated the hERα in MCF7 cells and was antagonised by ICI182780 however it did not activate the hERβ in HEK293 cells or H69 cells. hERα activation was confirmed by expression of TFF1 in MCF7 cells that was inhibited by ICI182780. Estrogens have been shown to induce cholestatic injury in the liver and one mechanism of this injury is via ERα mediated suppression of bile acid transporter expression in hepatocytes. Therefore, ER-mediate cholestatic injury could play a role in PBC development. As M8OI is a xenoestrogen it is possible that M8OI could activate the ERα and induce cholestatic effects. However further work is required to support this hypothesis.

Both *in vitro* and *in vivo* models have been used and various species (human, rat, mouse) have been used in the vitro models. This has shown some species differences in how M8OI acts, as it activated the murine ERβ but not the human ERβ and primary human hepatocytes were more efficient in metabolising M8OI compared to primary mouse hepatocytes and the rat derived B-13/H cells. Therefore, the use of primary human hepatocytes is vital in the further study into M8OI metabolism and xenoestrogenic effects may not be translatable across species. This suggests that the effects observed in the *in vivo* mouse model could differ in humans. However, the investigation into the toxic mechanism of action through the inhibition of oxidative phosphorylation is likely to be conserved across species and therefore the models used (B-13, B-13/H etc.) are translatable to potential human exposure. M8OI was found in the soil around a landfill site with a concentration of 94mg/kg soil (Probert *et al.*, 2018), but extent of human exposure to M8OI is not known as the route of exposure and the concentration of direct exposure to humans is yet to be fully determined.

Overall the data presented in this thesis demonstrates the application of *in vivo* and *in vitro* models to investigate drug and chemical toxicity. Using B-13/H cells an effective model of lipid dysregulation has been demonstrated that could therefore reduce the requirement of primary hepatocytes. Data has also shown the toxicity of M8OI to hepatocytes and hepatocyte progenitor cells *in vitro* and has demonstrated hepatic glycogen depletion *in vivo*. Additionally, the metabolism of M8OI to COOH7IM and the xenoestrogenic capability of M8OI has been shown. The presence of M8OI in the environment, M8OI-induced apoptosis of cells, metabolism to COOH7IM that can incorporate into PDC-E2 and the xenoestrogenic effects induced by M8OI could suggest a role of M8OI as one possible environmental trigger for PBC.

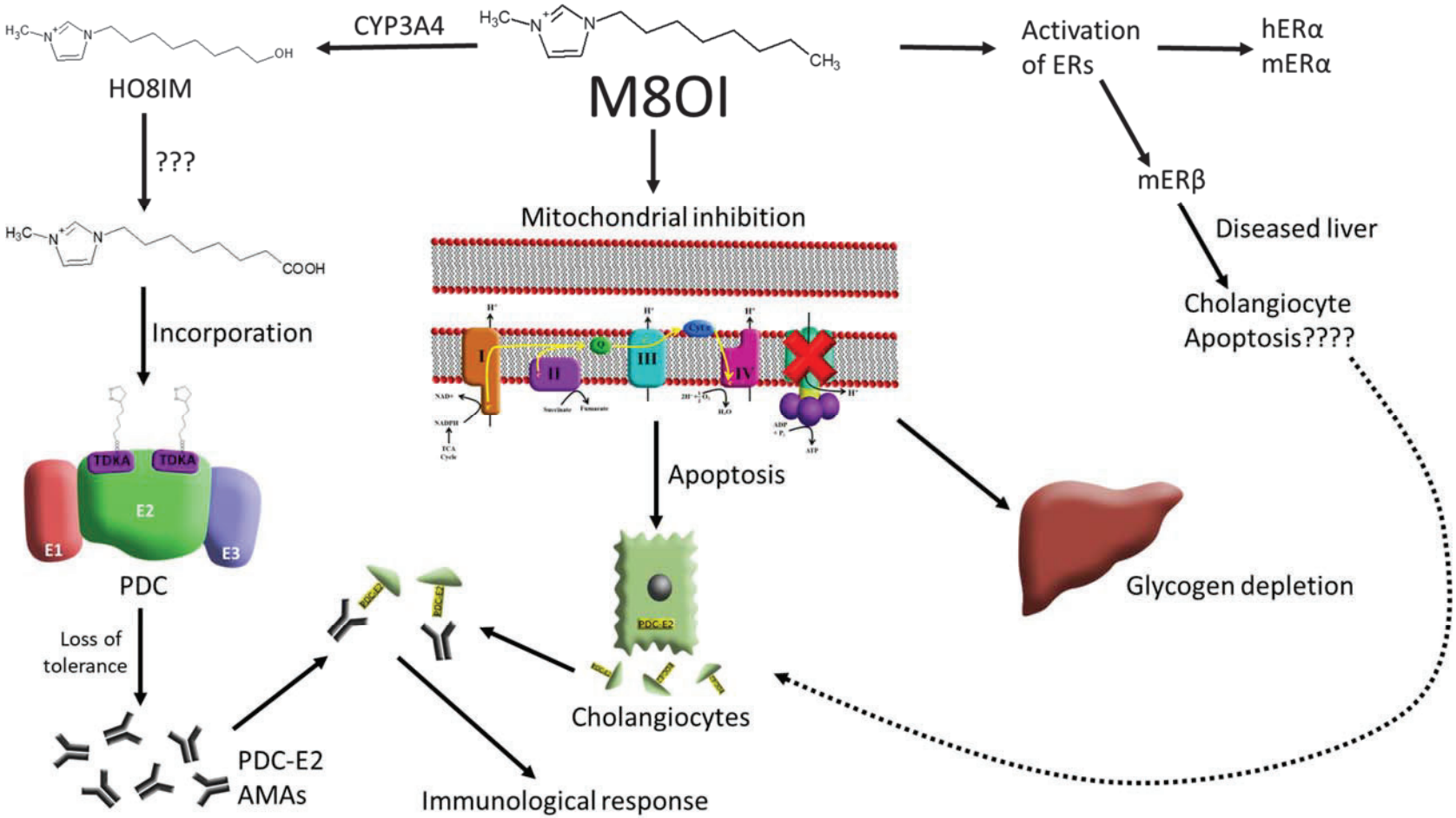

Figure 7.1: Summary of effects of M8OI.

References

Abid, A., Taha, O., Nseir, W., Farah, R., Grosovski, M. and Assy, N. (2009) 'Soft drink consumption is associated with fatty liver disease independent of metabolic syndrome', *J Hepatol*, 51(5), pp. 918-24.

Ahlbory-Dieker, D.L., Stride, B.D., Leder, G., Schkoldow, J., Trolenberg, S., Seidel, H., Otto, C., Sommer, A., Parker, M.G., Schutz, G. and Wintermantel, T.M. (2009) 'DNA binding by estrogen receptor-alpha is essential for the transcriptional response to estrogen in the liver and the uterus', *Mol Endocrinol*, 23(10), pp. 1544-55.

Ala, A., Stanca, C.M., Bu-Ghanim, M., Ahmado, I., Branch, A.D., Schiano, T.D., Odin, J.A. and Bach, N. (2006) 'Increased prevalence of primary biliary cirrhosis near Superfund toxic waste sites', *Hepatology*, 43(3), pp. 525-31.

Almela, M.J., Torres, P.A., Lozano, S. and Herreros, E. (2009) 'Characterization of the phospholipidogenic potential of 4(1H)-pyridone antimalarial derivatives', *Toxicol In Vitro*, 23(8), pp. 1528-34.

Alonso-Magdalena, P., Quesada, I. and Nadal, A. (2011) 'Endocrine disruptors in the etiology of type 2 diabetes mellitus', *Nature Reviews Endocrinology*, 7, p. 346.

Alvaro, D., Alpini, G., Onori, P., Perego, L., Svegliata Baroni, G., Franchitto, A., Baiocchi, L., Glaser, S.S., Le Sage, G., Folli, F. and Gaudio, E. (2000) 'Estrogens stimulate proliferation of intrahepatic biliary epithelium in rats', *Gastroenterology*, 119(6), pp. 1681-91.

Alvaro, D., Invernizzi, P., Onori, P., Franchitto, A., De Santis, A., Crosignani, A., Sferra, R., Ginanni-Corradini, S., Mancino, M.G., Maggioni, M., Attili, A.F., Podda, M. and Gaudio, E. (2004) 'Estrogen receptors in cholangiocytes and the progression of primary biliary cirrhosis', *J Hepatol*, 41(6), pp. 905-12.

Alvaro, D., Mancino, M.G., Onori, P., Franchitto, A., Alpini, G., Francis, H., Glaser, S. and Gaudio, E. (2006) 'Estrogens and the pathophysiology of the biliary tree', *World J Gastroenterol*, 12(22), pp. 3537-45.

Amacher, D.E. (2011) 'The mechanistic basis for the induction of hepatic steatosis by xenobiotics', *Expert Opin Drug Metab Toxicol*, 7(8), pp. 949-65.

Amacher, D.E. (2012) 'The primary role of hepatic metabolism in idiosyncratic drug-induced liver injury', *Expert Opin Drug Metab Toxicol*, 8(3), pp. 335-47.

Amano, K., Leung, P.S., Rieger, R., Quan, C., Wang, X., Marik, J., Suen, Y.F., Kurth, M.J., Nantz, M.H., Ansari, A.A., Lam, K.S., Zeniya, M., Matsuura, E., Coppel, R.L. and Gershwin, M.E. (2005) 'Chemical xenobiotics and mitochondrial autoantigens in primary biliary cirrhosis: identification of antibodies against a common environmental, cosmetic, and food additive, 2-octynoic acid', *J Immunol*, 174(9), pp. 5874-83.

Anderson, N. and Borlak, J. (2008) 'Molecular mechanisms and therapeutic targets in steatosis and steatohepatitis', *Pharmacol Rev*, 60(3), pp. 311-57.

Aninat, C., Piton, A., Glaise, D., Le Charpentier, T., Langouet, S., Morel, F., Guguen-Guillouzo, C. and Guillouzo, A. (2006) 'Expression of cytochromes P450, conjugating enzymes and nuclear receptors in human hepatoma HepaRG cells', *Drug Metab Dispos*, 34(1), pp. 75-83.

Antherieu, S., Chesne, C., Li, R., Guguen-Guillouzo, C. and Guillouzo, A. (2012) 'Optimization of the HepaRG cell model for drug metabolism and toxicity studies', *Toxicol In Vitro*, 26(8), pp. 1278-85.

Anttila, S., Hakkola, J., Tuominen, P., Elovaara, E., Husgafvel-Pursiainen, K., Karjalainen, A., Hirvonen, A. and Nurminen, T. (2003) 'Methylation of cytochrome P4501A1 promoter in the lung is associated with tobacco smoking', *Cancer Res*, 63(24), pp. 8623-8.

Asumda, F.Z., Hatzistergos, K.E., Dykxhoorn, D.M., Jakubski, S., Edwards, J., Thomas, E. and Schiff, E.R. (2018) 'Differentiation of hepatocyte-like cells from human pluripotent stem cells using small molecules', *Differentiation*, 101, pp. 16-24.

Attignon, E.A., Leblanc, A.F., Le-Grand, B., Duval, C., Aggerbeck, M., Rouach, H. and Blanc, E.B. (2017) 'Novel roles for AhR and ARNT in the regulation of alcohol dehydrogenases in human hepatic cells', *Arch Toxicol*, 91(1), pp. 313-324.

Axon, A., May, F.E., Gaughan, L.E., Williams, F.M., Blain, P.G. and Wright, M.C. (2012) 'Tartrazine and sunset yellow are xenoestrogens in a new screening assay to identify modulators of human oestrogen receptor transcriptional activity', *Toxicology*, 298(1-3), pp. 40-51.

Ayres, R.C., Neuberger, J.M., Shaw, J., Joplin, R. and Adams, D.H. (1993) 'Intercellular adhesion molecule-1 and MHC antigens on human intrahepatic bile duct cells: effect of pro-inflammatory cytokines', *Gut*, 34(9), pp. 1245-9.

Bass, A.S., Cartwright, M.E., Mahon, C., Morrison, R., Snyder, R., McNamara, P., Bradley, P., Zhou, Y.Y. and Hunter, J. (2009) 'Exploratory drug safety: a discovery strategy to reduce attrition in development', *J Pharmacol Toxicol Methods*, 60(1), pp. 69-78.

Beischlag, T.V., Luis Morales, J., Hollingshead, B.D. and Perdew, G.H. (2008) 'The aryl hydrocarbon receptor complex and the control of gene expression', *Crit Rev Eukaryot Gene Expr*, 18(3), pp. 207-50.

Bell, C.C., Hendriks, D.F., Moro, S.M., Ellis, E., Walsh, J., Renblom, A., Fredriksson Puigvert, L., Dankers, A.C., Jacobs, F., Snoeys, J., Sison-Young, R.L., Jenkins, R.E., Nordling, A., Mkrtchian, S., Park, B.K., Kitteringham, N.R., Goldring, C.E., Lauschke, V.M. and Ingelman-Sundberg, M. (2016) 'Characterization of primary human hepatocyte spheroids as a model system for drug-induced liver injury, liver function and disease', *Sci Rep*, 6, p. 25187.

Bellentani, S., Scaglioni, F., Marino, M. and Bedogni, G. (2010) 'Epidemiology of non-alcoholic fatty liver disease', *Dig Dis*, 28(1), pp. 155-61.

Bergheim, I., Weber, S., Vos, M., Kramer, S., Volynets, V., Kaserouni, S., McClain, C.J. and Bischoff, S.C. (2008) 'Antibiotics protect against fructose-induced hepatic lipid accumulation in mice: role of endotoxin', *J Hepatol*, 48(6), pp. 983-92.

Berthois, Y., Katzenellenbogen, J.A. and Katzenellenbogen, B.S. (1986) 'Phenol red in tissue culture media is a weak estrogen: implications concerning the study of estrogen-responsive cells in culture', *Proc Natl Acad Sci U S A*, 83(8), pp. 2496-500.

Beuers, U., Gershwin, M.E., Gish, R.G., Invernizzi, P., Jones, D.E., Lindor, K., Ma, X., Mackay, I.R., Pares, A., Tanaka, A., Vierling, J.M. and Poupon, R. (2015) 'Changing nomenclature for PBC: From 'cirrhosis' to 'cholangitis'', *J Hepatol*, 63(5), pp. 1285-7.

Beuers, U., Hohenester, S., de Buy Wenniger, L.J., Kremer, A.E., Jansen, P.L. and Elferink, R.P. (2010) 'The biliary HCO(3)(-) umbrella: a unifying hypothesis on pathogenetic and therapeutic aspects of fibrosing cholangiopathies', *Hepatology*, 52(4), pp. 1489-96.

Beuers, U., Kremer, A.E., Bolier, R. and Elferink, R.P. (2014) 'Pruritus in cholestasis: facts and fiction', *Hepatology*, 60(1), pp. 399-407.

Bełtowski, J. (2008) 'Liver X Receptors (LXR) as Therapeutic Targets in Dyslipidemia', *Cardiovascular Therapeutics*, 26(4), pp. 297-316.

Bianchi, I., Lleo, A., Gershwin, M.E. and Invernizzi, P. (2012) 'The X chromosome and immune associated genes', *J Autoimmun*, 38(2-3), pp. J187-92.

Bjornsson, E.S. (2015) 'Drug-induced liver injury: an overview over the most critical compounds', *Arch Toxicol*, 89(3), pp. 327-34.

Bogaards, J.J., Bertrand, M., Jackson, P., Oudshoorn, M.J., Weaver, R.J., van Bladeren, P.J. and Walther, B. (2000) 'Determining the best animal model for human cytochrome P450 activities: a comparison of mouse, rat, rabbit, dog, micropig, monkey and man', *Xenobiotica*, 30(12), pp. 1131-52.

Bogdanos, D.P., Baum, H., Grasso, A., Okamoto, M., Butler, P., Ma, Y., Rigopoulou, E., Montalto, P., Davies, E.T., Burroughs, A.K. and Vergani, D. (2004) 'Microbial mimics are major targets of crossreactivity with human pyruvate dehydrogenase in primary biliary cirrhosis', *J Hepatol*, 40(1), pp. 31-9.

Bondesson, M., Hao, R., Lin, C.Y., Williams, C. and Gustafsson, J.A. (2015) 'Estrogen receptor signaling during vertebrate development', *Biochim Biophys Acta*, 1849(2), pp. 142-51.

Bonner-Weir, S., Trent, D.F. and Weir, G.C. (1983) 'Partial pancreatectomy in the rat and subsequent defect in glucose-induced insulin release', *J Clin Invest*, 71(6), pp. 1544-53.

Bowlus, C.L. and Gershwin, M.E. (2014) 'The diagnosis of primary biliary cirrhosis', *Autoimmun Rev*, 13(4-5), pp. 441-4.

Brand, M.D. and Nicholls, D.G. (2011) 'Assessing mitochondrial dysfunction in cells', *Biochem J*, 435(2), pp. 297-312.

Browning, J.D. and Horton, J.D. (2004) 'Molecular mediators of hepatic steatosis and liver injury', *J Clin Invest*, 114(2), pp. 147-52.

Bruggraber, S.F., Leung, P.S., Amano, K., Quan, C., Kurth, M.J., Nantz, M.H., Benson, G.D., Van de Water, J., Luketic, V., Roche, T.E., Ansari, A.A., Coppel, R.L. and Gershwin, M.E. (2003) 'Autoreactivity to lipoate and a conjugated form of lipoate in primary biliary cirrhosis', *Gastroenterology*, 125(6), pp. 1705-13.

Burke, Z.D., Shen, C.N., Ralphs, K.L. and Tosh, D. (2006) 'Characterization of liver function in transdifferentiated hepatocytes', *J Cell Physiol*, 206(1), pp. 147-59.

Calkin, A.C. and Tontonoz, P. (2012) 'Transcriptional integration of metabolism by the nuclear sterol-activated receptors LXR and FXR', *Nat Rev Mol Cell Biol*, 13(4), pp. 213-24.

Cani, P.D. and Everard, A. (2015) 'Keeping gut lining at bay: impact of emulsifiers', *Trends Endocrinol Metab*, 26(6), pp. 273-4.

Cani, P.D., Possemiers, S., Van de Wiele, T., Guiot, Y., Everard, A., Rottier, O., Geurts, L., Naslain, D., Neyrinck, A., Lambert, D.M., Muccioli, G.G. and Delzenne, N.M. (2009) 'Changes in gut microbiota control inflammation in obese mice through a mechanism involving GLP-2-driven improvement of gut permeability', *Gut*, 58(8), pp. 1091-103.

Carlsen, H., Moskaug, J.O., Fromm, S.H. and Blomhoff, R. (2002) 'In vivo imaging of NF-kappa B activity', *J Immunol*, 168(3), pp. 1441-6.

Ceni, E., Mello, T. and Galli, A. (2014) 'Pathogenesis of alcoholic liver disease: role of oxidative metabolism', *World J Gastroenterol*, 20(47), pp. 17756-72.

Cha, J.Y. and Repa, J.J. (2007) 'The liver X receptor (LXR) and hepatic lipogenesis. The carbohydrate-response element-binding protein is a target gene of LXR', *J Biol Chem*, 282(1), pp. 743-51.

Chakravarthy, M.V., Lodhi, I.J., Yin, L., Malapaka, R.R., Xu, H.E., Turk, J. and Semenkovich, C.F. (2009) 'Identification of a physiologically relevant endogenous ligand for PPARalpha in liver', *Cell*, 138(3), pp. 476-88.

Chang, B.H., Li, L., Paul, A., Taniguchi, S., Nannegari, V., Heird, W.C. and Chan, L. (2006) 'Protection against fatty liver but normal adipogenesis in mice lacking adipose differentiation-related protein', *Mol Cell Biol*, 26(3), pp. 1063-76.

Chang, T.T. and Hughes-Fulford, M. (2009) 'Monolayer and spheroid culture of human liver hepatocellular carcinoma cell line cells demonstrate distinct global gene expression patterns and functional phenotypes', *Tissue Eng Part A*, 15(3), pp. 559-67.

Chassaing, B., Koren, O., Goodrich, J.K., Poole, A.C., Srinivasan, S., Ley, R.E. and Gewirtz, A.T. (2015) 'Dietary emulsifiers impact the mouse gut microbiota promoting colitis and metabolic syndrome', *Nature*, 519(7541), pp. 92-6.

Chatman, L.A., Morton, D., Johnson, T.O. and Anway, S.D. (2009) 'A strategy for risk management of drug-induced phospholipidosis', *Toxicol Pathol*, 37(7), pp. 997-1005.

Christophe, J. (1994) 'Pancreatic tumoral cell line AR42J: an amphicrine model', *Am J Physiol*, 266(6 Pt 1), pp. G963-71.

Chuang, Y.H., Lian, Z.X., Yang, G.X., Shu, S.A., Moritoki, Y., Ridgway, W.M., Ansari, A.A., Kronenberg, M., Flavell, R.A., Gao, B. and Gershwin, M.E. (2008) 'Natural killer T cells exacerbate liver injury in a transforming growth factor beta receptor II dominant-negative mouse model of primary biliary cirrhosis', *Hepatology*, 47(2), pp. 571-80.

Clemens, D.L., Halgard, C.M., Miles, R.R., Sorrell, M.F. and Tuma, D.J. (1995) 'Establishment of a recombinant hepatic cell line stably expressing alcohol dehydrogenase', *Arch Biochem Biophys*, 321(2), pp. 311-8.

Corpechot, C., Chretien, Y., Chazouilleres, O. and Poupon, R. (2010) 'Demographic, lifestyle, medical and familial factors associated with primary biliary cirrhosis', *J Hepatol*, 53(1), pp. 162-9.

Cowley, S.M., Hoare, S., Mosselman, S. and Parker, M.G. (1997) 'Estrogen receptors α and β form heterodimers on DNA', *Journal of Biological Chemistry*, 272(32), pp. 19858-19862.

Crichton, Paul G., Parker, N., Vidal-Puig, Antonio J. and Brand, Martin D. (2009) 'Not all mitochondrial carrier proteins support permeability transition pore formation: no involvement of uncoupling protein 1', *Bioscience Reports*, 30(Pt 3), pp. 187-192.

Criddle, D.N., Gillies, S., Baumgartner-Wilson, H.K., Jaffar, M., Chinje, E.C., Passmore, S., Chvanov, M., Barrow, S., Gerasimenko, O.V., Tepikin, A.V., Sutton, R. and Petersen, O.H. (2006) 'Menadione-induced reactive oxygen species generation via redox cycling promotes apoptosis of murine pancreatic acinar cells', *J Biol Chem*, 281(52), pp. 40485-92.

Dancygier, H. (2009) *Clinical Hepatology: Principles and Practice of Hepatobiliary Diseases*. Springer Berlin Heidelberg.

Daniel, E., Aylwin, S., Mustafa, O., Ball, S., Munir, A., Boelaert, K., Chortis, V., Cuthbertson, D.J., Daousi, C., Rajeev, S.P., Davis, J., Cheer, K., Drake, W., Gunganah, K., Grossman, A., Gurnell, M., Powlson, A.S., Karavitaki, N., Huguet, I., Kearney, T., Mohit, K., Meeran, K., Hill, N., Rees, A., Lansdown, A.J., Trainer, P.J., Minder, A.-E.H. and Newell-Price, J. (2015) 'Effectiveness of Metyrapone in Treating Cushing's Syndrome: A Retrospective Multicenter Study in 195 Patients', *The Journal of clinical endocrinology and metabolism*, 100(11), pp. 4146-4154.

Dara, L., Ji, C. and Kaplowitz, N. (2011) 'The contribution of endoplasmic reticulum stress to liver diseases', *Hepatology*, 53(5), pp. 1752-63.

Day, C.P. (2012) 'Clinical Spectrum and Therapy of Non-Alcoholic Steatohepatitis', *Digestive Diseases*, 30(suppl 1)(Suppl. 1), pp. 69-73.

de Graaf, E.L., Kench, J., Dilworth, P., Shackel, N.A., Strasser, S.I., Joseph, D., Pleass, H., Crawford, M., McCaughan, G.W. and Verran, D.J. (2012) 'Grade of deceased donor liver macrovesicular steatosis impacts graft and recipient outcomes more than the Donor Risk Index', *J Gastroenterol Hepatol*, 27(3), pp. 540-6.

di Masi, A., De Marinis, E., Ascenzi, P. and Marino, M. (2009) 'Nuclear receptors CAR and PXR: Molecular, functional, and biomedical aspects', *Mol Aspects Med*, 30(5), pp. 297-343.

Diamanti-Kandarakis, E., Bourguignon, J.P., Giudice, L.C., Hauser, R., Prins, G.S., Soto, A.M., Zoeller, R.T. and Gore, A.C. (2009) 'Endocrine-disrupting chemicals: an Endocrine Society scientific statement', *Endocr Rev*, 30(4), pp. 293-342.

Ding, X., Saxena, N.K., Lin, S., Xu, A., Srinivasan, S. and Anania, F.A. (2005) 'The roles of leptin and adiponectin: a novel paradigm in adipocytokine regulation of liver fibrosis and stellate cell biology', *Am J Pathol*, 166(6), pp. 1655-69.

Donaldson, P.T., Baragiotta, A., Heneghan, M.A., Floreani, A., Venturi, C., Underhill, J.A., Jones, D.E., James, O.F. and Bassendine, M.F. (2006) 'HLA class II alleles, genotypes, haplotypes, and amino acids in primary biliary cirrhosis: a large-scale study', *Hepatology*, 44(3), pp. 667-74.

Donnelly, K.L., Smith, C.I., Schwarzenberg, S.J., Jessurun, J., Boldt, M.D. and Parks, E.J. (2005) 'Sources of fatty acids stored in liver and secreted via lipoproteins in patients with nonalcoholic fatty liver disease', *J Clin Invest*, 115(5), pp. 1343-51.

Dooley, S. and ten Dijke, P. (2012) 'TGF-β in progression of liver disease', in *Cell Tissue Res*. Berlin/Heidelberg, pp. 245-56.

Douglass, A., Wallace, K., Parr, R., Park, J., Durward, E., Broadbent, I., Barelle, C., Porter, A.J. and Wright, M.C. (2008) 'Antibody-targeted myofibroblast apoptosis reduces fibrosis during sustained liver injury', *Journal of Hepatology*, 49(1), pp. 88-98.

Duarte-Rey, C., Bogdanos, D., Yang, C.Y., Roberts, K., Leung, P.S., Anaya, J.M., Worman, H.J. and Gershwin, M.E. (2012) 'Primary biliary cirrhosis and the nuclear pore complex', *Autoimmun Rev*, 11(12), pp. 898-902.

EFSA (2012) 'Guidance on selected default values to be used by the EFSA Scientific Committee, Scientific Panels and Units in the absence of actual measured data', *EFSA Journal*, 10(3), p. 2579.

Enomoto, N., Ikejima, K., Yamashina, S., Hirose, M., Shimizu, H., Kitamura, T., Takei, Y., Sato And, N. and Thurman, R.G. (2001) 'Kupffer cell sensitization by alcohol involves increased permeability to gut-derived endotoxin', *Alcohol Clin Exp Res*, 25(6 Suppl), pp. 51s-4s.

Fairhall, E.A., Charles, M.A., Probert, P.M., Wallace, K., Gibb, J., Ravindan, C., Soloman, M. and Wright, M.C. (2016) 'Pancreatic B-13 Cell Trans-Differentiation to Hepatocytes Is Dependent on Epigenetic-Regulated Changes in Gene Expression', *PLoS One*, 11(3), p. e0150959.

Fairhall, E.A., Charles, M.A., Wallace, K., Schwab, C.J., Harrison, C.J., Richter, M., Hoffmann, S.A., Charlton, K.A., Zeilinger, K. and Wright, M.C. (2013a) 'The B-13 hepatocyte progenitor cell resists pluripotency induction and differentiation to non-hepatocyte cells', *Toxicology Research*, 2(5), pp. 308-320.

Fairhall, E.A., Wallace, K., White, S.A., Huang, G.C., Shaw, J.A., Wright, S.C., Charlton, K.A., Burt, A.D. and Wright, M.C. (2013b) 'Adult human exocrine pancreas differentiation to hepatocytes - potential source of a human hepatocyte progenitor for use in toxicology research', *Toxicology Research*, 2(1), pp. 80-87.

Farfan Labonne, B.E., Gutierrez, M., Gomez-Quiroz, L.E., Konigsberg Fainstein, M., Bucio, L., Souza, V., Flores, O., Ortiz, V., Hernandez, E., Kershenobich, D. and Gutierrez-Ruiz, M.C. (2009) 'Acetaldehyde-induced mitochondrial dysfunction sensitizes hepatocytes to oxidative damage', *Cell Biol Toxicol*, 25(6), pp. 599-609.

Ferreyra, C., Vargas, F., Rodríguez-Gómez, I., Pérez-Abud, R., O'Valle, F. and Osuna, A. (2013) 'Preconditioning with Triiodothyronine Improves the Clinical Signs and Acute Tubular Necrosis Induced by Ischemia/Reperfusion in Rats', *PLoS ONE*, 8(9), p. e74960.

Fishbein, T.M., Fiel, M.I., Emre, S., Cubukcu, O., Guy, S.R., Schwartz, M.E., Miller, C.M. and Sheiner, P.A. (1997) 'Use of livers with microvesicular fat safely expands the donor pool', *Transplantation*, 64(2), pp. 248-51.

Fontana, R.J. (2014) 'Pathogenesis of idiosyncratic drug-induced liver injury and clinical perspectives', *Gastroenterology*, 146(4), pp. 914-28.

Fraczek, J., Bolleyn, J., Vanhaecke, T., Rogiers, V. and Vinken, M. (2013) 'Primary hepatocyte cultures for pharmaco-toxicological studies: at the busy crossroad of various anti-dedifferentiation strategies', *Arch Toxicol*, 87(4), pp. 577-610.

Francavilla, A., Polimeno, L., Dileo, A., Barone, M., Ove, P., Coetzee, M., Eagon, P., Makowka, L., Ambrosino, G., Mazzaferro, V. and Starzl Thomas, E. (1989) 'The effect of estrogen and tamoxifen on hepatocyte proliferation in Vivo and in Vitro', *Hepatology*, 9(4), pp. 614-620.

Franklin, M.R. and Hathaway, L.B. (2008) '2-Diethylaminoethyl-2,2-diphenylvalerate-HCl (SKF525A) revisited: comparative cytochrome P450 inhibition in human liver microsomes by SKF525A, its metabolites, and SKF-acid and SKF-alcohol', *Drug Metab Dispos*, 36(12), pp. 2539-46.

Friedman, S.L. (2008) 'Mechanisms of hepatic fibrogenesis', *Gastroenterology*, 134(6), pp. 1655-69.

Fujimura, H., Dekura, E., Kurabe, M., Shimazu, N., Koitabashi, M. and Toriumi, W. (2007) 'Cell-based fluorescence assay for evaluation of new-drugs potential for phospholipidosis in an early stage of drug development', *Exp Toxicol Pathol*, 58(6), pp. 375-82.

Gao, B. and Bataller, R. (2011) 'Alcoholic liver disease: pathogenesis and new therapeutic targets', *Gastroenterology*, 141(5), pp. 1572-85.

Gerets, H.H., Tilmant, K., Gerin, B., Chanteux, H., Depelchin, B.O., Dhalluin, S. and Atienzar, F.A. (2012) 'Characterization of primary human hepatocytes, HepG2 cells, and HepaRG cells at the mRNA level and CYP activity in response to inducers and their predictivity for the detection of human hepatotoxins', *Cell Biol Toxicol*, 28(2), pp. 69-87.

Gershwin, M.E., Selmi, C., Worman, H.J., Gold, E.B., Watnik, M., Utts, J., Lindor, K.D., Kaplan, M.M. and Vierling, J.M. (2005) 'Risk factors and comorbidities in primary biliary cirrhosis: a controlled interview-based study of 1032 patients', *Hepatology*, 42(5), pp. 1194-202.

Ghany, M.G., Strader, D.B., Thomas, D.L. and Seeff, L.B. (2009) 'Diagnosis, management, and treatment of hepatitis C: an update', *Hepatology*, 49(4), pp. 1335-74.

Glaser, S.S., Gaudio, E., Miller, T., Alvaro, D. and Alpini, G. (2009) 'Cholangiocyte proliferation and liver fibrosis', *Expert Rev Mol Med*, 11, p. e7.

Glock, M., Muehlbacher, M., Hurtig, H., Tripal, P. and Kornhuber, J. (2016) 'Drug-induced phospholipidosis caused by combinations of common drugs in vitro', *Toxicol In Vitro*, 35, pp. 139-48.

Goldring, C., Antoine, D.J., Bonner, F., Crozier, J., Denning, C., Fontana, R.J., Hanley, N.A., Hay, D.C., Ingelman-Sundberg, M., Juhila, S., Kitteringham, N., Silva-Lima, B., Norris, A., Pridgeon, C., Ross, J.A., Young, R.S., Tagle, D., Tornesi, B., van de Water, B., Weaver, R.J., Zhang, F. and Park, B.K. (2017) 'Stem cell-derived models to improve mechanistic understanding and prediction of human drug-induced liver injury', *Hepatology*, 65(2), pp. 710-721.

Gomez-Lechon, M.J. and Tolosa, L. (2016) 'Human hepatocytes derived from pluripotent stem cells: a promising cell model for drug hepatotoxicity screening', *Arch Toxicol*, 90(9), pp. 2049-61.

Gomez-Lechon, M.J., Tolosa, L. and Donato, M.T. (2016) 'Metabolic activation and drug-induced liver injury: in vitro approaches for the safety risk assessment of new drugs', *J Appl Toxicol*, 36(6), pp. 752-68.

Green, S., Walter, P., Kumar, V., Krust, A., Bornert, J.M., Argos, P. and Chambon, P. (1986) 'Human oestrogen receptor cDNA: sequence, expression and homology to v-erb-A', *Nature*, 320(6058), pp. 134-9.

Gripon, P., Rumin, S., Urban, S., Le Seyec, J., Glaise, D., Cannie, I., Guyomard, C., Lucas, J., Trepo, C. and Guguen-Guillouzo, C. (2002) 'Infection of a human hepatoma cell line by hepatitis B virus', *Proc Natl Acad Sci U S A*, 99(24), pp. 15655-60.

Guguen-Guillouzo, C. and Guillouzo, A. (2010) 'General review on in vitro hepatocyte models and their applications', *Methods Mol Biol*, 640, pp. 1-40.

Guo, L., Dial, S., Shi, L., Branham, W., Liu, J., Fang, J.L., Green, B., Deng, H., Kaput, J. and Ning, B. (2011) 'Similarities and differences in the expression of drug-metabolizing enzymes between human hepatic cell lines and primary human hepatocytes', *Drug Metab Dispos*, 39(3), pp. 528-38.

Habs, M., Shubik, P. and Eisenbrand, G. (1986) 'Carcinogenicity of methapyrilene hydrochloride, mepyramine hydrochloride, thenyldiamine hydrochloride, and pyribenzamine hydrochloride in Sprague-Dawley rats', *Journal of Cancer Research and Clinical Oncology*, 111(1), pp. 71-74.

Halliwell, W.H. (1997) 'Cationic amphiphilic drug-induced phospholipidosis', *Toxicol Pathol*, 25(1), pp. 53-60.

Hammes, S.R. and Levin, E.R. (2007) 'Extranuclear steroid receptors: nature and actions', *Endocr Rev*, 28(7), pp. 726-41.

Hankinson, O. (1995) 'The aryl hydrocarbon receptor complex', *Annu Rev Pharmacol Toxicol*, 35, pp. 307-40.

Hardy, T., Oakley, F., Anstee, Q.M. and Day, C.P. (2016) 'Nonalcoholic Fatty Liver Disease: Pathogenesis and Disease Spectrum', *Annu Rev Pathol*, 11, pp. 451-96.

Hasegawa, M., Kapelyukh, Y., Tahara, H., Seibler, J., Rode, A., Krueger, S., Lee, D.N., Wolf, C.R. and Scheer, N. (2011) 'Quantitative prediction of human pregnane X receptor and cytochrome P450 3A4 mediated drug-drug interaction in a novel multiple humanized mouse line', *Mol Pharmacol*, 80(3), pp. 518-28.

Heckenbach, M.E., Romero, F.N., Green, M.D. and Halden, R.U. (2016) 'Meta-analysis of ionic liquid literature and toxicology', *Chemosphere*, 150, pp. 266-274.

Hengstler, J.G., Utesch, D., Steinberg, P., Platt, K.L., Diener, B., Ringel, M., Swales, N., Fischer, T., Biefang, K., Gerl, M., Bottger, T. and Oesch, F. (2000) 'Cryopreserved primary hepatocytes as a constantly available in vitro model for the evaluation of human and animal drug metabolism and enzyme induction', *Drug Metab Rev*, 32(1), pp. 81-118.

Hernandez-Gea, V. and Friedman, S.L. (2011) 'Pathogenesis of liver fibrosis', *Annu Rev Pathol*, 6, pp. 425-56.

Hiraoka, M., Abe, A., Lu, Y., Yang, K., Han, X., Gross, R.W. and Shayman, J.A. (2006) 'Lysosomal phospholipase A2 and phospholipidosis', *Mol Cell Biol*, 26(16), pp. 6139-48.

Hirschfield, G.M., Dyson, J.K., Alexander, G.J.M., Chapman, M.H., Collier, J., Hubscher, S., Patanwala, I., Pereira, S.P., Thain, C., Thorburn, D., Tiniakos, D., Walmsley, M., Webster, G. and Jones, D.E.J. (2018) 'The British Society of Gastroenterology/UK-PBC primary biliary cholangitis treatment and management guidelines', *Gut*.

Hirschfield, G.M. and Gershwin, M.E. (2013) 'The immunobiology and pathophysiology of primary biliary cirrhosis', *Annu Rev Pathol*, 8, pp. 303-30.

Hirschfield, G.M., Mason, A., Luketic, V., Lindor, K., Gordon, S.C., Mayo, M., Kowdley, K.V., Vincent, C., Bodhenheimer, H.C., Jr., Pares, A., Trauner, M., Marschall, H.U., Adorini, L., Sciacca, C., Beecher-Jones, T., Castelloe, E., Bohm, O. and Shapiro, D. (2015) 'Efficacy of obeticholic acid in patients with primary biliary cirrhosis and inadequate response to ursodeoxycholic acid', *Gastroenterology*, 148(4), pp. 751-61.e8.

Honkakoski, P. and Negishi, M. (2000) 'Regulation of cytochrome P450 (CYP) genes by nuclear receptors', *Biochem J*, 347(Pt 2), pp. 321-37.

Houck, K.A., Borchert, K.M., Hepler, C.D., Thomas, J.S., Bramlett, K.S., Michael, L.F. and Burris, T.P. (2004) 'T0901317 is a dual LXR/FXR agonist', *Molecular Genetics and Metabolism*, 83(1), pp. 184-187.

Huch, M., Gehart, H., van Boxtel, R., Hamer, K., Blokzijl, F., Verstegen, M.M., Ellis, E., van Wenum, M., Fuchs, S.A., de Ligt, J., van de Wetering, M., Sasaki, N., Boers, S.J., Kemperman, H., de Jonge, J., Ijzermans, J.N., Nieuwenhuis, E.E., Hoekstra, R., Strom, S., Vries, R.R., van der Laan, L.J., Cuppen, E. and Clevers, H. (2015) 'Long-term culture of genome-stable bipotent stem cells from adult human liver', *Cell*, 160(1-2), pp. 299-312.

Invernizzi, P., Miozzo, M., Battezzati, P.M., Bianchi, I., Grati, F.R., Simoni, G., Selmi, C., Watnik, M., Gershwin, M.E. and Podda, M. (2004) 'Frequency of monosomy X in women with primary biliary cirrhosis', *Lancet*, 363(9408), pp. 533-5.

Invernizzi, P., Ransom, M., Raychaudhuri, S., Kosoy, R., Lleo, A., Shigeta, R., Franke, A., Bossa, F., Amos, C.I., Gregersen, P.K., Siminovitch, K.A., Cusi, D., de Bakker, P.I., Podda, M., Gershwin, M.E. and Seldin, M.F. (2012) 'Classical HLA-DRB1 and DPB1 alleles account for HLA associations with primary biliary cirrhosis', *Genes Immun*, 13(6), pp. 461-8.

Invernizzi, P., Selmi, C. and Gershwin, M.E. (2010) 'Update on primary biliary cirrhosis', *Dig Liver Dis*, 42(6), pp. 401-8.

Iredale, J.P., Benyon, R.C., Pickering, J., McCullen, M., Northrop, M., Pawley, S., Hovell, C. and Arthur, M.J. (1998) 'Mechanisms of spontaneous resolution of rat liver fibrosis. Hepatic stellate cell apoptosis and reduced hepatic expression of metalloproteinase inhibitors', *Journal of Clinical Investigation*, 102(3), pp. 538-549.

Issa, R., Williams, E., Trim, N., Kendall, T., Arthur, M.J., Reichen, J., Benyon, R.C. and Iredale, J.P. (2001) 'Apoptosis of hepatic stellate cells: involvement in resolution of biliary fibrosis and regulation by soluble growth factors', *Gut*, 48(4), pp. 548-57.

James, L.P., Mayeux, P.R. and Hinson, J.A. (2003) 'Acetaminophen-induced hepatotoxicity', *Drug Metab Dispos*, 31(12), pp. 1499-506.

Jennen, D.G., Magkoufopoulou, C., Ketelslegers, H.B., van Herwijnen, M.H., Kleinjans, J.C. and van Delft, J.H. (2010) 'Comparison of HepG2 and HepaRG by whole-genome gene expression analysis for the purpose of chemical hazard identification', *Toxicol Sci*, 115(1), pp. 66-79.

Johnson, E.F., Hsu, M.H., Savas, U. and Griffin, K.J. (2002) 'Regulation of P450 4A expression by peroxisome proliferator activated receptors', *Toxicology*, 181-182, pp. 203-6.

Jones, D.E. (2007) 'Pathogenesis of primary biliary cirrhosis', *Gut*, 56(11), pp. 1615-24.

Jungnickel, C., Łuczak, J., Ranke, J., Fernández, J.F., Müller, A. and Thöming, J. (2008) 'Micelle formation of imidazolium ionic liquids in aqueous solution', *Colloids and Surfaces A: Physicochemical and Engineering Aspects*, 316(1-3), pp. 278-284.

Kao, T.L., Kuan, Y.P., Cheng, W.C., Chang, W.C., Jeng, L.B., Yeh, S. and Ma, W.L. (2018) 'Estrogen receptors orchestrate cell growth and differentiation to facilitate liver regeneration', *Theranostics*, 8(10), pp. 2672-2682.

Kaplan, M.M. and Gershwin, M.E. (2005) 'Primary biliary cirrhosis', *N Engl J Med*, 353(12), pp. 1261-73.

Kasahara, T., Tomita, K., Murano, H., Harada, T., Tsubakimoto, K., Ogihara, T., Ohnishi, S. and Kakinuma, C. (2006) 'Establishment of an in vitro high-throughput screening assay for detecting phospholipidosis-inducing potential', *Toxicol Sci*, 90(1), pp. 133-41.

Ke, P.Y. and Chen, S.S. (2012) 'Hepatitis C virus and cellular stress response: implications to molecular pathogenesis of liver diseases', *Viruses*, 4(10), pp. 2251-90.

Khanna, A. and Jones, D.E. (2017) 'Novel strategies and therapeutic options for the management of primary biliary cholangitis', *Therap Adv Gastroenterol*, 10(10), pp. 791-803.

Kia, R., Sison, R.L., Heslop, J., Kitteringham, N.R., Hanley, N., Mills, J.S., Park, B.K. and Goldring, C.E. (2013) 'Stem cell-derived hepatocytes as a predictive model for drug-induced liver injury: are we there yet?', *Br J Clin Pharmacol*, 75(4), pp. 885-96.

Kita, H., Matsumura, S., He, X.S., Ansari, A.A., Lian, Z.X., Van de Water, J., Coppel, R.L., Kaplan, M.M. and Gershwin, M.E. (2002) 'Quantitative and functional analysis of PDC-E2-specific autoreactive cytotoxic T lymphocytes in primary biliary cirrhosis', *J Clin Invest*, 109(9), pp. 1231-40.

Klaunig, J.E., Babich, M.A., Baetcke, K.P., Cook, J.C., Corton, J.C., David, R.M., DeLuca, J.G., Lai, D.Y., McKee, R.H., Peters, J.M., Roberts, R.A. and Fenner-Crisp, P.A. (2003) 'PPARalpha agonist-induced rodent tumors: modes of action and human relevance', *Crit Rev Toxicol*, 33(6), pp. 655-780.

Kleine, M., Riemer, M., Krech, T., DeTemple, D., Jager, M.D., Lehner, F., Manns, M.P., Klempnauer, J., Borlak, J., Bektas, H. and Vondran, F.W. (2014) 'Explanted diseased livers - a possible source of metabolic competent primary human hepatocytes', *PLoS One*, 9(7), p. e101386.

Klinge, C.M. (2001) 'Estrogen receptor interaction with estrogen response elements', *Nucleic Acids Res*, 29(14), pp. 2905-19.

Kotokorpi, P., Ellis, E., Parini, P., Nilsson, L.M., Strom, S., Steffensen, K.R., Gustafsson, J.A. and Mode, A. (2007) 'Physiological differences between human and rat primary hepatocytes in response to liver X receptor activation by 3-[3-[N-(2-chloro-3-trifluoromethylbenzyl)-(2,2-diphenylethyl)amino]propyloxy]phe nylacetic acid hydrochloride (GW3965)', *Mol Pharmacol*, 72(4), pp. 947-55.

Krizhanovsky, V., Yon, M., Dickins, R.A., Hearn, S., Simon, J., Miething, C., Yee, H., Zender, L. and Lowe, S.W. (2008) 'Senescence of activated stellate cells limits liver fibrosis', *Cell*, 134(4), pp. 657-67.

Kuntz, E. and Kuntz, H.D. (2009) *Hepatology: Textbook and Atlas*. Springer Berlin Heidelberg.

Kurash, J.K., Shen, C.N. and Tosh, D. (2004) 'Induction and regulation of acute phase proteins in transdifferentiated hepatocytes', *Exp Cell Res*, 292(2), pp. 342-58.

Kuribayashi, S., Goto, K., Naito, S., Kamataki, T. and Yamazaki, H. (2009) 'Human cytochrome P450 1A2 involvement in the formation of reactive metabolites from a species-specific hepatotoxic pyrazolopyrimidine derivative, 5-n-butyl-7-(3,4,5-trimethoxybenzoylamino)pyrazolo[1,5-a]pyrimidine', *Chem Res Toxicol*, 22(2), pp. 323-31.

Kyffin, J.A., Sharma, P., Leedale, J., Colley, H.E., Murdoch, C., Mistry, P. and Webb, S.D. (2018) 'Impact of cell types and culture methods on the functionality of in vitro liver systems - A review of cell systems for hepatotoxicity assessment', *Toxicol In Vitro*, 48, pp. 262-275.

Lan, R.Y., Cheng, C., Lian, Z.X., Tsuneyama, K., Yang, G.X., Moritoki, Y., Chuang, Y.H., Nakamura, T., Saito, S., Shimoda, S., Tanaka, A., Bowlus, C.L., Takano, Y., Ansari, A.A., Coppel, R.L. and Gershwin, M.E. (2006) 'Liver-targeted and peripheral blood alterations of regulatory T cells in primary biliary cirrhosis', *Hepatology*, 43(4), pp. 729-37.

Larosche, I., Letteron, P., Fromenty, B., Vadrot, N., Abbey-Toby, A., Feldmann, G., Pessayre, D. and Mansouri, A. (2007) 'Tamoxifen inhibits topoisomerases, depletes mitochondrial DNA, and triggers steatosis in mouse liver', *J Pharmacol Exp Ther*, 321(2), pp. 526-35.

Lee, H.J., Yeon, J.E., Ko, E.J., Yoon, E.L., Suh, S.J., Kang, K., Kim, H.R., Kang, S.H., Yoo, Y.J., Je, J., Lee, B.J., Kim, J.H., Seo, Y.S., Yim, H.J. and Byun, K.S. (2015) 'Peroxisome proliferator-activated receptor-delta agonist ameliorated inflammasome activation in nonalcoholic fatty liver disease', *World J Gastroenterol*, 21(45), pp. 12787-99.

Leite, S.B., Wilk-Zasadna, I., Zaldivar, J.M., Airola, E., Reis-Fernandes, M.A., Mennecozzi, M., Guguen-Guillouzo, C., Chesne, C., Guillou, C., Alves, P.M. and Coecke, S. (2012) 'Three-dimensional HepaRG model as an attractive tool for toxicity testing', *Toxicol Sci*, 130(1), pp. 106-16.

Leung, P.S., Quan, C., Park, O., Van de Water, J., Kurth, M.J., Nantz, M.H., Ansari, A.A., Coppel, R.L., Lam, K.S. and Gershwin, M.E. (2003) 'Immunization with a xenobiotic 6-bromohexanoate bovine serum albumin conjugate induces antimitochondrial antibodies', *J Immunol*, 170(10), pp. 5326-32.

Li, T.K. and Theorell, H. (1969) 'Human liver alcohol dehydrogenase: inhibition by pyrazole and pyrazole analogs', *Acta Chem Scand*, 23(3), pp. 892-902.

Li, X., Ma, J., Jing, C. and Wang, J. (2013) 'Expression alterations of cytochromes P4501A1, 2E1, and 3A, and their receptors AhR and PXR caused by 1-octyl-3-methylimidazolium chloride in mouse mammary carcinoma cells', *Chemosphere*, 93(10), pp. 2488-92.

Li, X.-Y., Jing, C.-Q., Zang, X.-Y., Yang, S. and Wang, J.-J. (2012) 'Toxic cytological alteration and mitochondrial dysfunction in PC12 cells induced by 1-octyl-3-methylimidazolium chloride', *Toxicology in Vitro*, 26(7), pp. 1087-1092.

Liang, T.J. and Ghany, M.G. (2013) 'Current and future therapies for hepatitis C virus infection', *N Engl J Med*, 368(20), pp. 1907-17.

Liaskou, E., Hirschfield, G.M. and Gershwin, M.E. (2014) 'Mechanisms of tissue injury in autoimmune liver diseases', *Semin Immunopathol*, 36(5), pp. 553-68.

Liu, X., Chism, J.P., LeCluyse, E.L., Brouwer, K.R. and Brouwer, K.L. (1999) 'Correlation of biliary excretion in sandwich-cultured rat hepatocytes and in vivo in rats', *Drug Metab Dispos*, 27(6), pp. 637-44.

Liu, Y.L., Patman, G.L., Leathart, J.B., Piguet, A.C., Burt, A.D., Dufour, J.F., Day, C.P., Daly, A.K., Reeves, H.L. and Anstee, Q.M. (2014) 'Carriage of the PNPLA3 rs738409 C >G polymorphism confers an increased risk of non-alcoholic fatty liver disease associated hepatocellular carcinoma', *J Hepatol*, 61(1), pp. 75-81.

Lleo, A., Marzorati, S., Anaya, J.M. and Gershwin, M.E. (2017) 'Primary biliary cholangitis: a comprehensive overview', *Hepatol Int*, 11(6), pp. 485-499.

Longnecker, D.S., Lilja, H.S., French, J., Kuhlmann, E. and Noll, W. (1979) 'Transplantation of azaserine-induced carcinomas of pancreas in rats', *Cancer Lett*, 7(4), pp. 197-202.

Longnus, S.L., Wambolt, R.B., Parsons, H.L., Brownsey, R.W. and Allard, M.F. (2003) '5-Aminoimidazole-4-carboxamide 1-beta -D-ribofuranoside (AICAR) stimulates myocardial glycogenolysis by allosteric mechanisms', *Am J Physiol Regul Integr Comp Physiol*, 284(4), pp. R936-44.

Loor, G., Kondapalli, J., Schriewer, J.M., Chandel, N.S., Vanden Hoek, T.L. and Schumacker, P.T. (2010) 'Menadione triggers cell death through ROS-dependent mechanisms involving PARP activation without requiring apoptosis', *Free Radic Biol Med*, 49(12), pp. 1925-36.

Lu, W.Y., Bird, T.G., Boulter, L., Tsuchiya, A., Cole, A.M., Hay, T., Guest, R.V., Wojtacha, D., Man, T.Y., Mackinnon, A., Ridgway, R.A., Kendall, T., Williams, M.J., Jamieson, T., Raven, A., Hay, D.C., Iredale, J.P., Clarke, A.R., Sansom, O.J. and Forbes, S.J. (2015) 'Hepatic progenitor cells of biliary origin with liver repopulation capacity', *Nat Cell Biol*, 17(8), pp. 971-983.

Ma, Q. and Lu, A.Y. (2007) 'CYP1A induction and human risk assessment: an evolving tale of in vitro and in vivo studies', *Drug Metab Dispos*, 35(7), pp. 1009-16.

Malarkey, D.E., Johnson, K., Ryan, L., Boorman, G. and Maronpot, R.R. (2005) 'New insights into functional aspects of liver morphology', *Toxicol Pathol*, 33(1), pp. 27-34.

Marek, C.J., Cameron, G.A., Elrick, L.J., Hawksworth, G.M. and Wright, M.C. (2003) 'Generation of hepatocytes expressing functional cytochromes P450 from a pancreatic progenitor cell line in vitro', *Biochem J*, 370(Pt 3), pp. 763-9.

Markiewicz, M., Jungnickel, C. and Arp, H.P. (2013) 'Ionic liquid assisted dissolution of dissolved organic matter and PAHs from soil below the critical micelle concentration', *Environ Sci Technol*, 47(13), pp. 6951-8.

Markiewicz, M., Jungnickel, C., Cho, C.W. and Stolte, S. (2015) 'Mobility and biodegradability of an imidazolium based ionic liquid in soil and soil amended with waste sewage sludge', *Environ Sci Process Impacts*, 17(8), pp. 1462-9.

Marzioni, M., Torrice, A., Saccomanno, S., Rychlicki, C., Agostinelli, L., Pierantonelli, I., Rhonnstad, P., Trozzi, L., Apelqvist, T., Gentile, R., Candelaresi, C., Fava, G., Semeraro, R., Benedetti, A., Gaudio, E., Franchitto, A., Onori, P., De Minicis, S., Carpino, G., Kallin, E., Alvaro, D. and Nilsson, S. (2012) 'An oestrogen receptor beta-selective agonist exerts anti-neoplastic effects in experimental intrahepatic cholangiocarcinoma', *Dig Liver Dis*, 44(2), pp. 134-42.

Mashima, H., Ohnishi, H., Wakabayashi, K., Mine, T., Miyagawa, J., Hanafusa, T., Seno, M., Yamada, H. and Kojima, I. (1996a) 'Betacellulin and activin A coordinately convert amylase-secreting pancreatic AR42J cells into insulin-secreting cells', *J Clin Invest*, 97(7), pp. 1647-54.

Mashima, H., Shibata, H., Mine, T. and Kojima, I. (1996b) 'Formation of insulin-producing cells from pancreatic acinar AR42J cells by hepatocyte growth factor', *Endocrinology*, 137(9), pp. 3969-76.

Mattison, D.R., Karyakina, N., Goodman, M. and LaKind, J.S. (2014) 'Pharmaco- and toxicokinetics of selected exogenous and endogenous estrogens: a review of the data and identification of knowledge gaps', *Crit Rev Toxicol*, 44(8), pp. 696-724.

Mauvais-Jarvis, F., Clegg, D.J. and Hevener, A.L. (2013) 'The Role of Estrogens in Control of Energy Balance and Glucose Homeostasis', *Endocrine Reviews*, 34(3), pp. 309-338.

Mello, T., Ceni, E., Surrenti, C. and Galli, A. (2008) 'Alcohol induced hepatic fibrosis: role of acetaldehyde', *Mol Aspects Med*, 29(1-2), pp. 17-21.

Meyer, S.K., Probert, P.M., Lakey, A.K., Leitch, A.C., Blake, L.I., Jowsey, P.A., Cooke, M.P., Blain, P.G. and Wright, M.C. (2017a) 'Environmental Xenoestrogens Super-Activate a Variant Murine ER Beta in Cholangiocytes', *Toxicol Sci*, 156(1), pp. 54-71.

Meyer, S.K., Probert, P.M.E., Lakey, A.F., Axon, A.R., Leitch, A.C., Williams, F.M., Jowsey, P.A., Blain, P.G., Kass, G.E.N. and Wright, M.C. (2017b) 'Hepatic effects of tartrazine (E 102) after systemic exposure are independent of oestrogen receptor interactions in the mouse', *Toxicol Lett*, 273, pp. 55-68.

Michalopoulos, G.K. (2010) 'Liver Regeneration after Partial Hepatectomy: Critical Analysis of Mechanistic Dilemmas', *The American Journal of Pathology*, 176(1), pp. 2-13.

Miwa, S., St-Pierre, J., Partridge, L. and Brand, M.D. (2003) 'Superoxide and hydrogen peroxide production by Drosophila mitochondria', *Free Radic Biol Med*, 35(8), pp. 938-48.

Monga, S.P.S. and Cagle, P.T. (2010) *Molecular Pathology of Liver Diseases*. Springer US.

Morozov, V.A. and Lagaye, S. (2018) 'Hepatitis C virus: Morphogenesis, infection and therapy', *World J Hepatol*, 10(2), pp. 186-212.

Mousa, H.S., Lleo, A., Invernizzi, P., Bowlus, C.L. and Gershwin, M.E. (2015) 'Advances in pharmacotherapy for primary biliary cirrhosis', *Expert Opin Pharmacother*, 16(5), pp. 633-43.

Muehlbacher, M., Tripal, P., Roas, F. and Kornhuber, J. (2012) 'Identification of drugs inducing phospholipidosis by novel in vitro data', *ChemMedChem*, 7(11), pp. 1925-34.

Mutoh, S., Sobhany, M., Moore, R., Perera, L., Pedersen, L., Sueyoshi, T. and Negishi, M. (2013) 'Phenobarbital indirectly activates the constitutive active androstane receptor (CAR) by inhibition of epidermal growth factor receptor signaling', *Sci Signal*, 6(274), p. ra31.

Naik, A., Belic, A., Zanger, U.M. and Rozman, D. (2013) 'Molecular Interactions between NAFLD and Xenobiotic Metabolism', *Front Genet*, 4, p. 2.

Narayan, P., Duan, B., Jiang, K., Li, J., Paka, L., Yamin, M.A., Friedman, S.L., Weir, M.R. and Goldberg, I.D. (2016) 'Late intervention with the small molecule BB3 mitigates postischemic kidney injury', *American Journal of Physiology - Renal Physiology*, 311(2), pp. F352-F361.

Nativ, N.I., Yarmush, G., Chen, A., Dong, D., Henry, S.D., Guarrera, J.V., Klein, K.M., Maguire, T., Schloss, R., Berthiaume, F. and Yarmush, M.L. (2013) 'Rat hepatocyte culture model of macrosteatosis: effect of macrosteatosis induction and reversal on viability and liver-specific function', *J Hepatol*, 59(6), pp. 1307-14.

Nguyen, D.G., Funk, J., Robbins, J.B., Crogan-Grundy, C., Presnell, S.C., Singer, T. and Roth, A.B. (2016) 'Bioprinted 3D Primary Liver Tissues Allow Assessment of Organ-Level Response to Clinical Drug Induced Toxicity In Vitro', *PLoS One*, 11(7), p. e0158674.

Nguyen, P., Leray, V., Diez, M., Serisier, S., Le Bloc'h, J., Siliart, B. and Dumon, H. (2008) 'Liver lipid metabolism', *J Anim Physiol Anim Nutr (Berl)*, 92(3), pp. 272-83.

Odin, J.A., Huebert, R.C., Casciola-Rosen, L., LaRusso, N.F. and Rosen, A. (2001) 'Bcl-2-dependent oxidation of pyruvate dehydrogenase-E2, a primary biliary cirrhosis autoantigen, during apoptosis', *J Clin Invest*, 108(2), pp. 223-32.

Oliver, J.D. and Roberts, R.A. (2002) 'Receptor-mediated hepatocarcinogenesis: role of hepatocyte proliferation and apoptosis', *Pharmacol Toxicol*, 91(1), pp. 1-7.

Ono, S., Hatanaka, T., Hotta, H., Satoh, T., Gonzalez, F.J. and Tsutsui, M. (1996) 'Specificity of substrate and inhibitor probes for cytochrome P450s: evaluation of in vitro metabolism using cDNA-expressed human P450s and human liver microsomes', *Xenobiotica*, 26(7), pp. 681-93.

Ozkan, S., Ceylan, Y., Ozkan, O.V. and Yildirim, S. (2015) 'Review of a challenging clinical issue: Intrahepatic cholestasis of pregnancy', *World J Gastroenterol*, 21(23), pp. 7134-41.

Paradis, V., Perlemuter, G., Bonvoust, F., Dargere, D., Parfait, B., Vidaud, M., Conti, M., Huet, S., Ba, N., Buffet, C. and Bedossa, P. (2001) 'High glucose and hyperinsulinemia stimulate connective tissue growth factor expression: a potential mechanism involved in progression to fibrosis in nonalcoholic steatohepatitis', *Hepatology*, 34(4 Pt 1), pp. 738-44.

Park, S., Choi, Y.J. and Lee, B.H. (2012) 'In vitro validation of drug-induced phospholipidosis', *J Toxicol Sci*, 37(2), pp. 261-7.

Pascussi, J.M., Drocourt, L., Fabre, J.M., Maurel, P. and Vilarem, M.J. (2000) 'Dexamethasone induces pregnane X receptor and retinoid X receptor-alpha expression in human hepatocytes: synergistic increase of CYP3A4 induction by pregnane X receptor activators', *Mol Pharmacol*, 58(2), pp. 361-72.

Peekhaus, N.T., Chang, T., Hayes, E.C., Wilkinson, H.A., Mitra, S.W., Schaeffer, J.M. and Rohrer, S.P. (2004) 'Distinct effects of the antiestrogen Faslodex on the stability of estrogen receptors-alpha and -beta in the breast cancer cell line MCF-7', *J Mol Endocrinol*, 32(3), pp. 987-95.

Pelden, S., Insawang, T., Thuwajit, C. and Thuwajit, P. (2013) 'The trefoil factor 1 (TFF1) protein involved in doxorubicininduced apoptosis resistance is upregulated by estrogen in breast cancer cells', *Oncol Rep*, 30(3), pp. 1518-26.

Pernak, J., Rzemieniecki, T. and Materna, K. (2016) 'Ionic liquids" in a nutshell"(history, properties and development)', *Chemik*, 70(9), pp. 471-475.

Petit, P.X., Goubern, M., Diolez, P., Susin, S.A., Zamzami, N. and Kroemer, G. (1998) 'Disruption of the outer mitochondrial membrane as a result of large amplitude swelling: the impact of irreversible permeability transition', *FEBS Letters*, 426(1), pp. 111-116.

Pfleger, J., He, M. and Abdellatif, M. (2015) 'Mitochondrial complex II is a source of the reserve respiratory capacity that is regulated by metabolic sensors and promotes cell survival', *Cell Death Dis*, 6, p. e1835.

Poupon, R. (2015) 'Liver alkaline phosphatase: a missing link between choleresis and biliary inflammation', *Hepatology*, 61(6), pp. 2080-90.

Prince, M.I., Chetwynd, A., Diggle, P., Jarner, M., Metcalf, J.V. and James, O.F. (2001) 'The geographical distribution of primary biliary cirrhosis in a well-defined cohort', *Hepatology*, 34(6), pp. 1083-8.

Probert, P.M., Chung, G.W., Cockell, S.J., Agius, L., Mosesso, P., White, S.A., Oakley, F., Brown, C.D. and Wright, M.C. (2014) 'Utility of B-13 progenitor-derived hepatocytes in hepatotoxicity and genotoxicity studies', *Toxicol Sci*, 137(2), pp. 350-70.

Probert, P.M., Leitch, A.C., Dunn, M.P., Meyer, S.K., Palmer, J.M., Abdelghany, T.M., Lakey, A.F., Cooke, M.P., Talbot, H., Wills, C., McFarlane, W., Blake, L.I., Rosenmai, A.K., Oskarsson, A., Figueiredo, R., Wilson, C., Kass, G.E., Jones, D.E., Blain, P.G. and Wright, M.C. (2018) 'Identification of a xenobiotic as a potential environmental trigger in primary biliary cholangitis', *J Hepatol*.

Probert, P.M., Palmer, J.M., Alhusainy, W., Amer, A.O., Rietjens, I., White, S.A., Jones, D.E. and Wright, M.C. (2016) 'Progenitor-derived hepatocyte-like (B-13/H) cells metabolise 1'-hydroxyestragole to a genotoxic species via a SULT2B1-dependent mechanism', in *Toxicol Lett*. pp. 98-110.

Probert, P.M.E., Meyer, S.K., Alsaeedi, F., Axon, A.A., Fairhall, E.A., Wallace, K., Charles, M., Oakley, F., Jowsey, P.A., Blain, P.G. and Wright, M.C. (2015) 'An expandable donor-free supply of functional hepatocytes for toxicology', *Toxicology Research*, 4(2), pp. 203-222.

Public Health England (2017) *The 2nd Atlas of variation in risk factors and healthcare for liver disease in England* https://fingertips.phe.org.uk/profile/atlas-of-variation: (last accessed September 01, 2018). [Online]. Available at: https://fingertips.phe.org.uk/profile/atlas-of-variation.

Pyper, S.R., Viswakarma, N., Yu, S. and Reddy, J.K. (2010) 'PPARalpha: energy combustion, hypolipidemia, inflammation and cancer', *Nucl Recept Signal*, 8, p. e002.

Quinlan, C.L., Perevoshchikova, I.V., Hey-Mogensen, M., Orr, A.L. and Brand, M.D. (2013) 'Sites of reactive oxygen species generation by mitochondria oxidizing different substrates', *Redox Biol*, 1, pp. 304-12.

Rae, J.M., Johnson, M.D., Lippman, M.E. and Flockhart, D.A. (2001) 'Rifampin Is a Selective, Pleiotropic Inducer of Drug Metabolism Genes in Human Hepatocytes: Studies with cDNA and Oligonucleotide Expression Arrays', *Journal of Pharmacology and Experimental Therapeutics*, 299(3), p. 849.

Ramachandran, P. and Iredale, J.P. (2009) 'Reversibility of liver fibrosis', *Ann Hepatol*, 8(4), pp. 283-91.

Rasola, A. and Bernardi, P. (2007) 'The mitochondrial permeability transition pore and its involvement in cell death and in disease pathogenesis', *Apoptosis*, 12(5), pp. 815-833.

Ratra, G.S., Morgan, W.A., Mullervy, J., Powell, C.J. and Wright, M.C. (1998) 'Methapyrilene hepatotoxicity is associated with oxidative stress, mitochondrial disfunction and is prevented by the Ca2+ channel blocker verapamil', *Toxicology*, 130(2), pp. 79-93.

Raucy, J.L., Lasker, J., Ozaki, K. and Zoleta, V. (2004) 'Regulation of CYP2E1 by ethanol and palmitic acid and CYP4A11 by clofibrate in primary cultures of human hepatocytes', *Toxicol Sci*, 79(2), pp. 233-41.

Reel, J.R., Lamb, I.J. and Neal, B.H. (1996) 'Survey and assessment of mammalian estrogen biological assays for hazard characterization', *Fundam Appl Toxicol*, 34(2), pp. 288-305.

Repa, J.J., Liang, G., Ou, J., Bashmakov, Y., Lobaccaro, J.M., Shimomura, I., Shan, B., Brown, M.S., Goldstein, J.L. and Mangelsdorf, D.J. (2000) 'Regulation of mouse sterol regulatory element-binding protein-1c gene (SREBP-1c) by oxysterol receptors, LXRalpha and LXRbeta', *Genes Dev*, 14(22), pp. 2819-30.

Rieger, R., Leung, P.S., Jeddeloh, M.R., Kurth, M.J., Nantz, M.H., Lam, K.S., Barsky, D., Ansari, A.A., Coppel, R.L., Mackay, I.R. and Gershwin, M.E. (2006) 'Identification of 2-nonynoic acid, a cosmetic component, as a potential trigger of primary biliary cirrhosis', *J Autoimmun*, 27(1), pp. 7-16.

Roberts, R.A., Ganey, P.E., Ju, C., Kamendulis, L.M., Rusyn, I. and Klaunig, J.E. (2007) 'Role of the Kupffer cell in mediating hepatic toxicity and carcinogenesis', *Toxicol Sci*, 96(1), pp. 2-15.

Rodrigo-Torres, D., Affo, S., Coll, M., Morales-Ibanez, O., Millan, C., Blaya, D., Alvarez-Guaita, A., Rentero, C., Lozano, J.J., Maestro, M.A., Solar, M., Arroyo, V., Caballeria, J., van Grunsven, L.A., Enrich, C., Gines, P., Bataller, R. and Sancho-Bru, P. (2014) 'The biliary epithelium gives rise to liver progenitor cells', *Hepatology*, 60(4), pp. 1367-77.

Saito, J., Okamura, A., Takeuchi, K., Hanioka, K., Okada, A. and Ohata, T. (2016) 'High content analysis assay for prediction of human hepatotoxicity in HepaRG and HepG2 cells', *Toxicol In Vitro*, 33, pp. 63-70.

Salabei, J.K., Gibb, A.A. and Hill, B.G. (2014) 'Comprehensive measurement of respiratory activity in permeabilized cells using extracellular flux analysis', *Nat Protoc*, 9(2), pp. 421-38.

Sanyal, A.J., Campbell-Sargent, C., Mirshahi, F., Rizzo, W.B., Contos, M.J., Sterling, R.K., Luketic, V.A., Shiffman, M.L. and Clore, J.N. (2001) 'Nonalcoholic steatohepatitis: association of insulin resistance and mitochondrial abnormalities', *Gastroenterology*, 120(5), pp. 1183-92.

Savas, U., Machemer, D.E., Hsu, M.H., Gaynor, P., Lasker, J.M., Tukey, R.H. and Johnson, E.F. (2009) 'Opposing roles of peroxisome proliferator-activated receptor alpha and growth hormone in the regulation of CYP4A11 expression in a transgenic mouse model', *J Biol Chem*, 284(24), pp. 16541-52.

Sconce, E.A., Khan, T.I., Wynne, H.A., Avery, P., Monkhouse, L., King, B.P., Wood, P., Kesteven, P., Daly, A.K. and Kamali, F. (2005) 'The impact of CYP2C9 and VKORC1 genetic polymorphism and patient characteristics upon warfarin dose requirements: proposal for a new dosing regimen', *Blood*, 106(7), pp. 2329-33.

Seki, E., De Minicis, S., Osterreicher, C.H., Kluwe, J., Osawa, Y., Brenner, D.A. and Schwabe, R.F. (2007) 'TLR4 enhances TGF-beta signaling and hepatic fibrosis', *Nat Med*, 13(11), pp. 1324-32.

Selmi, C., Balkwill, D.L., Invernizzi, P., Ansari, A.A., Coppel, R.L., Podda, M., Leung, P.S., Kenny, T.P., Van De Water, J., Nantz, M.H., Kurth, M.J. and Gershwin, M.E. (2003) 'Patients with primary biliary cirrhosis react against a ubiquitous xenobiotic-metabolizing bacterium', *Hepatology*, 38(5), pp. 1250-7.

Selmi, C., Mayo, M.J., Bach, N., Ishibashi, H., Invernizzi, P., Gish, R.G., Gordon, S.C., Wright, H.I., Zweiban, B., Podda, M. and Gershwin, M.E. (2004) 'Primary biliary cirrhosis in monozygotic and dizygotic twins: genetics, epigenetics, and environment', *Gastroenterology*, 127(2), pp. 485-92.

Shanle, E.K. and Xu, W. (2011) 'Endocrine disrupting chemicals targeting estrogen receptor signaling: Identification and mechanisms of action', *Chemical research in toxicology*, 24(1), pp. 6-19.

Shayman, J.A. and Abe, A. (2013) 'Drug induced phospholipidosis: an acquired lysosomal storage disorder', *Biochim Biophys Acta*, 1831(3), pp. 602-11.

Shen, C.N., Slack, J.M. and Tosh, D. (2000) 'Molecular basis of transdifferentiation of pancreas to liver', *Nat Cell Biol*, 2(12), pp. 879-87.

Shuai, Z., Wang, J., Badamagunta, M., Choi, J., Yang, G., Zhang, W., Kenny, T.P., Guggenheim, K., Kurth, M.J., Ansari, A.A., Voss, J., Coppel, R.L., Invernizzi, P., Leung, P.S.C. and Gershwin, M.E. (2017) 'The fingerprint of antimitochondrial antibodies and the etiology of primary biliary cholangitis', *Hepatology*, 65(5), pp. 1670-1682.

Song, X., Vasilenko, A., Chen, Y., Valanejad, L., Verma, R., Yan, B. and Deng, R. (2014) 'Transcriptional dynamics of bile salt export pump during pregnancy: mechanisms and implications in intrahepatic cholestasis of pregnancy', *Hepatology*, 60(6), pp. 1993-2007.

Spitzer, A.L., Lao, O.B., Dick, A.A., Bakthavatsalam, R., Halldorson, J.B., Yeh, M.M., Upton, M.P., Reyes, J.D. and Perkins, J.D. (2010) 'The biopsied donor liver: incorporating macrosteatosis into high-risk donor assessment', *Liver Transpl*, 16(7), pp. 874-84.

Staels, B., Rubenstrunk, A., Noel, B., Rigou, G., Delataille, P., Millatt, L.J., Baron, M., Lucas, A., Tailleux, A., Hum, D.W., Ratziu, V., Cariou, B. and Hanf, R. (2013) 'Hepatoprotective effects of the dual peroxisome proliferator-activated receptor alpha/delta agonist, GFT505, in rodent models of nonalcoholic fatty liver disease/nonalcoholic steatohepatitis', *Hepatology*, 58(6), pp. 1941-52.

Stieger, B., Fattinger, K., Madon, J., Kullak-Ublick, G.A. and Meier, P.J. (2000) 'Drug- and estrogen-induced cholestasis through inhibition of the hepatocellular bile salt export pump (Bsep) of rat liver', *Gastroenterology*, 118(2), pp. 422-30.

Sun, J.M., Spencer, V.A., Li, L., Yu Chen, H., Yu, J. and Davie, J.R. (2005) 'Estrogen regulation of trefoil factor 1 expression by estrogen receptor alpha and Sp proteins', *Exp Cell Res*, 302(1), pp. 96-107.

Sun, M. and Kisseleva, T. (2015) 'Reversibility of liver fibrosis', *Clin Res Hepatol Gastroenterol*, 39 Suppl 1, pp. S60-3.

Sun, M.G., Williams, J., Munoz-Pinedo, C., Perkins, G.A., Brown, J.M., Ellisman, M.H., Green, D.R. and Frey, T.G. (2007) 'Correlated three-dimensional light and electron microscopy reveals transformation of mitochondria during apoptosis', *Nature Cell Biology*, 9, p. 1057.

Sun, Y., Haapanen, K., Li, B., Zhang, W., Van de Water, J. and Gershwin, M.E. (2015) 'Women and primary biliary cirrhosis', *Clin Rev Allergy Immunol*, 48(2-3), pp. 285-300.

Szabo, G. (2015) 'Gut-liver axis in alcoholic liver disease', *Gastroenterology*, 148(1), pp. 30-6.

Takayama, K., Inamura, M., Kawabata, K., Sugawara, M., Kikuchi, K., Higuchi, M., Nagamoto, Y., Watanabe, H., Tashiro, K., Sakurai, F., Hayakawa, T., Furue, M.K. and Mizuguchi, H. (2012) 'Generation of metabolically functioning hepatocytes from human pluripotent stem cells by FOXA2 and HNF1alpha transduction', *J Hepatol*, 57(3), pp. 628-36.

Tanaka, A., Leung, P.S. and Gershwin, M.E. (2018) 'Environmental basis of primary biliary cholangitis', *Exp Biol Med (Maywood)*, 243(2), pp. 184-189.

Tanimizu, N. and Mitaka, T. (2014) 'Re-evaluation of liver stem/progenitor cells', *Organogenesis*, 10(2), pp. 208-15.

Tetsuka, K., Ohbuchi, M. and Tabata, K. (2017) 'Recent Progress in Hepatocyte Culture Models and Their Application to the Assessment of Drug Metabolism, Transport, and Toxicity in Drug Discovery: The Value of Tissue Engineering for the Successful Development of a Microphysiological System', *J Pharm Sci*, 106(9), pp. 2302-2311.

Thomas, P. and Smart, T.G. (2005) 'HEK293 cell line: a vehicle for the expression of recombinant proteins', *J Pharmacol Toxicol Methods*, 51(3), pp. 187-200.

Thuy Phuong, N.T., Kim, J.W., Kim, J.A., Jeon, J.S., Lee, J.Y., Xu, W.J., Yang, J.W., Kim, S.K. and Kang, K.W. (2017) 'Role of the CYP3A4-mediated 11,12-epoxyeicosatrienoic acid pathway in the development of tamoxifen-resistant breast cancer', *Oncotarget*, 8(41), pp. 71054-71069.

Timsit, Y.E. and Negishi, M. (2007) 'CAR and PXR: the xenobiotic-sensing receptors', *Steroids*, 72(3), pp. 231-46.

Tolosa, L., Gomez-Lechon, M.J., Perez-Cataldo, G., Castell, J.V. and Donato, M.T. (2013) 'HepG2 cells simultaneously expressing five P450 enzymes for the screening of hepatotoxicity: identification of bioactivable drugs and the potential mechanism of toxicity involved', *Arch Toxicol*, 87(6), pp. 1115-27.

Tosh, D., Shen, C.N. and Slack, J.M. (2002) 'Differentiated properties of hepatocytes induced from pancreatic cells', *Hepatology*, 36(3), pp. 534-43.

Triger, D.R. (1980) 'Primary biliary cirrhosis: an epidemiological study', *Br Med J*, 281(6243), pp. 772-5.

Tsai, M.J. and O'Malley, B.W. (1994) 'Molecular mechanisms of action of steroid/thyroid receptor superfamily members', *Annu Rev Biochem*, 63, pp. 451-86.

Umeda, M., Hiramoto, M. and Imai, T. (2015) 'Partial hepatectomy induces delayed hepatocyte proliferation and normal liver regeneration in ovariectomized mice', *Clin Exp Gastroenterol*, 8, pp. 175-82.

van Herwaarden, A.E., Wagenaar, E., van der Kruijssen, C.M., van Waterschoot, R.A., Smit, J.W., Song, J.Y., van der Valk, M.A., van Tellingen, O., van der Hoorn, J.W., Rosing, H., Beijnen, J.H. and Schinkel, A.H. (2007) 'Knockout of cytochrome P450 3A yields new mouse models for understanding xenobiotic metabolism', *J Clin Invest*, 117(11), pp. 3583-92.

Wakabayashi, K., Lian, Z.X., Leung, P.S., Moritoki, Y., Tsuneyama, K., Kurth, M.J., Lam, K.S., Yoshida, K., Yang, G.X., Hibi, T., Ansari, A.A., Ridgway, W.M., Coppel, R.L., Mackay, I.R. and Gershwin, M.E. (2008) 'Loss of tolerance in C57BL/6 mice to the autoantigen E2 subunit of pyruvate dehydrogenase by a xenobiotic with ensuing biliary ductular disease', *Hepatology*, 48(2), pp. 531-40.

Walden, H.R., Kirby, J.A., Yeaman, S.J., Gray, J., Jones, D.E. and Palmer, J.M. (2008) 'Xenobiotic incorporation into pyruvate dehydrogenase complex can occur via the exogenous lipoylation pathway', *Hepatology*, 48(6), pp. 1874-84.

Wallace, K., Burt, A.D. and Wright, M.C. (2008) 'Liver fibrosis', *Biochem J*, 411(1), pp. 1-18.

Wallace, K., Fairhall, E.A., Charlton, K.A. and Wright, M.C. (2010a) 'AR42J-B-13 cell: an expandable progenitor to generate an unlimited supply of functional hepatocytes', *Toxicology*, 278(3), pp. 277-87.

Wallace, K., Flecknell, P.A., Burt, A.D. and Wright, M.C. (2010b) 'Disrupted pancreatic exocrine differentiation and malabsorption in response to chronic elevated systemic glucocorticoid', *Am J Pathol*, 177(3), pp. 1225-32.

Wallace, K., Long, Q., Fairhall, E.A., Charlton, K.A. and Wright, M.C. (2011) 'Serine/threonine protein kinase SGK1 in glucocorticoid-dependent transdifferentiation of pancreatic acinar cells to hepatocytes', *J Cell Sci*, 124(Pt 3), pp. 405-13.

Wallace, K., Marek, C.J., Currie, R.A. and Wright, M.C. (2009) 'Exocrine pancreas trans-differentiation to hepatocytes--a physiological response to elevated glucocorticoid in vivo', *J Steroid Biochem Mol Biol*, 116(1-2), pp. 76-85.

Wang, Y.M., Ong, S.S., Chai, S.C. and Chen, T. (2012) 'Role of CAR and PXR in xenobiotic sensing and metabolism', *Expert Opin Drug Metab Toxicol*, 8(7), pp. 803-17.

Wardell, S.E., Marks, J.R. and McDonnell, D.P. (2011) 'The turnover of estrogen receptor alpha by the selective estrogen receptor degrader (SERD) fulvestrant is a saturable process that is not required for antagonist efficacy', *Biochem Pharmacol*, 82(2), pp. 122-30.

Westerink, W.M. and Schoonen, W.G. (2007a) 'Cytochrome P450 enzyme levels in HepG2 cells and cryopreserved primary human hepatocytes and their induction in HepG2 cells', *Toxicol In Vitro*, 21(8), pp. 1581-91.

Westerink, W.M. and Schoonen, W.G. (2007b) 'Phase II enzyme levels in HepG2 cells and cryopreserved primary human hepatocytes and their induction in HepG2 cells', *Toxicol In Vitro*, 21(8), pp. 1592-602.

Wilkening, S., Stahl, F. and Bader, A. (2003) 'Comparison of primary human hepatocytes and hepatoma cell line Hepg2 with regard to their biotransformation properties', *Drug Metab Dispos*, 31(8), pp. 1035-42.

Williams, D.P., Shipley, R., Ellis, M.J., Webb, S., Ward, J., Gardner, I. and Creton, S. (2013) 'Novel in vitro and mathematical models for the prediction of chemical toxicity', *Toxicol Res (Camb)*, 2(1), pp. 40-59.

Williams, P.A., Cosme, J., Vinkovic, D.M., Ward, A., Angove, H.C., Day, P.J., Vonrhein, C., Tickle, I.J. and Jhoti, H. (2004) 'Crystal structures of human cytochrome P450 3A4 bound to metyrapone and progesterone', *Science*, 305(5684), pp. 683-6.

Williams, R., Aspinall, R., Bellis, M., Camps-Walsh, G., Cramp, M., Dhawan, A., Ferguson, J., Forton, D., Foster, G., Gilmore, I., Hickman, M., Hudson, M., Kelly, D., Langford, A., Lombard, M., Longworth, L., Martin, N., Moriarty, K., Newsome, P., O'Grady, J., Pryke, R., Rutter, H., Ryder, S., Sheron, N. and Smith, T. (2014) 'Addressing liver disease in the UK: a blueprint for attaining excellence in health care and reducing premature mortality from lifestyle issues of excess consumption of alcohol, obesity, and viral hepatitis', *Lancet*, 384(9958), pp. 1953-97.

Woolbright, B.L. and Jaeschke, H. (2012) 'Novel insight into mechanisms of cholestatic liver injury', *World J Gastroenterol*, 18(36), pp. 4985-93.

Wright, M.C., Issa, R., Smart, D.E., Trim, N., Murray, G.I., Primrose, J.N., Arthur, M.J.P., Iredale, J.P. and Mann, D.A. (2001) 'Gliotoxin stimulates the apoptosis of human and rat hepatic stellate cells and enhances the resolution of liver fibrosis in rats', *Gastroenterology*, 121(3), pp. 685-698.

Wright, M.C., Paine, A.J., Skett, P. and Auld, R. (1994) 'Induction of rat hepatic glucocorticoid-inducible cytochrome P450 3A by metyrapone', *J Steroid Biochem Mol Biol*, 48(2-3), pp. 271-6.

Xie, W., Barwick, J.L., Simon, C.M., Pierce, A.M., Safe, S., Blumberg, B., Guzelian, P.S. and Evans, R.M. (2000) 'Reciprocal activation of xenobiotic response genes by nuclear receptors SXR/PXR and CAR', *Genes Dev*, 14(23), pp. 3014-23.

Xu, J., Oda, S. and Yokoi, T. (2018) 'Cell-based assay using glutathione-depleted HepaRG and HepG2 human liver cells for predicting drug-induced liver injury', *Toxicol In Vitro*, 48, pp. 286-301.

Xuan, J., Chen, S., Ning, B., Tolleson, W.H. and Guo, L. (2016) 'Development of HepG2-derived cells expressing cytochrome P450s for assessing metabolism-associated drug-induced liver toxicity', *Chem Biol Interact*, 255, pp. 63-73.

Yamamoto, Y., Moore, R., Hess, H.A., Guo, G.L., Gonzalez, F.J., Korach, K.S., Maronpot, R.R. and Negishi, M. (2006) 'Estrogen receptor alpha mediates 17alpha-ethynylestradiol causing hepatotoxicity', *J Biol Chem*, 281(24), pp. 16625-31.

Yi, P., Driscoll, M.D., Huang, J., Bhagat, S., Hilf, R., Bambara, R.A. and Muyan, M. (2002) 'The effects of estrogen-responsive element- and ligand-induced structural changes on the recruitment of cofactors and transcriptional responses by ER alpha and ER beta', *Mol Endocrinol*, 16(4), pp. 674-93.

Yokoyama, Y., Sasaki, Y., Terasaki, N., Kawataki, T., Takekawa, K., Iwase, Y., Shimizu, T., Sanoh, S. and Ohta, S. (2018) 'Comparison of Drug Metabolism and Its Related Hepatotoxic Effects in HepaRG, Cryopreserved Human Hepatocytes, and HepG2 Cell Cultures', *Biol Pharm Bull*, 41(5), pp. 722-732.

Yu, M., Li, S.M., Li, X.Y., Zhang, B.J. and Wang, J.J. (2008) 'Acute effects of 1-octyl-3-methylimidazolium bromide ionic liquid on the antioxidant enzyme system of mouse liver', *Ecotoxicol Environ Saf*, 71(3), pp. 903-8.

Zanger, U.M. and Schwab, M. (2013) 'Cytochrome P450 enzymes in drug metabolism: regulation of gene expression, enzyme activities, and impact of genetic variation', *Pharmacol Ther*, 138(1), pp. 103-41.

Zeilinger, K., Freyer, N., Damm, G., Seehofer, D. and Knospel, F. (2016) 'Cell sources for in vitro human liver cell culture models', *Exp Biol Med (Maywood)*, 241(15), pp. 1684-98.

Zhang, Y., Klein, K., Sugathan, A., Nassery, N., Dombkowski, A., Zanger, U.M. and Waxman, D.J. (2011) 'Transcriptional profiling of human liver identifies sex-biased genes associated with polygenic dyslipidemia and coronary artery disease', *PLoS One*, 6(8), p. e23506.

Zhao, C., Dahlman-Wright, K. and Gustafsson, J.A. (2008) 'Estrogen receptor beta: an overview and update', *Nucl Recept Signal*, 6, p. e003.

Zhou, Z., Wang, L., Song, Z., Lambert, J.C., McClain, C.J. and Kang, Y.J. (2003) 'A critical involvement of oxidative stress in acute alcohol-induced hepatic TNF-alpha production', *Am J Pathol*, 163(3), pp. 1137-46.

Zoeller, R.T., Brown, T.R., Doan, L.L., Gore, A.C., Skakkebaek, N.E., Soto, A.M., Woodruff, T.J. and Vom Saal, F.S. (2012) 'Endocrine-disrupting chemicals and public health protection: a statement of principles from The Endocrine Society', *Endocrinology*, 153(9), pp. 4097-110.

Appendix A. Published papers